CRYSTALLOGRAPHIC STUDIES FOR THE RATIONAL DESIGN OF

N-FUNCTIONALIZED PHOSPHONIC ACID COORDINATION POLYMERS

By

JULIE ANN FRY

Bachelor of Arts, 1989
Rice University
Houston, Texas

Submitted to the Graduate Faculty of the
College of Science and Engineering
Texas Christian University
in partial fulfillment of the requirements
for the degree of

Doctor of Philosophy

December 2011

CRYSTALLOGRAPHIC STUDIES FOR THE RATIONAL DESIGN OF N-FUNCTIONALIZED PHOSPHONIC ACID COORDINATION POLYMERS
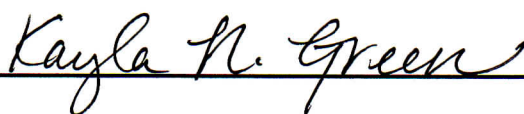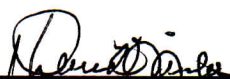
By

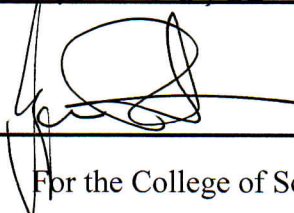Julie A. Fry

Dissertation approved:

Robert H. Neilson
Major Professor

Kayla N. Green

Tracy A. Hanna

Robert Doyle

For the College of Science and Engineering

ACKNOWLEDGEMENTS

TABLE OF CONTENTS

CHAPTER 1
Metal Organic Frameworks

CHAPTER 2
A Mild Synthetic Route to Zinc, Cadmium, and Silver Polymers with 2-(pyridyl) phosphonic Acid: Synthesis and Analysis

iv

CHAPTER 3
2-(pyridylmethyl)phosphonic acid: A flexible, multi-dentate ligand for metal phosphonates.

CHAPTER 4
(Aminomethyl)phosphonic acid: A flexible, multi-dentate ligand for metal phosphonates.

CHAPTER 5
Investigative Studies with 2-(pyridylmethyl)phosphonic Acid and its Isomers

Vita

Abstract

LIST OF ABBREVIATIONS

1D	One dimension, unidimensional
2D	Two dimensions, bidimensional
3D	Three dimensions, tridimensional
$2PyHPO_3H$	2-(pyridyl)phosphonic acid
$3PyHPO_3H$	3-(pyridyl)phosphonic acid
$4PyHPO_3H$	4-(pyridyl)phosphonic acid
$2PyCH_2PO_3H_2$	2-(pyridylmethyl)phosphonic acid
$3PyCH_2PO_3H_2$	3-(pyridylmethyl)phosphonic acid
$3PyCH_2PO_3H_2$	4-(pyridylmethyl)phosphonic acid
AFM	Atomic Force Microscopy
Ampa	Aminomethylphosphonic acid
Bdc	Benzene dicarboxylic acid
Bipy	Bipyridine
Bpp	1,3-bis(4-pyridyl)propane
CNS	Coordination Network Solid
COF	Covalent Organic Framework
DEF	N-N-diethylformamide
DMMB	Methyl-3,5-dimethylbenzoate
DPPF	1,1'-bis(diphenylphosphino)ferrocene
EtOH	Ethanol
HDS	Hydrodesulfurization
Hetz	3,5-diethyl-1,2,4-triazole
HKUST	Hong Kong University of Science and Technology
H_3NTB	4,4',4"-nitrilotrisbenzoic acid

ICP	Infinite Coordination Network
IR	Infrared
IRMOF	Isoreticular Metal-Organic Framework
IUPAC	International Union of Pure and Applied Chemistry
LLCT	Ligand-Ligand Charge Transfer
LMCT	Ligand-Metal Charge Transfer
MeOH	Methanol
MLCT	Metal-Ligand Charge Transfer
MOF	Metal-Organic Framework
MOM	Metal-Organic Materials
NMR	Nuclear Magnetic Resonance
PCP	Porous Coordination Polymer
PCN	Porous Coordination Network
pH	Measure of hydrogen ion potential
pKa	Negative logarithm (base 10) of the acid dissociation constant
PMP	Pinacolyl methylphosphonate
Py	Pyridine
SBU	Secondary Building Unit
SMM	Single Molecule Magnets
TGA	Thermogravimetric Analysis
THF	Tetrahydrofuran
TMSBr	Trimethylsilyl bromide
TPT	2,4,6-tris(4-pyridyl)triazine
XPS	X-ray Photoelectron Spectroscopy
ZIF	Zeolitic Imidazolate Framework

LIST OF FIGURES

LIST OF EQUATIONS

LIST OF SCHEMES

LIST OF TABLES

Chapter 1

Metal Organic Frameworks and their Applications

1.1 Introduction

Over the last twenty years, an explosion of new research in the area of coordination polymers has begun to bear rich fruit: the emergence of rigid, crystalline "sponge" metal-organic frameworks (MOFs).[1] Many of these dynamic one-, two-, and three-dimensional networks reveal unprecedented gas adsorption and storage capabilities, catalytic function, and other useful physical and/or chemical properties such as luminescence and magnetism.[2] This field has developed from the rudimentary goal of engineering crystalline structures with specific physical and/or chemical properties in mind.[3]

The extended arrays of these networks are composed of highly labile metal ions or clusters and bridging polydentate organic ligands. Depending on the preferred geometries of the metal, the degree of chelation available to the organic linker, and other significant factors that can affect the chemical environment (pH, counterions, solvent, temperature), products with differing dimensionalities can result.[4] A simplified illustration of how network topologies depend on the geometric nature of the building blocks is shown in Scheme 1; steric restraints,[5] rare-earth cations participating in high coordination numbers,[6] flexible organic ligands,[7] and the presence of secondary ligands[8] can all contribute to irregular topologies.

Functionalized organic acids play a critical role in the development of mono-, bi-, and tri-dimensional structures due to the strong covalent nature of the metal-oxygen bonds.[9] These groups can be readily deprotonated forming anionic ligands that can coordinate to metal centers and compensate for charge. Non-acidic moieties can give increased rigidity to the ligand,[10] as well as provide additional sites for metal coordination,[11] influencing the structure through non-

1

covalent forces,[12] and interacting with solvent and guest molecules to affect the function of the
network.[13] Examples of multidentate ligands are shown in Figure 1.1.
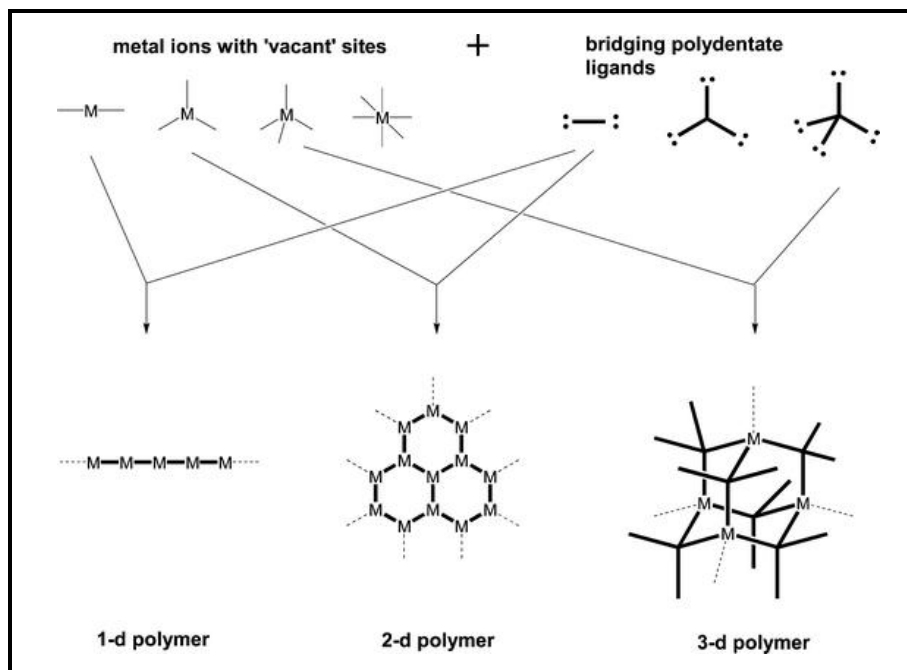
Scheme 1 Metal centers act like "joints"; ligands are the "struts." Adapted from Reference 1.
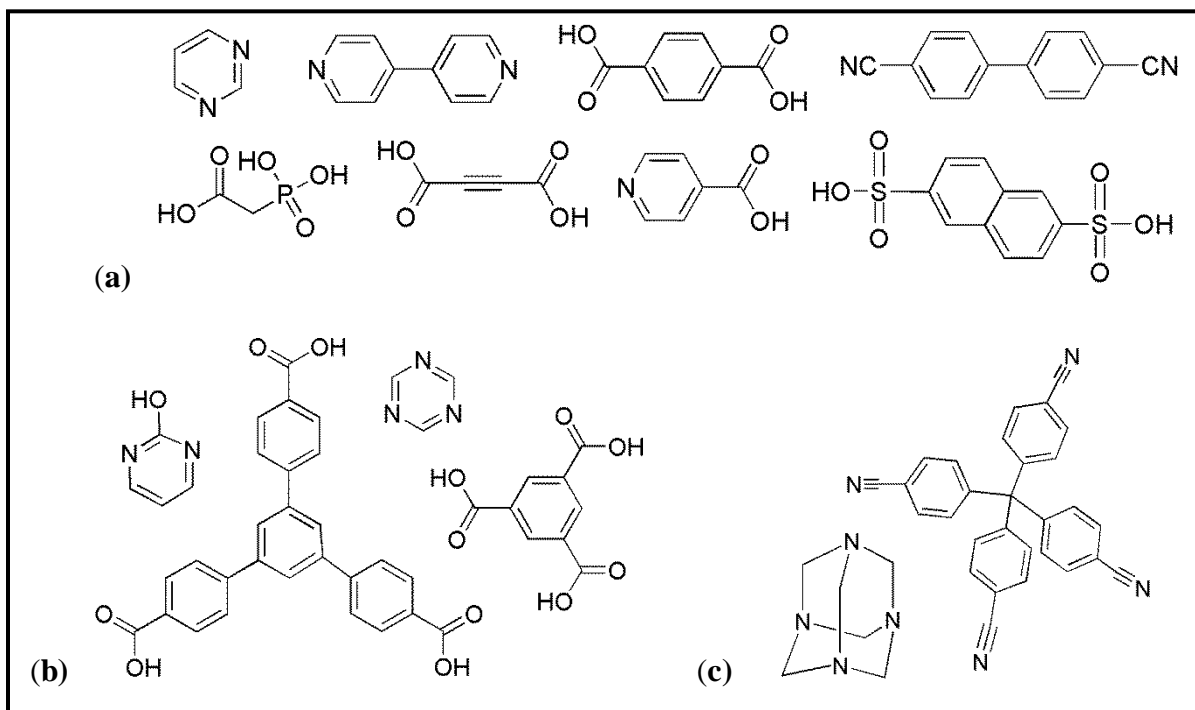
Figure 1.1 Common organic linkers: **(a)** Bidentate **(b)** Tridentate **(c)** Tetradentate.

While we begin to see many possibilities for applications of these new polymers and 3D networks,[14] the goal of true rational design of such materials will only be achieved on the basis of intensive systematic investigations.[15] Our project research goals were two-fold:

- Utilize mild, "green" methods to synthesize and analyze novel homo- and heterometallic polymers for the purpose of future applications, using bifunctional phosphonic acids to extend product dimensionality.
- Investigate factors that control the structure of crystalline, thermally stable coordination polymers, such as preferred metal geometry and coordination modes, ligand flexibility, counterion, solvent, and pH.

The following five chapters will detail our efforts to advance these research goals. Chapter 1 continues the discussion of concepts needed to fully appreciate our research with functionalized acid polymers.

Chapter 2 describes the synthesis and analysis of five new metal pyridylphosphonate polymers employing a bifunctional 2-(pyridyl)phosphonic acid ligand and salts of Zn(II), Cd(II), Hg(II), and Ag(I). Room-temperature aqueous conditions were utilized in this synthesis.

Chapter 3 reports the influence that preferred metal geometry and coordination preferences of the more flexible ligand 2-(pyridylmethyl)phosphonic acid have on the dimensionality and structure of eight products. Physical properties of Mn(II), Co(II), Fe(II), Fe(III), Ag(I), and Pb(II) phosphonates are contrasted, as well as compared, to a bimetallic Ag(I)/Pb(II) structure.

Chapter 4 explores the use of aminomethyl phosphonic acid (ampa) as a bifunctional organic linker for the production of coordination polymers. The substitution of the amino group for the rigid heterocyclic ring of 2-(pyridylmethyl)phosphonic acid results in two-dimensional

organophosphonate frameworks with Zn(II), Mn(II), Co(II), Cu(II), Gd(III), Sm(III), and Yb(III) cations.

Chapter 5 relates our efforts to evaluate the relationships between metal choice, counter-ion, and ligand geometric constraints on polymer architectures. Reactions with 2-(pyridylmethyl)phosphonic acid and bromide and perchlorate salts of Ca(II), the nitrate salt of Co(II), and chloride, nitrate, and perchlorate salts of Zn(II) produced both dimers and two-dimensional polymers. Polymers were also obtained from reactions between 3-(pyridylmethyl)phosphonic acid and triflate and nitrate salts of Ag(I), as well as between 4-(pyridylmethyl)phosphonic acid and the nitrate salt of Zn(II).

1.2 Terminology

The term "coordination polymer" has been around since the 1960's, and refers to a coordination compound whose metal centers are bridged by ligands to create a repeating array, considered officially by the IUPAC as a one-dimensional structure.[16] In general, the scientific community considers coordination polymers as extended complexes in one, two, or three dimensions, and these polymers have been prevalent in the literature for decades. However, in 1989, Robson et $al.$ introduced the first representative of a new class of highly porous, rigid coordination polymers with his synthesis of $[Cu^I\{C(C_6H_4CN)_4\}]_n^{n+}$, a "deliberately designed and constructed infinite framework consisting of tetrahedral centers linked together by rod-like units."[10] This significant achievement was quickly followed in kind by Yaghi with MOF-2[17] and MOF-4,[13] and the ground-breaking MOF-5 in 1999[18] (Figure 1.2). The latter was the first of these geometrically-planned 3D complexes to maintain crystallinity after being fully desolvated. MOF-5 displayed a surface area and uniform pore volume greater than the average zeolites,

which are rigid aluminosilicate solids widely used in industry as "molecular sieves" and catalysts. [19]
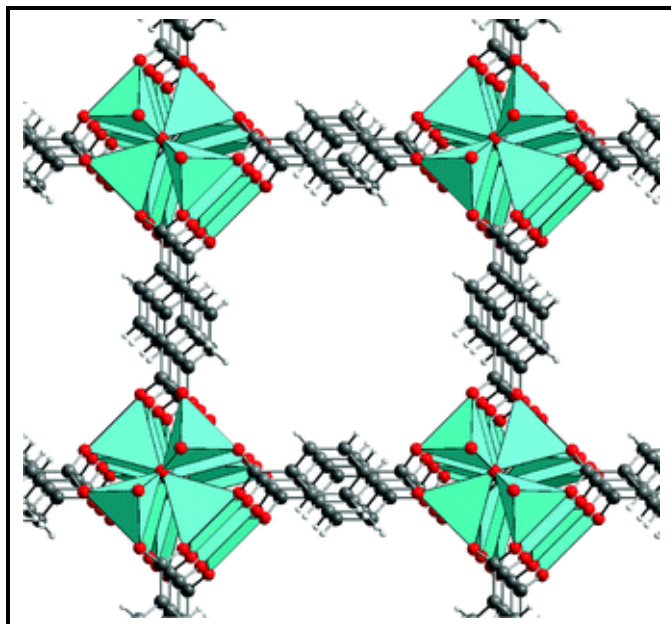
Figure 1.2 Cubic porous network MOF-5: $Zn_4O(BDC)_3\cdot(DMF)_8(C_6H_5Cl)$ units composed of octahedral $Zn_4O(CO_2)_6$ secondary building units (SBUs) linked to linear 1,4-benzenedicarboxylate (BDC). Solvent molecules omitted for clarity. Adapted from Reference 18.

The clamor for porous materials analogous to zeolites, but with the capacity for rationally-designed chemical modification, has paved the way for an avalanche of research world-wide. The accompanying new vocabulary is a veritable vegetable soup of acronyms used to classify types of coordination polymers as well as name individual structures. MOF is a general term (metal-organic framework), similar to the COF for covalent organic framework,[20] but is also used to name structures (MOF-n) as seen in Figure 1.2. Further examples of nomenclature are IRMOF-n (isoreticular metal-organic framework)[21] and ZIF-n (zeolitic imidazolate framework)[22], which are descriptive in nature, and MIL-n (Materiaux de l'Institut Lavoisier)[23] and HKUST-n (Hong Kong University of Science and Technology)[24] which refer to the laboratory of origin. More generalized terms such as PCP (porous coordination polymer), PCN

(porous coordination network), ICP (infinite coordination polymer), MOM (metal-organic materials), and CNS (coordination network solid) have also proven useful. Added to the mix is the label "organic-inorganic hybrid material," which is a very general term for such materials.

While the exact definition of a metal-organic framework has not been published by the IUPAC at this time,[25] some attempts have been made to make communication within the scientific community more effective. Classification schemes can focus on the types of physical linkages[26] occurring (Figure 1.3), the bond characteristics present,[14] and the dimensionality of the material (Figure 1.4).[27]
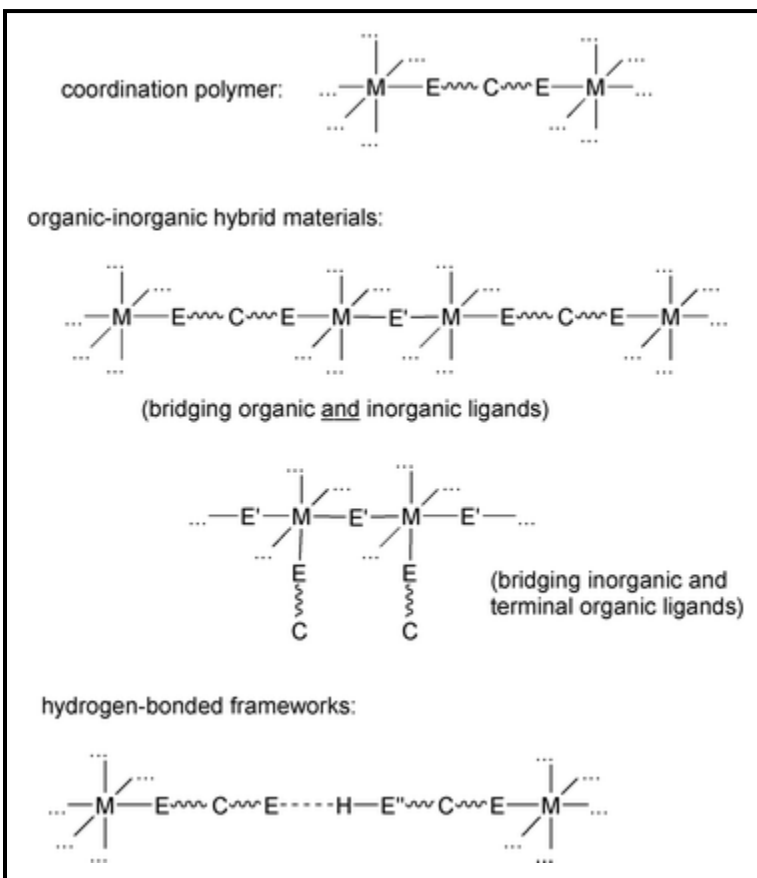
Figure 1.3 Christoph Janiak's terminology, which focuses on connections between the metal centers. M = metal cation; E = oxygen or similar atom; C =carbon. Adapted from Reference 26.
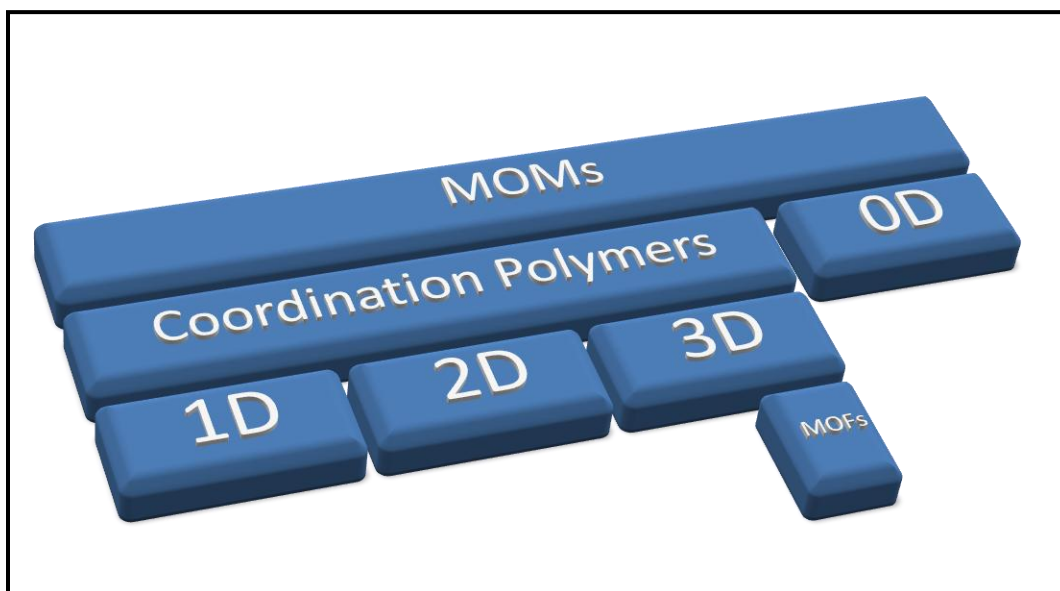
Figure 1.4 Classification scheme focusing solely on dimensionality, with Metal-Organic Frameworks (MOFs) as a subset of 3D Coordination Polymers. MOMs = Metal-organic Materials; 0D = discrete clusters or cages; 1D = Chains, ladders; 2D = Sheets, bilayers. Modified from Reference 27.

In this work, the term "coordination polymer" will be a general term used to indicate an infinite array in one, two, or three dimensions utilizing M-L-M connections, where the ligand may or may not connect to the metal center via a carbon atom. The primary bonding interactions in these coordination polymers are covalent and coordinate bonds, with additional interactions occurring to help maintain polymer stability (e.g. Ag-Ag interactions, hydrogen bonding, $\pi\cdots\pi$ interactions). "Hybrid organic-inorganic" will be used for those coordination polymers that contain organic moieties, but the metals are not connected through carbon atoms in at least one dimension (i.e. only through the phosphonate moiety rather than the pyridine ring of 2-pyridyl phosphonic acid). The term metal-organic framework (MOF) will be reserved for three-dimensional, porous structures where metal atoms or metal clusters are connected solely by covalent bonds,[28] with metal to metal connections always occurring via an organic linkage, as pictured by MOF-5 in Figure 1.2.

7

1.3 Structure and Dimensionality

A unique feature of these novel network solids is that, unlike the majority of organic polymers which are linear in nature, many support channels and pores that can maintain their structure with or without the presence of guest molecules (such as solvent or adsorbed gases). Zeolites[1] and amorphous carbon materials[29] are currently used for applications related to their microporous structures, however the chemical versatility and additional functionalities that can be introduced through the incorporation of a judicial choice of organic linker makes the metal-organic frameworks and other coordination network solids highly desirable materials for investigation.[2]

1.3.1   1D Polymers

1D coordination polymers that generate useful channels or cavities are those that can organize into helical and ladder architectures.   The helical structure of [Ni(bipy)(benzoate)$_2$(MeOH)$_2$] ·PhNO$_2$ is attained by the linking of octahedral metal moieties with linear organic linkers (Figure 1.5).[30] Nitrobenzene guest molecules are trapped in 500 Å^3 cavities produced by the packing of adjacent helices. An interesting note is that the resulting bulk crystals are polar, as the helices are all oriented in the same direction.

If the stoichiometry of the reagents is 1:1.5 instead of the 1:1 used to produce the helices, then 1D ladders can result.   The first example of a metal-organic supramolecular ladder, connected solely by metal-ligand coordination bonds, was reported by Fujita *et al*. in 1995.[31] Cadmium(II) ions were combined with a pyridine-functionalized ligand, 1,4-bis(4-pyridylmethyl)-benzene, to produce a 4-fold interpenetrated 1D architecture, where the ligand participates as both rung and rail of the ladder, with the metal center as the vertex.
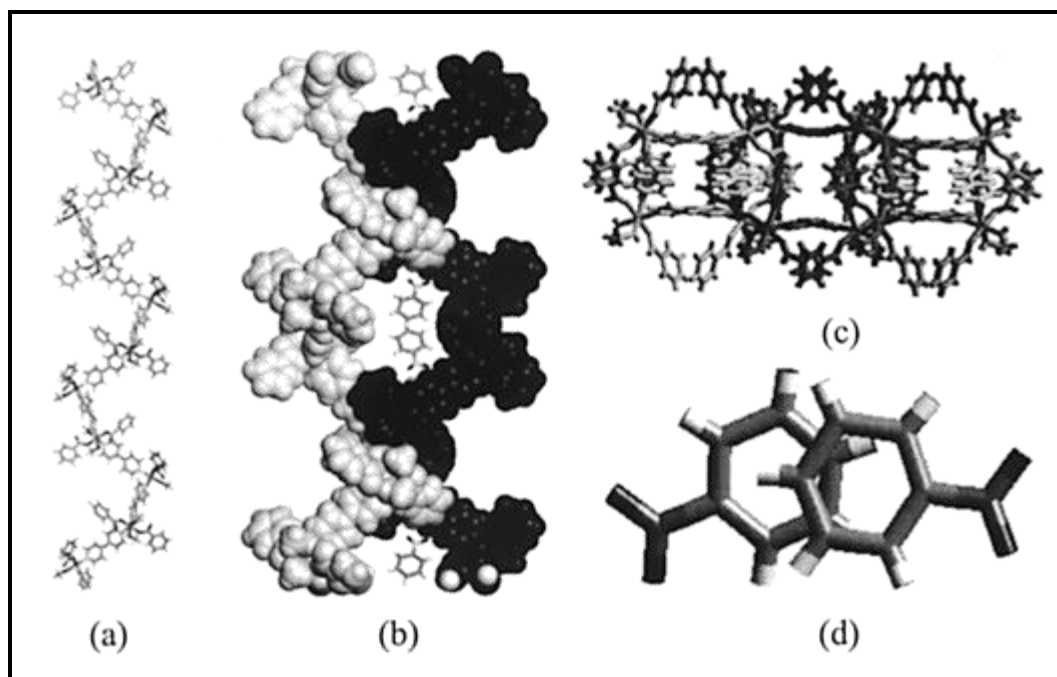
Figure 1.5. [Ni(bipy)(benzoate)$_2$(MeOH)$_2$]·PhNO$_2$ a) Single helical chain   b) Nitrobenzene dimers occupying cavities formed by packing of adjacent helices (c) Overhead view (d) Clathrated nitrobenzene dimer. Adapted from Reference 12a.

1.3.2 2D Polymers

Some common 2D architectures utilizing M-L-M connectivity in both dimensions are illustrated in Figure 1.6. Factors affecting the network topology are metal:ligand ratios and the degree of chelation.[12a]
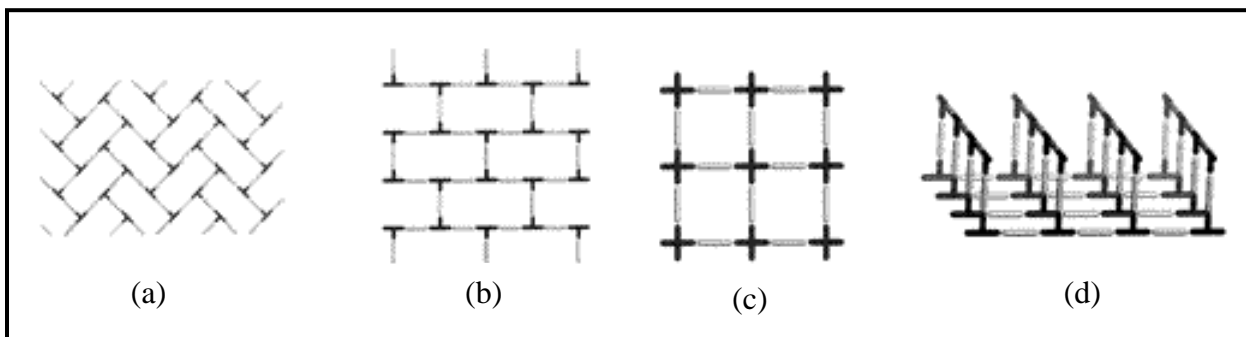
Figure 1.6   Representations of 2D networks reported for metal-organic polymers.   (a) Herringbone or ''Parquet Floor'' (b) Brick Wall (c) Square Grid (d) Bilayer. Adapted from Reference 12a.

The square grid topology is fairly common, and can be seen in MOF-2 (Figure 1.7).[17] The 2D microporous layers are held together by hydrogen-bonding interactions between Zn(II)-coordinated water molecules from one layer and carboxylate oxygens from an adjacent layer.
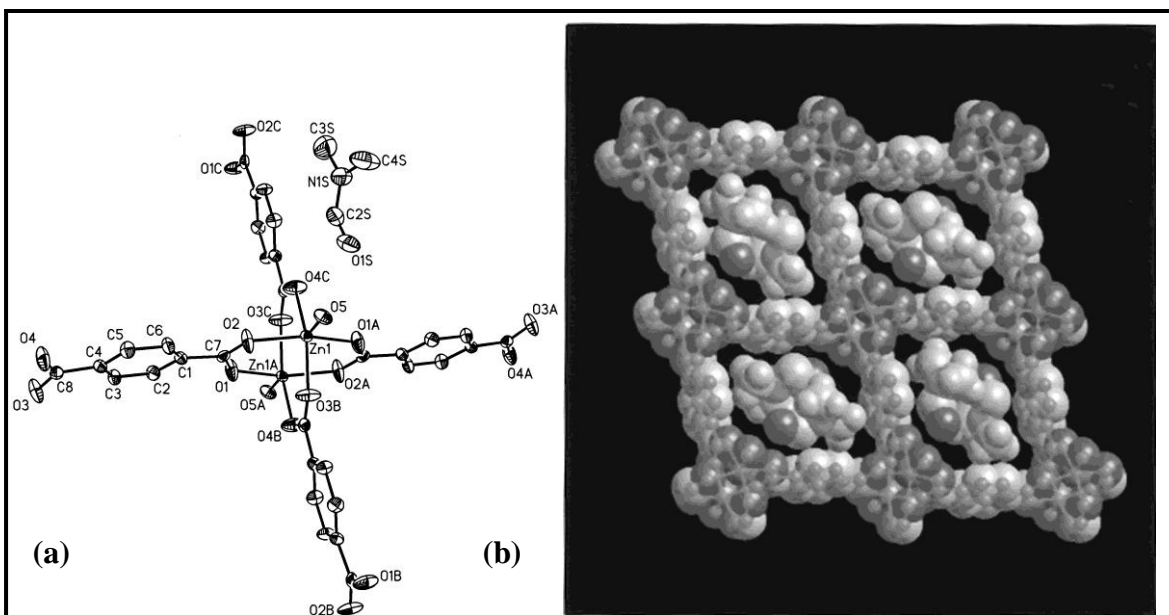
Figure 1.7 MOF-2: Zn(BDC)·(DMF)(H$_2$O) (BDC = 1,4-benzenedicarboxylate). **(a)** MOF-2's building block unit, including the asymmetric unit. Atoms of the DMF guest molecule are labeled with an "S." **(b)** MOF-2's crystal structure showing one 2D layer and DMF guest molecules occupying 1D channels. Adapted from Reference 17.

The most prevalent form of metal phosphonate is a two-dimensional layered structure, where the connectivity results from metal-oxygen-metal coordination in one dimension with the organic moieties pointing between the layers. The 2D hydrated structure [Cd$_3$(H$_2$O)$_3$(O$_3$PCH$_2$)$_2$(NH-CH$_2$C$_6$H$_4$-COOH)$_2$]·11H$_2$O, containing 1D channels, exemplifies this motif (Figure 1.8).[32] Layers are formed by Cd$_2$O$_{10}$ and octahedral CdO$_6$ vertices connecting with tetrahedral phosphonate groups, and the Cd(II)-phosphonate layers are themselves attracted to each other by hydrogen-bonding interactions. Interestingly, the cadmium cations preferentially coordinate to the phosphonate oxygens compared to the carboxylic oxygens.
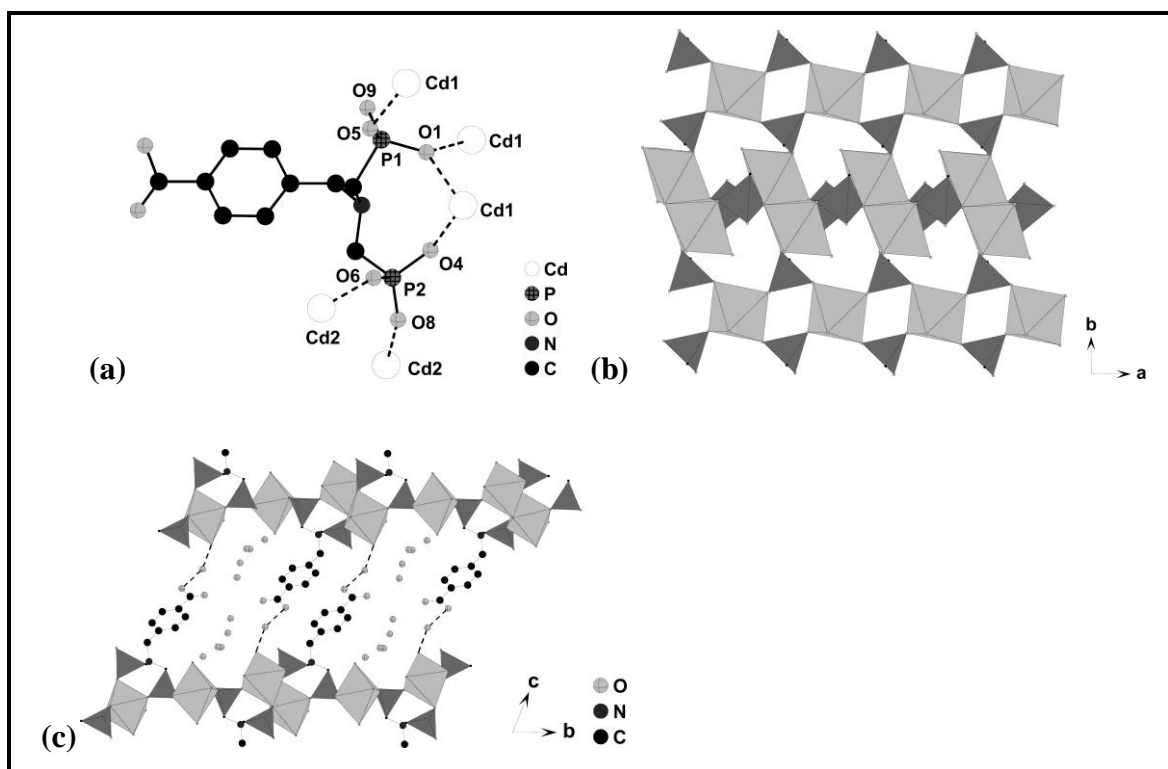
Figure 1.8 2D polymer [Cd$_3$(H$_2$O)$_3$((O$_3$PCH$_2$)$_2$NH-CH$_2$C$_6$H$_4$-COOH)$_2$]·11H$_2$O
(a) Coordination environment of the ligand **(b)** 2D inorganic layer composed of the metal centers and phosphonate moieties **(c)** 1D channels formed between layers held together by H-bonds (-C-OH…H$_2$O…H$_2$O-Cd^{2+}). Adapted from Reference 32.

1.3.3   3D Polymers

The most influential of 3D networks might be said to be MOF-5, reported in 1999 by Yaghi (Figure 1.2).[20b] Using the inorganic octahedral Zn$_4$O cluster as nodes, this research group has capitalized on the regular geometric arrangements possible when metal clusters are viewed as polyhedrons, and organic linkers are chosen with specific 3D motifs in mind. Numerous networks have since been synthesized, by their group as well as others world-wide, that utilize polyhedral "secondary building units" (SBUs) in place of single metal cations of simpler coordination polymers.[28] Selecting different organic linkers to combine with a given SBU can result in significantly different pore dimensions.[21]

11

When the cavities of porous 3D materials reach a certain size, many 3D structures begin to interweave or catenate as they are assembled, resulting in multiple interpenetrations of the networks. This phenomenon vastly reduces the network's pore sizes as it increases its stability. Three-fold interpenetration is exhibited by a 3D adamantoid network, $[\{Cu_4(4,4'\text{-bipy})_4(SO_4)\}_n \cdot 2n(C_6H_5SO_4)]$ based on the tetrahedral SBU $[Cu_4(\mu_4\text{-}SO_4)]$ and is stabilized by $\pi \cdots \pi$ interactions between adjacent 4,4'-bipyridine molecules (Figure 1.9).[33]
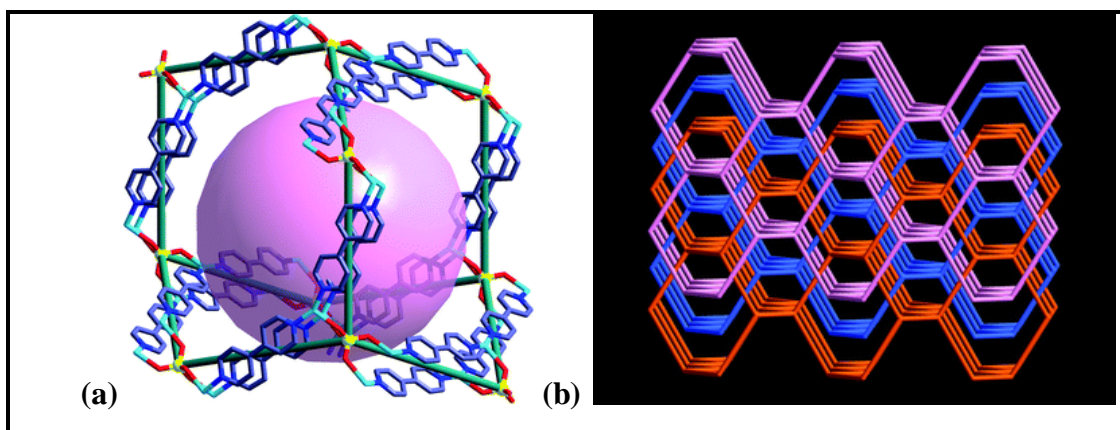
Figure 1.9 $\{[Cu_4(4,4'\text{-bipy})_4(SO_4)]_n \cdot 2n(C_6H_5SO_4)\}$ (4,4'-bipy = 4,4'-bipyridine) **(a)** Single adamantoid cage; pore dimensions are represented by the purple sphere **(b)** Three mutually-interpenetrated 3D networks of this complex. Adapted from Reference 33.

3D networks resulting from more than one organic ligand have a greater architectural versatility, as do those resulting from the use of two or more different metals. The coordination polymer with the general formula $[Zn_3(OH)_2(L^M)_2]$ is an example of a bimetallic structure (M = Cu(II), Ni(II), and Co(II); L^M is a Schiff base-type metalloligand $[M(salphdc)]^{2-}$, Figure 1.10).[34] The unique feature of this 3D polymer (Figure 1.11) is that the Zn(II) centers function as the connectors while the unsaturated copper centers are immobilized in the pore walls of the network. Half of the Zn^{2+} ions are in a typical tetrahedral environment, while the dimensionality is increased via the octahedral coordination of the other crystallographically distinct zinc cations. Heterometallic coordination polymers can be constructed to take

advantage of the metals' individual preferences (such as coordination geometry or attraction to "hard" or "soft" atoms)[35] for structural reasons, as well as to functionalize pores/channels for use as catalysts, molecular-based magnets, sensors, etc.
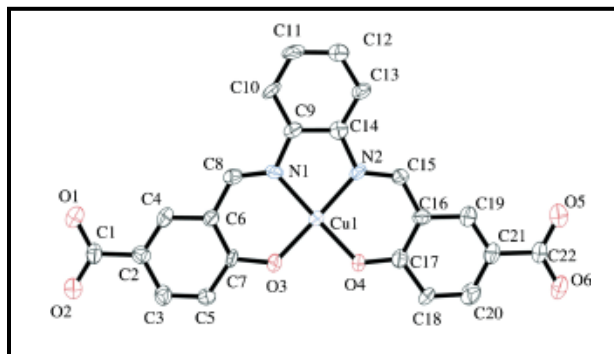
Figure 1.10 Metalloligand L^M, [M(salphdc)]$^{2-}$, where M = Cu(II) and salphdc = *N,N'*-phenylenebis(salicylideneimine)dicarboxylate. Adapted from Reference 34.
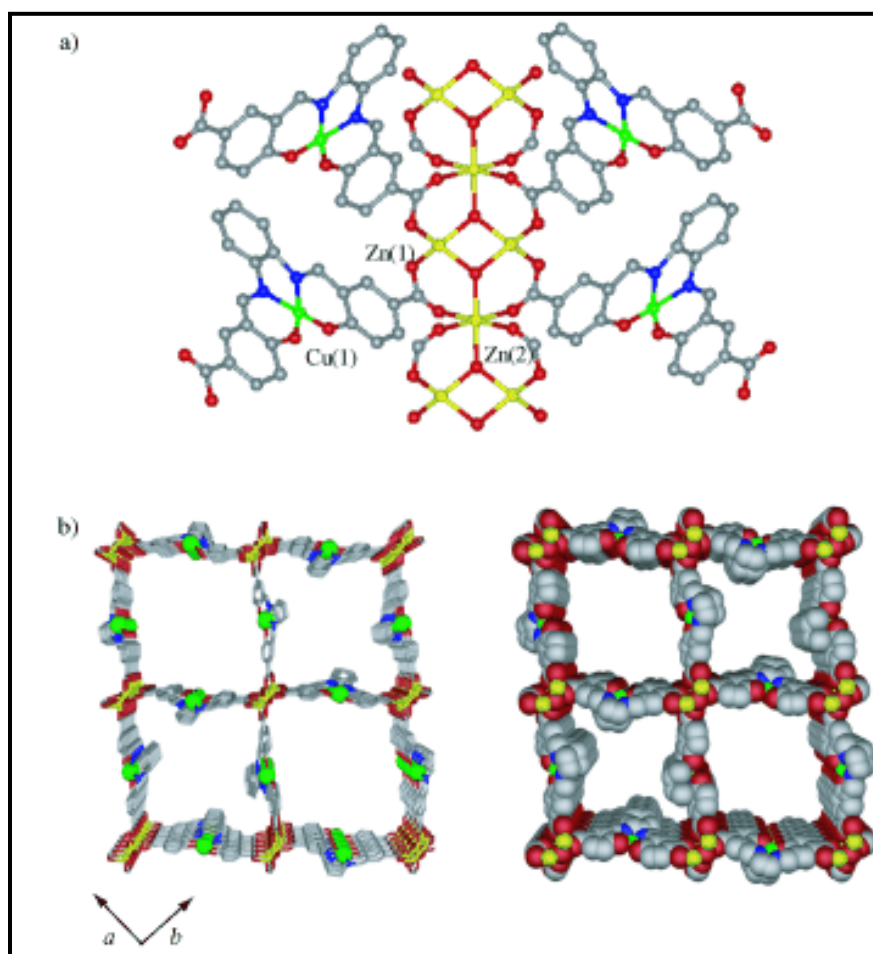
Figure 1.11 [Zn$_3$(OH)$_2$(L^{Cu})$_2$] **(a)** Building unit: Zn, yellow; Cu, green; O, red; C, gray; N, blue **(b)** 3D porous structure viewed down *c* axis. Adapted from Reference 34.

13

1.3.4   3rd-Generation 3D

A relevant classification of 3D coordination networks proposed by Kitagawa *et al.*[14] is based upon the transformative nature of some porous MOFs. In their opinion, 1st-Generation MOFs are networks that collapse upon removal of solvent or guest molecules, 2nd-Generation MOFs are those that remain rigid and robust independent of any solvent, while 3rd-Generation MOFs are those demonstrating dynamic structural rearrangement due to flexibility in their frameworks. Wanting to capitalize on the increased versatility this property can give to coordination polymers, focused attention has been given to the investigation of such processes. For example, reversible crystal-to-crystal transformations have been found to occur in 3D networks formed from trivalent cations such as Cr(III) and bridging benzene-1,4-dicarboxylate (Figure 1.12).[36] The hydrated form of this thermally-stable polymer is actually contracted compared to its dehydrated form; the unusual flexibility of the framework allows hydrogen bonding between guest water molecules and the linker's carboxylate groups to decrease the pore dimensions.
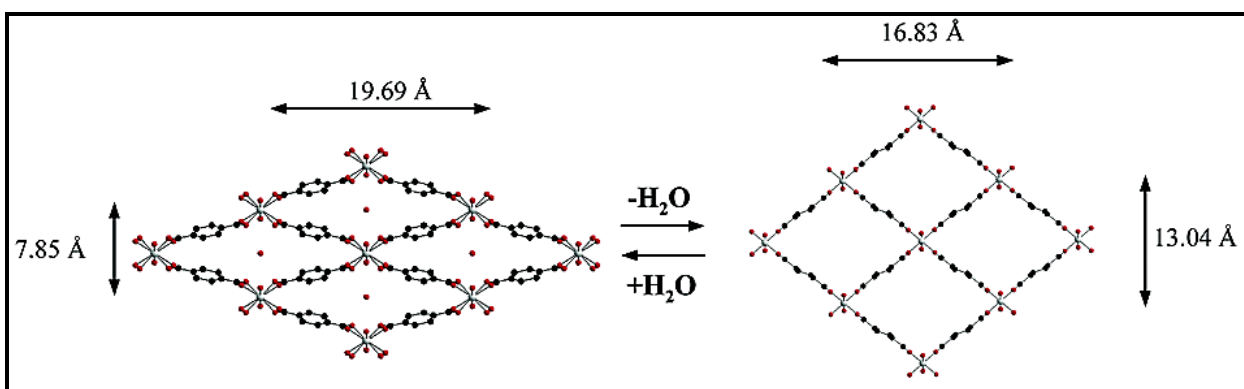
Figure 1.12.   MIL-53: $Cr^{III}(OH) \cdot \{O_2C-C_6H_4-CO_2\} \cdot H_2O$ reversibly transforms to its anhydrous form, $Cr^{III}(OH) \cdot \{O_2C-C_6H_4-CO_2\}$, upon heating. Taken from Reference 36.

Crystal transformations within a dynamic framework can result from elongation sites along Jahn-Teller distortions, rotations around coordination bonds and single covalent bonds, breaking of hydrogen or photoactive bonds, π-stacking interactions, and even as a result of the

slipping/sliding motion of interpenetrated frameworks upon adsorption and desorption of guest molecules. The latter phenomenon has been dubbed "breathing" and is simply illustrated in Figure 1.13, where the presence of nitrobenzene guest molecules in the PCP $[\{(ZnI_2)_3(TPT)_2 \cdot 6C_6H_5NO_2\}_n]$ (TPT = 2,4,6-tris(4-pyridyl)triazine) is thought to induce rotation of the Zn-N coordination bonds, resulting in increased pore dimensions.[37] This notable characteristic holds great promise for future applications of these materials.
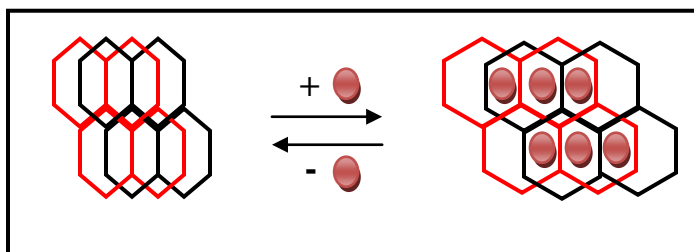
Figure 1.13. Doubly interpenetrated $[\{(ZnI_2)_3(TPT)_2 \cdot 6C_6H_5NO_2\}_n]$ (TPT = 2,4,6-tris(4-pyridyl)triazine), demonstrating the sliding of networks upon inclusion of nitrobenzene. Modified from Reference 37.

1.4 Applications

The initial excitement over the discovery of the highly porous metal-organic frameworks in the 1990's was due to the potential for fine-tuning pore dimensions and characteristics by manipulating the organic linkers. Immediate possibilities came to mind as gas storage and separation materials similar to the useful and ubiquitous zeolites. Combined with the relatively predictable topologies taken from analogous inorganic solid-state structures, these materials were seen as the source of an almost limitless array of new and exciting materials for both current and undiscovered applications.

1.4.1 Gas Adsorption and Separation

Early discoveries of rigid MOFs, with permanent porosity and behaviors similar to zeolite molecular sieves, may have initiated research in the area of gas adsorption and separations, but the flexible, dynamic frameworks that are beginning to be investigated show sensitivities to external stimuli beyond the scope of the traditional zeolites and activated carbons.[38] Although

separations and adsorption isotherms based solely upon size exclusions have been demonstrated,[39] the behaviors of networks that illustrate selective adsorptions based upon adsorbate-guest interactions that can induce structural changes in the solid show great promise for future applications. The degree of porosity of MOF materials is often determined by the amount of N_2 gas adsorbed (cm^3/g) as a function of pressure. Type I isotherms shown in Figure 1.14 are indicative of a microporous structure, where adsorbates line the surfaces of pores in the 0.05-2 nm range; Type II behavior is typical of nonporous surface-adsorption.[40] The dark line in this figure illustrates induced porosity as a result of structural changes caused by gate-opening pressure effects[14] and/or physical stimuli[41] at point A. Point B represents the pressure at which crystal transformation has been completed. As investigations continue into the cooperative framework-guest relationship, third-generation coordination polymers capable of solid structure shifts, similar to the induced-fit of proteins, show great promise in separation applications, among others.
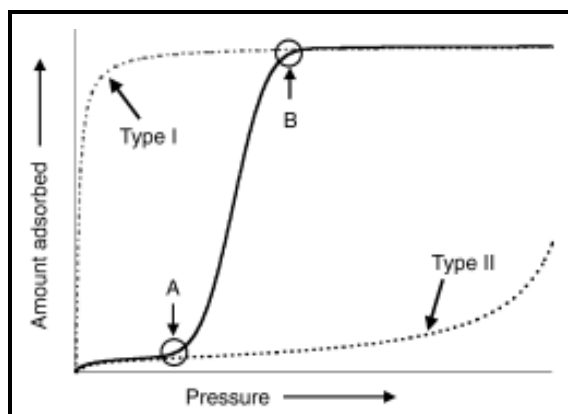
Figure 1.14. Generic adsorption isotherms illustrating microporous structures (Type I), nonporous structures (Type II), and the typical isotherm observed for solids undergoing structural transformation from nonporous to porous (solid line). Gate-opening and –closing pressures indicated by points A and B, respectively. Adapted from Reference 14.

One coordination polymer that exemplifies both size/shape exclusion as well as guest-molecule-triggered structural transformation is the flexible porous solid MAF-2, [Cu(etz)] (Hetz = 3,5-diethyl-1,2,4-triazole; MAF = metal azolate framework).[42] This network contains large

cavities connected by small openings guarded by pendant ethyl groups (Figure 1.15). Selective

adsorption of benzene over cyclohexane occurs because benzene, with a smaller cross-section,

can diffuse through the channels and fill the micropores of the network, whereas the bulkier

cyclohexane is only adsorbed minimally at the solid surface.
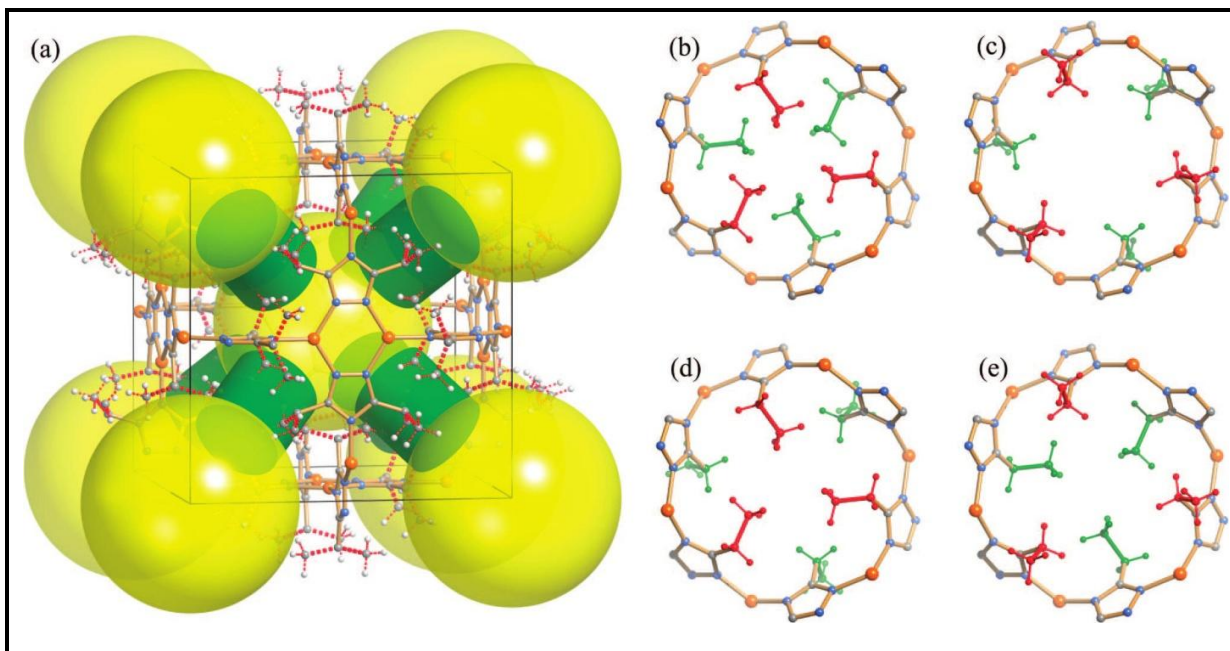
Figure 1.15. [Cu(etz)]. **(a)** Yellow spheres represent pores within the cuprous triazolate scaffold. Green cylinders represent hydrophobic channels physically blocked by swinging ethyl groups. **(b)**-**(e)** Viewed down the "gated" channels with passages that are double closed, double open, closed-open, and open-closed, respectively (ethyl groups are colored in red and green to highlight the two different gates). Adapted from Reference 42.

Concomitant with this size-exclusion behavior is the preferred adsorption of small molecules

such as MeOH, EtOH, and MeCN compared to that of H_2O. The organic molecules are able to

access the pore cavities after inducing the ethyl groups to swing out of the way, a consequence

of hydrophobic interactions. A Type I isotherm is shown in Figure 1.16 for these molecules,

demonstrating classic microporous uptake. Potential applications in organic solvent/water

separations are quite evident.
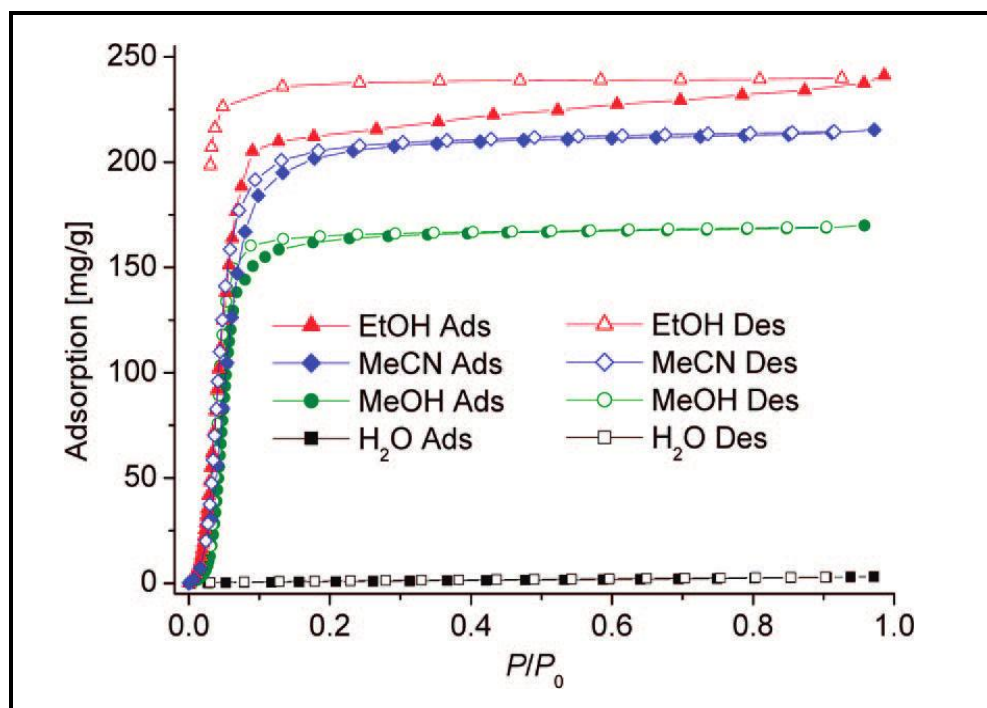
Figure 1.16. Adsorption (Ads) and desorption (Des) isotherms for water, ethanol, methanol, and acetonitrile measured at 298 K. Only slight surface adsorption is in evidence for water; no water has diffused through the channels to reach the pores. P_0 is the saturation pressure. Adapted from Reference 42.

1.4.2 Hydrogen Storage

The search for efficient, inexpensive hydrogen fuel cell storage materials has led to the possible utilization of porous metal-organic frameworks. Yaghi *et al*. have paved the way with their research related to MOF-5 and MOF-177, {$Zn_4O(1,3,5$-benzenetribenzoate$)_2$},[43] which have been reported to adsorb hydrogen at 7.1 wt % (40 bar/77 K) [44] and 7.5 wt % (70 bar/77 K),[45] respectively. To put this in perspective, the US Department of Energy stated their goal of achieving 5.5 wt % by the year 2015, with the ultimate goal of 7.5%.[46] A comparison of MOF-177's hydrogen gas uptake with that of other MOFs, a zeolite, and an empty tank is shown in Figure 1.17.[47] Most recently, several more ultrahigh-porosity MOFs (MOF-200, MOF-210)

have been synthesized with initial reports of H_2 adsorption in the range of 17%, which approaches the "absolute adsorption limit for solid materials."[48]
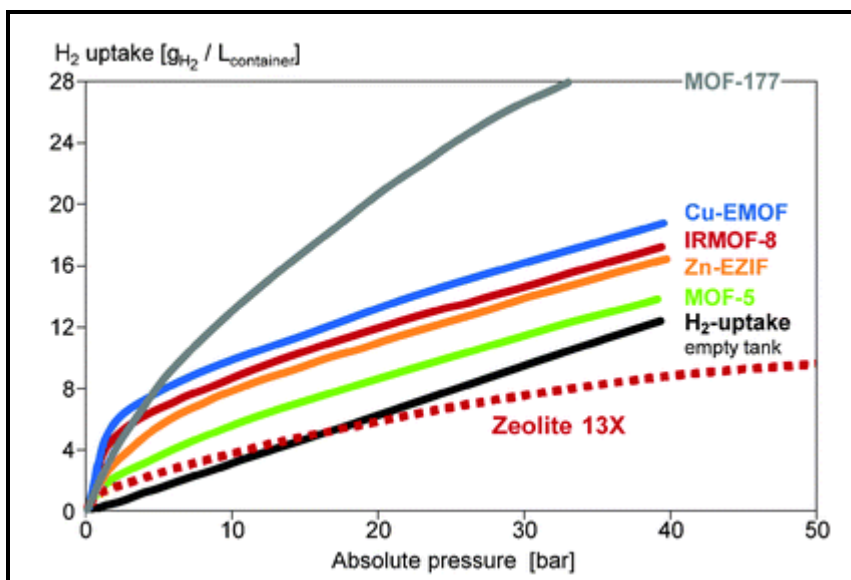
Figure 1.17. H_2-storage capacities measured at 77 K. Adapted from Reference 47.

Not only must the ideal storage material have uniform pore volumes for consistent storage parameters, but the diameters should be similar to those of the adsorbates to maximize the attractive forces between the pore walls and the adsorbed guests. Therefore, many of the frameworks with the largest pores would not be suitable for the adsorption and storage of hydrogen gas. However, in many cases as pore volume increases, the degree of interpenetration does as well.[1] Instead of decreasing available storage space, Yaghi has shown that interpenetrating nets may actually improve the storage capacity of the material.[49]

The presence of coordinatively-unsaturated metal sites for H_2 binding is also desirable, and can significantly increase hydrogen adsorption percentages.[50] This is possible through the thermally-induced removal of terminal-ligand solvent molecules to expose framework metal cations,[51] as well as by designing metalloligands that encourage "open" metal sites, such as through square planar geometries,[52] as shown in Figures 1.10 and 1.11.

MOF-storage for fuel-related hydrogen has the advantages of being fully reversible and quickly accomplished.[47] The outlook is positive, but there is still much work to be done to allow MOFs to adsorb hydrogen sufficiently at room temperature[53] (as opposed to 77 K) and in the presence of moisture, which can cause structural disintegration of the porous network.[54]

1.4.3 Catalysis

While the pores present in coordination network solids are physically useful in the applications just described in Sections 1.4.1 and 1.4.2, the chemical environment of the pores can also participate in catalytic activity potentially different, and critically more tunable, than those of zeolites. Heterogeneous catalysis is crucial in industry; approximately 90% of modern chemical processes depend on such catalysts.[55] Due to the highly porous nature of many MOFs, they have a low percentage of "dead volume" that can increase the gravimetric efficiency of a potential catalyst, resulting in a high density of available active sites per volume.[56] Other valuable characteristics are the size/shape selectivity crucial for catalytic efficiency and the compartmentalization that provides spatial separation of critical active sites, which can prevent excess side reactions and catalyst deactivation.[57] Some catalysis experiments have even shown enantioselectivity, a characteristic not seen in inorganic zeolite-like catalysts.[57] A few disadvantages are the smaller temperature tolerances of MOFs compared to zeolites, the fact that substrate access to framework catalytic metal centers is often completely blocked by coordinated solvents and ligands, and the moisture sensitivities of some MOFs. [58]

The first reported case of catalysis supported by an established MOF was published by Fujita *et al.* in 1994. Cyanosilylation of aldehydes demonstrated the Lewis-acid properties of a 2D square-grid network, $[Cd(4,4'-bipy)_2(NO_3)_2]$. Size- and shape-selectivity of substrate was

observed (Figure 1.18).[59]   The authors attribute cavity size limitations as the cause of the differences in product yield.
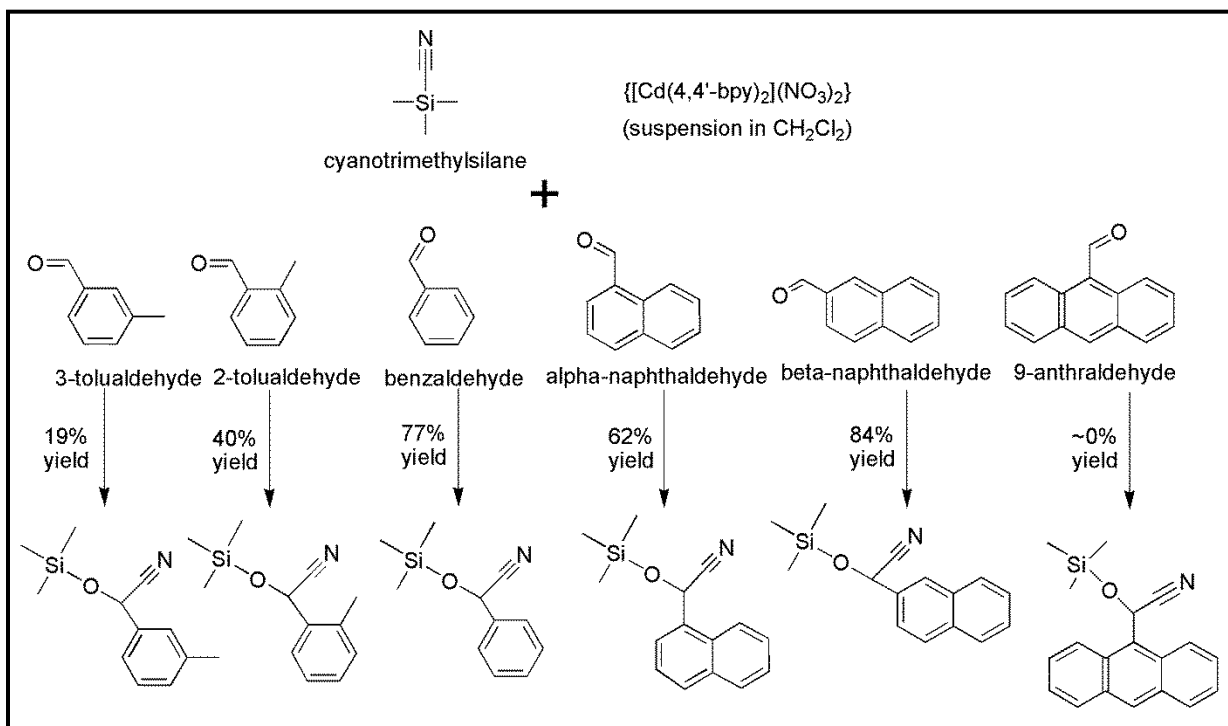
Figure 1.18 Experimental product yields for various cyanosilylation reactions when catalyzed by the intact polymer, [Cd(4,4'-bpy)$_2$(NO$_3$)$_2$].[59]   No reaction took place when using Cd(NO$_3$)$_2$ or 4,4'-bpy (polymer starting materials), or the supernatant.

Investigations into catalytic activity have increased tremendously since the turn of the century. The porosity of these materials can provide interesting backbones for heterogeneous catalysis, with some catalysts behaving as a kind of "nano"-reaction vessel.[58] However, the most common type of MOF catalyst uses coordinatively-unsaturated metal centers that are embedded in pore walls or present as critical structural components, as mentioned in Section 1.4.2. Terminal ligands (e.g. coordinated water, acetonitrile, methanol) can be evacuated leaving ample room for coordination by Lewis-base substrates, which is one reason that lanthanides, with their large coordination sphere, have been investigated as possible catalytic

21

sources. A recent example of a lanthanide-organic framework catalyst utilizing open-metal active sites is a polymer of ytterbium(III) succinate, $[Yb(C_4H_4O_4)_{1.5}]$, (Figure 1.19).[60] As well as showing ability as a Lewis-acid catalyst, crystals of this solid were also successful in catalyzing thiophene hydrodesulfurization (HDS), a "Green-Chemistry" process commonly used to remove sulfur compounds from natural gas and fossil fuels (Equation 1.1).[61] The reaction proceeds through initial coordination of the sulfur atom to Yb(III), and of the two active polymorphs of this polymer, the highest activity results from the structure with the lower coordination number for Yb. The polymorph with c.n. = 7 is thought to allow greater passage of substrates to the active site compared to the form with c.n. = 8.[60]

Equation 1.1 Hydrodesulfurization proceeding via hydrogenolysis of C-S bonds after S-Yb coordination.[60]
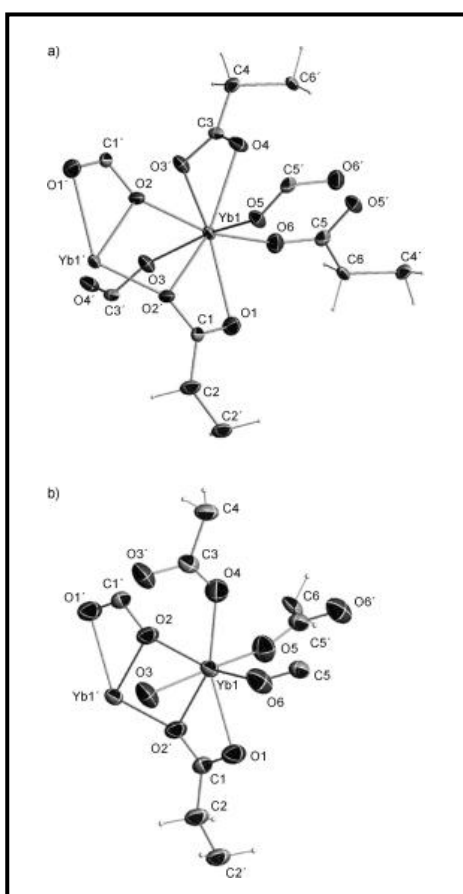
Figure 1.19 (a) α-$[Yb(C_4H_4O_4)_{1.5}]$ **(b)** β-$[Yb(C_4H_4O_4)_{1.5}]$. Adapted from Reference 60.
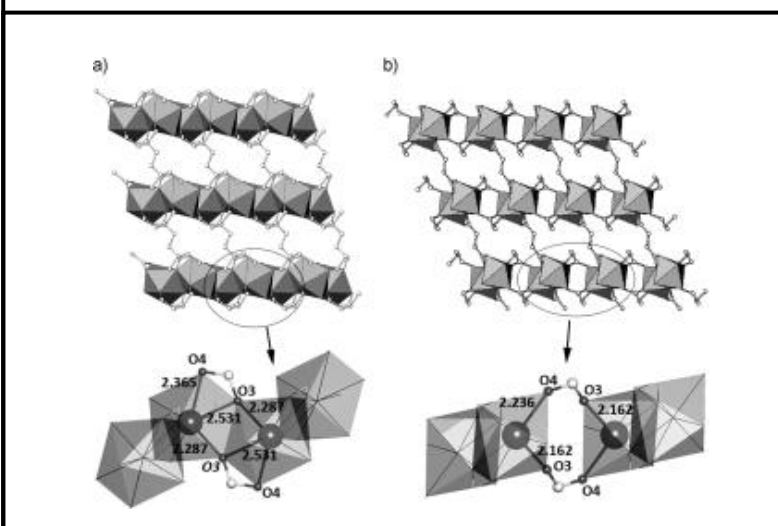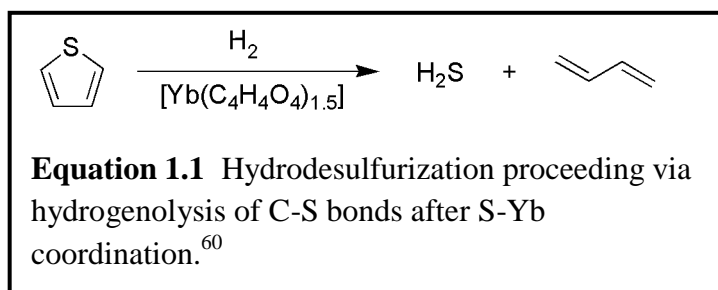
Figure 1.20 (a) α-$[Yb(C_4H_4O_4)_{1.5}]$ **(b)** β-$[Yb(C_4H_4O_4)_{1.5}]$, showing differences in geometry around the Yb(III) ions. Adapted from Reference 60.

1.4.4 Luminescent Sensors

Studies into luminescent MOFs are still in the early stages, but a number of important observations indicate great promise for current and future sensing applications of this class of materials. Their increased thermal stability compared to pure organic lumiphores, the ability of incorporated metals to affect emission wavelength, as well as their unique combination of chemical versatility, porosity, and increasing structural predictability can all be used to create metal-organic systems with tailored luminescent properties.[62]

Organic lumiphores typically have aromaticity or some degree of π-conjugation. The presence of metal centers that organize organic molecules in space can provide stability, separation, and orientation to the lumiphores and in the process limit ligand-ligand-charge-transfer (LLCT) signal interference caused by interactions such as π-stacking. Increasing porosity can also decrease the density of the emitting organic molecules to alleviate some of the broadening of emissions and red-shift compared to their solid-state spectra.[63] A 3D cadmium framework, [Cd(1,4-bdc)(py)], has been shown to enhance the fluorescent intensity of the free 1,4-bdc ligand by a factor of 100,[64] and in a comparative study of emission spectra of two zinc(II) complexes with the same ligand (Figure 1.21), the differences have been credited to the decrease of interligand $\pi\cdots\pi$ interactions in the lower-density polymer. The relative densities of the three-dimensional Structure 2, the two-dimensional Structure 1, and the powder sample of the ligand are revealed by the broadening and lengthening of the emission bandwidths in Figure 1.22.[65]
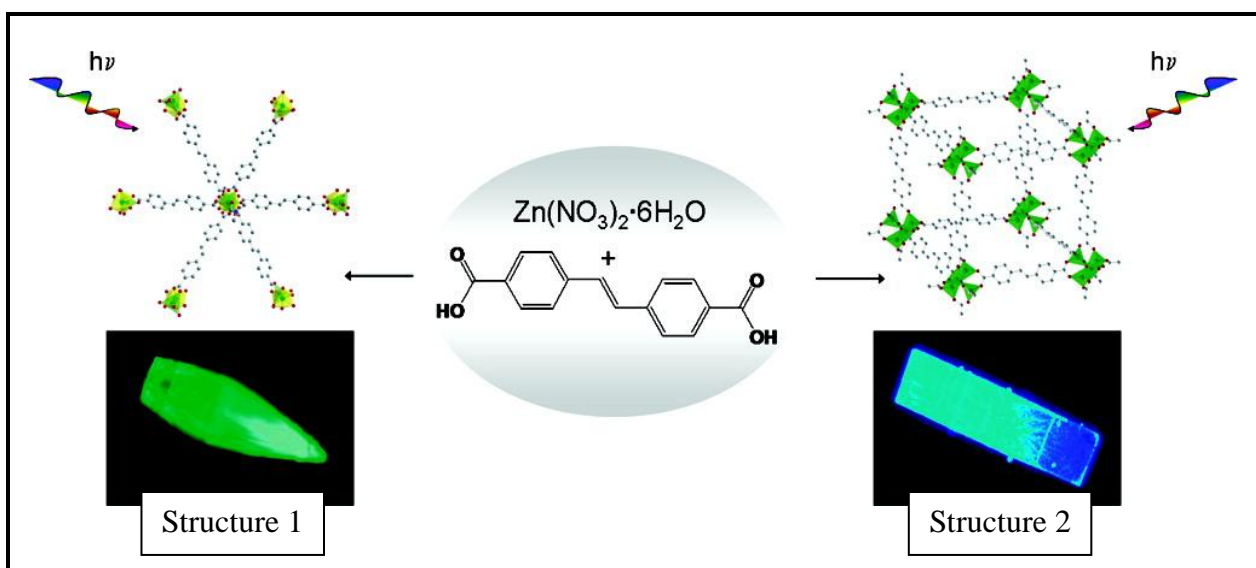
Figure 1.21 [Zn(1,4-bdc)] polymer starting materials in the center; 2D higher-density architecture on left; 3D lower-density architecture on right. Adapted from Reference 65.
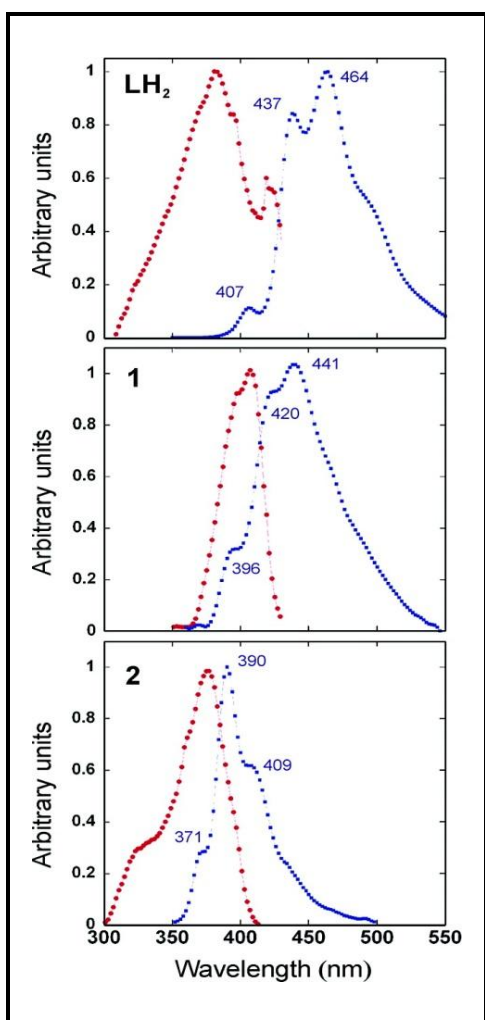
Figure 1.22 Phospholuminescence spectra Top: Powdered ligand LH$_2$ = [Zn(1,4-bdc)]; Middle: 2D Structure 1; Bottom: 3D Structure 2. Red lines represent excitation spectra; blue lines represent emission. Less red-shift and broadening of ligand emission occurs with network solid 2. Adapted from Reference 65.

The identity of the metal ions and presence of guest molecules can also significantly affect the luminescence of a given hybrid polymer. Paramagnetic transition-metal ions can quench electronic transitions to some degree,[66] diamagnetic d^{10} species can participate in ligand-metal-charge-transfer (LMCT) and metal-ligand-charge-transfer (MLCT) to enhance them,[67] and modulation of the phospholuminescent signal can occur by the intentional ratio of such metals.[68] Quenching effects can also occur due to the presence of molecules containing hydroxyl groups as is shown by the luminescence of dehydrated vs. hydrated forms of $[Cd_3(2,6\text{-di-}(4\text{-triazolyl})pyridine)_6](BF_4)_2(SiF_6)(OH)_2 \cdot 13\frac{1}{2}H_2O$ (Figure 1.23).[69] The anhydrous form of this polymer participates in LMCT producing 438 nm emissions. When lattice water molecules are present they effectively quench energy transfer from the linker to the cadmium centers, resulting in ligand-only luminescence at 382 nm.
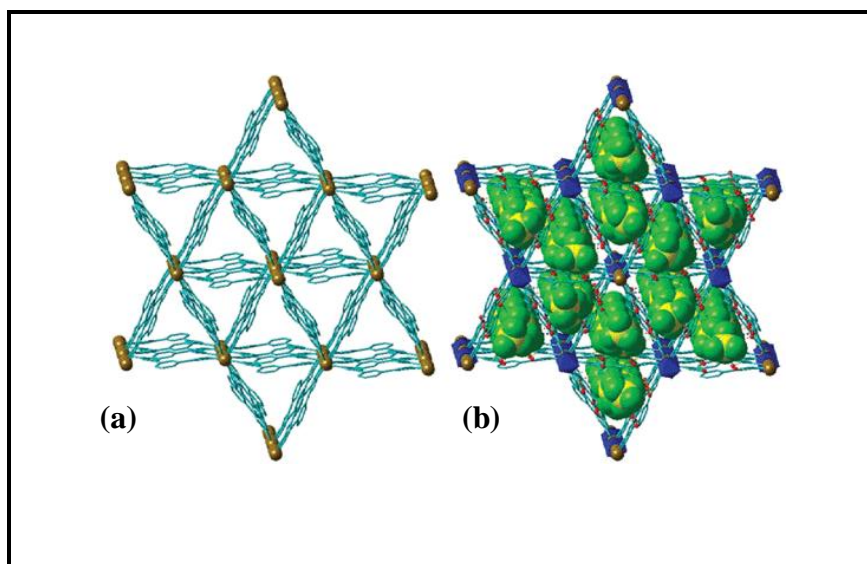
Figure 1.23 $[Cd_3(2,6\text{-di-}(4\text{-triazolyl})pyridine)_6](BF_4)_2(SiF_6)(OH)_2 \cdot 13\frac{1}{2}H_2O$ **(a)** Without water or anions **(b)** Water and anions present. Cd = brown, O= red, SiF_6^{2-} = blue polyhedron, BF_4^- = green and yellow. Adapted from Reference 69.

Lanthanide(III) ions are also well-known for their intense excitation and emission peaks when combined with chemical "antenna" molecules that can transfer photon energy at the appropriate metal energy level.[62] Europium(III)-phosphonate-based luminescent sensors have been developed that are highly sensitive and specific, able to detect an analyte in the parts-per-trillion range. For example, an optic fiber coated with the polymer $Eu(DMMB)_3(NO_3)_3$, (DMMB = methyl-3,5-dimethylbenzoate), can reversibly bond with a hydrolysis product of the nerve agent Soman (pinacolyl methylphosphonate—PMP) to produce a new complex that emits a distinctive peak at 610 nm when excited by a 466-nm laser. Figure 1.24 illustrates how this Eu(III)-phosphonate complex produces a unique signal that cannot be confused with those generated by common pesticides with structures similar to the analyte.[70]
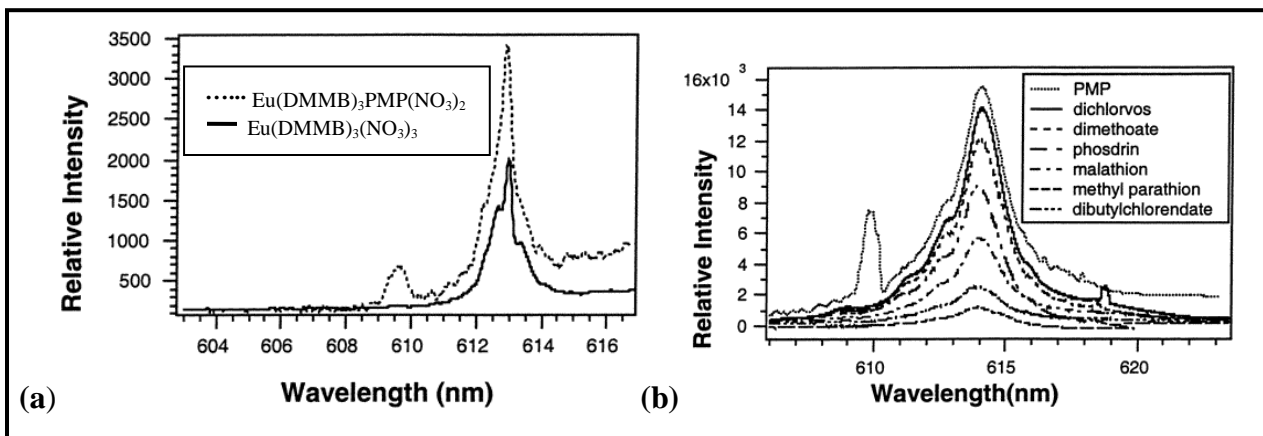
Figure 1.24 (a) Laser-excited luminescence spectra of $Eu(DMMB)_3PMP(NO_3)_2$ and $Eu(DMMB)_3(NO_3)_3$ **(b)** Response of the sensor to selected interferences. Adapted from Reference 70.

The ability to tune a polymer product for specific luminescent applications by varying the lumiphore type, rigidity/flexibility, and coordination environments is a powerful reason for increased investigations in this area. The modulation, initiation, or loss of luminescent emissions from metal-organic frameworks can be sensitively used to signal changes in polymer environments.

1.5 Synthetic Methodologies

1.5.1 Hydrothermal Synthesis

In the overwhelming majority of examples discussed so far, the experimental protocols involved hydrothermal, or solvothermal, synthesis. This is a "one-pot" methodology whereby solvent and stoichiometric amounts of metal salt(s) and organic ligand(s) of interest are added to a stainless steel or Teflon tube, sealed, and placed in a programmable furnace/autoclave for a period of 2 to 3 days.[71] The advantage of this method is that quite often X-ray quality single crystals can be produced without the need for recrystallization. X-ray crystallography is the most-utilized method for characterization of coordination network solids due to the high degree of insolubility of these materials in common solvents, therefore experimental protocols and selection of starting materials are quite often skewed to favor the production of high-quality single crystals.

Disadvantages of hydrothermal synthesis are the length of time it requires and the possibility of decomposition of thermally-sensitive reagents. Modifications of this technique involve biphasic conditions using immiscible solvents, where the crystals form at the solvent barrier[72] and microwave-assisted solvothermal synthesis, where reaction times are reduced significantly.[73]

1.5.2 Mechanochemical Synthesis

Mechanochemical synthesis,[74] of which "grinding" and "ballmilling" are the most common examples, is a method that is solvent-free, or "solvent-assisted"[75] if using minimal solvent. Motivations for selecting this method range from the practical (solvents can affect ligand protonation and product architectures) to the ideal (the search for "greener" synthetic protocols).

Green chemistry has been defined as a method that "efficiently utilizes (preferably renewable) raw materials, eliminates waste and avoids the use of toxic and/or hazardous reagents and solvents in the manufacture and application of chemical products."[76] Therefore, any method that eliminates the need for solvents entirely can be viewed as a "green" method and a step towards increased sustainability of our finite resources. There is also evidence that mechanochemical synthesis can result in much quicker reaction times than traditional methods; for example, the reaction of [(ethylenediamine)Pt(NO$_3$)$_2$] with 4,4'-bpy to produce a coordination macrocycle was completed in 10 minutes at room temperature when ground together without solvents,[77] while it can take as long as 4 weeks at 100 °C.[78]

The biggest disadvantage of mechanochemical methods is that the micro-crystalline products are not suitable for single-crystal X-ray analysis, which is the bread-and-butter for coordination polymer structure determination. However, several research groups are finding ways to work around this sometimes insurmountable problem. A few have been able to produce X-ray quality crystals utilizing seed crystals,[79] while an increasing number of groups are using computer software to predict the most probable network topologies.[80] Simulated X-ray powder diffraction patterns are created, which can then be matched to the diffraction patterns of the bulk solid to identify the most likely product architecture.[81]

1.5.3 Mild Conditions

In keeping with the theme of Green Chemistry, water is a non-toxic, non-flammable, abundant, and inexpensive resource. When considering additional choices of "green" solvents, the energy required to manufacture and utilize the solvent must be considered, as well as the

health hazards. Simple organic molecules such as methanol and ethanol are excellent choices, given their low energy requirements for synthesis and low toxicity.[82]

Although a large majority of coordination polymer crystals are obtained through hydrothermal means, mild conditions are also desirable. Temperature has been shown to affect solid architecture,[83] and certain framework topologies could remain undiscovered if only high-temperature methods are utilized. Additionally, thermally reactive salts such as perchlorates can more reasonably be selected for use as reagents at lower temperatures. This dissertation will describe how mild-condition methods have been successful in the synthesis of a range of multi-dimensional products.   The protocol involves the addition of the metallic precursor to an aqueous/alcoholic solution of organic ligand, and subsequent stirring at room temperature or temperatures from 50-100 °C. Slow evaporation of solvent can produce X-ray quality crystals.

1.6   Implications for Rational Design

1.6.1   Self-Assembly

The assembly of coordination polymers is a dynamic process, however studies are ongoing regarding the detailed mechanisms. The basic concept of crystallization involves soluble chemical species forming clusters under supersaturation conditions. Nucleation leads to the development of a miniscule solid crystal, which then grows under ambient conditions into its final form, be that single crystals or a polycrystalline solid. During nucleation, clusters of the soluble species continually form and dissociate due to local concentration changes, with critical nuclei forming that represent the supramolecular transition states. When a critical nucleus reaches a certain size, the crystal develops into the most stable lattice structure under a given set of experimental conditions.[84]

When describing the self-assembly process in his landmark paper, Robson stated that if a "wrong step is taken" the assembly can "backtrack to eliminate the error,"[85] which is possible when coordinate bonds with labile cations and weaker interactions such as hydrogen bonding are involved, thus forming a product with the lowest potential energy possible. Ramanan and Whittingham describe crystallization as a self-assembly process that involves molecular recognition, and provide a mechanistic explanation of MOF formation that emphasizes the formation of point zero charge (*pzc*) molecules.[86] In aqueous solution, the recognition occurs between the solvent-coordinated metal cations and the specific functional groups of the organic ligands, with geometric preferences leading the way. For example, to balance charge, aqueous zinc(II) would form an *in situ* tetrahedral $Zn(OH)_2(H_2O)_2$ complex. The *pzc* complexes would then approach an organic acid ligand, directed by hydrogen-bonding interactions. As water molecules are eliminated, the *pzc* components would assemble into the final structure. Recent experiments using atomic force microscopy (AFM) to probe the surface of a developing HKUST-1 crystal have revealed that measured heights of a crystal were not multiples of the dimensions of the network's SBU.[87] Therefore, rather than thinking of MOFs clicking together in large Lego-like sections, these results suggest that the growth mechanism occurs by the combination of individual solvated cations and ligand units to the growing crystal.[88]

1.6.2 Reagent Selection

The idea of intentionally modifying pore and/or channel size, shape, and surface functionality by the judicial selection of starting materials and reaction conditions is very appealing to the scientific community. While focusing primarily on the geometry of SBUs and linkers has produced a wealth of novel structures, it is much too simplistic to ignore the crucial structure-directing role of guest, counterion, and secondary ligand interactions. This is

especially significant when a given combination of metal precursor and organic ligand can result in a number of different polymorphs, depending on the actual reaction conditions employed.[12] As the chemistry of metal-organic frameworks is approaching the end of its second decade, an increasing number of studies into the factors affecting network topology are appearing in the literature.

1.6.2.1 Metal Choice

Coordinating abilities of metals can be drastically different from each other, with corresponding differences in network topology and physical properties when reacting with the same ligand (e.g. luminescence). However, other reagent combinations can result in isomorphous structures over a range of metal cations. A case in point is the reaction of divalent salts of nickel, copper, zinc, and cobalt with the bifunctional ligands 5- and 4-carboxylic acid pyrimidine).[89] The four isostructural products formed using the 5-carboxy ligand possessed identical six-coordinate octahedral geometry, with four equatorial water molecules and two doubly-deprotonated axial ligands coordinated at the N-2 position. All three of the polymers formed from the 4-carboxy ligand involved two chelating anions per metal center, coordinating at N-2 and the carboxylate group, and only two equatorial water molecules. Clearly, the identity of the metal ion had no effect on the coordinating motifs of these two ligands. Not all ligands are so predictable in their preferences, though, and some important characteristics to consider when selecting metal precursors are the preferred coordination number and geometry of the metal, desired physical properties (e.g. luminescence, metal-metal bond capability), ligand-coordination capability (e.g. hard/soft), cation charge, and electronic structure.

1.6.2.2 Solvent Choice

The solubility of the reagents is certainly a prime consideration when selecting solvents, as well as the ease of removal from the reaction products, but the interactions of the solvent with the growing crystalline solid can affect the overall crystal morphology tremendously. Not only can the solvent coordinate with the metal cations as terminal ligands and bridging ligands, but they can function as crucial structure-directing elements. This latter function is called a "templating effect," which is most relevant concerning flexible building blocks with more than one possible crystal structure when the solvent functions as a guest molecule or as a co-ligand. It depends on the physical dimensions of the solvent, as well as their weak interactions that can influence the developing architecture.[90] For example, the hydrothermal reaction of $Zn(NO_3)_2 \cdot 6H_2O$ and 4,4',4"-nitrilotrisbenzoic acid (H_3NTB) in a solvent mixture of $DEF/EtOH/H_2O$ (5:3:2, v/v) yielded a doubly interpenetrated 3D net structure (Figure 1.25a)[91] while the analogous reaction solely in EtOH produced a 3D polymer with 1D honeycomb channels (Figure 1.25b).[92]
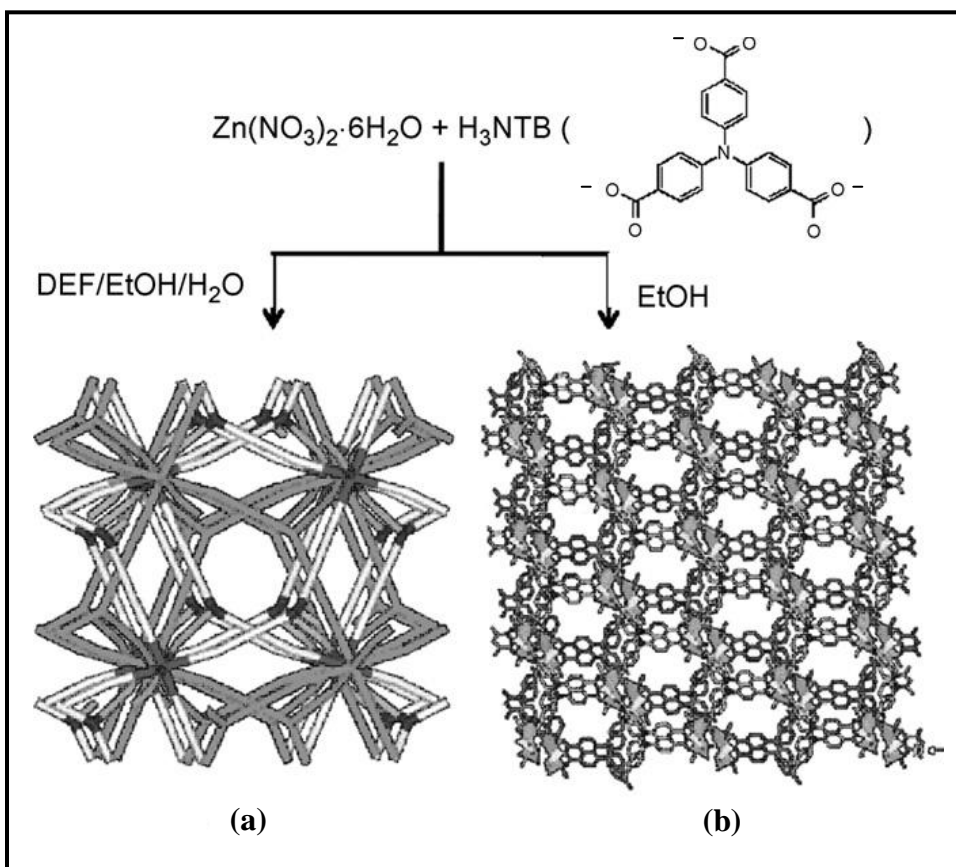
Figure 1.25 Different solvent templating effects yield two distinctly different topologies when identical reagents are combined. Adapted from Reference 52.

1.6.2.3 pH Effect

When selecting reagents, especially for aqueous reactions, pH is an important factor. At high pH, metal hydroxides tend to precipitate out of solution and thus do not allow the formation of extended polymeric frameworks; low and intermediate pH can affect the protonation of an organic acid ligand. A systematic investigation into the affect of pH on the polymers formed from $MnCl_2 \cdot 4H_2O$ and the bifunctional (phosphonomethyl)benzoate resulted in the discovery of three different structures. Low pH causes the deprotonation of only one oxygen on the phosphonate group and a 1D chain results. The second proton of that group is removed upon increasing pH, with the production of a 2D layered polymer, and a 3D structure is assembled once the carboxylate oxygen becomes deprotonated at the highest pH.[93]

1.6.2.4 Selection of Counterion

The anion present in the metal salt reagent can also play a key role in directing the polymer formation. The size and shape of the counter-ion can affect product architecture if it is incorporated into the crystal lattice, and there is a possibility of the anion coordinating to the metal and/or bridging metal centers. Bulky BF_4^- and PF_6^- anions are rarely incorporated into the lattice, while halides, nitrates, acetates, sulfates, and perchlorates can remain coordinated to the metal, and are capable of bridging metal centers to extend polymer dimensionality and direct the construction of the solid. For example, when silver nitrate reacts with bis(4-pyridyl)tetrazine, a helical staircase topology results—made possible through the connections of Ag(I) centers by bridging nitrates, giving a pseudo-square planar geometry at the Ag(I) center. When $AgPF_6$ and $AgBF_4$ are used, isomorphous pairs of 1D chains are formed, joined by Ag⋯Ag and π⋯ π interactions. One anion and one acetonitrile solvent molecule are coordinated to each silver(I), in place of a bridging nitrate in the helical polymer.[94] Without the bridging nitrate ions to "control" the architecture, there would have been no distinction between the structures.

Nitrate ions have also been associated with *in situ* oxidation of a phosphonic acid ligand,[95] and so care must be taken when selecting any counter-ion with the potential for side-reactions. Additional weak interactions between the anions and solvent or ligand should be considered, as well; for example, when a series of zinc(II) complexes were made with the flexible ligand methylenebis(3,5-dimethylpyrazole) in the presence of eight different anions, the most notable causes for structure variations (from discrete 0D to 3D) were weak interactions such as N-H⋯Cl, O⋯H_2O⋯H_2O⋯O, HOC=O⋯π, and N⋯H_2O⋯O.[96] Hydrogen bonds are much weaker than coordinate-covalent bonds, but strength in numbers can lead to a huge impact on the overall network structure.

1.6.2.5 Secondary Ligands

The presence of a co-ligand can be used to increase product dimensionality and aid in crystallization of materials;[97] when lanthanides are combined with oxalic acid as a co-ligand and 2-(pyridylmethyl)phosphonic acid ($2PyCH_2PO_3H_2$) as the primary organic linker, some very interesting isomorphic 2D and 3D structures result. The two ligands assemble into 2D layers with trivalent cations of Gd, Tb, and Dy, while Ho(III) and Yb(III) prefer a 3D architecture where the layers are cross-linked by $2PyCH_2PO_3H_2$.[98] Each oxalate anion chelates and bridges the metal atoms to contribute to the 2D and 3D topologies pictured in Figure 1.26. Not only do several of the structures produce characteristic sharp lanthanide phospholuminescent signals, but there is a distinct preference in structure type as the lanthanides increase in atomic number, thought to be a consequence of lanthanide contraction.

Figure 1.26
(a) Two-dimensional $[Gd_4(ox)_5(2PyCH_2PO_3H)_2(H_2O)_7]$ $\cdot 5H_2O$ showing $\{Gd_4(ox)_5\}_n$ extended network
(b) 2D polymer including phosphonate groups (pyridyl groups and water molecules omitted for clarity); half of the phosphonate groups are bidentate and half are tridentate
(c) Three-dimensional $[Ho_4(ox)_5(2PyCH_2PO_3H)_2(H_2O)_6]$ $\cdot 6H_2O$ with all phosphonate groups tridentate, resulting in the more complex topology. Adapted from Reference 98.

1.6.2.6 Ligand Choice

For the synthesis of functional coordination polymers, strong bonds are necessary to give strength and robustness to the framework, while weak interactions provide flexibility for dynamic transformations related to critical applications. Therefore, when selecting a ligand, not only geometry, but the possibilities for additional coordination sites that can aid in network stability and extend dimensionality should be considered.

36

Both neutral and charged ligands can be selected for use in the construction of these frameworks, however cationic ligands are uncommon due to their lower affinity for metal cations. Nitrogen-based ligands, such as 4,4'-bipyridine and triazine derivatives, have been prevalent in many of the earliest coordination polymers, with several examples described in this work; however oxygen-based organic acids probably hold the most prominent place in the formation of extended coordination polymers, especially MOFs.

MOFs have been dominated by the utilization of rigid, aromatic carboxylic acids— commonly bi- and tri-podal ligands as shown in Figure 1.1. Smaller organic acids such as succinic, gallic, and oxalic acids also hold significant roles in the literature, as just discussed in Section 1.6.2.5 and in Section 1.4.3 with Yb(III) succinate. However, carboxylic acids are limited by their trigonal geometry, and other classes of acids are capable of bonding motifs that are distinctly different.

Sulfonic acids are interesting choices, due to their spherical coordination mode, although they bond more weakly to metals than other acids such as carboxylic and phosphonic acids.[99] This can be an advantage by producing diverse architectures due to bond formation and reformation during the assembly process. Almost exclusively bonding as RSO_3^- monoanions, alkyl sulfonate groups are most often used as a secondary functional group appended to other acid moieties, such as 5-sulfosalicylic acid (Figure 1.27a).[100] Boronic acids (Figure 1.28b) are ubiquitous in literature dealing with the formation of covalent organic frameworks,[101] but the C-B bond is quite fragile and limited work has been done with metal-boronate coordination polymers.[102]
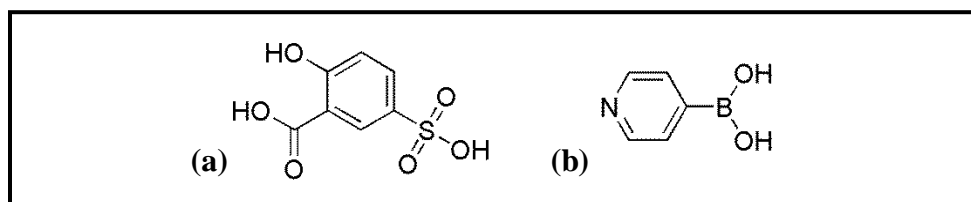
Figure 1.27 **(a)** 5-sulfosalicylic acid **(b)** 4-pyridyl boronic acid.

The focus of this dissertation is primarily centered on coordination polymers utilizing *N*-functionalized phosphonic acids. While there are significant challenges to this ligand class—their propensity to form dense-layered motifs that can inhibit porosity,[103] the difficulty in obtaining X-ray quality crystals due to frequent precipitation of solids as amorphous or oily insoluble phases, and the fact that their diverse coordination modes can be more unpredictable—the particular appeal of this type of ligand is that they *can* participate in multiple coordination modes.

1.7 Phosphonates

There are a large number of phosphorus-oxygen-bearing compounds that can form strong bonds with metals. But phosphonic acids can be distinguished from other phosphoric-acid derivatives by the number of alkyl groups attached (Figure 1.28).
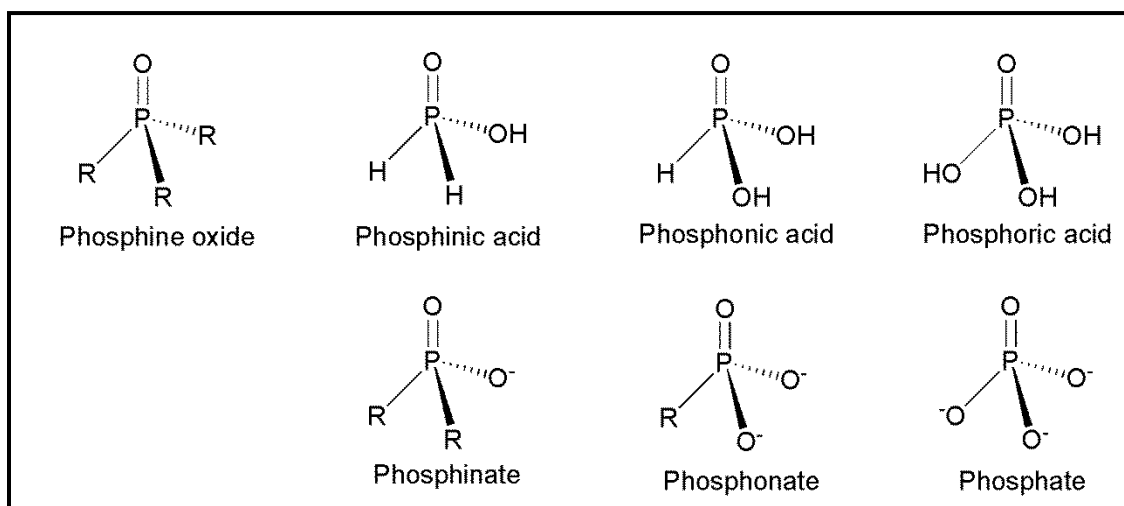
Figure 1.28 Distinctions between inorganic and organic phosphorus-oxygen compounds.

The biggest advantage of phosphonic acid ligands is their tendency to induce polymerization due to the strong interaction of the phosphonate group with the metal ion. Three possible binding sites on the phosphonate anion, combined with the ability to bond to more than one metal ion, or more than once to the same metal ion (see Figure 1.29), allow this ligand class to provide for diverse self-assembly of one-, two-, and three-dimensional polymeric structures.
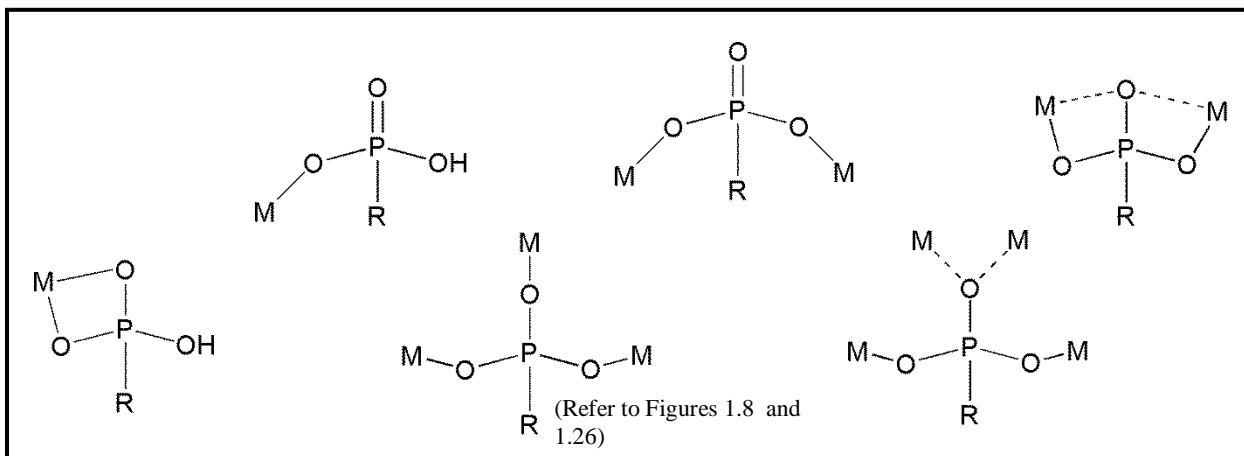
Figure 1.29 Multiple coordination modes are possible with phosphonic acid ligands.

Alberti *et al.* produced some of the first extended metal-phosphonate compounds, using Zr(IV).[104] The 1D zirconium bis(phenylphosphonate) hybrid pictured in Figure 1.30 possesses extended connectivities through the edge-to-edge interactions of stacked phenyl rings and tetrahedral metal geometry. Since that time, investigations have expanded to include di- and trivalent cations, including main group phosphonates[105] and transition and rare-earth metals, further examples of which will be discussed in Chapters 2-4.
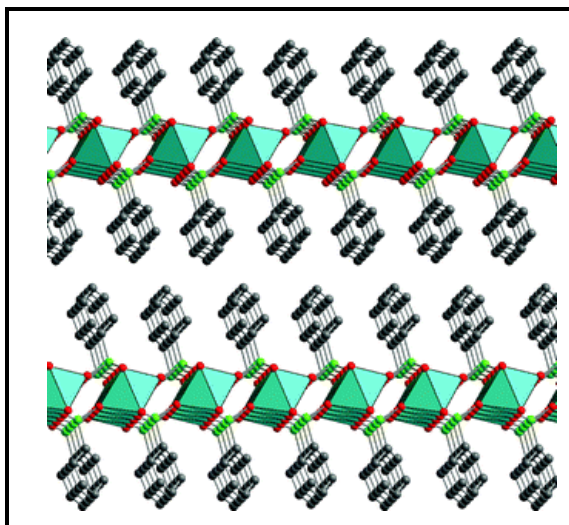
Figure 1.30 A side-view of the layered zirconium(IV) bis(phenylphosphonate). Adapted from Reference 4.

Phosphonic acids are easily synthesized and can be modified with almost any secondary organic functional group,[106] which makes them utilitarian building blocks for polymeric materials. Additionally, as illustrated in Sections 1.4.1 to 1.4.4, phosphonic acids are capable of supporting coordination polymers for a wide variety of applications, such as gas separation and storage, heterogeneous catalysis, and luminescent sensors.

1.8 Conclusion

As demonstrated, functionalized organic acids have played a critical role in the development of mono-, bi-, and tri-dimensional structures, with characteristics that have already provided opportunities for commercial applications. Continued investigations into preferred metal coordination geometries and pH, anion, and solvent effects are needed to improve our predictive abilities regarding network topologies. The control of polymeric architecture allows us to control physical and chemical properties, a necessary requirement in the design of functional materials.

Chapter 2

A Mild Synthetic Route to Zinc, Cadmium, and Silver Polymers with 2-(Pyridyl) phosphonic Acid: Synthesis and Analysis

2.1 Introduction

The chemistry of metal phosphonates has vastly increased in recent years, and is associated with many applications, including catalysis,[107] sensors,[108] and luminescence, as discussed in Chapter 1 Section 1.4.4. Initial evaluative studies into the catalytic capabilities of this class of materials have been underway for many years. An example of their utility in this capacity is the bisphosphonate [Sm(**LH₂**)(**LH₃**)(H₂O)₄]·xH₂O (x = 9-14, **LH₄** = 2,2'-diethoxy-1,1'-binapthalene -6,6'-bisphosphonic acid) (see Figure 2.1) that has been shown to catalyze the cyanosilylation of aldehydes, with 55-69% product yields, >98% recovery of the original catalyst, and without loss of catalytic activity.[109]
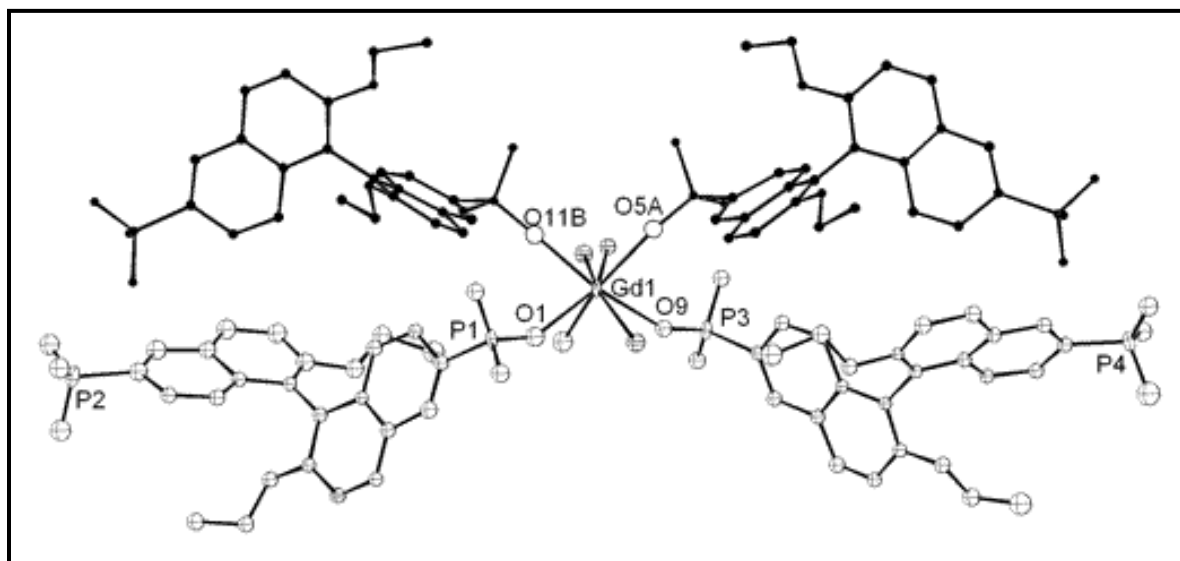
Figure 2.1 A series of isostructural polymers were formed through the reaction of Ln(III) nitrate and perchlorate salts with 2,2'-diethoxy-1,1'-binapthalene-6,6'-bisphosphonic acid. The Sm(III) analog was used to test for catalytic activity as a Lewis acid; the Gd(III) analog's single-crystal X-ray diffraction data was used to create the above figure. The asymmetric unit (excluding water guest molecules) is shown with ellipsoids at 30% probability. Taken from Reference 109.

A further example is the porous zirconium phosphonate compound, $Zr_2(PO_4(O_3PCH_2CH_2(viologen)CH_2CH_2PO_3)X_3 \cdot 3H_2O$ (X = halide), consisting of Zr-phosphate/phosphonate lamellae bridged by alkylviologen groups.[110] Guest halide ions are exchanged for $PtCl_4^{2-}$, which are subsequently reduced to give fine particles of elemental platinum, capable of photochemical production of $H_{2(g)}$ from water. These examples demonstrate how metal-phosphonate polymers with various dimensionalities show promise as heterogeneous catalysts—either as scaffolds for coordinatively-unsaturated metal centers, or as host-matrices for active catalysts.

2.1.1 Ligand Synthesis

In the pursuit of novel raw materials for potential applications, functionalized phosphonic acids are particularly interesting; they are easily synthesized and have coordination modes and possibilities for supramolecular assembly via hydrogen bonding or aromatic stacking originating from the additional functional groups. 2-(Pyridyl)phosphonic acid ($2PyHPO_3H$) has the capability for both of those interactions, with its heterocyclic nitrogen that can remain protonated and participate as a hydrogen donor, as well as its rigid aromatic ring. Multiple coordination sites are also available to the metal (Figure 2.2), increasing the potential for multidimensional products. We were particularly interested in the synthesis and investigation of thermally stable, crystalline, d^{10} metal frameworks with $2PyHPO_3H$, prepared from mild solution syntheses. Zinc, silver, mercury, and cadmium cations all have demonstrated abilities to coordinate to heterocyclic nitrogens,[111] and they were logical choices for reactions with this bifunctional ligand.
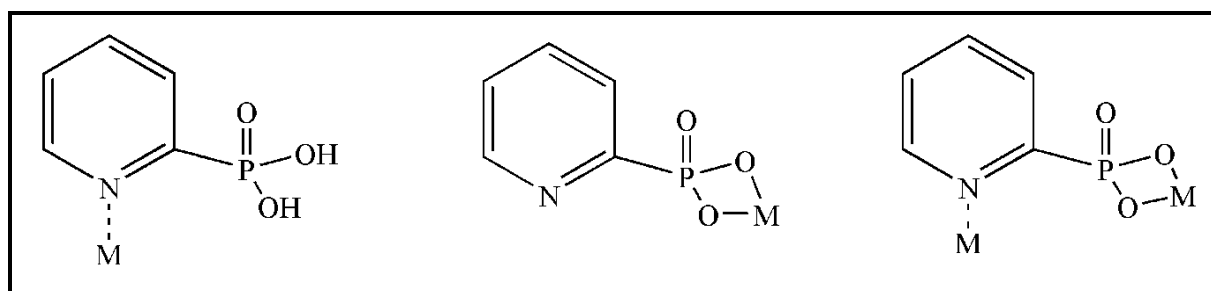
Figure 2.2 Various coordination modes of 2-(pyridyl)phosphonic acid.

For the synthesis of aryl and heteroaryl phosphonates, the modified Hirao cross-coupling scheme described by Montchamp *et al.* has been shown to be the most efficient and cost-effective method of production.[112] The desired heteroaryl halide is refluxed with diisopropyl phosphite in acetonitrile, using 1 mol % Pd(OAc)$_2$ and dppf as the catalyst. The resulting diester phosphonate is then deprotected by treatment with TMSBr following McKenna's protocol,[113] to obtain the heteroaryl phosphonic acid (Scheme 2.1).
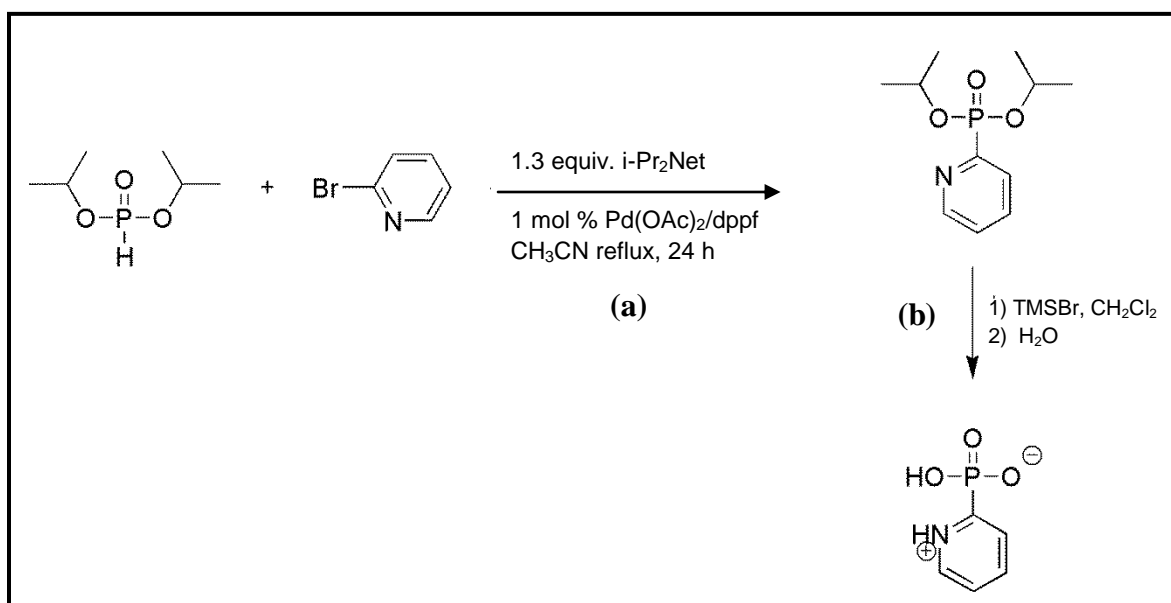
Scheme 2.1 **(a)** Modified Hirao cross-coupling to form the heteroaryl phosphonate **(b)** Deprotection with TMSBr, followed by hydrolysis, to form the heterocylic 2-(pyridyl) phosphonic acid. Modified from Reference 112.

2.1.2 Related Work

Early work by Foxman and co-workers using both 3- and 4-(pyridyl)phosphonic acids demonstrated this ligand class's ability to form polymeric frameworks. Unique coordination networks of divalent zinc, cadmium, copper, and cobalt were synthesized using hydrothermal means. For example, a one-dimensional ladder was formed using $3PyHPO_3H$ and zinc(II) (Figure 2.3). Each tetrahedral zinc center is coordinated to one bromide ion and three different μ_3-η^3-phosphonate units.[114]
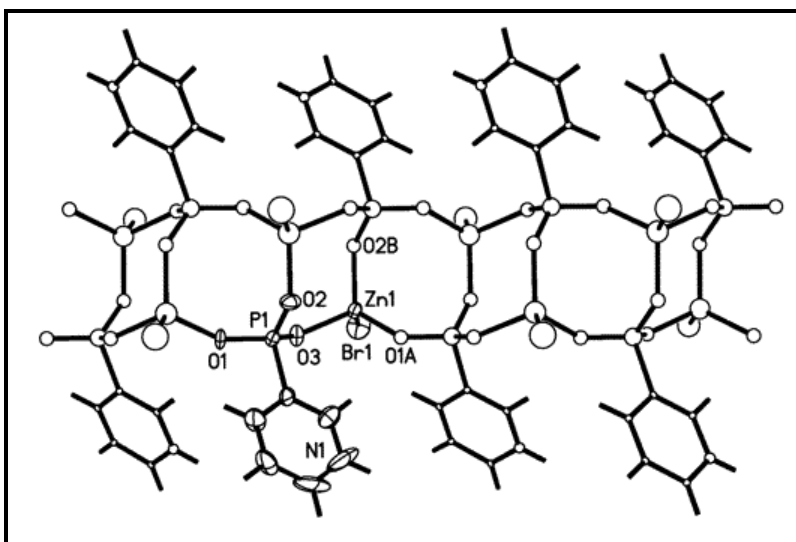
Figure 2.3 [Zn(3-pyridylphosphonate)Br]$_n$ in a 1D ladder topology. The asymmetric unit is shown with ellipsoids at 50% probability. Adapted from Reference 114.

Two distinct 3D frameworks were formed with Cd(II), both adopting slightly distorted octahedral geometries with coordination to four phosphonate groups in the equatorial positions and two pyridyl nitrogen atoms in the apical positions. However, when $3PyHPO_3H$ is utilized (see Figure 2.4a), the 3D network forms spherical cavities, while the $4PyHPO_3H$ network (see Figure 2.4b) consists of pillared layers with significant $\pi \cdots \pi$ interactions.[114]
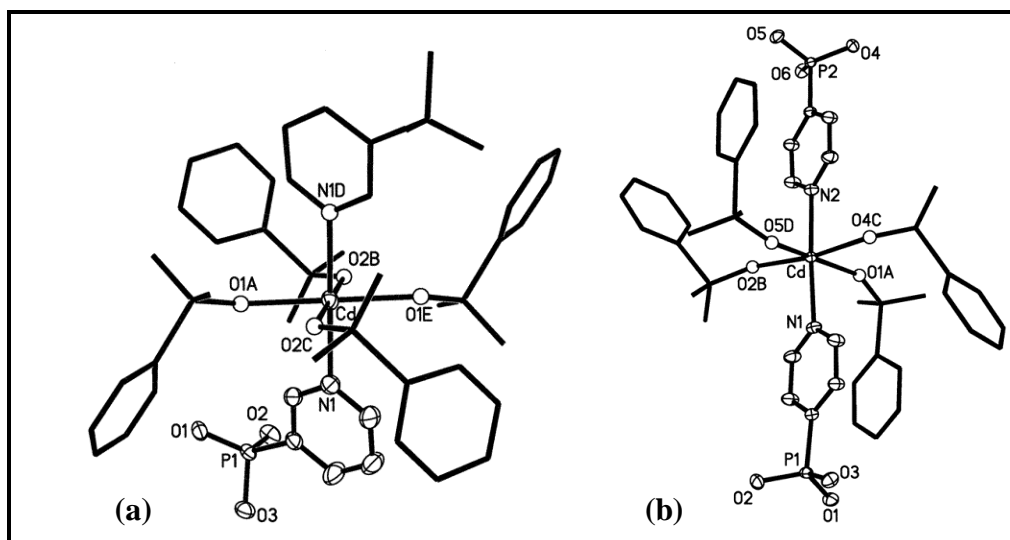
Figure 2.4 3D networks with Cd(II) and **(a)** 3-(pyridyl)phosphonic acid or **(b)** 4-(pyridyl)phosphonic acid. Asymmetric units displayed with ellipsoids at 50% probability. Adapted from Reference 114.

More recently, Clearfield *et al.* have used 4-(pyridyl)phosphonic acid under hydrothermal conditions to assemble multidimensional polymers with divalent cations of Cu, Mn, and Zn,[115] as well as with Sn(II).[116] Interestingly, the zinc complex is composed of a dimeric Zn(II) molecule with an extended series of hydrogen bonds transforming a 0D discrete unit into a 3D supramolecular network (Figure 2.5).
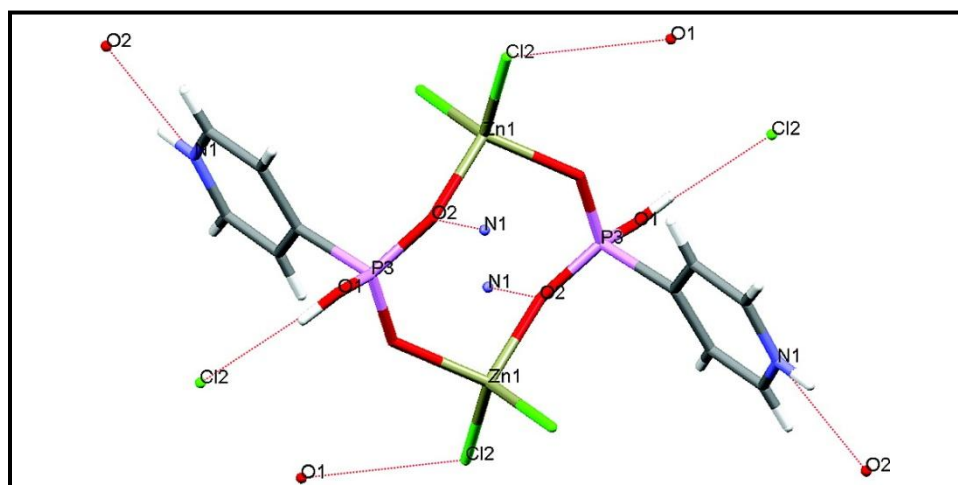
Figure 2.5 Stick representation of $[Zn_2(NHC_5H_4-PO_3H)_2Cl_4]$, with intermolecular hydrogen bonds shown as red lines. Adapted from Reference 115.

2-(Pyridyl)phosphonic acid has been less widely explored in comparison to other substituted derivatives as it was thought that the small bite angle associated with the 2-pyridyl substitution would limit the ability of the ligand to bridge, and rather than obtaining diverse frameworks, discrete structures would be formed. Despite these limitations, Zheng *et al.* have demonstrated the versatility of 2PyHPO$_3$H in the preparation of multidimensional polymers, albeit using hydrothermal synthetic methods.[117] Bimetallic, 3d-4f polymers incorporating 2PyHPO$_3$H, Zn(II)/Cu(II)/Co(II), and various trivalent lanthanides form isostructural open frameworks. The ligand employs both chelating and bridging modes, with the transition metal cations most often coordinating to both the heterocyclic nitrogen and one of the phosphonate oxygens (Figure 2.6). The "hard" lanthanide cation prefers binding to the phosphonate oxygens.
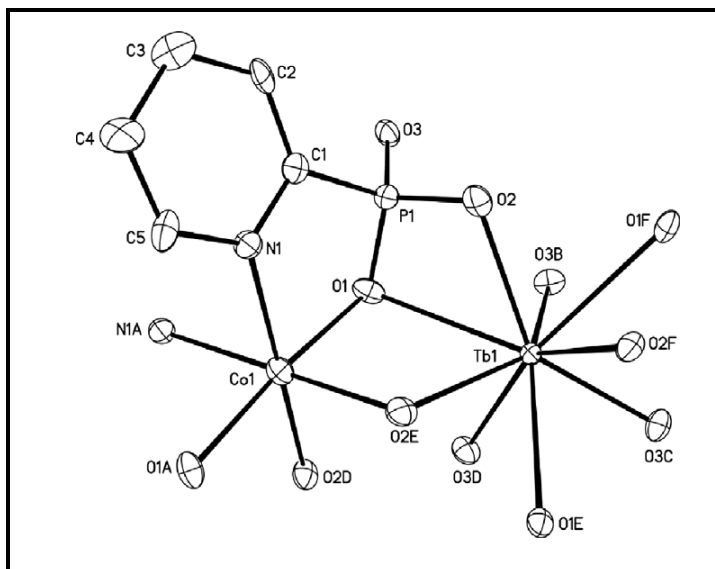
Figure 2.6 Representative asymmetric unit for the isostructural Ln$_2$M$_3$(2PyPO$_3$)$_6$·4H$_2$O, M = Zn(II), Cu(II), Co(II); Ln = trivalent cations of La, Ce, Pr, Nd, Sm, Gd, Tb, Dy. Adapted from Reference 117(c).

2.2 Results and Discussion

In contrast to methods employing high temperature hydrothermal conditions, we wished to examine the outcome of reactions performed at room temperature or with gentle heating, in order to obtain crystalline products from a reproducible, scalable synthesis to enable further chemical exploration. During our systematic investigations of 2-(pyridyl)phosphonic acid with metal salts under aqueous conditions, five novel coordination polymers were obtained. The reaction of 2-(pyridyl)phosphonic acid (2PyHPO$_3$H) with ZnX$_2$ (X = Cl, Br), CdCl$_2$, Hg(NO$_3$)$_2$ and Ag(SO$_3$CF$_3$) affords polymeric structures with varying structural motifs that range from interlinked cyclic cores of the zinc halide polymers, a highly symmetrical one-dimensional mercury polymer, and a complex two-dimensional silver triflate polymer with silver-silver interactions.

2.2.1 Discussion of Polymers 1, [Zn(Cl)(2PyHPO$_3$)]$_n$, and 2, [Zn(Br)(2PyHPO$_3$)]$_n$

The reactions of zinc(II) chloride and bromide with 2-(pyridyl)phosphonic acid under aqueous conditions in a 1:1 ratio afforded two-dimensional polymers (Figure 2.7).
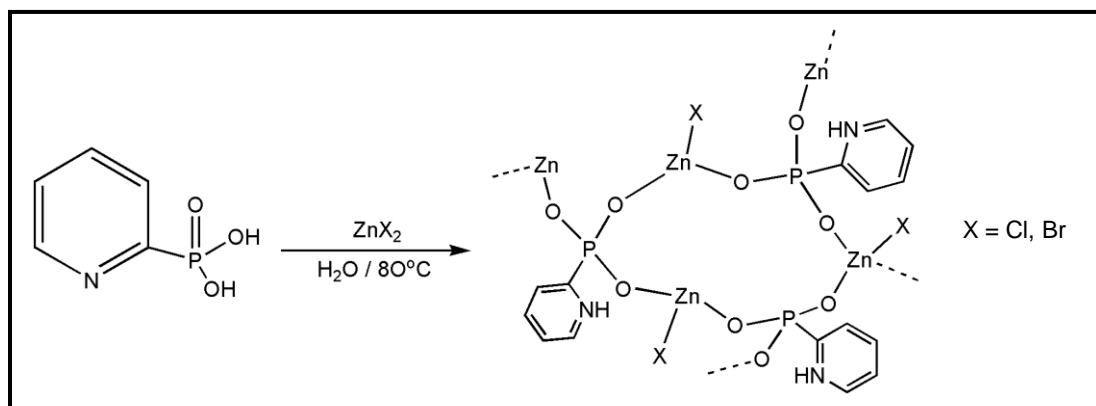
Figure 2.7 Synthesis of polymers **1** and **2**.

The network structures of zinc chloride and bromide are essentially similar although they crystallize in different space groups: the zinc chloride polymer **1** crystallizes in the monoclinic space group, $P2_1/c$, while the equivalent reaction with bromide affords colorless, crystalline needles that are orthorhombic, space group *Pbca*. The asymmetric unit and polymeric form of the zinc bromide reaction product are depicted in Figure 2.8.
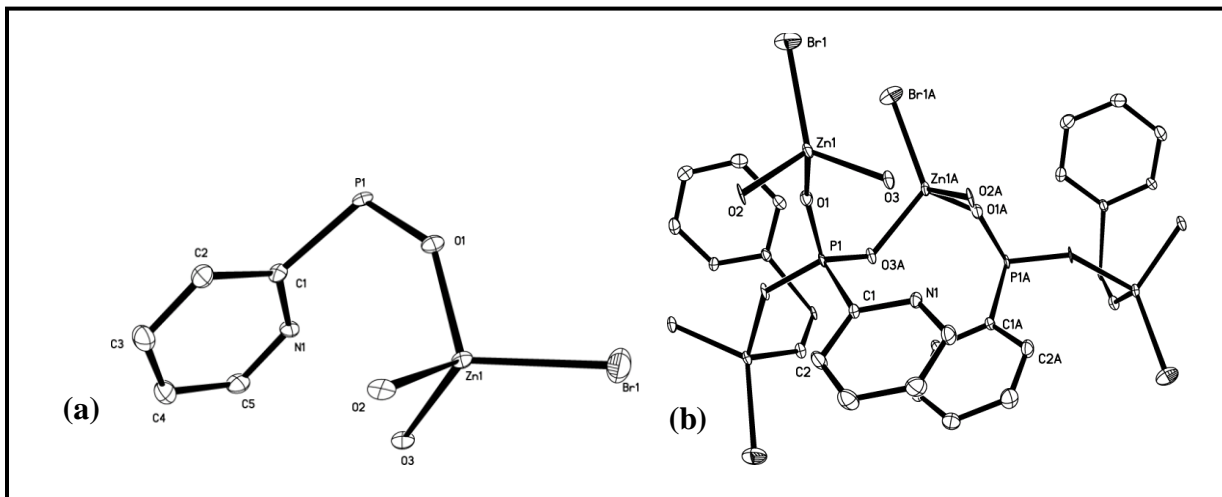
Figure 2.8 X-ray crystal structure of the **(a)** Asymmetric unit and **(b)** Polymeric form of $[ZnBr(2PyHPO_3)]_n$. Thermal ellipsoids are at 30% and hydrogen atoms are omitted for clarity.

The asymmetric unit of both **1** and **2** contains one zinc atom, a 2-(pyridyl)phosphonate molecule, and one halide atom. The zinc atoms have distorted tetrahedral geometry with each remaining coordination site occupied by an oxygen atom. The three oxygen atoms arise from the phosphonate moiety and bridge the zinc centers. It is difficult to determine from X-ray analysis the protonation of the phosphonate oxygen atoms. However, from the electron density difference map the pyridyl nitrogen is protonated, and for charge balance it is likely that the phosphonate group of the ligand is deprotonated.

The hydrogen atom attached to the pyridyl nitrogen atom is involved in hydrogen bonding to O1 of the phosphonate group; the distance between the two atoms (O and H) is 1.935 Å, and the N1–O1 distance of 2.754 Å is consistent with hydrogen bonding. No free water molecules are observed in the lattice of the solid-state material. The zinc-oxygen distances are between 1.923(2) and 1.9804(19) Å for **1** and 1.949(4) and 1.981(4) Å for **2**; these values are within the range of comparable Zn-O bonds.[118] Overall, the polymers are made up of 12-membered cyclic systems comprised of zinc, oxygen and phosphorus atoms surrounded by flanking halide and pyridyl groups (Figure 2.9). This type of ring motif is common for zinc phosphates and phosphonates, as is demonstrated by the 8-membered rings shown in Figures 2.3 and 2.5.[114,115] Around the cyclic core, the pyridyl groups adopt a "*cis*-type" geometry separated by a distance of 4.930 Å between parallel rings and a Zn-Zn distance of 5.166 Å. Polymer **2** has a py-py separation of 4.738 Å and a Zn-Zn distance of 4.502 Å. A terminal halide is present in polymers **1** and **2**, which limits polymer dimensionality.
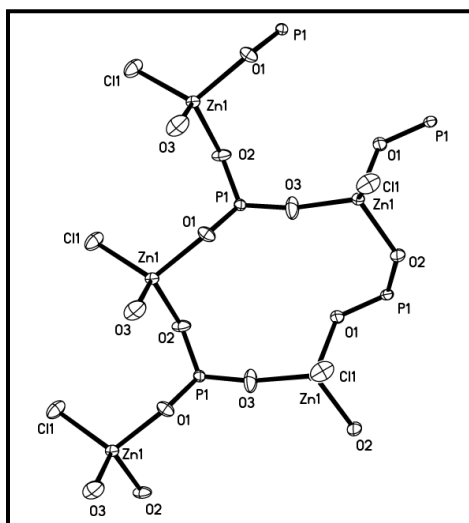
Figure 2.9 Crystal structure of the 12-membered cyclic core that makes up the polymer **1**. Thermal ellipsoids at 50% probability, hydrogen atoms and pyridyl rings are omitted for clarity. Selected bond lengths (Å) and angles (°): P1–O1 1.522(2), P1–O3 1.496(2), P1–O2 1.5032(19), Zn1–O1 1.9804(19), Zn1–O2 1.9487(19), Zn 1–O3 1.923(2), O3–Zn1–O2 108.66(9), O3–Zn1–O1 105.29(9), O3–Zn1–Cl1 117.36(7).

Infrared data of **1** show PO_3 stretching modes between 1284 and 962 cm^{-1}, and the NH stretch is at 3110 cm^{-1}. The C-C and C-N stretches associated with the pyridyl ligand occur between 1526 cm^{-1} and 1415 cm^{-1}. These values are consistent with recorded literature for systems with similar coordination modes.[119] Similar values are observed for **2**. The ^{31}P NMR spectra for each polymer displayed a single peak, indicating one phosphorus environment at $\delta = 1.2$ ppm (**1**) and one at 0.4 ppm (**2**). The free ligand has a phosphorus chemical shift at $\delta = -$ 3.2 ppm.[120] Polymers **1** and **2** are thermally robust, with no decomposition observed at 250 $^{\circ}$C; however, visually (during melting point measurements), some mass loss can be detected at around 45-50 $^{\circ}$C. TGA data were recorded on compounds **1** and **2**. Weight loss in this temperature range was found to be negligible, (0.23 and 0.19 % respectively) indicating that no free guest water molecules are present. A melting transition is observed for both polymers between 115 - 130 $^{\circ}$C, and no other changes are observed up to 400 $^{\circ}$C.

2.2.2 Discussion of Polymer 3: [Cd($_\mu$Cl)$_2$(2PyHPO$_3$)]$_n$

The 1:1 reaction of 2PyHPO$_3$H in water with CdCl$_2$·2.5H$_2$O afforded a one-dimensional framework. Colorless crystals of **3** suitable for single-crystal analysis were isolated from slow evaporation of an aqueous solution at room temperature. Single-crystal structural analysis on the crystals shows that **3** crystallizes in the orthorhombic space group *Pbca*. The crystal structure of **3** is shown in Figure 2.10.

The cadmium center has a slightly distorted octahedral geometry and consists of four μ_2-chlorine atoms and two apical phosphonate moieties. Both the chloride and oxygen bridges between the cadmium centers show small differences in their bond lengths but correspond well to other reported values.[121] The bridging oxygen atoms are deprotonated, and this, along with

the charge from the halides, indicate that the pyridyl nitrogen is protonated. The distance separating the cadmium centers is 3.7 Å. This is longer than the sum of the Van der Waals radii[122] and so Cd-Cd interaction is unlikely; π-π stacking is also ruled out, because the distance between the pyridyl groups is 7.4 Å and the optimal distance for π-stacking is ~3.9 Å.[123] TGA data on **3** showed no weight loss up to 400 °C, which corroborates that no guest water molecules are present.
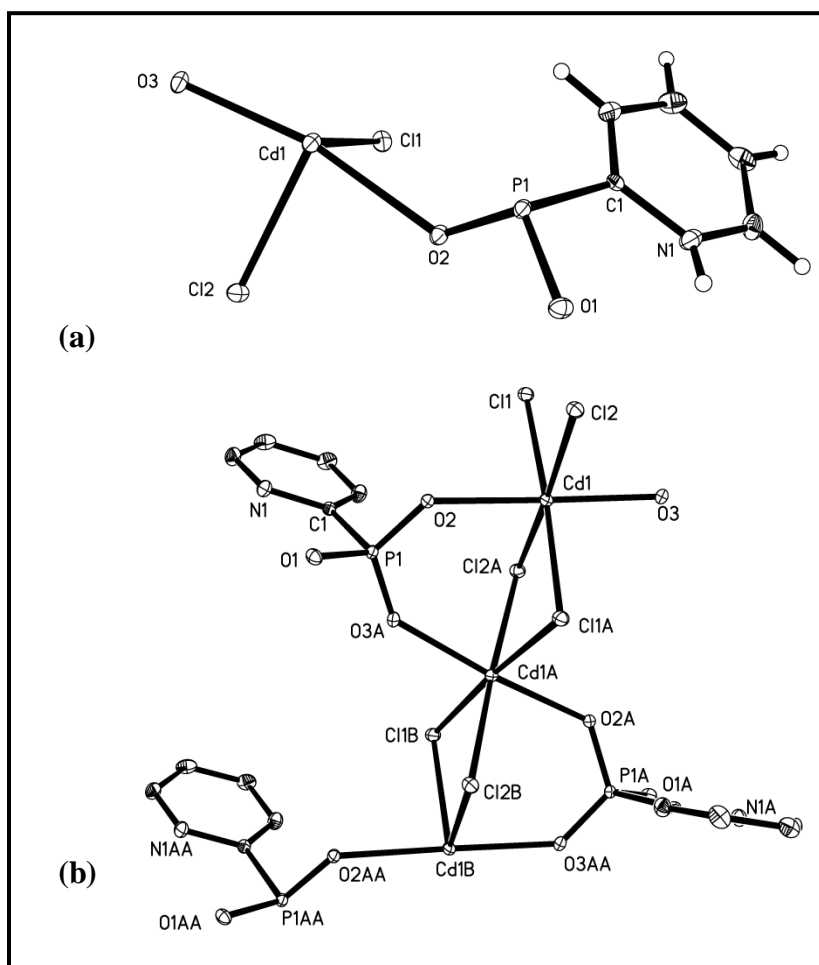
Figure 2.10 **(a)** Asymmetric unit of **3**; thermal ellipsoids at 30% probability. **(b)** Polymeric structure; hydrogen atoms are omitted for clarity. Selected bond lengths (Å) and angles (°): Cd1–Cl1 2.6223(15), Cd1–Cl2 2.5980(15), Cd1–O2 2.397(4), Cd1–O3 2.290(4), Cl2–Cd1–Cl1 86.43(5), Cl1–Cd1–O2 91.60(10), Cl2–Cd1–O3 83.07(11).

The structure of **3** can be compared with that of the 3D pillared coordination network isolated from the hydrothermal reaction of cadmium perchlorate with 4PyHPO$_3$H (the asymmetric unit is pictured in Figure 2.4b).[114] In the 4PyHPO$_3$H structure, the pyridyl groups participate in the octahedral geometry around the cadmium center and direct the polymer growth in the *c* direction. However, the 2PyHPO$_3$H ligand does not coordinate to the cadmium center via the pyridyl nitrogen; the proximity of the acidic functional group to the nitrogen position appears to constrain the geometry and limit the polymer to one-dimensional growth.

2.2.3 Discussion of Polymer 4: [{Hg(2PyPO$_3$H)$_2$}H$_2$O]$_n$

To extend the series, the preparations of mercury and silver frameworks were investigated. To maintain mild experimental conditions, halide precursors that have limited aqueous solubility were replaced with water-soluble precursors: mercury nitrate, silver nitrate, and silver triflate. The stoichiometric reaction of Hg(NO$_3$)$_2$ with 2PyHPO$_3$H afforded X-ray quality crystals of **4** in moderate yield at ambient temperature. The solid-state analysis of **4** (Figures 2.11 and 2.12) revealed that one molecule of 2PyHPO$_3$H and one mercury center are present in the asymmetric unit, as well as the presence of one water molecule in the crystal lattice. The mercury center is coordinated to the nitrogen atom of the pyridyl group and oxygen atoms of the phosphonate group and has a very slightly distorted octahedral geometry, with angles as expected for this geometry: N1–Hg1–N1A = 180° and N1–Hg1–O1 = 89.36(18)^o (Figure 2.11). The polymer is extended via the two bridging oxygen atoms of the phosphonate moiety.
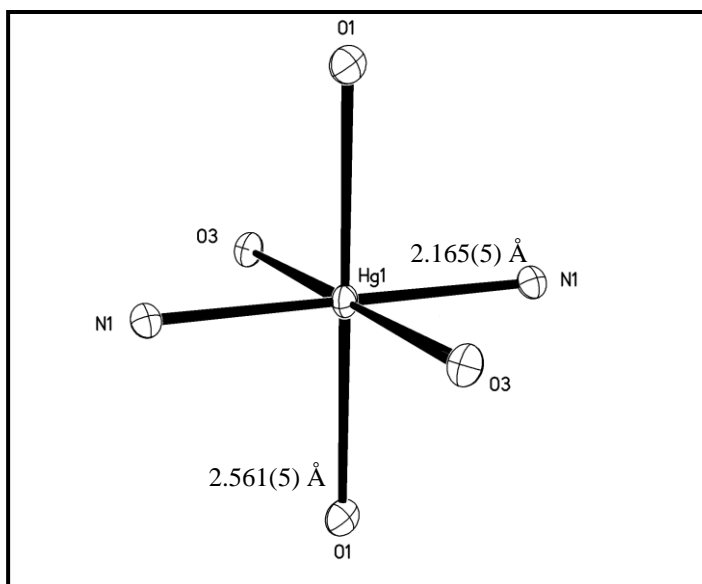
Figure 2.11 Diagram to display slightly distorted octahedral geometry around the Hg center. Thermal ellipsoids at 50% probability. Selected bond angles (^{o}): N1-Hg1-N1 180, O1-Hg1-N1 90.64(18), N1-Hg1-O3 79.54(17).
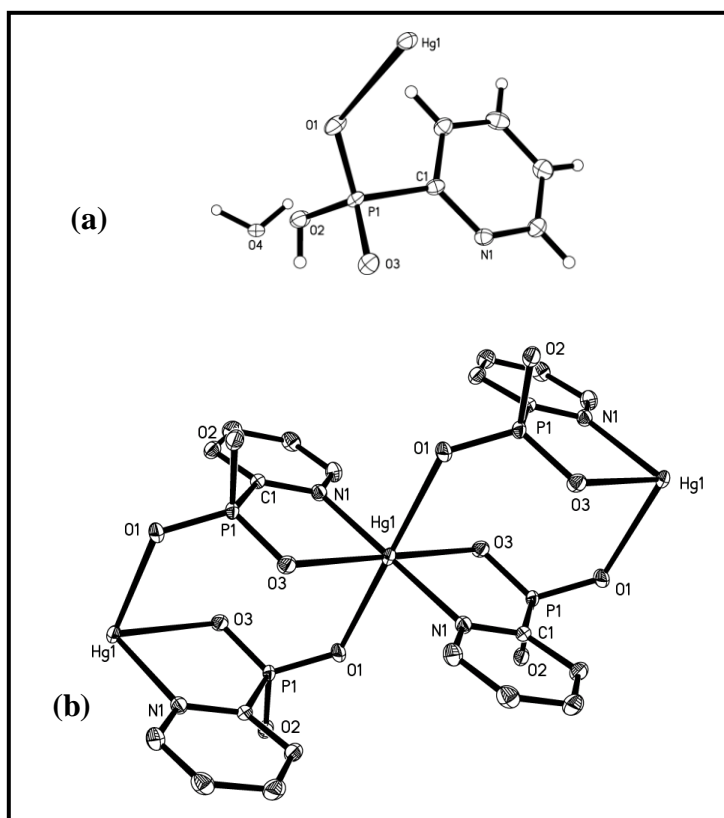
Figure 2.12 Structure of **4**, $[\{Hg(2PyPO_3H)_2\}H_2O]_n$ **(a)** Showing the asymmetric unit, **(b)** Showing the coordination environment of the metal center. H atoms are omitted for clarity, thermal ellipsoids at 30% probability. Other pertinent bond angles (^{o}) and lengths (Å): P1–O1 1.490(5), P1–O3 1.506(6), P1–O2 1.575(6), N1–Hg1–N1A 180.0(3), N1–Hg1–O1A 90.64(18), N1A–Hg1–O3A 79.54(17), O3A–Hg1– O3 180.00(19), O1–P1–O2 108.0(3).

The Hg-O distance of 2.561(5) Å is within the range of other characterized Hg-O species[124] but the Hg-N distance of 2.165(5) Å is shorter than those observed in similar Hg-Py systems, and could compensate for the weak interaction between the Hg and bridged oxygen atoms.[125] A distance of 5.7 Å between mercury centers limits any Hg-Hg interaction since it is almost double the value of the summed Van der Waals radii (1.70 Å – 2.0 Å).[126] Hydrogen bonding is present from the protonated phosphonate group to the lattice water molecule. Polymer **4** shows good thermal stability and appears stable up to 300 $^{\circ}$C (no visible decomposition). Crystalline **4** can be redissolved in water or ethanol, and heating of an aqueous solution to 100 $^{\circ}$C for one hour reveals no structural changes (checked by solution NMR and unit cell measurements following recrystallization from the aqueous solution). Infrared spectroscopy exhibited strong peaks at 3540 and 3500 cm^{-1}, which corresponds to the water, and at 1613 cm^{-1}, which is assigned to the bending vibration. In the ^{31}P solution NMR spectrum, a single phosphorus signal is observed at   -0.7 ppm. The TGA data shows a weight loss of 3.1% from 120 $^{\circ}$C to 136 $^{\circ}$C corresponding to the loss of water, which agrees with the theoretically calculated value of 3.3 %. Weight loss is also recorded between 195 and 211 $^{\circ}$C, corresponding to 8.1 % (calculated value 12 %), which likely corresponds to partial loss of the organic moiety. Decomposition occurs at 376 $^{\circ}$C.

2.2.4 Discussion of Polymer 5: [Ag$_3$(CF$_3$SO$_3$)$_2$(2PyHPO$_3$)]$_n$

It was anticipated that the diverse coordination geometries available to silver ions would result in a polymeric species. However, the reaction of AgNO$_3$ with 2PyHPO$_3$H afforded the recrystallized ligand. In order to obtain a polymeric network, other silver precursors were examined. Silver triflate was selected, as the CF$_3$SO$_3^-$ ion is considerably larger than NO$_3^-$ and

its oxygen atoms have a stronger coordinating ability than those of NO_3^-.[127] Framework **5** was isolated from the reaction of silver(I) triflate with 2-(pyridyl)phosphonic acid (Figure 2.13).
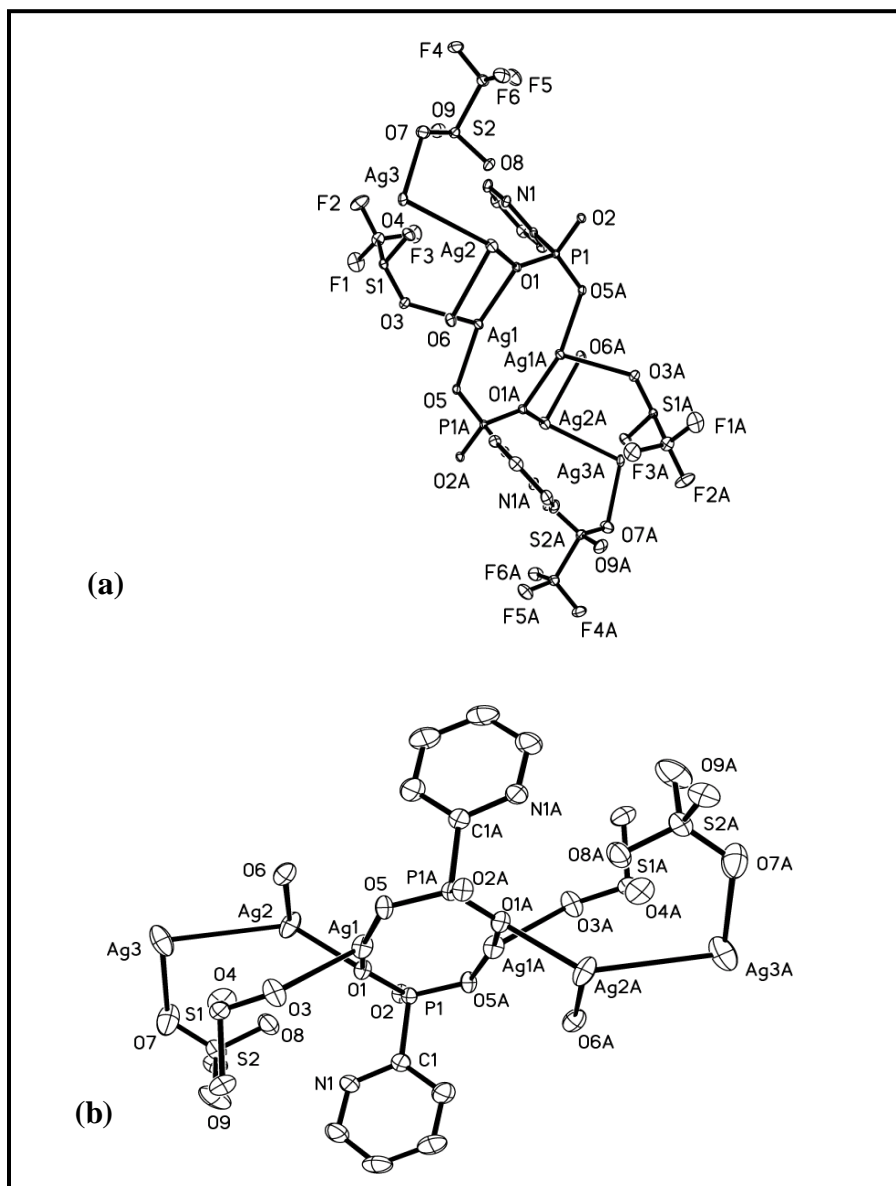
Figure 2.13 Thermal ellipsoid plots (30% probability) of the silver triflate polymer **5**, $[Ag_3(CF_3SO_3)_2(2PyHPO_3)]_n$. **(a):** Some of the triflate groups are removed for clarity. **(a)** and **(b):** H atoms are omitted for clarity.

In solid form, **5** shows good photostability, although in solution slow decomposition to metallic silver occurs. Coordination of the triflate anion is not common,[128] but in polymer **5** the triflate participates in bonding to the silver atom and also helps stabilize the framework.[129] This

occurs in conjunction with Ag-Ag interactions, which, according to Schröder,[130] help stabilize the polymeric network, as the energy of the Ag-Ag closed-shell interaction falls into the same range as aromatic stacking. The silver-silver distances of 3.3627(5) Å (Ag1-Ag2) and 3.0543(6) Å (Ag2-Ag3) fall within the range of documented Ag-Ag interactions (3.091-3.474 Å).[131] The variation of observed Ag-Ag distances is due to the relatively weak Ag-Ag contacts and their fairly small interaction. The silver ions form a zig-zag chain in which every silver atom is five-coordinate and has a distorted trigonal bipyramidal geometry (Figure 2.14).
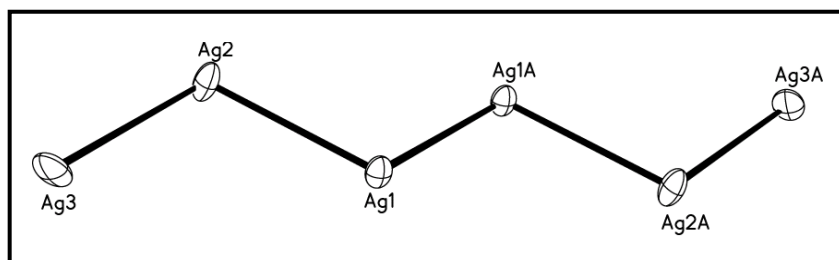
Figure 2.14 Zig-zag arrangement of the Ag atoms in **5**. Ag1–Ag2 3.3627(5) Å, Ag2–Ag3 3.0543(6) Å.

Examination of the repeating unit reveals three different silver environments. Ag1 is coordinated to two oxygen atoms from the phosphonate group and the oxygen atom of a triflate group. The oxygen atoms from the phosphonate bridge a second silver center, Ag2. Ag2 has a relatively short Ag-Ag distance to Ag3 [3.0543(6)Å] to which the triflate ion is attached. This short Ag-Ag interaction has a similar value to the Ag-Ag distance of 3.089(1) Å in polymeric Ag[(bpp)](CF$_3$SO$_3$)·EtOH (bpp = 1,3-bis(4-pyridyl)propane).[132] Thus, overall in the asymmetric unit, there are three silver centers, two triflate ions, and one phosphonate ion. The distance between the pyridyl rings is 9.567Å; this distance is too large for π-π stacking interactions. Selected bond lengths and angles are given in Figure 2.15.
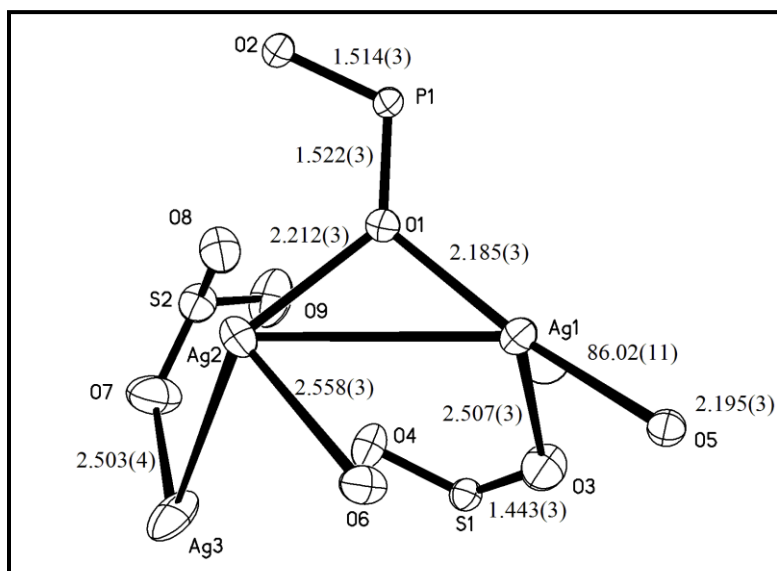
Figure 2.15 Selected bond lengths (Å) (in figure) and bond angles (°) of polymer **5**: O3-Ag1-Ag2 95.08(8), O3-Ag1-O5 86.02(11).

Thermal gravimetric analysis of **5** showed a melting transition at 176 $^{\circ}$C, (melting point recorded at 172 $^{\circ}$C when the sample became brown). Further heating results in a weight loss of ~38.7 % from 226–384 $^{\circ}$C, which is associated with loss of the triflate and 2PyHPO$_3$H groups (calculated value = 38.5 %). No further change was observed up to 500 $^{\circ}$C.

2.2.5 Luminescence Studies

Many d^{10} systems have shown promise as light emitting diodes,[133] as the advantage of metal-containing frameworks is that their absorption and emission can be altered by changing the metal environment. To probe the potential of these systems, luminescence properties were investigated. Emission of the free ligand was recorded at excitation wavelengths 250, 275, 300, 350, and 375 nm, and emission wavelengths were recorded at 306 and 331 nm. At the same wavelengths, luminescence experiments of the frameworks were performed. Polymers **1-4** showed no luminescence at ambient temperature. Polymer **5** (silver triflate polymer), when

dissolved in acetonitrile, had weak emission at 313 and shoulders associated with the ligand in its spectrum. It is thought that room temperature luminescence is too weak to be detected and requires low temperature measurements.

2.3 Conclusion

Several solid-state structures, **1-5**, were prepared under mild conditions and characterized by X-ray diffraction. 2-(Pyridyl)phosphonic acid (2PyHPO$_3$H) serves as a useful ligand for the synthesis of various metal-organic frameworks. In the past, emphasis was placed on other isomers of (pyridyl)phosphonic acid. This work demonstrates that the less common 2-isomer also provides interesting materials. The control of molecular structure depends both on the phosphorus-containing ligand and on the metal (and metal precursor) employed. 2PyHPO$_3$H has been shown to act in μ_3-η^3, μ_2-$\eta^3$and μ_2-η^2 modes—the first with the two zinc polymers, **1** and **2**, the second with the mercury compound, **4**, and the third with the cadmium and silver frameworks, **3** and **5**. The zinc polymers exhibited the expected tetrahedral geometries and ring structures and yet retained their bi-dimensionality due to the fact that all three of the phosphonate oxygens participated in coordination to the metal centers. The cadmium compound, **3**, while limited to one-dimension due to the bridging chlorides, was still able to polymerize through the μ_2-ligand. The silver compound, **5**, employed a μ_2-η^2-ligand as well, but also contained the coordinating triflate counterion which connected two of the three unique silver centers. Only one of the five compounds demonstrated metal-coordination to the pyridyl nitrogen, although all metals were chosen with that capability in mind. Polymer **4** utilized a chelating mode of the 2-(pyridyl)phosphonic acid ligand to coordinate the mercury center to the oxygen from one ligand and an oxygen and nitrogen from a second ligand. This resulted in the two-dimensional framework where two ligands bridged the same two mercury centers, and each

mercury(II) was coordinated to a total of four ligands in an octahedral environment. The 2-(pyridyl)phosphonic ligand has thus been shown to support a variety of coordination modes with d^{10} metal cations, allowing the growth of polymeric structures.

2.4 Materials and Methods

2-(Pyridyl)phosphonic acid was prepared as described in Section 2.1.1. Other materials were purchased from Aldrich and used as received. IR spectra were recorded from KBr pellets on a MIDAC M4000 FT-IR spectrometer. Thermogravimetric analyses (TGA) were carried out on a Seiko 220 instrument at a heating rate of 5 ^{o}C/ min. ^{1}H and ^{31}P{H} NMR spectra were recorded in solution on a Varian Mercury 300 MHz spectrometer. Due to limited solubility in common deuterated solvents no meaningful ^{13}C data could be collected. Fluorescence was recorded using a Shimadzu 5301PC spectrofluorimeter at ambient temperature. Elemental analysis was carried out by Schwarzkopf Microanalytical Laboratory in Woodside, NY.

X-ray data collection of the compounds were performed at -60 ^{o}C on a Bruker SMART 1000 diffractometer, using Mo Kα radiation (0.71073Å), and equipped with cryostream. Crystals were mounted on glass fibers using paratone oil. *SAINT* was used for data reduction and cell refinement,[134] and SADABS[134] was run for absorption correction on all data. Crystal structures were solved using direct methods and refined with full-matrix least squares treatment (SHELXL).[134] Crystallographic data are summarized in Table 2.1.

2.5 General Experimental

2.5.1 Synthesis of 1, [Zn(Cl)(2PyHPO$_3$)]$_n$:

A solution containing 0.10 g (0.63 mmol) of 2PyHPO$_3$H and 0.09 g of ZnCl$_2$ (1 mmol) dissolved in ~ 5 mL of water in a vial was stirred at room temperature for 30 minutes. The initial crystals were obtained from a flask that was heated for an additional 20 minutes at 70 $^{\circ}$C, however on repeating the reaction, the product can be formed at room temperature. Colorless crystals suitable for X-ray diffraction were obtained by slow evaporation of the solution at room temperature. Yield = 0.067 g (41 %). Melting point > 250 $^{\circ}$C; on slow heating of the crystalline material, contraction of the solid is visible between 40 – 50 $^{\circ}$C. This corresponds with results obtained by TGA (see text). IR (KBr pellets): 3224 (m), 3110 (m), 3019 (m), 3008 (m), 2919 (m), 2862 (m), 1607 (s), 1526 (s), 1440 (s), 1415 (m), 1284 (m), 1170 (s), 1152 (s), 992 (s), 962 (m), 910 (w) cm^{-1}. Elemental Analysis: (C$_5$H$_5$ClNO$_3$PZn, 258.89) C: 23.78, H 1.89, N 5.61 Calc: C (23.19) H (1.94) N (5.41). ^{1}H NMR (300 MHz, 25 $^{\circ}$C, D$_2$O): δ 8.8 (m, 1 H), 8.5 (m, 1 H), 8.2 (m, 1 H), 8.0 (m, 1 H), ppm (all broad signals). ^{31}P{H} NMR (121 MHz, 25 $^{\circ}$C, D$_2$O): δ 1.0 ppm.

2.5.2 Synthesis of 2, [Zn(Br)(2PyHPO$_3$)]$_n$:

A solution containing 0.10 g (0.63 mmol) of 2PyHPO$_3$H and 0.14 g of ZnBr$_2$ (0.63 mmol) dissolved in ~ 5 mL of water in a vial was stirred at room temperature for 30 minutes. Colorless crystals suitable for X-ray diffraction were obtained by evaporation of the solution by heating at ~ 100 $^{\circ}$C. Yield = 0.15 g (81 %). Melting point > 250 $^{\circ}$C; on slow heating of the crystalline material, contraction of the solid is visible between 40 – 50 $^{\circ}$C. This corresponds with results obtained by TGA (see text). IR (KBr pellets): 3216 (s), 3085 (s), 1604 (s), 1523 (s), 1440 (s),

1288 (s), 1202 (s), 1108 (s), 1081 (s), 1108 (s), 1016 (s), 952 (s), 779 (s), 722 (s), 625 (m), 555 (s), 448 (m), 419 (m) cm^{-1}. ^{1}H NMR (300 MHz, 25 ^{o}C, D$_2$O): δ 8.8 (d, J = 6.0 Hz, 1 H), 8.5 (m, 1 H), 8.2 (t, J = 7.5 Hz, 1 H), 8.0 (m, 1 H) ppm (all broad signals). ^{31}P{H} NMR (121 MHz, 25 ^{o}C, D$_2$O): δ 0.4 ppm.

2.5.3 Synthesis of 3, [Cd($_\mu$Cl)$_2$(2PyHPO$_3$)]$_n$:

A solution containing 0.10 g (0.63 mmol) of 2PyHPO$_3$H and 0.14 g of CdCl$_2$·2.5H$_2$O (0.63 mmol) dissolved in ~ 5 mL of water in a vial was stirred at room temperature for 15 minutes, followed by heating for an additional 20 minutes at 70 ^{o}C. The solution was filtered and concentrated by heating to 100 ^{o}C for ~ 10 minutes. Colorless crystals suitable for X-ray diffraction were obtained by slow evaporation of the solution at room temperature. Yield = 0.13 g (62 %). Melting point > 250 ^{o}C; on slow heating of the crystalline material, contraction of the solid is visible between 40 – 50 ^{o}C. IR (KBr pellets): 3210 (s), 3163 (s), 3088 (s), 1595 (m), 1519 (m), 1443 (m), 12034 (s), 1154 (m), 1204 (m), 1080 (s), 1031 (s), 1009 (m), 947 (m), 874 (m), 816 (m), 763 (s), 719 (s), 562 (s), 532 (s), 495 (s) cm^{-1}.   Elemental Analysis: (C$_5$H$_7$CdCl$_2$NO$_3$P, 343.39) C: 17.68, H 2.10, N 4.36   Calc: C (17.49) H (2.05) N (4.08). ^{1}H NMR (300 MHz, 25 ^{o}C, D$_2$O): δ 8.8 (d, J = 6.0 Hz, 1 H), 8.6 (tm, J = 8.0 Hz, 1 H), 8.3 (t, J = 7.5 Hz, 1 H), 8.1 (t, J = 7.5 Hz, 1 H) ppm. ^{31}P{H} NMR (121 MHz, 25 ^{o}C, D$_2$O): δ -1.0 ppm.

2.5.4 Synthesis of 4, [{Hg(2PyPO$_3$H)$_2$}H$_2$O]$_n$:

A solution containing 0.10 g (0.62 mmol) of 2PyHPO$_3$H and 0.21 g (0.64 mmol) of Hg(NO$_3$)$_2$·H$_2$O dissolved in a vial containing 5 mL of water was stirred at 100 ^{o}C. After 2 hours, the suspension was filtered. The solid residue was discarded and the clear solution was

kept. From the solution, crystals suitable for X-ray diffraction were obtained. Melting point >300 ^{o}C. Yield = 0.25 g (66 %). IR (KBr pellets): 3540 (s), 3500 (s), 2925 (s), 2905 (m), 1613 (s), 1386 (s), 1013 (m), 929 (s), 770 (m), 733 (m) cm^{-1}. Elemental Analysis: ($C_{10}H_{14}HgN_2O_8P_2$ 552.76), C: 20.68, H 2.19, N 5.15 Calc: C (21.72) H (2.55) N (5.07). ^{1}H NMR (300 MHz, 25 ^{o}C, D$_2$O): δ 8.8 (d, J = 6.0 Hz, 1 H), 8.5 (d, J = 6.0 Hz, 1 H), 8.2 (t, J = 6.8 Hz, 1 H), 8.1 ppm (t, J = 7.0 Hz, 1 H). ^{31}P{H} NMR (121 MHz, 25 ^{o}C, D$_2$O): δ -1.0 ppm.

2.5.5 Synthesis of 5, [Ag$_3$(CF$_3$SO$_3$)$_2$(2PyHPO$_3$)]$_n$:

A solution of 0.10 g (0.63 mmol) 2PyHPO$_3$H was made with 3 mL of water and added to a 2 mL ethanol solution containing 0.16 g (0.63 mmol) of silver(I) trifluoromethanesulfonate. The resulting mixture was stirred at room temperature, under aluminum foil, for 1 hour. The reaction mixture was filtered, the solution kept, and the solid residue (some Ag) was discarded. From the aluminum foil covered solution, crystals suitable for X-ray diffraction were obtained. Melting point: decomposes at 172 ^{o}C. Yield = 0.090 g (22 %). IR (KBr pellets): 3470 (m), 3242 (w), 3173 (w), 3105 (m), 3053 (w), 1623 (s), 1454 (m), 1266 (s), 1172 (s), 1033 (s), 643 (s) cm^{-1}. Elemental Analysis: ($C_7H_5Ag_3F_6NO_9PS_2$, 779.82) C: 10.81, H 0.92, N 1.92 Calc: C (10.78) H (0.65) N (1.8). ^{1}H NMR (300 MHz, 25 ^{o}C, D$_2$O): δ 8.8 (d, J = 6.0 Hz, 1 H), 8.4 (m, 1 H), 8.2 (t, J = 8.0 Hz, 1 H), 8.1 (t, J = 7.2 Hz, 1 H) ppm. ^{31}P{H} NMR (121 MHz, 25°C, D$_2$O): δ -1.0 ppm. ^{19}F{H} NMR (282 MHz, 25 ^{o}C, D$_2$O): δ -79 ppm.

Table 2.1 Crystal Data for Compounds 1-5:

Compound Name with precursor	**1**: $ZnCl_2$	**2**: $ZnBr_2$	**3**: $CdCl_2$	**4**: $Hg(NO_3)_2$	**5**: $Ag(OTf)$
Chemical Formula	$C_5H_5ClNO_3PZn$	$C_5H_5BrNO_3PZn$	$C_5H_7CdCl_2NO_3P$	$C_{10}H_{14}HgN_2O_8P_2$	$C_7H_5Ag_3F_6NO_9PS_2$
Formula Weight	258.89	303.35	343.39	552.76	779.82
Crystal System	Monoclinic	Orthorhombic	Orthorhombic	Monoclinic	Triclinic
Space Group	$P2_1/c$	Pbca	Pbca	$P2_1/n$	P-1
T(K)	213(2)	213(2)	213(2)	213(2)	213(2)
a (Å)	4.9295(5)	9.8688(14)	7.3883(13)	10.9312(15)	9.1388(8)
b (Å)	20.8947(19)	8.5984(12)	15.627(3)	5.6500(8)	9.5668(8)
c (Å)	8.2886(8)	20.49(3)	15.832(3)	12.3486(17)	12.2093(11)
α (°)	90	90	90	90	93.112(2)
β (°)	110.328(5)	90	90	97.920(2)	106.4150(10)
γ (°)	90	90	90	90	117.7150(10)
V (Å^3)	829.90(13)	1738.8(4)	1827.8(6)	755.39(18)	884.52(13)
Z	4	8	8	2	2
Reflections collected	4934	8393	8485	3359	5811
Independent reflections	1956	1756	1649	1348	3954
Data/restraints/ parameter ratio	1953/0/113	1756/6/113	1649/0/122	1348/2/115	3954/2/266
Unique Data (R int)	0.0369	0.0545	0.0538	0.0348	0.0185

D_{calc} (Mg/m^3)	2.072	2.318	2.496	2.430	2.928
F(000)	516	1168	1320	524	736
R indices (all data)	R1 = 0.0380, wR2 = 0.0859	R1 = 0.0595, wR2 = 0.1203	R1 = 0.0588, wR2 = 0.0735	R1 = 0.0704 wR2 = 0.1836	R1 = 0.0396 wR2 = 0.0955
Final R indices [I > 2σ(I)]	R1 = 0.0314, wR2 = 0.0806	R1 = 0.0420, wR2 = 0.1047	R1 = 0.0297, wR2 = 0.0580	R1 = 0.0674 wR2 = 0.1753	R1 = 0.0349 wR2 = 0.0910
Largest difference in peak and hole (e Å^{-3})	0.632 and -0.722	1.111 and -1.115	0.774 and -0.580	6.046 and − 5.119[†]	2.718 and − 2.781[†]

[†] The large electron density peak found in the difference map is associated with the Hg and Ag centers. Various crystals from different samples, solvents and attempts to vary crystal size all resulted in the same problem.

Chapter 3

2-(pyridylmethyl)phosphonic acid: A flexible, multi-dentate ligand for metal phosphonates.

3.1 Introduction

The outcomes of reactions involving functionalized phosphonic acids, RPO_3H_2, with metal salts have shown that the presence of nitrogen donors provides further coordination capabilities affording cages, 1-3D polymers and bimetallic frameworks.[117b,135] Multi-dimensional metal-phosphonate polymers have been discussed as significant platforms for catalysis and luminescent sensors; however, transition-metal-phosphonate cages and clusters are interesting, as well. The synthesis of cages and clusters containing paramagnetic ions is of increasing interest since the early 1990's, after the synthesis of metal-oxalate 2D networks[136] and manganese clusters such as $[Mn_{12}O_{12}(O_2CR)_{16}(H_2O)_4]$[137] were shown to have very unusual magnetic properties. The field of single-molecule magnets (SMM) has widespread applications, but specifically it would allow the development of materials that could provide a higher density of magnetic information storage than current nanoscale ferromagnetic materials.

Metal phosphonates with Fe(III), Co(II), and Cr(III) have been shown to exhibit slow relaxation of magnetization[138] and studies by Winpenny,[139] Chandrasekhar,[140] Zubieta,[141] and Clearfield[138a] into the synthesis of metal phosphonate cages and clusters have begun to catalog magnetic susceptibilities for an increasing number of compounds. The primary advantage of using phosphonates as ligands for the creation of magnetic materials is the presence of three donor oxygen atoms per phosphonate moiety. However, limited solubility in various solvents has stimulated the development of various synthetic strategies to overcome this problem: the addition of co-ligands to help increase solubility was pioneered by Chandrasekhar,[140] Winpenny

has utilized preformed carboxylate cages as reagents,[139] while Zubieta has focused on the use of hydrothermal techniques.[141]

Variation of ligand R groups allows chemical functionality to be introduced into solid frameworks and provides an opportunity to design robust, yet flexible solids with desired physical and chemical properties. Most reports involving functionalized aryl phosphonic acids have employed rigid molecules with the phosphonic acid moiety attached directly to the aromatic ring, which somewhat promotes product predictability.[114,117a,142] Metal phosphonates assembled from the reactions of more flexible ligands, (*i.e.* with a carbon between the aromatic and phosphonic acid groups), *e.g.* (pyridylmethyl)phosphonic acids, are not so well studied, possibly because a serendipitous assembly is more likely.[143] Nevertheless, these ligands may show more interesting properties and afford porous structures that can be compared with products obtained from the analogous carbon-containing acids, pyridine methyl carboxylic acids (PyCH$_2$COOH), that have been used to synthesize monomers, dimers and polymers.[144]

3.1.1 Ligand Synthesis

Based on our previous successful work with 2-(pyridyl)phosphonic acid,[135a] 2-(pyridylmethyl)phosphonic acid, 2PyCH$_2$PO$_3$H$_2$ (Py = pyridine), was selected for our studies, with the rationale being that the additional CH$_2$ group between the functionalities would yield a more flexible ligand, promoting higher dimensional polymeric materials. Surprisingly, studies involving 2PyCH$_2$PO$_3$H$_2$ are limited[98,143b,145] despite complexes with Tc and Pt showing anti-tumor activity in rats.[146] The reaction of hydroxyl(2-pyridyl)methyl phosphonic acid with zinc(II) sulfate produced a hepta-nuclear cluster (Figure 3.1),[145] and the *N*-oxide of the ligand has been shown to react with rare-earth hydroxides to form hydrogen-bonded frameworks

(Figure 3.2).[7,143b] More recent compounds composed of this ligand, the oxalate ion, and lanthanide cations have been shown to support room temperature luminescence, as described in Section 1.6.2.5.[98]
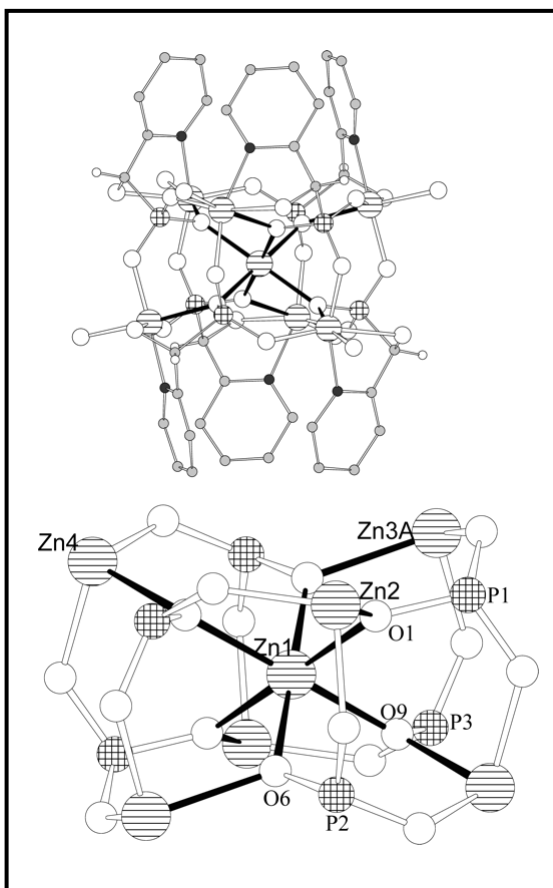
Figure 3.1 Heptanuclear cluster of $[Zn_7\{2\text{-}C_5H_4N)CH(OH)PO_3\}_6(H_2O)_6]SO_4 \cdot 4H_2O$ (top) and inorganic core of cluster (bottom). Taken from Reference 145.
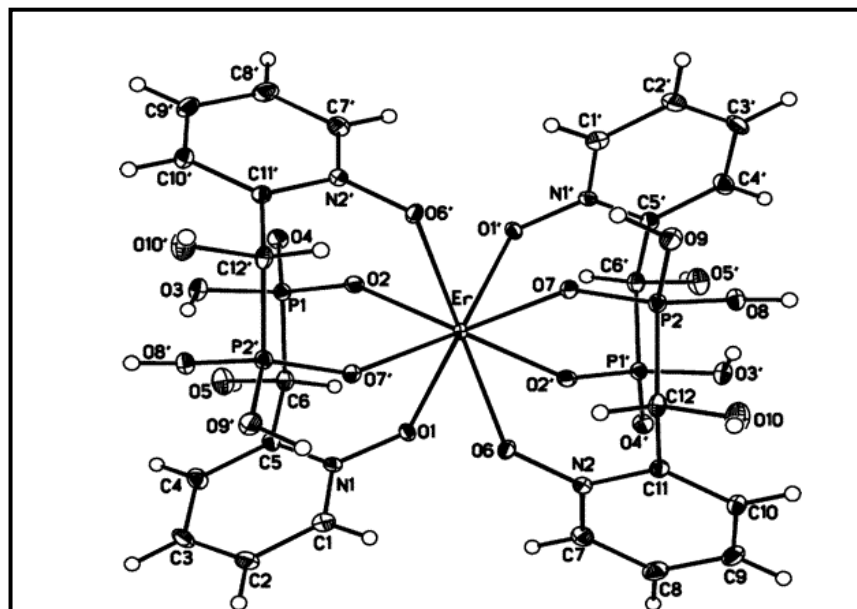
Figure 3.2 Molecular structure for
Er{[(HO)-(O)P(O)C(H)(OH)]C_5H_4NO-}$_3${[(HO)$_2$P(O)C(H)(OH)]C_5H_4NO}·8H_2O, containing three deprotonated ligands and one protonated ligand. Each metal complex is hydrogen bonded with adjacent complexes to form a 3D framework. Adapted from Reference 143b.

Ligand 2PyCH$_2$PO$_3$H$_2$ can be prepared by a modified literature method.[143b] 2-(bromomethyl)pyridine hydrobromide is dissolved in toluene and 40 % NaOH added until strongly basic (Scheme 3.1). Under a nitrogen atmosphere, a solution of n-butyl lithium is added slowly to diethyl phosphite at -78 °C to produce (EtO)$_2$POLi. The room-temperature addition of the lithiated salt to the organic phase from the first step (containing 2-(bromomethyl)pyridine) is followed by overnight reflux, the addition of 6M HCl, and extraction with diethyl ether. Acid hydrolysis of the phosphonate ester, followed by concentration and dissolution of the resulting solid with methanol, yields 2-(pyridylmethyl)phosphonic acid.
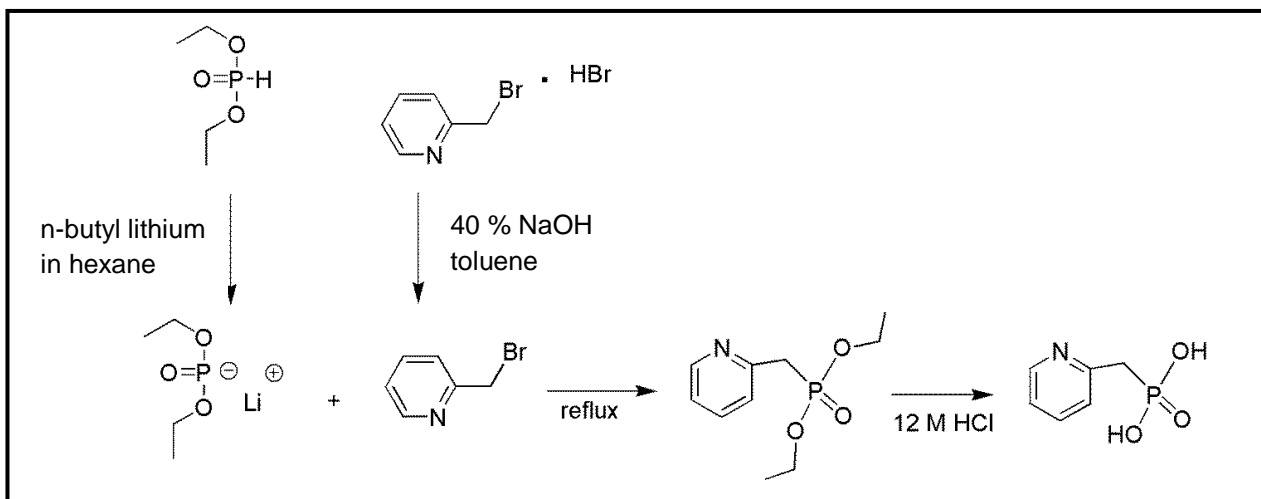
Scheme 3.1 Synthesis of 2-(pyridylmethyl)phosphonic acid.

Our goal was to examine the coordination preferences of 2-(pyridylmethyl)phosphonic acid to construct homo- and heterometal phosphonates and further examine their properties. An overriding aim of this study is that by investigating factors that influence the coordination modes of designed ligands, a strategy to manipulate the resultant structural motif could be developed. Herein we report the synthesis and characterization of a series of metal phosphonates and highlight the diverse potential of functionalized phosphonic acids.

3.2 Results and Discussion

In a typical experiment stoichiometric quantities of the ligand and metal salt were dissolved in water and/or ethanol and placed in an open scintillation vial. The reactions were stirred at room temperature or with gentle heating for ~3 hours. Crystalline materials were obtained by filtration of the reaction mixture to remove any impurities followed by slow evaporation of the solution at room temperature. The structures of all the compounds were determined by single crystal X-ray analysis. A comparison of the experimental powder diffraction data with that

simulated from the single crystal data confirmed that the single crystal structures are representative of the bulk material (excluding **6**, *vide infra*).

In order to examine products based on preferred metal geometry and ligand coordination preferences, metal cations with open coordination sites were selected from the p and d block. Metal perchlorate salts[147] were selected based on their solubility and the lability of the ClO_4^- group, which provides a source of 'free' metal ions for ligand coordination and generally yields crystalline products.

3.2.1 Discussion of Polymers 6 and 7: $[\{M(2PyHCH_2PO_3H)_2(H_2O)_2\}(ClO_4)_2]_n$, M = Mn (6) and Co (7)

The stoichiometric reaction of manganese(II) and cobalt(II) perchlorate with 2-(pyridylmethyl)phosphonic acid dissolved in a 50/50 mixture of ethanol and water at 100 ^{o}C afforded two-dimensional isostructural products **6** and **7**, Figure 3.3, that crystallize in the monoclinic space group $P2_1/c$. The cobalt and manganese atoms exhibit octahedral geometry, with four of the six octahedral sites occupied by oxygen atoms from the phosphonate group. The remaining two sites are occupied by water molecules in a *trans* arrangement. The bond lengths and bond angles of **6** and **7** are similar to other reported manganese and cobalt phosphonates.[148] The phosphonate group links two metal centers via the formation of μ_2-η^2-phosphonato groups and the P-O bonds involved have similar bond lengths of 1.504(5) Å (P1-O1) in **6** and 1.508(3) Å (P1-O3) in **7**. In both, the remaining uncoordinated phosphorus oxygen atoms are protonated (O3 in **6** and O2 in **7**) with longer P-O bond lengths of 1.579(5) Å and 1.576(3) Å, respectively, and each has a protonated heterocyclic nitrogen atom. In **6** the hydrogen atom on O3 could not be located from the difference map, probably because of unresolved twinning that could not be resolved using rotational twin laws.
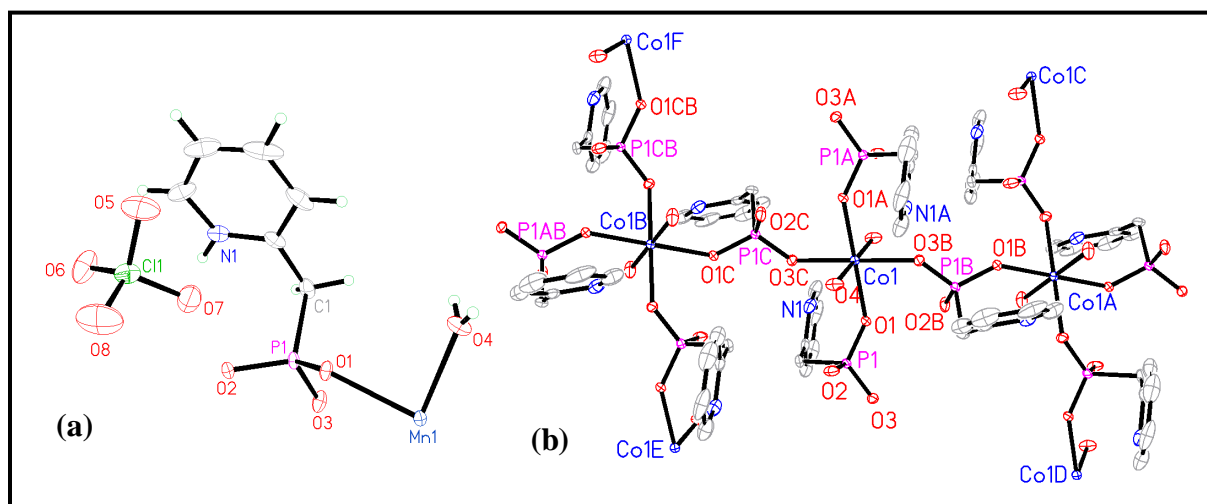
Figure 3.3 (a) Asymmetric unit of **6**. **(b)** Polymeric structure of **7**. Thermal ellipsoids drawn at 30% probability and hydrogen atoms on **7** are omitted for clarity. Selected bond lengths (Å) and angles (^{o}) **6**: Mn1-O1 2.224(4), Mn1-O4 2.172(5), P1-O1 1.504(5), P1-O2 1.501(5), P1-O3 1.579(5), O1-Mn1-O4 87.8(2), O2-P1-O3 106.5(3). **7**: Co1-O1 2.143(2), Co1-O4 2.099(3), P1-O1 1.512(2), P1-O2 1.576(3), P1-O3 1.508(3), O4-Co1-O1 92.59(11), O1-P1-O2 106.22(16).

In the extended polymeric structure the metallic octahedral arrangements are interconnected via tetrahedral [PCO_3] units creating 16-membered rings via bridged oxygen atoms. Within the 16-membered cores, it is possible to observe the alternating arrangement of the pyridine rings throughout the polymer (Figure 3.3). The displaced perchlorate ions are located in the lattice, sandwiched between layers made up of O-Co/Mn-O rings in an arrangement that maximizes hydrogen bonding interactions. Hydrogen bonding occurs between the protonated nitrogen atom of the pyridyl group and the oxygen atom at the metal center from the phosphonate group (N1-O3 in **7**). The distance separating the manganese and cobalt is ~6.5 Å, which indicates no measurable magnetic communication would occur.

The purity of the bulk material was confirmed by powder X-ray diffraction which was compared to the simulated pattern produced from the single crystal CIF file. UV/Vis spectra of

6 and **7** exhibited low-intensity absorbance due to the ligand at 268 nm, however low intensities of octahedral Mn/Co(II) complexes are not unusual.[149] The IR spectra of complexes **6** and **7** have numerous characteristic peaks. Evidence for the presence of perchlorate ions can be obtained from the asymmetric stretch occurring around 1100 cm^{-1}, a sharp band at 625 cm^{-1} attributed to the asymmetric bend, and the weak absorption at 940 – 945 cm^{-1} due to the symmetric stretch.[119a,150] The coordinated water molecules are clearly observed in the infrared spectra, with the bending/stretching vibrations observed at 1600–1650 cm^{-1} and a sharp peak at ~3400 cm^{-1}. In an electrochemical study of **6**, irreversible one-electron reduction of the ligand was observed, as well as a one-electron irreversible oxidation of the metal. The chemical composition of **6** and **7** was confirmed by mass spectrometry.

3.2.2 Discussion of Polymer 8: [Fe$_4$(PyHCH$_2$PO$_3$)$_4$(H$_2$O)$_{12}$(Cl)(ClO$_4$)$_7$·xH$_2$O]

Continuing with the investigation of transition metal salts, the aqueous reaction of iron(II) perchlorate with 2PyCH$_2$PO$_3$H$_2$ was performed, Equation 3.1. Following slow evaporation of the reaction mixture, colorless crystals of **8** were isolated.
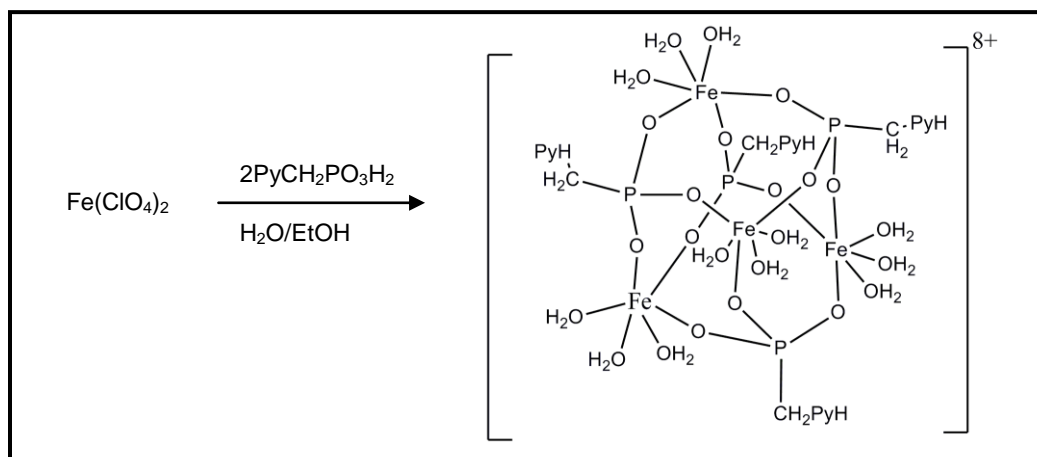
Equation 3.1: Synthesis of the iron(III) phosphonate cage, **8**.

Single crystal X-ray analysis of **8** revealed a tetrameric iron cage, Figure 3.4, in which the iron atoms are linked by bridged oxygen atoms from the phosphonate groups. The cage contains four octahedrally-coordinated iron centers arranged in a cubane type structure. Three of the octahedral coordination sites are occupied by oxygen atoms from the phosphonate groups and the remaining three sites are occupied by water molecules. Each of the remaining vertices has a tetrahedral phosphorus atom that links to the oxygen atoms occupying all midpoints of the cube, forming Fe-O-P bonds.
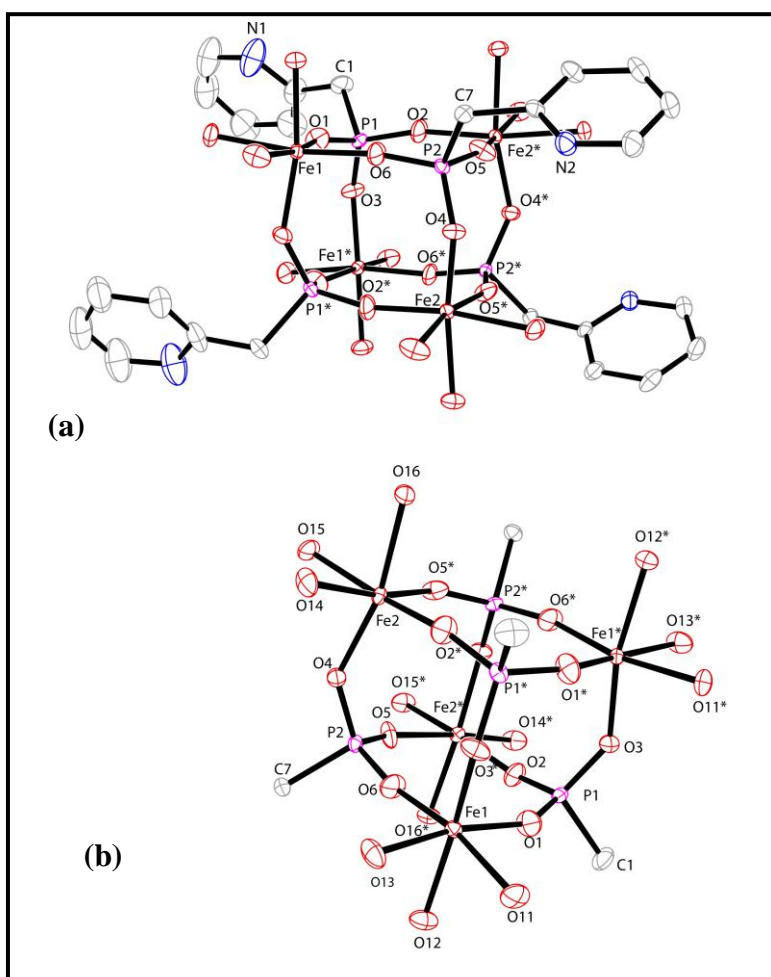
Figure 3.4 Molecular structure of **8**. **(a)** Full molecule **(b)** Fe-O-P core. Thermal ellipsoids drawn at 30% probability and hydrogen atoms are omitted for clarity. Selected bond lengths (Å) and angles (°): Fe1-O1 1.917(4), Fe1-O6 1.888(4), Fe1-O11 2.061(4), Fe2-O4 1.952(4), Fe2-O14 2.055(4), P1-O1 1.507(4), P1-O2 1.494(4), P1-O3 1.524(4), P2-O4 1.518(4), P2-O5 1.514(4), P2-O6 1.493(4), O1-Fe1-O6 97.7(2), O6-Fe1-O11 169.7(2), O4-Fe2-O14 89.52(18).

Compound **8** is fairly unusual as metal phosphonate cages usually require a co-ligand along with the phosphonic acid to circumvent polymerization.[151] In addition, phosphonic acids are not often used for the synthesis of discrete molecules because of their limited solubility.[140,152] However, tetranuclear iron phosphates and phosphonates have been previously documented[153] and have been fairly well studied because tetranuclear iron(III) complexes are known to occur in nature and have been used as model systems for heme proteins.[154]

The seven perchlorate ions, one chloride ion and four doubly deprotonated phosphonate groups bring the total negative charge to -16. With the pyridyl nitrogen atoms protonated, this leaves a charge of +3 to be assigned to each iron atom.

The source of Cl^- in the lattice is likely from reduction of a ClO_4^- anion, as no other chloride source was present. The lattice chloride ion lies on a two-fold axis and plays an important role in the extended structure. The packing diagram of **8** shows four water molecules in a tetrahedral arrangement around each chloride ion, two water molecules from each tetranuclear cage. A polymeric chain is generated from chloride-bridged tetranuclear molecules in the *a* direction, with the perchlorate ions arranged in channels between the tetranuclear units (Figures 3.5 and 3.6).
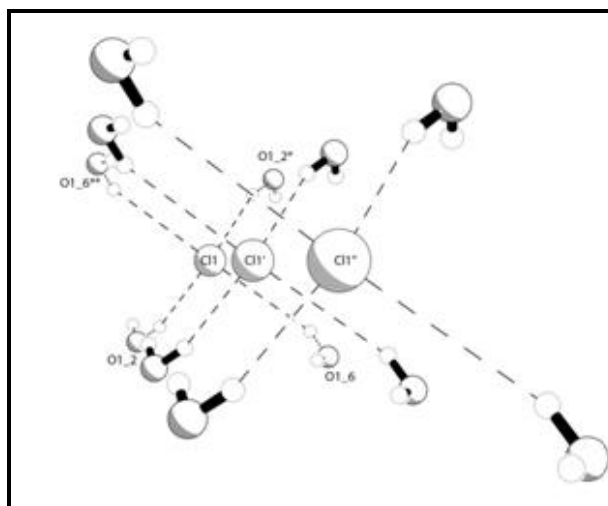
Figure 3.5 Diagram depicting the chloride bridges in the packing diagram
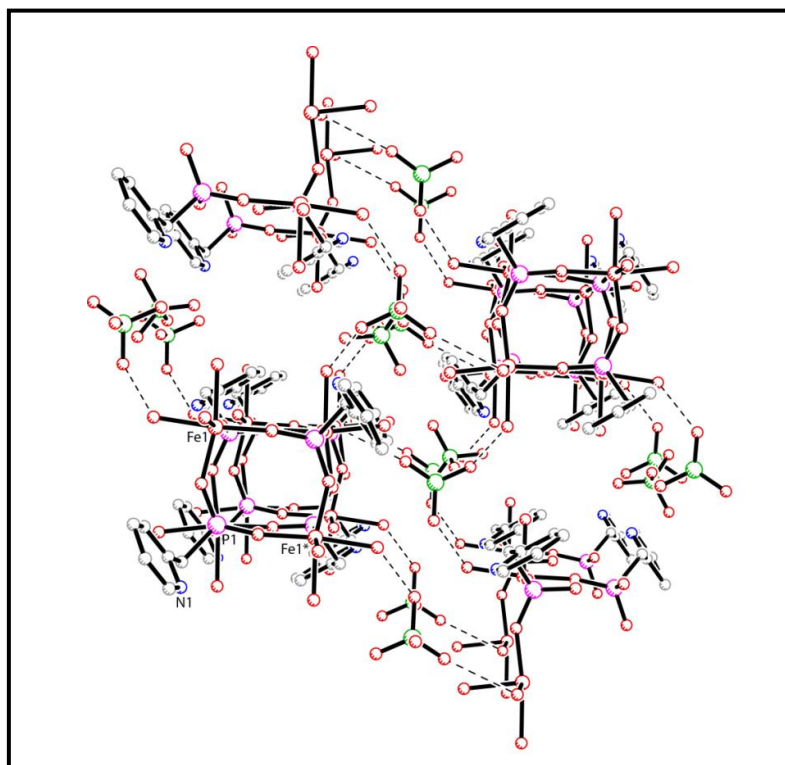
Figure 3.6 Packing arrangement of **8**, showing the perchlorate ions between the tetranuclear cages looking down the *b*-axis. Thermal ellipsoids are drawn at 30% probability. Atom colors: nitrogen = blue, chlorine = green, carbon = grey, phosphorus = pink, iron and oxygen = red.

The Fe-O (phosphonate) bonds in **8** (e.g. Fe1-O1 1.917(4), Fe1-O6 1.888(4)) are slightly longer than those in related iron phosphonate cages[155] but this is possibly due to the greater steric hindrance of the ligand compared to structures generated from unsubstituted phosphoric acids.[151,155] Experimental efforts to prevent protonation of the pyridine nitrogen atom by addition of various bases (sodium hydroxide, triethylamine, and pyridine) were all unsuccessful and led to crystallization of various inorganic salts.

NMR confirms the paramagnetic nature of **8**, with very broad signals being observed. However, the ^{31}P NMR spectrum exhibited three broad peaks at 66, 50 and 19 ppm, indicating possible decomposition upon redissolution. Attempts to recrystallize the solution from the NMR tube to examine decomposition products were unsuccessful.

As seen in **6** and **7**, the UV/VIS spectrum of **8** showed an absorption band at 268 nm that can be assigned to the ligand with no other absorption observed. Infrared spectroscopy of **8** shows a peak at 798 cm^{-1} that can be assigned to the asymmetric Fe-O-Fe stretch vibration and is comparable with other oxo-bridged Fe species.[138a,156] An electrochemical study of **8** in aqueous and DMF solutions revealed that **8** displayed a irreversible one-electron reduction (Fe^{3+} $\rightarrow$ Fe^{2+}). Continuous scanning saw passivation of the electrode and a decrease in response. To confirm the oxidation state of the iron atoms, XPS (X-ray photoelectron spectroscopy) analysis of **8** was performed. High-resolution spectra were acquired for the principal photoelectron peaks of several of the elements detected for the sample. The Fe 2p doublet had the broad, asymmetric structure typical of compounds in which the metal has unpaired d electrons. The more intense Fe 2p 3/2 component was centered at a binding energy of 712.5 eV. This value is at the high end of the range of binding energies reported for Fe compounds (707.4 eV – 712.8 eV),[157] and suggests that the metal is present as Fe(III); however, binding energies reported for Fe(II) and

Fe(III) complexes overlap each other to a great extent. According to the NIST (National Institute of Standards and Technology) XPS database, the binding energy measured for Fe 2p 3/2 in $FePO_4$ is 712.8 eV, which is close to that measured for **8**.[157]

3.2.3 Discussion of Polymers 9 and 10: $[\{Fe_2(2PyHCH_2PO_3H)_6\}(ClO_4)_6]_n$ and $[\{Fe(2PyHCH_2PO_3H)_2(H_2O)_2\}(ClO_4)_2]_n$

As a continuation of the work on iron cages, we were interested in investigating iron precursors with different anions and varied solvent systems. To this end iron(II) nitrate, bromide, and oxalate were reacted with $2PyCH_2PO_3H_2$ in a range of solvents: DMF, CH_3NO_2, MeOH etc. All reactions yielded oily or amorphous material. However, the stoichiometric reaction of $2PyCH_2PO_3H_2$ with $Fe(ClO_4)_2$ in D_2O yielded a crystalline product. D_2O was selected as it is known to alter molecular interactions and can perturb the usual crystallization process.[158] Examination of the crystals under the microscope revealed two types of crystals—colorless blocks, **9**, and colorless plates, **10**. A single-crystal X-ray diffraction study of **9** found it to crystallize in the trigonal space group, $R\overline{3}$, and **9** is an aesthetically pleasing Fe(III) phosphonate chain with three-fold symmetry along the main axis. Figure 3.7 depicts the atom connectivity and the highly symmetrical packing arrangement of the polymeric material. In the asymmetric unit of **9** are found one zwitterionic ligand and two iron centers; each iron(III) cation is at $1/6^{th}$ occupancy. The charge is balanced by the presence of a single lattice perchlorate molecule. Each iron atom exists in close to perfect octahedral geometry and every coordinated oxygen atom is from a phosphonate group that bridges the iron centers.

Single crystal X-ray analysis of **10**, the crystalline plate, found it to be monoclinic, space group $P2_1/c$ (Figure 3.8). Crystalline **10** forms a polymeric sheet network that shows structural similarity to **6** and **7**. The asymmetric unit has one iron atom on an inversion center, a

phosphonic acid ligand, and one disordered perchlorate anion. As with **9**, the iron is found in an octahedral environment; however, a water molecule occupies one of the coordination sites that in **9** is occupied by an oxygen atom from the phosphonate group.
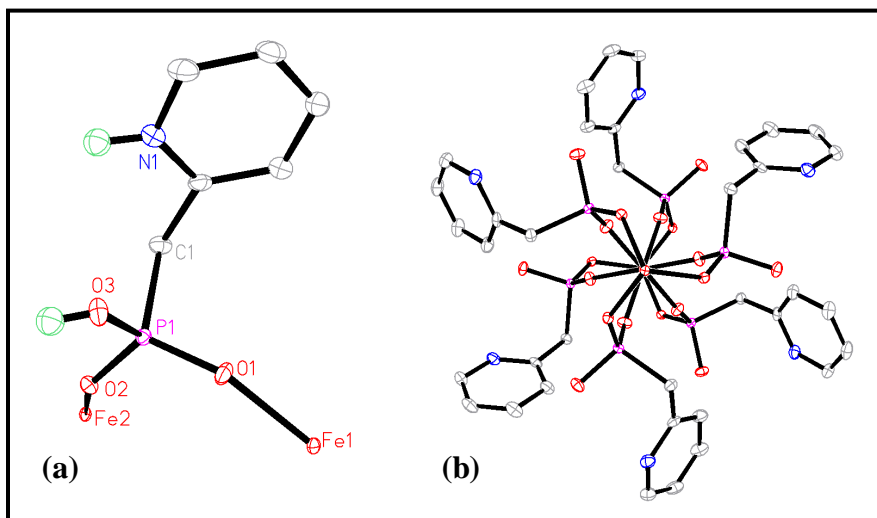
Figure 3.7 **(a)** The asymmetric unit of **9**, hydrogen atoms other than those on O3 and N1 are omitted for clarity. **(b)** The symmetrical polymeric chain arrangement of **9**, all hydrogen atoms are omitted for clarity. Thermal ellipsoids of both are drawn at 30% probability. Selected bond lengths (Å) and angles (^{o}): Fe1-O1 1.9870(17), Fe2-O2 1.9873(16), P1-O1 1.4921(17), P1-O2 1.5013(17), P1-O3 1.5624(18).
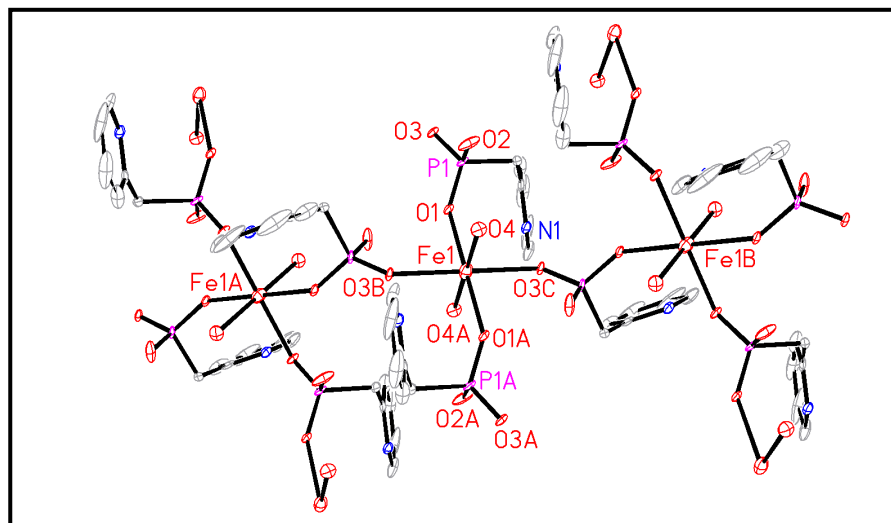
Figure 3.8 Molecular structure of polymeric **10**. Thermal ellipsoids drawn at 30% probability, hydrogen atoms and the disordered perchlorate ion are omitted for clarity. Selected bond lengths (Å) and angles (^{o}): Fe1-O1 2.292(4), Fe1-O4 2.343(5), Fe1-O3 2.354(4), P1-O1 1.504(4), P1-O2 1.570(5), O1-Fe1-O4 93.59(15).

The Fe-O bond lengths of **9** and **10** show distinct differences, with distances ~1.9 – 2.0 Å in **9**, and 2.2 – 2.3 Å in **10**. These differences are likely due to the different oxidation states of the iron centers; in **9**, the iron centers are Fe^{3+} with smaller ionic radii than the Fe^{2+} of **10**.[159] These bond lengths and angles are comparable to other documented species in similar oxidation states.[160] A visible survey of the crystalline product under the microscope found **9** to be the major product, but due to the small size and similar crystal color, attempts at separation proved futile. Attempts to generate individual products of **9** and **10,** such as by performing the reaction under N_2 etc., were unsuccessful.

3.2.4 Discussion of Polymer 11: [AgPb(2PyCH$_2$PO$_3$)(NO$_3$)]$_n$

Bimetallic metal phosphonates of the late transition metals still remain fairly limited;[161] however, they may have useful properties not available to single metal systems. For the synthesis of bimetallic polymers, metal-salt solubility, the coordination preference of the reactant metals, and potential metathesis reactions need to be considered. With these factors in mind, the reaction of silver(I) triflate, lead(II) nitrate, and 2-(pyridylmethyl)phosphonic acid was performed in a 1:1:1 ratio. Slow evaporation of the solution resulted in the isolation of colorless crystals of **11**. Single crystal determination showed that **11** crystallizes in the monoclinic space group *P*2$_1$/*c*. The asymmetric unit of **11** contains one silver atom, a lead atom, one ligand, and a coordinated nitrate ion (Figure 3.9).
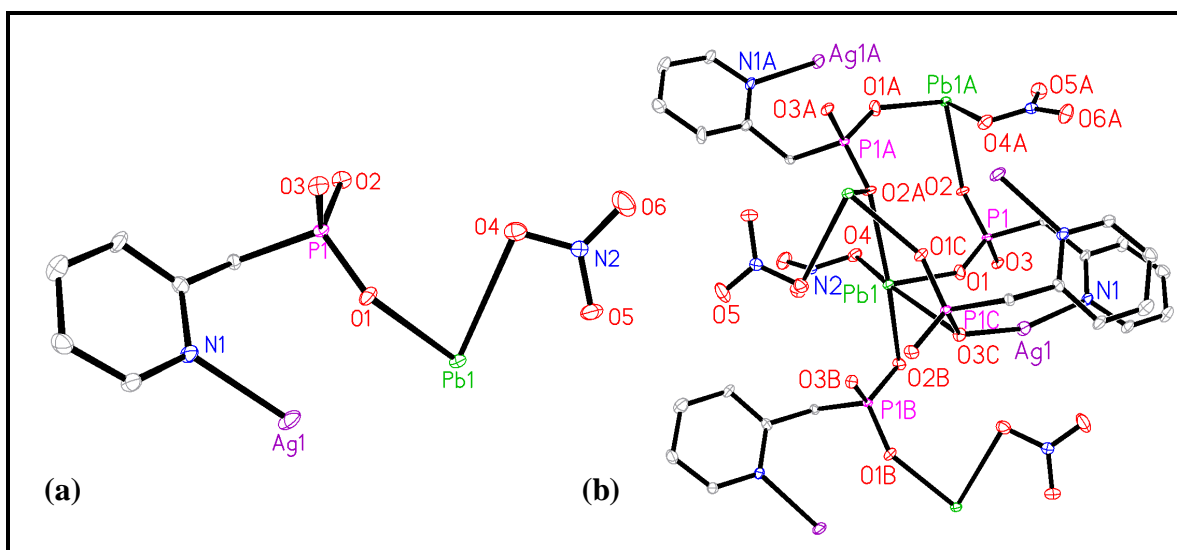
Figure 3.9 Molecular structure of **11**. **(a)** Asymmetric unit **(b)** Polymeric arrangement. Hydrogen atoms are omitted for clarity, thermal ellipsoids drawn at 30% probability level. Selected bond lengths (Å) and angles (°): N1-Ag1 2.197(9), Ag1-O3 2.183(6), Pb1-O1 2.383(7), Pb1-O4 2.737(8), P1-O1 1.518(8), P1-O2 1.519(7), P1-O3 1.550(6), N1-Ag1-O3A 161.5(3), O1-Pb1-O4 76.2(2), O1–P1-O2 115.8(4).

Unlike in polymeric **6** and **7**, the pyridyl nitrogen atom participates in bonding. Although silver-nitrogen coordination did not occur with polymer **5**, which utilized 2-(pyridyl)phosphonic acid, this coordination is still not too surprising considering the coordination preference of silver.[162] The silver atom is ligated to the pyridyl nitrogen atom and a symmetry-generated phosphonate oxygen atom (O3) that forms a bridge between the silver and lead centers. The geometry around the silver atom is distorted from linear geometry with an angle of 161.5(3)°.

The coordination sphere of the lead atom is occupied by oxygen atoms with Pb-O bond lengths between 2.383(7) - 2.757(7) Å that show no unusual discrepancies. If Pb-O distances of less than 2.8 Å are considered, then each lead center is five-coordinate in distorted square pyramidal geometry; but if the Pb-O distance is increased to 2.8 Å, then the lead atom would have seven-coordinate geometry. The overall structural motif of **11** is quite complicated and

when assembled in two dimensions, the anti-parallel packing arrangement of the pyridyl rings and nitrate groups can be observed, possibly because of the need to minimize lone pair repulsions. Overall, there are layers of Pb-O centers that are linked by phoshonate groups and pyridyl-Ag-O bridges. The phosphonic acid is doubly deprotonated and, along with a nitrate ion, balances the +3 cationic charge, Figure 3.10.
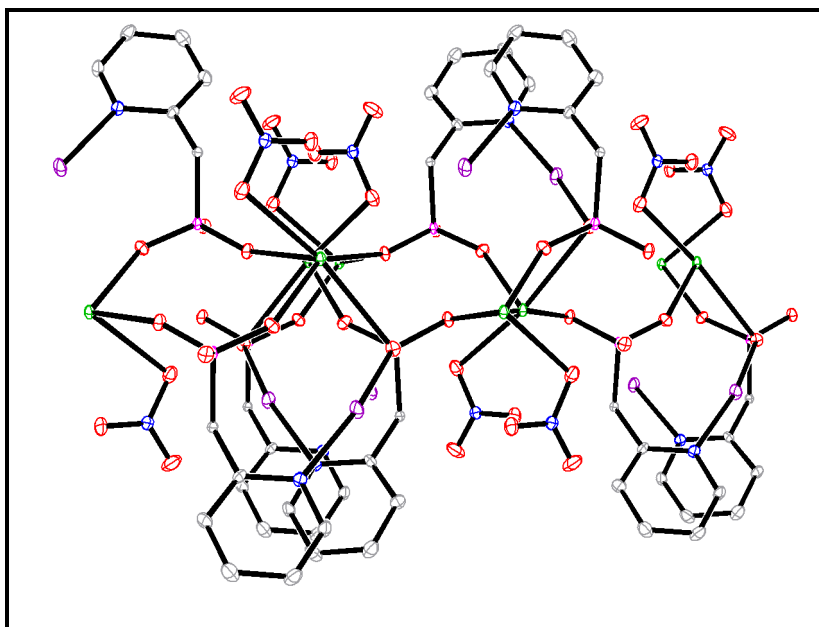
Figure 3.10   Polymeric structure of the bimetallic phosphonate, **11**, oxygen atoms = red, nitrogen atoms = blue, carbon = grey, phosphorus = pink, silver = purple, lead = green

XPS studies on **11** confirmed the presence of both Pb and Ag; the Pb 4f 7/2 component of the 4f doublet was located at 138.7 eV, which is within the range of values reported for Pb(II) compounds (137.7 eV – 139.5 eV).[157] This value can be compared with the binding energy reported for the Pb 4f 7/2 component in $Pb_3(PO_4)_2$ of 138.6 eV.[157]   The binding energies reported for Ag 3d 5/2 in silver and its compounds do not differ substantially, making it difficult to determine the oxidation state of silver in an unknown sample. It is possible to distinguish the element from its compounds by also measuring the kinetic energy of the MNN Auger peaks and

calculating the Auger parameter. The binding energy of the Ag 3d 5/2 peak in **11** was 367.9 eV and the kinetic energy of the Ag MNN peak 350.2 eV, yielding a modified Auger parameter of 718.1 eV. From this, it can be concluded that Ag is present as either Ag(I) or Ag(II), however, as earlier stated, for charge balance, and based on previous results, Ag(I) is more likely. X-ray powder diffraction on bulk **11** did not match the simulated diffraction pattern. The XPS analysis showed the presence of sulfur and fluorine in the bulk powder, which arises from the triflate precursor. Therefore, IR and NMR analyses were performed using crystalline material.

3.2.5   Discussion of Polymer 12: [Pb(2PyHCH₂PO₃H)(NO₃)₂]ₙ and Polymer 13, [Ag₃(2PyCH₂PO₃H)(SO₃CF₃)₂]ₙ

In light of the isolation of the bimetallic Pb/Ag polymer, the separate reactions of both metal salts were performed to compare the individual metal structural motifs and to gain insight into the prediction of material architecture. Furthermore, compared to transition metal phosphonates, main group metal phosphonates remain much less well studied, with the exception of aluminum and calcium.[163] Lead(II) has been shown to exhibit different structural geometry from the similarly charged transition metals (Cd, Zn, Hg) due to the presence of lone pair electrons.[164] With this in mind, the individual stoichiometric reactions of lead(II) nitrate and silver triflate with 2PyCH₂PO₃H₂ were performed. From the reaction of lead(II) nitrate with 2PyCH₂PO₃H₂ colorless crystals of **12** were isolated, Figure 3.11. In the asymmetric unit of **12** is one lead atom, one phosphonate ligand and two nitrate ions. The phosphonic acid is singly deprotonated while the pyridyl nitrogen atom is protonated. The Pb1-O2 distance of 2.257(5) Å is on the shorter end of Pb-O distances but not unprecedented; the pillared, layered structure of catena-(bis(μ₅-carboxyethylphosphonato)-trilead) has a Pb-O distance of ~2.26 Å.[165a] Other Pb-O distances in the range 2.595 – 2.718(6) Å are comparable to those observed in other lead(II)

phosphonates.[163,165] The one-dimensional chain arises from bridged nitrate ions that link the lead centers. **12** is not as thermally stable as expected (no coordinated or lattice water molecules) and melts at 125–127 °C; the thermal gravimetric analysis (TGA) shows decomposition of the organic ligand in this temperature range.
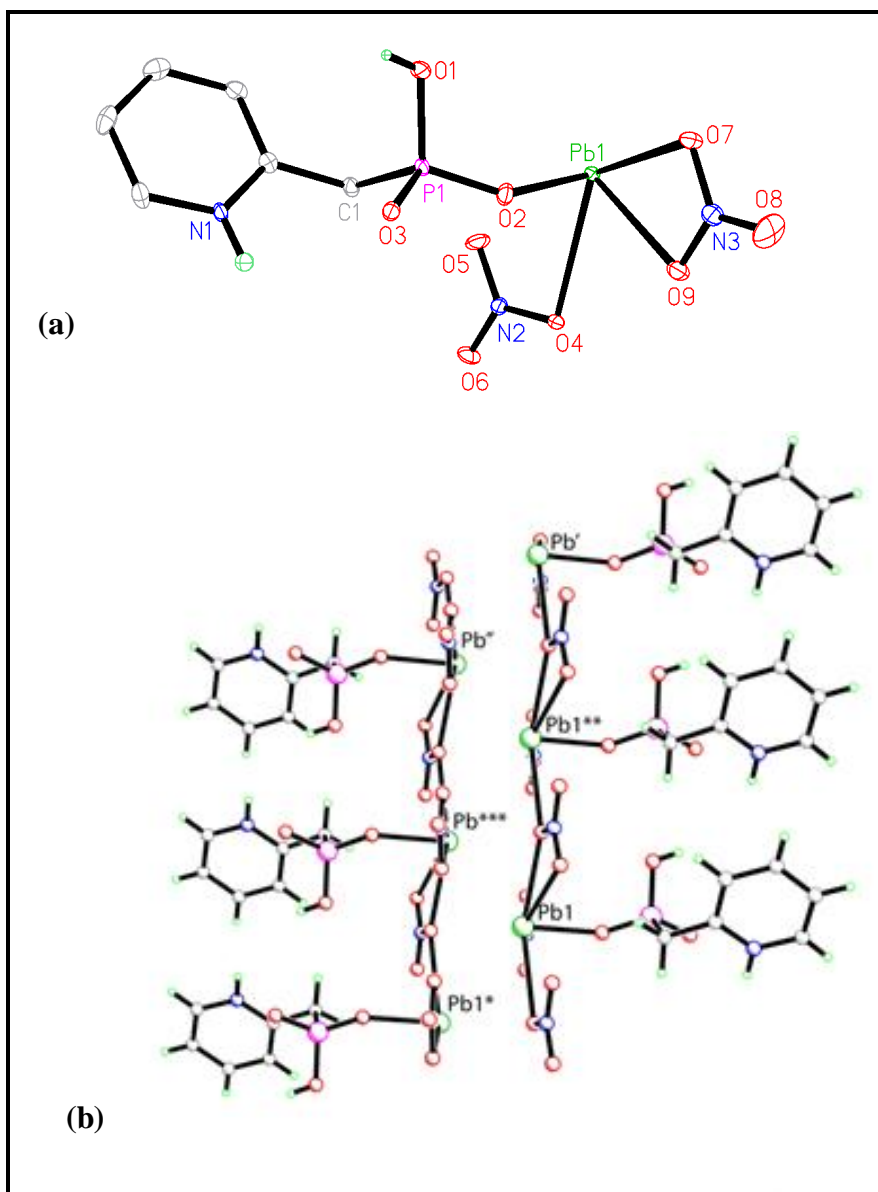
Figure 3.11 Crystal structure of **12**, $[Pb(2PyHCH_2PO_3)(NO_3)_2]_n$, thermal ellipsoids at 30% probability. Hydrogen atoms excluding H-O1 and H-N1 are omitted for clarity. **(a)** Asymmetric unit, **(b)** Polymeric chain. Selected bond lengths (Å) and angles (°): Pb1-O2 2.257(5), Pb1-O4 2.757(5), Pb1-O7 2.594(6), Pb1-O9 2.651(6), P1-O1 1.568(5), P1-O2 1.506(5), P1-O3 1.516(5), O2-Pb1-O7 79.93(18), O2-Pb1-O4 81.19(18), O1-P1-O2 110.3(3).

From the silver triflate reaction, concomitant with a metallic silver deposit, colorless crystals of **13** were isolated. Solid state analysis of these crystals revealed a two-dimensional polymer, Figure 3.12.
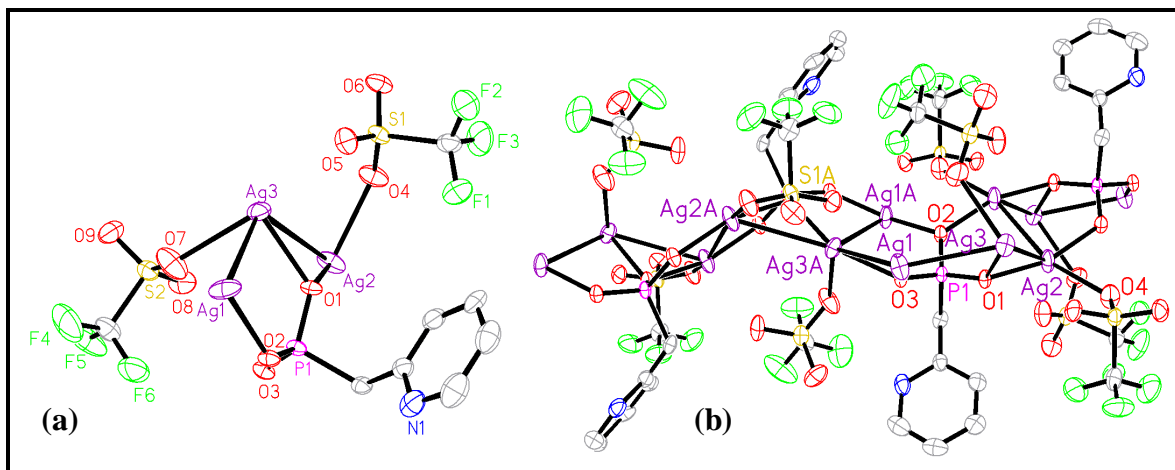
Figure 3.12 **(a)** Asymmetric unit of **13,** $[Ag_3(2PyCH_2PO_3H)(SO_3CF_3)_2]_n$, and **(b)** Polymeric form. Thermal ellipsoids at 30% probability level; hydrogen atoms are omitted for clarity. In the polymeric form oxygen = red, nitrogen = blue, carbon = grey, phosphorus = pink, silver = purple, fluorine = green, sulfur = yellow. Selected bond lengths (Å) and angles (°): Ag1-O3 2.154(5), Ag1-Ag3 3.091(2) , Ag2-O1 2.200(5), Ag3-O1 2.279(5), Ag3-O7 2.547(7), Ag2-Ag3 3.233(2), P1-O1 1.522(5), P1-O2 1.521(6), P1-O3 1.518(5), O1-Ag3-O7 92.5(3), O3-Ag1-Ag3 88.57(14), Ag1-Ag3-Ag2 , O3-P1-O1 112.2(3).

A single-crystal diffraction study on **13**, Figure 3.12, revealed that the asymmetric unit has three crystallographically unique silver atoms, which in the extended structure form a zig-zag chain. The doubly-deprotonated phosphonate ligand links the silver atoms with O1 to bridge Ag2 and Ag3, while O2 bonds to Ag1. Each of the silver atoms has a different coordination sphere, and interestingly, when compared to the bimetallic polymer **11**, there is no coordination to the unprotonated pyridyl nitrogen atoms. Ag1 is four-coordinate, with two Ag interactions (Ag3, Ag3A) and bonds to bridged oxygen atoms from the phosphonate moiety. Ag2 is five-coordinate, with argentophilic interactions to Ag3 and a symmetry equivalent Ag2A. The remaining three coordination sites are taken up by an oxygen atom from the triflate anion (O4)

and two phosphonate oxygen atoms (O1, O2). With a coordination number of six, Ag3 has three Ag-bonding interactions (Ag1, Ag2, Ag1A) and the remaining sites are occupied by oxygen atoms—one triflate (O7) and two phosphonate oxygen atoms (O1, O3)), Figure 3.13.
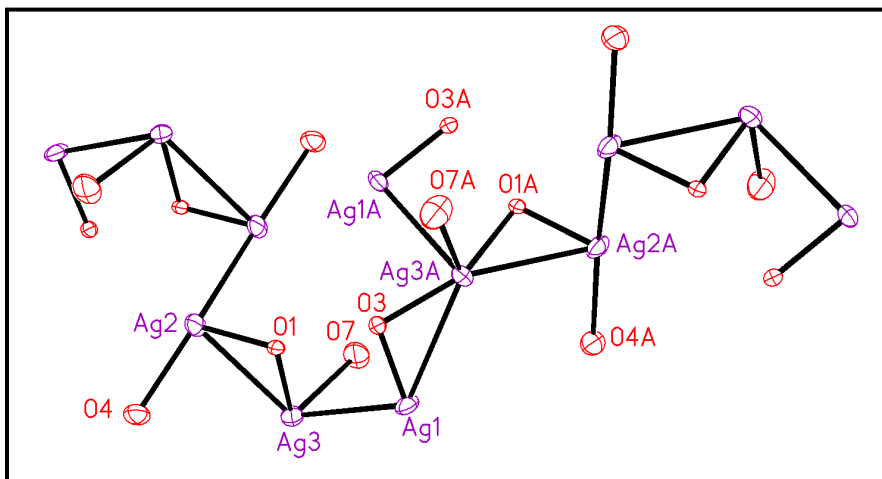
Figure 3.13 A diagram depicting the argentophilic interactions in **13**. Selected bond lengths (Å): Ag1- Ag3 3.091(2), Ag2 - Ag3 3.233(2).

Coordination of the triflate anion is not common,[128] being a labile leaving group, but in polymer **13**, two triflate groups participate in bonding to two silver atoms, (Ag2 and Ag3), as seen previously with polymer **5** (Section 2.2.4). Counter-ion coordination and Ag–Ag interactions[129] both help to stabilize the polymeric network. The silver–silver distances fall on the shorter end of documented Ag–Ag interactions, which vary from 3.091 – 3.474 Å.[131,132] The mass spectral analysis showed a fragmentation pattern consistent with the X-ray structural determination and the [107]Ag, [109]Ag isotope pattern was clearly observed.

The presence of fairly short argentophilic interactions,[166] Figure 3.13, prompted us to investigate the luminescence of **13**. Excitation at 280 nm produced an intense emission peak at 580 nm, and a broad emission at 340 nm (Figure 3.14).
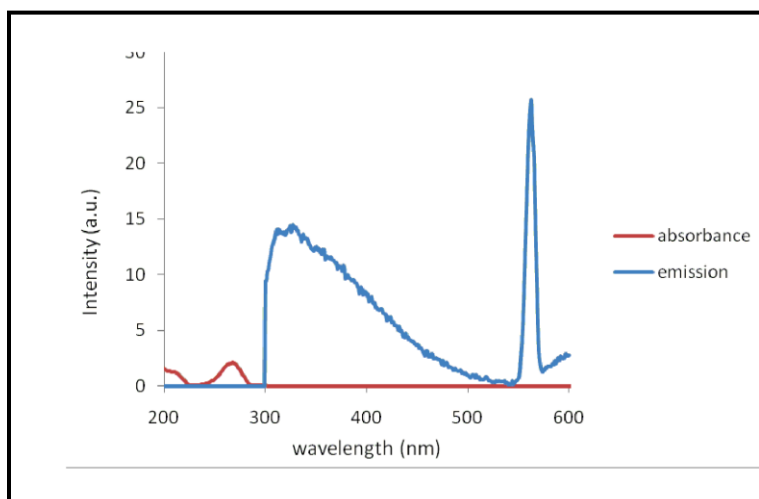
Figure 3.14 Emission spectrum of **13**, [Ag$_3$(2PyCH$_2$PO$_3$H)(SO$_3$CF$_3$)$_2$]$_n$. Excitation at 280 nm.

Excitation of the free ligand at 265 nm shows emission at 326 nm and 623 nm. The broad peak observed at 340 nm is attributed to emission from the ligand. In the solid state, **13** shows good photostability, although in solution slow decomposition to metallic silver occurs. Polymeric **13** is thermally stable with decomposition occurring at 250 - 256 ^{o}C.

3.3 Conclusion

The results demonstrate that modification of the organic moieties of the phosphonate ligand RPO$_3^{2-}$ can significantly influence the structure of the final products. A number of new coordination polymers with 2-(pyridylmethyl)phosphonic acid have been synthesized and show the varying coordination modes possible and the rich variety of structures that can be obtained. In the majority of isolated structures the pyridine nitrogen atom did not coordinate to the metal centers. Nonparticipation of the pyridine group is quite unusual,[167] but is probably due to the acidic medium and subsequent protonation of the heterocyclic nitrogen atom, which in turn limits polymer dimensionality. When comparing the bimetallic coordination polymer, **11**, to the individual components, **12** (Pb) and **13**, (Ag), it is clear that the goal of crystals by design

remains an ongoing challenge. However, one can observe the important role that the anion plays in stabilizing the polymers and cages through hydrogen bonding. In our studies, employing perchlorate salts proved useful for obtaining crystalline products but always afforded complexes with lattice incorporated perchlorate anions, which can reduce polymer dimensionality and porosity.

Isolation of the tetrametric iron phosphonates, **8**, demonstrates how functionalized phosphonic acids could be used as support ligands for the preparation of paramagnetic transition metal cages, and as possible biological mimics. One advantage of working with phosphonate ligands is the diverse geometries possible with the tetrahedral PO_3 bridging unit; if the growth of two-dimensional lattices could be stopped before 2D frameworks form, the resulting structural anisotropy might lead to the generation of magnetic anisotropy.[138b] The recent work investigating magnetic susceptibility of iron cages shows promise for the usefulness of phosphonate polymers as potential magnetic materials, and plans for future SQUID (superconducting quantum interference device) analysis with the iron cage, **8**, are underway.

3.4 Materials and Methods

All manipulations were performed under aerobic conditions. All reagents were purchased from Aldrich and used as received. Crystal data were collected with a Bruker SMART 1000 or Oxford Gemini diffractoometer, molybdenum radiation (λ = 0.7107 Å) at –50, -60 or -100 ^{o}C. Crystals were mounted on glass fibers using paratone oil. The data were corrected for absorption. Structures were solved by direct methods[134] and refined[134] via full-matrix least squares. Crystal data for **6** − **13** can be found in Table 3.1. Hydrogen atoms were placed in idealized positions except certain H_2O molecules and NH atoms that were localized from the

electron density map and refined with distant restraints. The ^{1}H spectra were recorded at 300 MHz on a Varian Mercury spectrometer or on a Bruker Avance 500 MHz instrument. IR analysis was conducted as KBr discs on a MIDAC M4000 FT IR spectrometer, and mass spectrometry analysis was carried out using an Ultraflex III tof/tof mass spectrometer (Bruker Daltonics, Germany), and run under positive ionization mode using α-cyano 4-hydroxy cinnamic acid as the matrix. XPS analysis was run at La Trobe Centre for Materials and Surface Science, in Melbourne, Australia. Fluorescence measurements were recorded on a Varian Cary Eclipse fluorescence spectrophotometer and analyzed using Cary Eclipse Scan Application v 1.1(132). X-ray powder diffraction spectra were recorded using Siemens Kristalloflex Diffraktometer D5000. Simulation of powder diffraction patterns were obtained using Mercury, V: 2.3. Melting points were determined in capillaries and are uncorrected.

3.5 General Experimental

In order to elucidate the optimal experimental conditions for metal phosphonate formation, a combinatorial approach was used that examined metal precursors, solvent, temperature and pH. From this study it was found that metal perchlorates and nitrates were generally the most conducive to yielding crystalline material. Using a mixture of EtOH/H_2O as a solvent provided the correct balance for solubility and generating crystalline material by evaporation in a reasonable time frame (1 – 2 days). Performing the reactions under basic conditions (NaOH, pyridine, or addition of NEt$_3$) proved unsuccessful, affording either metal hydroxides or non-crystalline material.

3.5.1 Synthesis of 2-(pyridylmethyl)phosphonic acid

A 15.8-gram sample of 2-(bromomethyl)pyridine hydrobromide was dissolved in 50 mL of toluene and 40 % NaOH was added, using an ice bath, until strongly basic. The organic phase was extracted and dried over $MgSO_{4(s)}$. At the same time, under a nitrogen atmosphere, a hexane solution of n-butyl lithium (55 mL) was added slowly to diethyl phosphite (56 mL) via addition funnel at -78 °C using an acetone/dry ice bath. Once the addition was completed, the reaction mixture was allowed to warm up to room temperature. Eighty mL of the $(EtO)_2POLi$ solution was added at room temperature under a nitrogen atmosphere to the previously obtained organic phase. The resulting mixture was refluxed overnight. Heating was stopped and 6 M HCl and diethyl ether were added to the aqueous phase and it was extracted with ether. The ether was dried and concentrated, checking the purity of the product by ^{31}P NMR.[7] The product was then hydrolyzed using 12 M HCl and monitored by ^{31}P NMR. The aqueous phase was concentrated and the remnant solid was redissolved in methanol. Methyl oxirane was added, monitoring pH, to eliminate excess acid, yielding the 2-(pyridylmethyl)phosphonic acid.

3.5.2 Synthesis of 6, [{Mn(2PyHCH$_2$PO$_3$H)$_2$(H$_2$O)$_2$}(ClO$_4$)$_2$]$_n$

The reagents, 0.10 g (0.58 mmol) of 2-pyridylmethylphosphonic acid and 0.14 g (0.55 mmol) of manganese perchlorate hexahydrate, were added to 3 mL of 50/50 EtOH/H_2O solution and stirred until the reactants dissolved. The mixture was heated at 100 °C. After 3 hours, the reaction was filtered and the pale pink filtrate kept. From the solution, pale pink crystals of **6** suitable for X-ray crystallography were obtained. Yield = 0.057 g (16%). Melting point: 157 - 160 °C. IR (KBr pellet, cm^{-1}): 3336(s), 1629(s), 1534(m), 1473(m), 1420(m), 1386(w), 1306(w), 1249(w), 1143(s), 1086(s), 956(m), 941(m), 800(s), 838 (m), 751(m), 717(w). No signals were

detected in the ^{1}H NMR experiment or the ^{31}P NMR experiment. MS obs, (calc): 520.654 (519), M$^+$ - H$_2$O – ClO$_4^-$.

3.5.3 Synthesis of 7, [{Co(2PyHCH$_2$PO$_3$H)$_2$(H$_2$O)$_2$}(ClO$_4$)$_2$]$_n$

Compound **7** was prepared by the same method as was used for **6**. A 0.10-gram sample (0.58 mmol) of 2-pyridylmethylphosphonic acid and 0.21 g (0.58 mmol) of cobalt perchlorate hexahydrate were combined.   Yield = 0.026 g (7.1 %). At 63 ℃ color changed from pink to purple and shrinkage was observed at 76 ℃. Melting point: 102 – 105 ℃. IR (KBr pellet, cm^{-1}): 3412 - 3390 (s), 1633(s), 1618(s), 1542(w), 1470(w), 1390(w), 1413(w), 1310(w), 1135(s), 1101(s), 1082(s), 941(m), 792(m), 701(m), 626(s). No signals were detected in the ^{1}H NMR experiment or the ^{31}P NMR experiment. MS obs, (calc): 604.18 (604.07), M$^+$ - 2H$_2$O.

3.5.4 Synthesis of 8, [Fe$_4$PyHCH$_2$PO$_3$)$_4$(H$_2$O)$_{12}$(Cl)(ClO$_4$)$_7$·xH$_2$O]

In a glass scintillation vial, Fe(ClO$_4$)$_2$ (0.074 g, 0.29 mmol) and 2-pyridylmethylphosphonic acid (0.050 g 0.29 mmol) were dissolved in 3 mL of 50/50 EtOH/H$_2$O and gently heated to ~60 ^{o}C with stirring. After 3 hours, the pale brown colored mixture was filtered. After evaporation of the filtrate, colorless crystals suitable for X-ray crystallography were obtained. Yield = 0.10 g (22%). Melting point: sweat observed at 93 - 94 ℃, melting point at 110 - 103 ℃.   IR (KBr pellet, cm^{-1}): 2702–3600 (v. broad strong stretch), 2358 (w), 1616 (s), 1541 (m), 1415 (w), 1388 (w), 1143 (s), 941 (m), 833 (w), 798 (m), 721 (w). ^{1}H NMR spectrum not observed. ^{31}P NMR spectrum: very broad signals observed at 19, 53, and 66 ppm. MS obs, (calc): 664 (664) ½ M$^+$ - 2ClO$_4^-$, Cl$^-$, 1253.46 (1255), M+ - 2ClO$_4^-$, Cl$^-$, -4H$_2$O.

3.5.5 Synthesis of 9 and 10, [{Fe$_2$(2PyHCH$_2$PO$_3$H)$_6$}(ClO$_4$)$_6$]$_n$ and [{Fe(2PyHCH$_2$PO$_3$H)$_2$(H$_2$O)$_2$}(ClO$_4$)$_2$]$_n$

In a glass scintillation vial, Fe(ClO$_4$)$_2$ (0.074 g, 0.29 mmol) and 2-pyridylmethylphosphonic acid (0.050 g, 0.29 mmol) were dissolved in 3 mL D$_2$O and gently heated to ~60 ^{o}C with stirring. After 3 hours, the pale brown colored mixture was filtered. After slow evaporation of the filtrate, colorless crystals suitable for X-ray crystallography were obtained. Two types of crystals were observed under the microscope, colorless blocks, **9**, and colorless plates, **10** (minor product).

3.5.6 Synthesis of 11, [AgPb(2PyCH$_2$PO$_3$)(NO$_3$)]$_n$

In a glass scintillation vial, 2-pyridylmethylphosphonic acid (0.10 g, 0.58 mmol), lead(II) nitrate (0.19 g, 0.58 mmol), and silver(I) triflate (0.15 g, 0.58 mmol) were added to 3 mL of 50/50 EtOH/H$_2$O solution. The mixture was stirred until all reactants dissolved and then covered with aluminum foil. The mixture was heated at 150 ^{o}C, and after 3 hours the reaction was filtered. The filtrate was kept in the dark. Colorless crystals suitable for X-ray crystallography were obtained by slow evaporation of the solution. Yield = 0.022 g (6.9 %). Melting point: 205 – 207 ^{o}C. IR (KBr pellet, cm^{-1}): 3440(s), 1629(s), 1384(s), 1299(m), 1253(m), 1170(m), 1098(m), 1074(m), 1035(m), 915(w), 800(w), 722(w), 642(m). ^{1}H NMR (D$_2$O, 300 MHz, 25 ^{o}C): 3.7 (br d, 2H), 6.3 (m, 2H), 6.8 – 7.4 (m, 2H) ppm. ^{31}P NMR 13 ppm (s).

3.5.7 Synthesis of 12, [Pb(2PyHCH$_2$PO$_3$H)(NO$_3$)$_2$]$_n$

In a small beaker, 2-pyridylmethylphosphonic acid (0.10 g, 0.58 mmol) and lead(II) nitrate (0.19 g, 0.58 mmol) were dissolved in 3 mL of 50/50 EtOH/H$_2$O solution. The mixture was

stirred at 150 $^{\circ}$C. After 3 hours, the reaction was filtered to remove any precipitate and the filtrate stored at room temperature. Colorless crystals suitable for X-ray crystallography were obtained after 7 days. Yield = 0.042 g (14 %). Melting point: 125 – 127 $^{\circ}$C. IR (KBr pellet, cm^{-1}): 3371(s), 1641(s), 1622(s), 1543(m), 1473(s), 1417(m), 1397(m), 1311(m), 1143(s), 1086(s), 1004(s), 914(s), 834(m), 801(s), 713(m), 627(s). ^{1}H NMR (D$_2$O, 300 MHz, 25 $^{\circ}$C): 1.7 (s, 2H), 5.8 (br d, 2H), 6.3 (s, 1H), 6.9 (s, 1H). ^{31}P NMR 13 ppm (s).

3.5.8 Synthesis of 13, [Ag$_3$(2PyCH$_2$PO$_3$H)(SO$_3$CF$_3$)$_2$]$_n$

In an amber-colored scintillation vial, 2-pyridylmethylphosphonic acid (0.05 g, 0.29 mmol) and AgSO$_3$CF$_3$ (0.074 g, 0.29 mmol) were added to 3 mL of 50/50 EtOH/H$_2$O solution until the reactants dissolved. The reaction mixture was stirred at 60 $^{\circ}$C for 2 hours, after which time the grey-colored mixture was filtered to remove any traces of deposited silver or precipitate. The resulting clear solution was stored at room temperature to yield colorless crystals of **13**. Yield = 0.070 g (31%). Melting point: 60 ℃ "sweat", 90 ℃ (bubbling, loss of H$_2$O), 250 - 256 ℃ color change from brown to metallic silver (decomposition). IR (KBr pellet, cm^{-1}) 3469 (w), 2104 (m), 1624 (s), 1544 (m), 1473 (s), 1227(s), 1168 (s), 1006 (w), 937 (w), 792 (s), 711 (s). ^{1}H NMR (D$_2$O, 300 MHz, 25 $^{\circ}$C): 8.5 (br, s), 8.4 (br, tr) 7.8 (br, dd). ^{31}P NMR 12 ppm (s). MS obs, (calc): 296.743 (295), 298.736 (297) PyHCH$_2$PO$_3$AgO, (Ag^{107}, Ag^{109}), 395.55 (395), 397.55 (397), Ag$_2$(trif)O$_2$ (Ag^{107}, Ag^{109}), 485.32 (486), 487.32 (487) Ag$_3$(trif)O, (Ag^{107}, Ag^{109}).

Table 3.1: Crystal Data for Compounds 6 - 13

Compound Name	6	7	8	9
Chemical Formula	$C_{12}H_{18}Cl_2Mn_1N_2O_{16}P_2$	$C_{12}H_{20}Cl_2Co_1N_2O_{16}P_2$	$C_{24}H_{54}Cl_8Fe_4N_4O_{53}P_4$	$C_{18}H_{24}Cl_3Fe_1N_3O_{21}P_3$
Formula Weight	636.08	640.07	1877.59	873.51
Crystal System	Monoclinic	Monoclinic	Monoclinic	Trigonal
Space Group	$P2_1/c$	$P2_1/c$	$P2/n$	$R\text{-}3$
T(K)	213(2)	213(2)	213(2)	173(2)
a (Å)	13.3278(17)	13.398(3)	11.051(3)	23.6196(7)
b (Å)	8.2658(10)	8.2442(19)	14.563(4)	23.6196(7)
c (Å)	10.1631(13)	10.040(2)	20.651(6)	9.5024(3)
α (°)	90	90	90	90
β (°)	97.450(2)	97.348(4)	92.526(6)	90
γ (°)	90	90	90	120
V (Å^3)	1110.2(2)	1099.9(4)	3320.4(17)	4591.0(2)
Z	2	2	2	6
Reflections collected	9359	6462	19115	14286
Independent reflections	2645	2546	7772	2581
Data/restraints /parameter ratio	2645/0/160	2546/3/174	7772 / 2215 / 684	2851/0/149
Unique Data (R int)	0.0352	0.0311	0.0316	0.0497
D_{calc} (Mg/m^3)	1.897	1.933	1.878	1.896

F(000)	642	650	1900	2658
R indices (all data)	R1 = 0.0893 wR2 = 0.2525	R1 = 0.0702 wR2 = 0.1396	R1 = 0.0971, wR2 = 0.2009	R1 = 0.0664, wR2 = 0.0904
Final R indices [I > 2σ(I)]	R1 = 0.0749 wR2 = 0.2358	R1 = 0.0486 wR2 = 0.1233	R1 = 0.0666, wR2 = 0.1756	R1 = 0.0407, wR2 = 0.0823
Largest difference in peak and hole (e Å^{-3})	2.190 and –0.766	1.312 and –0.563	1.418 and -1.050	0.469 and -0.497

Compound Name	10	11	12	13
Chemical Formula	$C_{12}H_{20}Cl_2Fe_1N_2O_{16}P_2$	$C_6H_6Ag_1N_2O_6P_1Pb_1$	$C_6H_8N_3O_9P_1Pb_1$	$C_8H_7Ag_3F_6N_1O_9P_1S_2$
Formula Weight	636.99	548.16	504.31	793.85
Crystal System	Monoclinic	Monoclinic	Triclinic	Monoclinic
Space Group	P2$_1$/c	P2$_1$/c	P-1	P2$_1$/c
T(K)	173(2)	213(2)	213(2)	298(2)
a (Å)	13.5170(8)	13.9027(19)	5.4028(4)	13.144(10)
b (Å)	8.2636(4)	9.8255(14)	10.1360(8)	9.394(8)
c (Å)	10.3910(4)	7.9178(11)	11.8724(9)	16.244(13)
α (º)	90	90	73.6130(10)	90
β (º)	97.108(4)	104.871(2)	84.5320(10)	108.812(15)
γ (º)	90	90	82.5930(10)	90
V (Å^3)	1151.75(10)	1045.4(3)	617.36(8)	1899(3)
Z	2	4	2	4

Reflections collected	8350	5763	3575	11025
Independent reflections	2322	2384	2708	4308
Data/restraints /parameter ratio	2322/4/173	2384/0/154	2708 / 0 / 189	4308/0/271
Unique Data (*R int*)	0.0342	0.0451	0.0188	0.0661
Dcalc (Mg/m^3)	1.837	3.483	2.713	2.777
F(000)	648	992	468	1504
R indices (all data)	R1 = 0.1014 wR2 = 0.2536	R1 = 0.0557 wR2 = 0.1080	R1 = 0.0406 wR2 = 0.0955	R1 = 0.1294 wR2 = 0.1180
Final R indices [I > 2σ(I)]	R1 = 0.0803 wR2 = 0.2291	R1 = 0.0425, wR2 = 0.0993	R1 = 0.0366 wR2 = 0.0922	R1 = 0.0446 wR2 = 0.0848
Largest difference in peak and hole (e Å^{-3})	0.935 and -1.845	3.251 and -1.976	2.678 and -3.558	0.742 and -1.118

Chapter 4

(Aminomethyl)phosphonic acid: A flexible, multi-dentate ligand for metal phosphonates.

4.1 Introduction

Bifunctional ligands provide twice as many opportunities for metal coordination, and thus increase the likelihood of expanding a given polymer into more than one dimension. The utilization of the rigid heterocylic 2-(pyridyl)phosphonic acid and the more flexible 2-(pyridylmethyl)phosphonic acid have demonstrated the ability of bifunctional phosphonic acids to form multidimensional polymers. However, the limited coordination of the pyridyl nitrogen to transition metal cations in these polymers prompted us to investigate the possibility for multidimensional products using the flexible bifunctional (aminomethyl)phosphonic acid (ampa). While this ligand lacks the potential for stabilizing π-stacking interactions, it does provide a stronger Lewis base for coordination by Lewis acid cations. The coordination properties of this ligand have been limited and the solid-state analysis even more so.[168] Most of the work that has been done is related to the fact that ampa is the main metabolic product of the environmental decomposition of a common broad-spectrum herbicide, N-(phosphomethyl)glycine.[169] Ampa has been shown to inhibit a zinc(II)-metalloenzyme, which indicates the presence of metal-coordination interactions.[170] Discrete complexes of ampa with Fe(III) and Mg(II) have been analyzed,[171] and more recently, our group reported the synthesis and characterization of one silver dimer and seven polymeric species with ampa and Zn(II), Cd(II), Pb(II), Hg(II), Ag(I), and Cu(II)/Ag(I).[172]

(Aminomethyl)phosphonic acid participates in several ionization reactions as shown in Table 4.1, with Equation 4.2 being the most significant in aqueous systems. There is only a 1 in

500 chance for the amino group to be deprotonated before the second phosphonate oxygen, and therefore the rare microform, $H_2NCH_2PO_2OH^-$, will not be of concern in this discussion.[173]

	Ionization reaction	pK_a
Equation 4.1	$^+H_3NCH_2PO(OH)_2 \rightleftarrows H^+ + {}^+H_3NCH_2PO_2OH^-$ (H_3ampa^+) ($H_2ampa^\pm$)	$pK^H_{H3ampa} \approx 0.4$
Equation 4.2	$^+H_3NCH_2PO_2OH^- \rightleftarrows H^+ + {}^+H_3NCH_2PO_3^{2-}$ ($H_2ampa^\pm$) ($Hampa^-$)	$pK^H_{H2ampa} = 5.4 \pm 0.01$
Equation 4.3	$^+H_3NCH_2PO_3^{2-\ -} \rightleftarrows H^+ + H_2NCH_2PO_3^{2-}$ ($Hampa^-$) ($ampa^{2-}$)	$pK^H_{Hampa} = 10.08 \pm 0.01$

Table 4.1 Modified from Reference 173.

Stability constants of coordination complexes with ampa and transition metals indicate a distinct favoring of the forward reaction in Equation 4.4, whereby chelation occurs via the amino and phosphonate groups. Therefore, it is reasonable to expect that transition-metal coordination polymers incorporating ampa would demonstrate this chelating mode as well, and thus increase the dimensionality of the polymer. Potential coordination sites are illustrated in Figure 4.1 where various bonding motifs are shown.
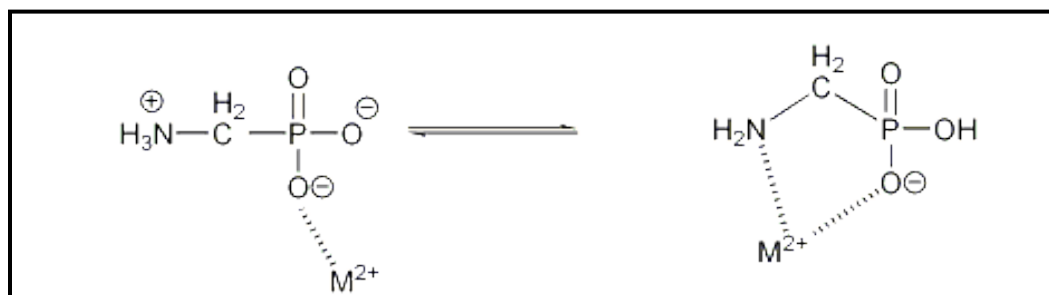
Equation 4.4   Stability constants indicate the forward reaction is favored for complexes of (aminomethyl)phosphonic acid and transition metal divalent cations. Modified from Reference 173.
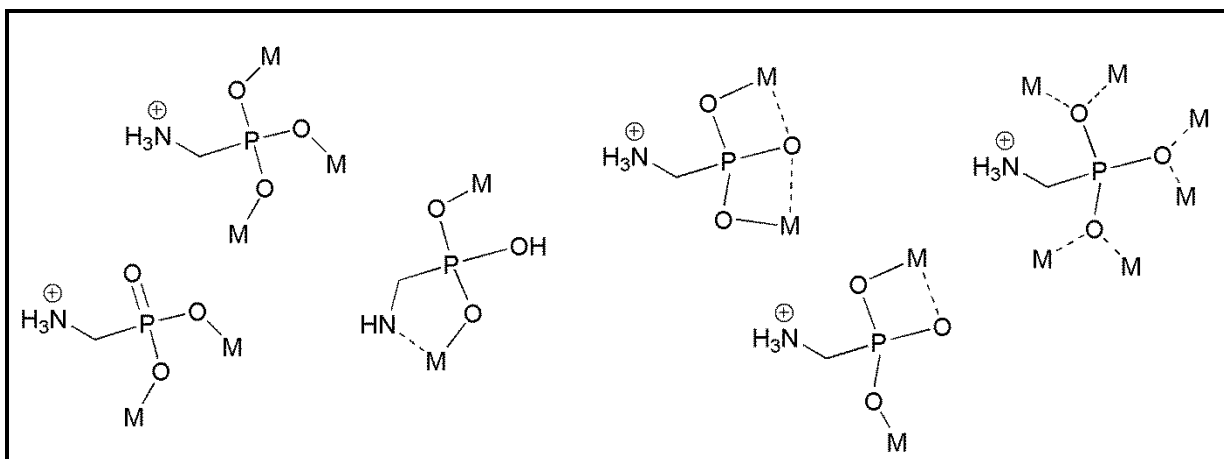
Figure 4.1 Possible coordination modes for (aminomethyl)phosphonic acid and transition metal cations.

4.2 Ligand Synthesis

Phosphonic acid derivatives can be formed via the Michaelis-Arbuzov reaction between a nucleophilic trialkyl phosphite and an alkyl halide. Specifically, (aminomethyl)phosphonic acid is synthesized by the reaction of triethyl phosphite and *N*-(bromomethyl)phthalimide, with the removal of the ethyl bromide byproduct.[174] The resulting diethyl phosphonate is then hydrolyzed and treated with methyl oxirane to remove excess acid,[175] yielding the zwitterion $H_3NCH_2PO_3H$ (Scheme 4.1).
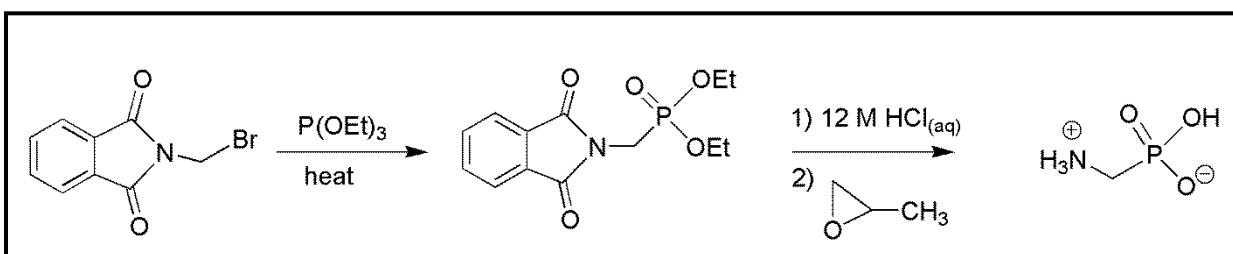
Scheme 4.1 Synthetic pathway for (aminomethyl)phosphonic acid utilizing a Michaelis-Arbuzov rearrangement and acid hydrolysis of the phosphonate ester to produce the phosphonic acid.

4.3 Results and Discussion

Continuing with our desire to pursue the use of mild synthetic methods, the stoichiometric reactions of ampa with divalent transition metal perchlorate salts and trivalent lanthanide nitrate salts in aqueous and EtOH/H$_2$O solvents yielded a series of seven two-dimensional polymeric structures, **14-20** (Scheme 4.2). Hydrogen-bonding interactions are present between the layers, adding to the stability of these frameworks, and thermal stability is exhibited by all of these compounds, with four of them stable above 300 °C.
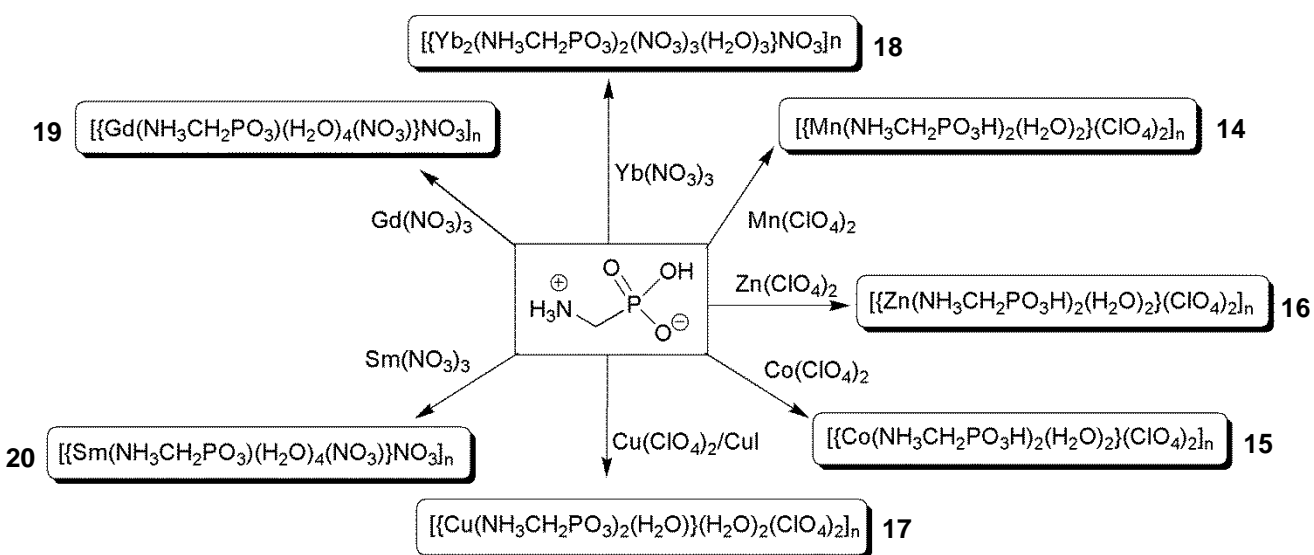
Scheme 4.2 Summary of the reactions of ampa with metal precursors.

4.3.1 Discussion of Polymer 14: [{Zn(NH$_3$CH$_2$PO$_3$H)$_2$(H$_2$O)$_2$}(ClO$_4$)$_2$]$_n$

To investigate the effect of counter ion on the framework structural motif, the mild aqueous reaction of zinc(II) perchlorate with ampa was performed. We hoped to avoid the limited dimensionality of the polymer [Zn(ampa)Cl]$_n$ that resulted from coordinated terminal chloride

ions with $ZnCl_2$ as the metal precursor as shown in Figure 4.2.[172] The perchlorate salt was selected since it has been shown to be capable of bridging metal centers, as well as remaining out of the crystal lattice when not needed for charge balance. The combination of stoichiometric amounts of zinc perchlorate hexahydrate with ampa in an $EtOH/H_2O$ solvent yielded the two-dimensional polymer **14** (Figure 4.3).
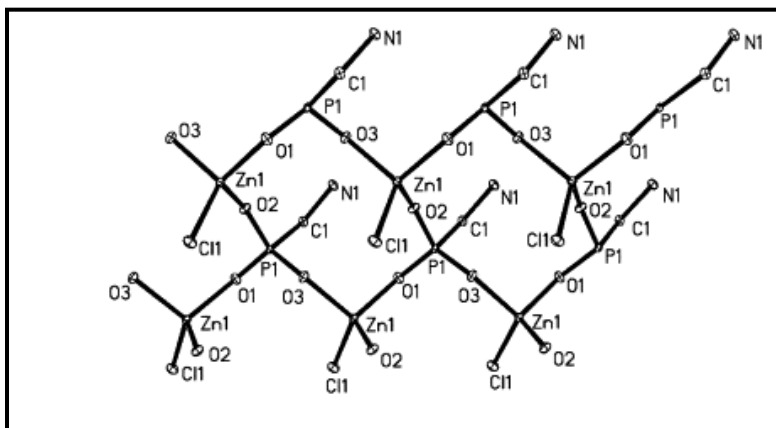
Figure 4.2 Main structural motif for the 2D ampa polymer, $[Zn(NH_3CH_2PO_3H)Cl]_n$. Thermal ellipsoids at 30% probability; hydrogen atoms omitted for clarity. Taken from Reference 172.
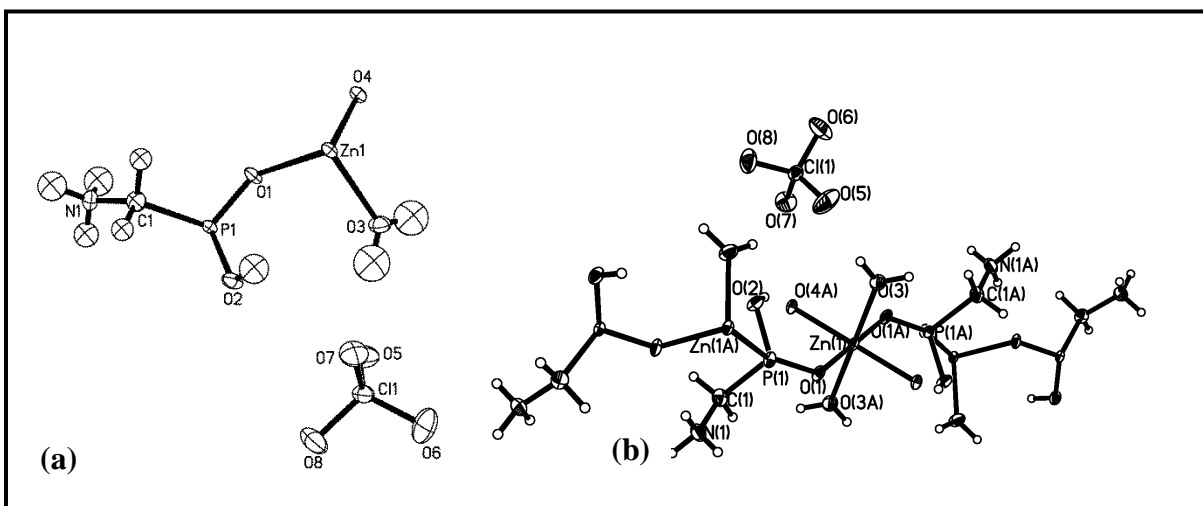
Figure 4.3 **(a)** Asymmetric unit of **14** **(b)** Polymeric form of **14** (thermal ellipsoids at 30% probability). Selected bond lengths (Å) and angles (°): Zn1-O1 2.1038(19), Zn1-O3 2.104(2), Zn1-O4 2.0826(18), P1-O1 1.498(2), P1-O2 1.566(2), P1-O4A 1.5037(19), O4A-Zn1-O4 180.0, O1-Zn1-O1A 180.0, O3-Zn1-O3A 180.0, O4-Zn1-O1A 90.23(7), O4-Zn1-O3 91.07(9).

Polymer **14**, [{Zn(NH$_3$CH$_2$PO$_3$H)$_2$(H$_2$O)$_2$}(ClO$_4$)$_2$]$_n$, crystallizes in the monoclinic space group *P*2$_1$/*c*. The zinc cation is in an almost perfect octahedral environment, with four monodentate ligands in the two axial positions and two equatorial ones. The remaining equatorial positions are taken by two water molecules. The asymmetric unit contains one zinc center at half-occupancy, one zwitterionic ligand molecule, one coordinated water, and one lattice perchlorate ion. The ligand exists with a protonated amino group and a singly deprotonated phosphonate group, resulting in a net charge of zero. The bond length between the protonated oxygen and the phosphorus atom is therefore slightly longer at 1.566(2) Å, when compared to the others (P1-O1 1.498(2) and P1-O4A 1.5037(19)). Hydrogen bonds located between the lattice counterions and the coordinated waters (2.079(13) Å) and amino groups (2.46 - 2.93 Å) help stabilize the 2D layers.

The layers themselves contain 16-membered rings with alternating Zn-O-P-O segments (Figure 4.4). This is larger than the 12-membered rings seen in polymers **1** and **2,** Section 2.2.1, and in the the polymer using ZnCl$_2$ as a precursor (Figure 4.3). The largest dimension of the ring is 7.7 Å between opposing phosphorus atoms, and the narrowest dimension is 2.7 Å between opposite hydroxyl and methylene groups. The net-like layers have a metal-phosphonate lamella with amino groups exposed on the outside of the layers as shown in Figure 4.5. While the nitrate counterion did not limit the dimensionality of **14**, the zinc's waters of hydration and the ligand's monoprotonated oxygen served to inhibit the growth of the polymer. The Zn-O bond lengths are slightly longer than those of the tetrahedral ZnCl$_2$ polymer (ranging from 2.08 to 2.10 Å as opposed to 1.93 to 1.97 Å), but are comparable to other octahedral structures, with Zn-O distances of 2.06 to 2.14 Å.[176]
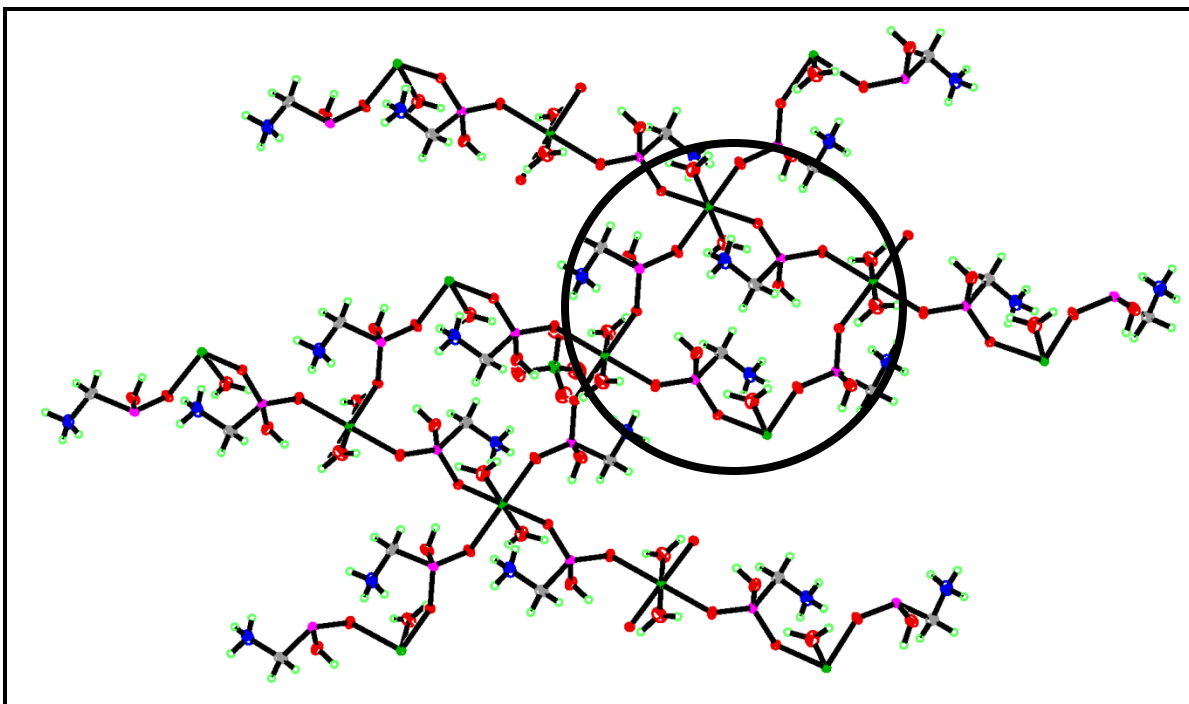
Figure 4.4 Extended framework of **14,** $[\{Zn(NH_3CH_2PO_3H)_2(H_2O)_2\}(ClO_4)_2]_n$. The 16-membered ring is circled. Thermal ellipsoids at 30% probability. Green = zinc, pink = phosphorus, red = oxygen, grey = carbon, blue = nitrogen, light green = hydrogen.
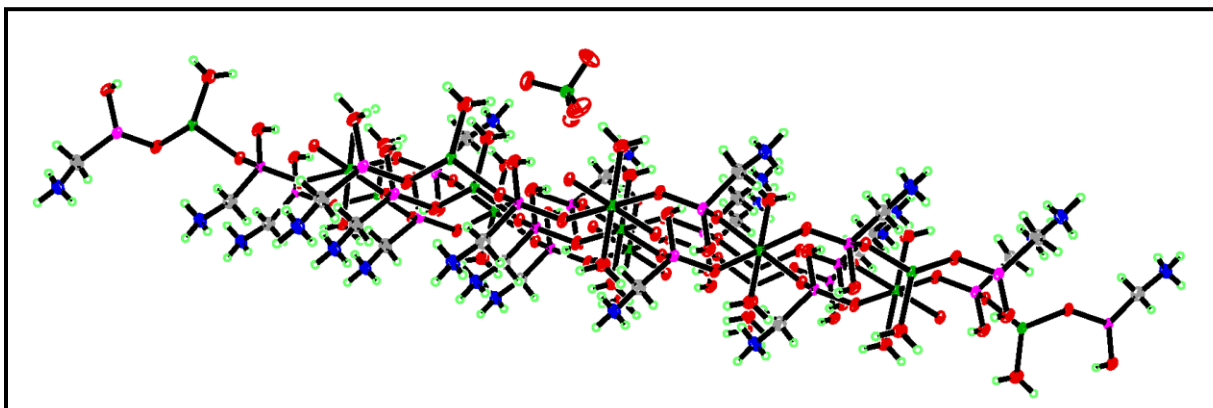
Figure 4.5 One representative layer of polymer **14,** $[\{Zn(NH_3CH_2PO_3H)_2(H_2O)_2\}(ClO_4)_2]_n$. The zinc phosphonate core is shown in dark green, pink, and red (zinc, phosphorus, and oxygen atoms repectively). The amino groups cover the outside of the layer (blue nitrogen, grey carbon, and light green hydrogen atoms).

The solid-state IR spectrum of **14** is in good agreement with the single-crystal X-ray data. The P=O from the free ampa ligand (1216 cm^{-1}) is low-frequency shifted to 1150 cm^{-1} ($\Delta\nu = 66$

cm^{-1}) indicating coordination of the oxygen atom to zinc, which is also verified by the bond distance, as previously mentioned.[177] The peak at 3503 cm^{-1} corresponds to the stretching frequency of water, with the bending/stretching vibrations observed at 1622 cm^{-1}. The presence of the lattice perchlorate ion is indicated by the strong band near 1100 cm^{-1}, the sharp band at 627 cm^{-1}, and the medium band at 940 cm^{-1} attributed to the asymmetric stretch, asymmetric bend, and symmetric stretch of the perchlorate, respectively.[119a,150] Several other bands are related to the phosphonate core: the strong band at 1083 cm^{-1} can be attributed to the POH bending vibration,[178] and the weak bands between 540 cm^{-1} and 415 cm^{-1} are from the O-P-O deformations.[179] The Zn-O stretches also occur in this region (600 - 200 nm).[180] The peak at 2358 cm^{-1} is due to the protonated phosphonate OH stretch (POOH), and the weak peak at 2950 cm^{-1} corresponds to the stretching vibration of the CH$_2$ group, with the bending vibrations located at 1429 and 1306 cm^{-1}.[181] The strong peak at 1514 cm^{-1} can be attributed to the NH symmetric bend from the protonated amino group. [181]

The existence of blue fluorescent emission by d^{10} Zn(II) in other complexes[182] suggested that polymer **14** may fluoresce. When excited with 350 nm light, there was a weak emission at 384 nm, just outside the visible spectrum. The ampa molecule itself emits in the blue region at λ_{em} = 488 nm when excited at λ_{ex} = 244 nm, as well as a strong emission in the non-visible range: λ_{em} = 304 nm, λ_{ex} = 608 nm.

TGA (thermogravimetric analysis) revealed two shallow endotherms centered at 70 and 107 ^{o}C as the sample lost coordinated water molecules (the observed and calculated weight loss are 7.4 % and 6.70 % respectively). A sharp exotherm at 246 ^{o}C corresponds to the combustion of the organic material.

4.3.2 Discussion of Polymers 15: $[\{Co(NH_3CH_2PO_3H)_2(H_2O)_2\}(ClO_4)_2]_n$ and 16: $[\{Mn(NH_3CH_2PO_3H)_2(H_2O)_2\}(ClO_4)_2]_n$

Continuing with our investigation of divalent cations, (aminomethyl)phosphonic acid was reacted with perchlorate salts of manganese(II), cobalt(II), and iron(II), where we could also compare potential structures with those obtained from reaction with $2pyCH_2PO_3H_2$ (Polymers **6-10**), with the free amino group in place of the more rigid heterocycle. Even though dimeric species of ampa with Fe(III) have been reported using a perchlorate precursor, no crystalline material was formed,[171a] and all attempts using the current mild methodologies with iron(II) and (III) nitrates, perchlorates, and halides produced amorphous precipitates and films. However, the crystalline products **15**, $[\{Co(NH_3CH_2PO_3H)_2(H_2O)_2\}(ClO_4)_2]_n$, and **16**, $[\{Mn(NH_3CH_2PO_3H)_2(H_2O)_2\}(ClO_4)_2]_n$, resulted from the stoichiometric reaction of the perchlorate Co(II)/Mn(II) precursors and ampa with only mild heating in $EtOH/H_2O$.

The asymmetric units of **15** and **16** exist as a divalent metal cation at half-occupancy, one zwitterionic ampa ligand, one coordinated water molecule, and one lattice perchlorate ion. The ligand contains a protonated amino group and a singly protonated phosphonate group, resulting in a net charge of zero. The protonated oxygen is pendant, with the other two phosphonate oxygens bonding to the metal center. The bond lengths between the phosphorus and oxygen atoms support this: O2-P1 1.568(2) Å, P1-O1 1.5024(18) Å, and P1-O4B 1.5036(18) Å, where O2 is the protonated oxygen, all values for the Mn(II) polymer. The Mn(II) is in an almost perfect octahedral environment, with 180º between each phosphonate oxygen and its symmetry pair, for a total of four equatorial oxygen atoms coordinated to the metal. The axial water molecules are also at 180º from each other, and the equatorial bond angles between the oxygens and Mn(II) range from 89.52(7) to 90.48(7)º. The presence of the axial waters limits the

dimensionality of this polymer, as shown in Figures 4.6b and 4.7 where the structure only extends in two directions.
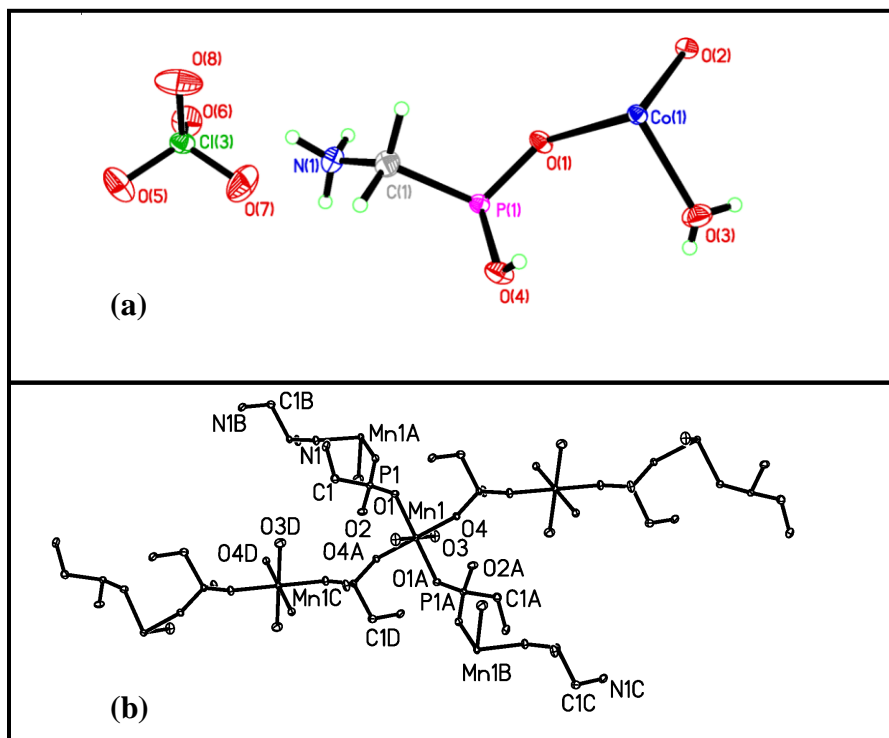
Figure 4.6 (**a**) Asymmetric unit of **15** (**b**) Polymeric form of **16**; thermal ellipsoids at 30% probability. Selected bond lengths (Å) and angles (°): **15:** Co1-O3A 2.099(3), Co1-O3 2.099(3), Co1-O1 2.099(2) Co1-O1A 2.099(2), Co1-O4 2.104(2), Co1-O4A 2.104(2), P1-O1 1.503(2), P1-O4A 1.504(2), P1-O2 1.568(2), O3A-Co1-O3 180.00(7), O3A-Co1-O1 89.23(10), O3-Co1-O1 90.77(10), O1-Co1-O1A 180.00(9), O4-Co1-O4A 180.0, O1-P1-O4B 115.33(12), O1-P1-O2 111.20(12), O4B-P1-O2 108.22(13), C1-N1-H1#1 120.0, C1-N1-H1#1 120.0, H1#1-N1-H1#2 120.0; **16:** Mn1-O4A 2.1465(16), Mn1-O4 2.1465(16), Mn1-O1 2.1692(17), Mn1-O1A 2.1692(17), O2-P1 1.568(2), P1-O1 1.5024(18), P1-O4B 1.5036(18), O4A-Mn1-O4 180.00(1), O4A-Mn1-O1 89.52(7), O1-Mn1-O1A 180.0, O3A-Mn1-O3 180.0, H3A-N1-H2 109(3), H2A-N1-H2 110(3), H3A-N1-H2A 103(3).
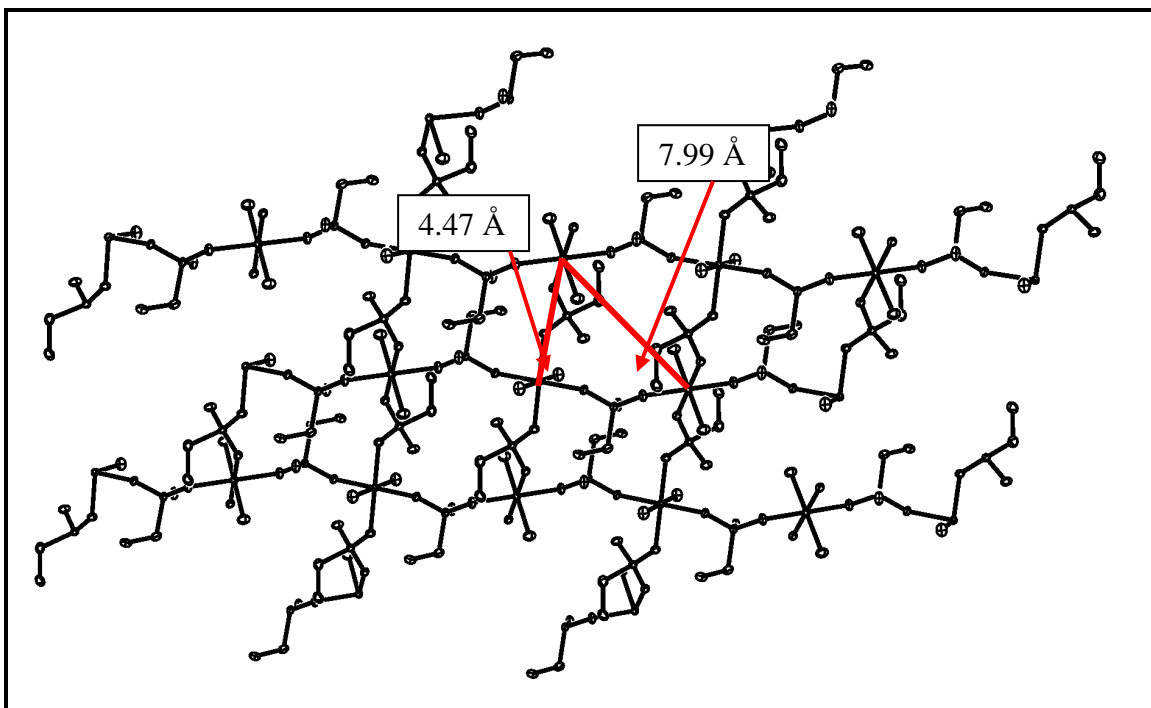
Figure 4.7 Extended framework of polymer **15** (**16** is identical). Thermal ellipsoids at 30% probability; hydrogen atoms omitted for clarity. Metal-to-metal distances shown down the side of a 16-membered ring and across an *a*-axis pore.

The two-dimensional extended structure of these two polymers (Figure 4.7) contains pores generated along the *a*-axis that are 7.99 Å metal-to-metal and occluded by the methylene and phosphonic acid hydrogen atoms, with a 2.75 Å space between them. Hydrogen-bonding interactions exist between the lattice perchlorate oxygen atoms and ligand hydrogen atoms on adjacent layers. Interlayer distances are measured at 4.155 Å on the Mn(II) structure.

The infrared absorption spectra for polymers **15** and **16** are similar to that of polymer **14**, which is expected due to their analogous framework structure. The phosphonic acid POH absorptions are more defined, however, and occur at 2873, 2525, 2289, and 2024 cm^{-1} for **15** and 2530, 2348, 2285, and 2020 cm^{-1} for **16**.

Comparing structures **15** and **16** with those obtained with 2-(pyridylmethyl)phosphonic acid, polymers **6** and **7**, it can be observed that the ligand's charge is the same: a protonated nitrogen on both and a single protonated phosphonate oxygen results in an overall neutral ligand. Both sets of structures exhibit octahedral metal geometry and 16-membered rings formed from bridging phosphonate oxygens and four metal centers. The hydrogen-bonded layered architecture and the alternating up-down arrangement of the pendant portion of the ligand are observed in both sets of structures, as well.

4.3.3 Discussion of Polymer 17: $[\{Cu(NH_3CH_2PO_3H)_2(H_2O)\}(H_2O)_2(ClO_4)_2]_n$

Given the affinity of copper(II) for nitrogen coordination, the perchlorate salt of this cation was reacted with ampa in the hopes that the chelation of the ligand could increase the dimensionality of the product. However, the combination of these reagents in water or EtOH/water only afforded metal hydroxides and amorphous materials. The aqueous reaction mixtures containing $Cu(ClO_4)_2/CuI$ and $Cu(ClO_4)_2/CuI/AgCN$ both produced the same aqua, monoclinic crystals in space group C2/C. The CuI and AgCN were insoluble in the reaction media and were filtered out before crystal formation. The Cu(II) is at half-occupancy, as well as the lone axial water molecule, with the asymmetric unit containing one zwitterionic ligand and one lattice perchlorate ion and water molecule (Figure 4.8a). Each copper center exists in a five-coordinate, square-pyramidal geometry, bonded to four bridging phosphonate groups and a single water molecule, which alternates up and down across a chain as shown in Figure 4.8b. Other copper(II) structures exhibiting this geometry are discrete molecules with two diphosphonic acids and one water molecule coordinated to the copper(II) center.[183] The Cu(II)-O bond lengths of polymer **17** (1.96 – 1.97 Å for Cu-O-P and 2.21 Å for the Cu-OH$_2$) are similar to published values, which range from 1.90 – 1.99 and 2.12 – 2.30 Å, respectively.[183]
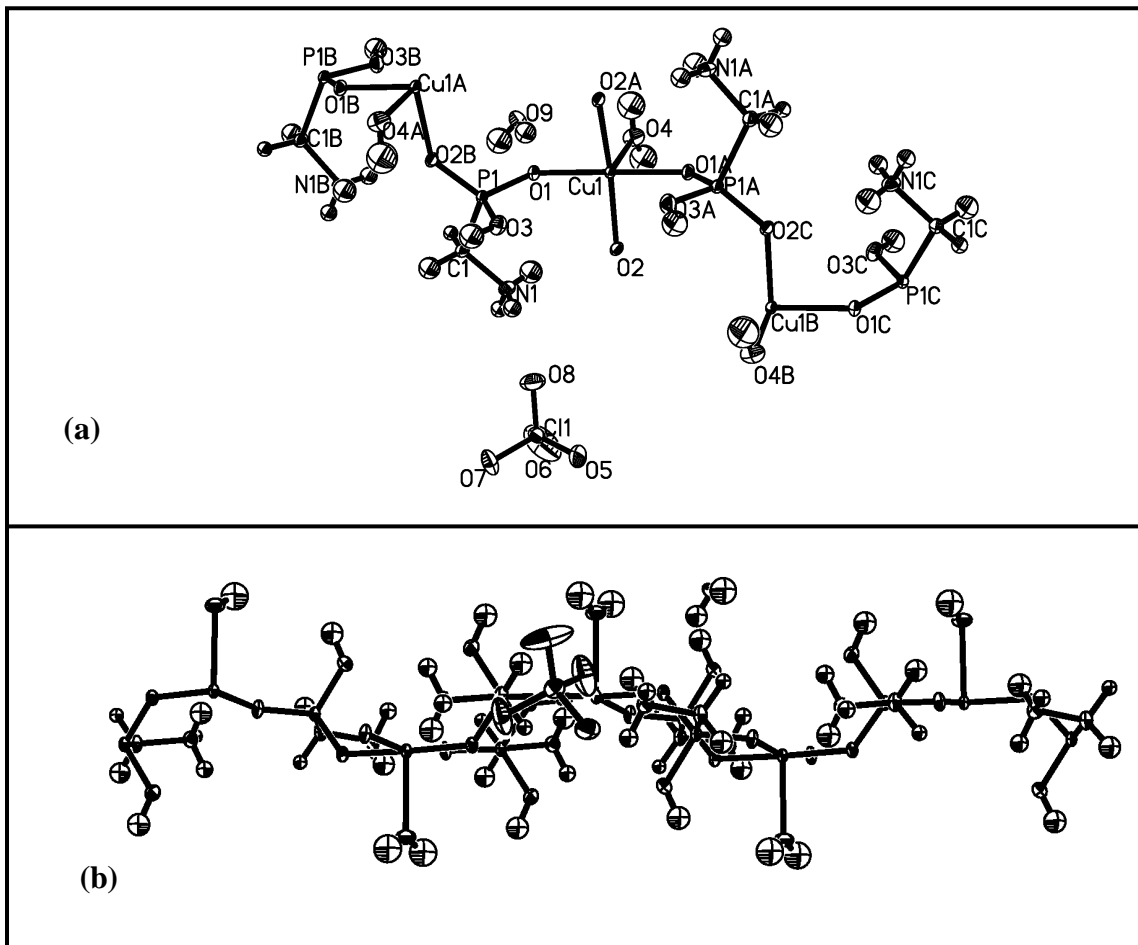
Figure 4.8 Polymer **17**, [{Cu(NH$_3$CH$_2$PO$_3$H)$_2$(H$_2$O)}(H$_2$O)(ClO$_4$)$_2$]$_n$, **(a)** polymeric form illustrating the geometry around the metal center **(b)** 2-D chain showing the alternating up and down axial water molecules. Thermal ellipsoids drawn at 30% probability. Selected bond lengths (Å) and angles (°): Cu1-O1 1.9645(15), Cu1-O2 (1.9727(16), Cu1-O4 2.213(2), O1-P1 1.5123(15), O2-P1 1.5554(16), O3-P1 1.5061(16), O1-Cu1-O1A 177.92(8), O2-Cu1-O1 90.49(6), O2-Cu1-O1A 89.27(6), O2-Cu1-O2A 166.89(10), O4-Cu1-O1 91.04(4), P1-O1-Cu1 131.43(9), O2-P1-O1 106.84(9), O3-P1-O1 117.34(9), O3-P1-O2 114.49(10), C1-P1-O1 106.60(10).

The orientational disorder of the perchlorate ion results in high thermal parameters for O6; however, this is not unusual for structures containing nearly spherical counter ions.[184] The perchlorate ions participate in hydrogen-bonding interactions with the lattice water molecules and the ligand, stabilizing the 2-D layered network.

4.3.4 Discussion of Polymer 18: $[\{Yb_2(NH_3CH_2PO_3)_2(NO_3)_3(H_2O)_3\}NO_3]_n$

Lanthanide phosphonates have demonstrated room-temperature luminescence, as discussed in Section 1.4.4, and as the larger coordination sphere of these metals could encourage polymer growth in multiple directions, we were interested in the synthesis of such frameworks using (aminomethyl)phosphonic acid. Equimolar amounts of the nitrate salt of Yb(III) and ampa were combined in distilled water, and within a few minutes, a fine precipitate was formed. The powder was tested for IR absorption and produced identical bands to those observed for the crystalline material. Single crystals for X-ray diffraction were obtained from slow evaporation of the mother liquor.

Crystallographic analysis of polymer **18**, $[\{Yb_2(NH_3CH_2PO_3)_2(NO_3)_3(H_2O)_3\}NO_3]_n$, revealed the presence of two unique ytterbium atoms in the asymmetric unit (Figure 4.9). The seven-coordinate, distorted octahedral environment of Yb1 includes one chelating nitrate ion, two coordinated water molecules, and three phosphonate oxygens from separate ampa ligands. The Yb2 center is eight-coordinate with *trans*-chelating nitrate ions, rotated perpendicular to each other, two axial phosphonate oxygen atoms, a third oxygen atom from a separate phosphonate group, and one water molecule. One lattice nitrate ion is present for charge balance, supporting the fact that both of the ampa ligands are doubly deprotonated on the phosphonate moiety and protonated on the amino group, with a net 1- charge. Each ampa ligand bridges three different metal centers, bonding through each phosphonate oxygen atom, with pendant amino groups. Hydrogen-bonding interactions serve to stabilize the 2D polymeric sheets; interactions between lattice nitrate ions occur with coordinated water molecules and amino groups, and interlayer hydrogen bonding occurs between the coordinated nitrate ions and ligand amino groups from adjacent layers.
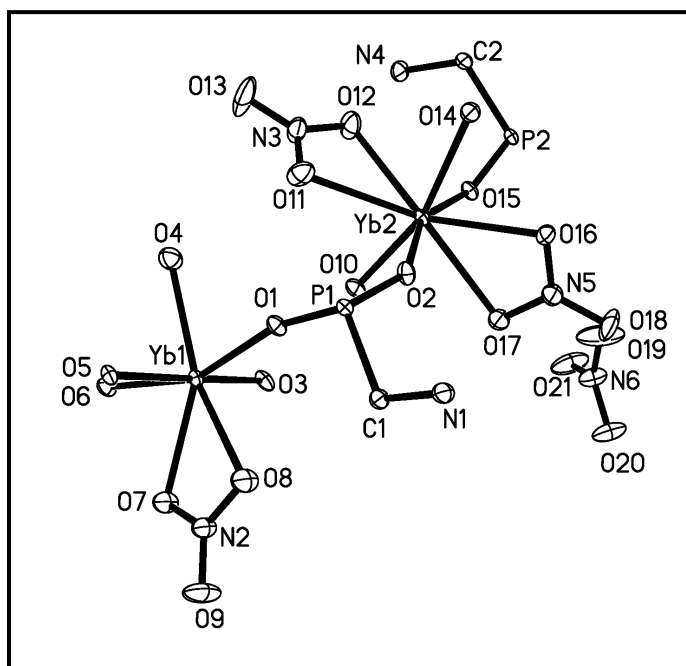
Figure 4.9 Asymmetric unit of **18**, [{Yb$_2$(NH$_3$CH$_2$PO$_3$)$_2$(NO$_3$)$_3$(H$_2$O)$_3$}NO$_3$]$_n$, showing the two different ytterbium environments (thermal ellipsoids shown at 30% probability). Selected bond lengths (Å) and angles (°): Yb1-O1 2.145(3), Yb1-O3 2.150(3), Yb1-O6 2.195(3), Yb1-O7 2.388(3), Yb1-O8 2.416(4), Yb1-O4 2.341(4), Yb1-O5 2.315(3), Yb2-O10 2.152(3), Yb2-O2 2.183(3), Yb2-O15 2.226(3), P1-O2 1.504(3), P1-O1 1.511(3), P1-O6C 1.533(3), P2-O10D 1.508(3), P2-O3D 1.520(3), P2-O15 1.524(3), O1-Yb1-O3 92.14(12), O1-Yb1-O6 92.81(11), O3-Yb1-O6 174.19(11), O7-Yb1-O8 52.89(12), O10-Yb2-O2 92.18(12), O10-Yb2-O15 90.31(10), O2-Yb2-O15 158.71(11), O16-Yb2-O17 51.56(12), O12-Yb2-O11 50.58(12), O2-P1-O1 114.35(19), O2-P1-O6C 110.90(17), O1-P1-O6C 112.45(18).

Only one other ytterbium(III)-phosphonate structure has been published, catena-(bis(1-hydroxy-1,1-diphosphonato)-ytterbium pentahydrate, and the metal-to-oxgyen bond lengths range from 2.198 – 2.370 Å.[185] Polymer **18** has Yb(III)-phosphonate oxygen bond distances between 2.145(3) and 2.195(3) Å, which are somewhat shorter than the aforementioned structure, however other bond lengths in the asymmetric unit agree with published results. The bond lengths between the Yb(III) centers and the bidentate nitrate ions (~2.4 Å) and the

distances from the Yb(III) to the aqua ligand (~2.3 Å) are comparable to other existing structures.[98,186]

Solid-state IR analysis confirms the presence of the bidentate nitrate ions, with a band at 1472 cm^{-1} attributed to their stretching frequency. Curtis and Curtis reported stretching frequencies from 1475–1490 cm^{-1} when nitrate ions were bidentate and between 1412-1440 cm^{-1} when monodentate.[187] The presence of the lattice nitrate ion is indicated by the sharp band at 1383 cm^{-1}.[187] TGA shows several endotherms prior to decomposition with accompanying weight loss at each step: 70 °C (2.1 % weight loss), 107 °C (1.9 %), 138 °C (1.4 %), and 196 °C (5.0 %). These can be attributed to the loss of volatile components from the coordinated water and nitrate ions. The first step agrees with the loss of one water (2.1 % observed, 2.09 % calculated), the second step with the second water (1.9 % observed), and the third step with the third water (1.4 % observed). The fourth step, with an observed weight loss of 5.0 %, is slightly less than that calculated for the loss of one of the nitrate ions (7.19 % calculated). Upon examination of polymer **18**'s room temperature luminescence, the polymer was found to give a sharp emission at 487 nm when excited at 244 nm.

4.3.5 Discussion of Polymer 19: [{Gd(NH$_3$CH$_2$PO$_3$)(H$_2$O)$_4$(NO$_3$)}NO$_3$]$_n$ and Polymer 20: [{Sm(NH$_3$CH$_2$PO$_3$)(H$_2$O)$_4$(NO$_3$)}NO$_3$]$_n$

When nitrate salts of Gd(III) and Sm(III) were reacted in a 1:1 ratio with (aminomethyl)phosphonic acid, isostructural 2D polymers resulted. The two polymers crystallize in the monoclinic space group $P2_1/c$ and, unlike the ytterbium polymer, there is only one crystallographically unique metal center. One zigzag chain of the gadolinium(III) structure, [{Gd(NH$_3$CH$_2$PO$_3$)(H$_2$O)$_4$(NO$_3$)}NO$_3$]$_n$, is shown in Figure 4.10 as a representative of both polymers. Each lanthanide cation has a common eight-coordinate geometry, with three of the

more equatorial positions occupied by phosphonate oxygens from separate tridentate ligands. The remaining coordination sites belong to one monodentate nitrate ion and four water molecules, with one lattice nitrate ion. As seen in the ytterbium polymer, the ligand has a protonated amino group and a doubly-deprotonated phosphonate group, with a net charge of 1-. The nonbonding, pendant amino group is visible in Figure 4.11, a one-dimensional chain of polymer **20**. When observing the bond lengths of the phosphonate moiety, the three P-O bond distances in **19** are similar: P1-O1 1.516(3), P1-O2A 1.503(3), and P1-O8B 1.511(3) Å, and comparable to those from the ytterbium polymer (1.50 – 1.53 Å), thus reaffirming the deprotonated state of both of the ligand's oxygens. Metal-oxygen bond lengths for polymers **19** and **20** are comparable to other literature values.[98, 117b]
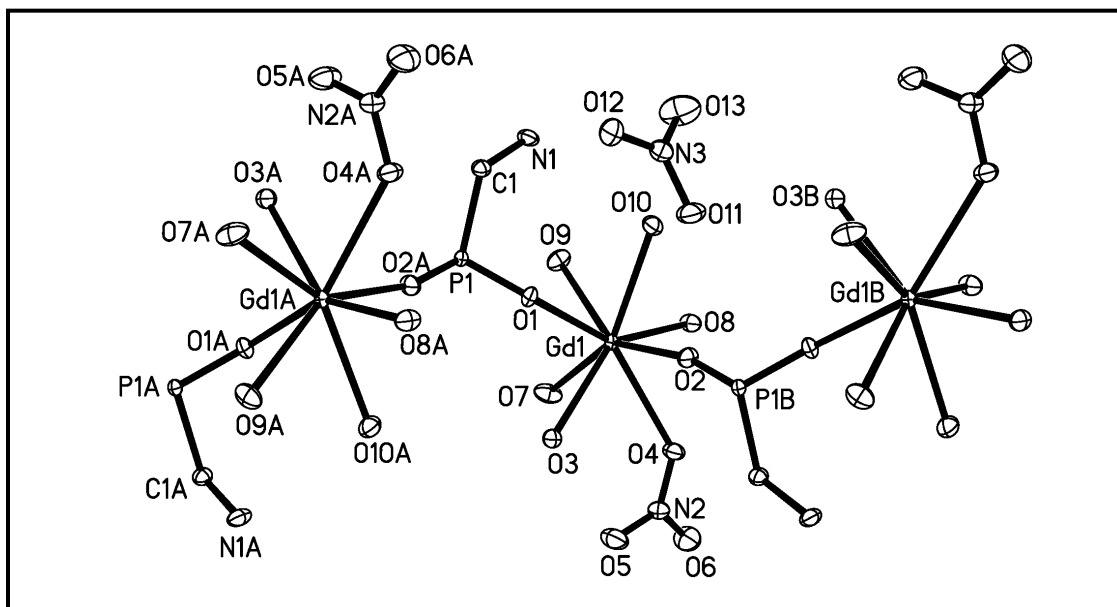
Figure 4.10 Zigzag chain of the 2D polymer **19**, $[\{Gd(NH_3CH_2PO_3)(H_2O)_4(NO_3)\}NO_3]_n$ (thermal ellipsoids shown at 30% probability). Selected bond lengths (Å) and angles (°): Gd1-O1 2.300(3), Gd1-O2 2.243(3), Gd1-O3 2.477(3), Gd1-O4 2.622(3), Gd1-O7 2.414(4), Gd1-O8 2.271(3), Gd1-O9 2.461(3), Gd1-O10 2.506(3), P1-O1 1.516(3), P1-O2A 1.503(3), P1-O8B 1.511(3), O2-Gd1-O8 92.66(13), O2-Gd1-O1 92.58(11), O8-Gd1-O1 147.45(10), O2-Gd1-O7 145.87(12), O1-P1-O2A 112.57(17).
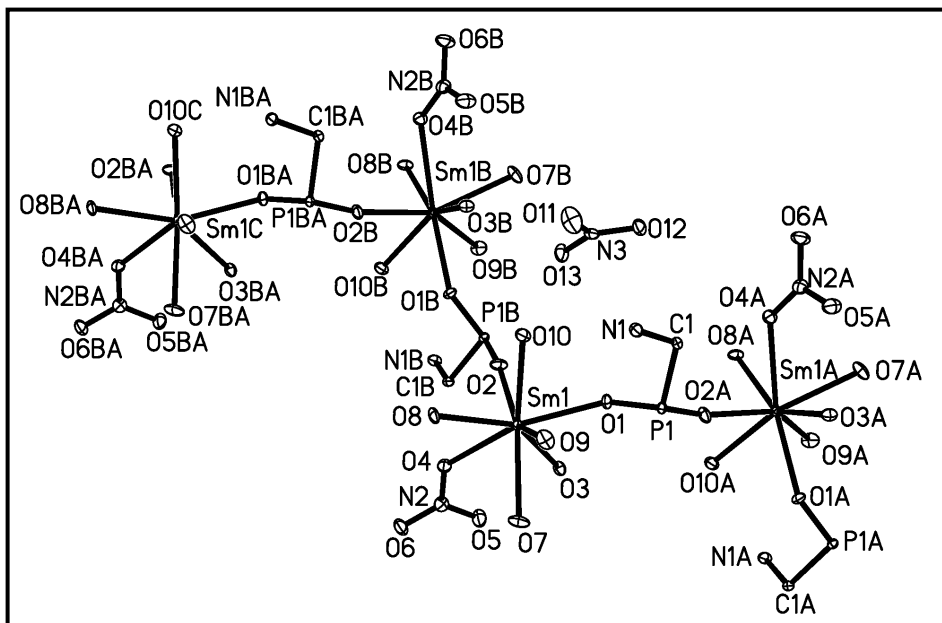
Figure 4.11 Polymer **20**, emphasizing the nonbonding portion of the ligand as it alternates up and down. Thermal ellipsoids at 30% probability, hydrogens omitted for clarity.

IR peaks that occurred at 1472 cm^{-1} for the bidentate nitrate ions in the ytterbium polymer (**18**) are now seen at 1422 cm^{-1} in polymer **19** and 1424 cm^{-1} in polymer **20**, agreeing with the literature value of 1420 cm^{-1} for monodentate coordination.[187] No luminescence was observed by polymer **20**, and only a weak emission at 393 nm was observed for polymer **19**.

Hydrogen bonding is observed between the aqua ligands and the ampa amino groups and coordinated nitrate ions (~2.5 and 1.9 Å distances, respectively). The polymer layers are held together in the third dimension by hydrogen bonding interactions with the lattice nitrate ions sandwiched between the layers. The expanded framework of polymer **19** is shown in Figure 4.12, viewed down each axis; the inter-layer nitrate ions can be clearly seen. The packing diagram includes a rectangular box displaying the *a*, *b*, and *c* axes and one or more unit cells whose geometric centers lie within the default packing range of 0.0 to 1.0 crystallographic coordinates.
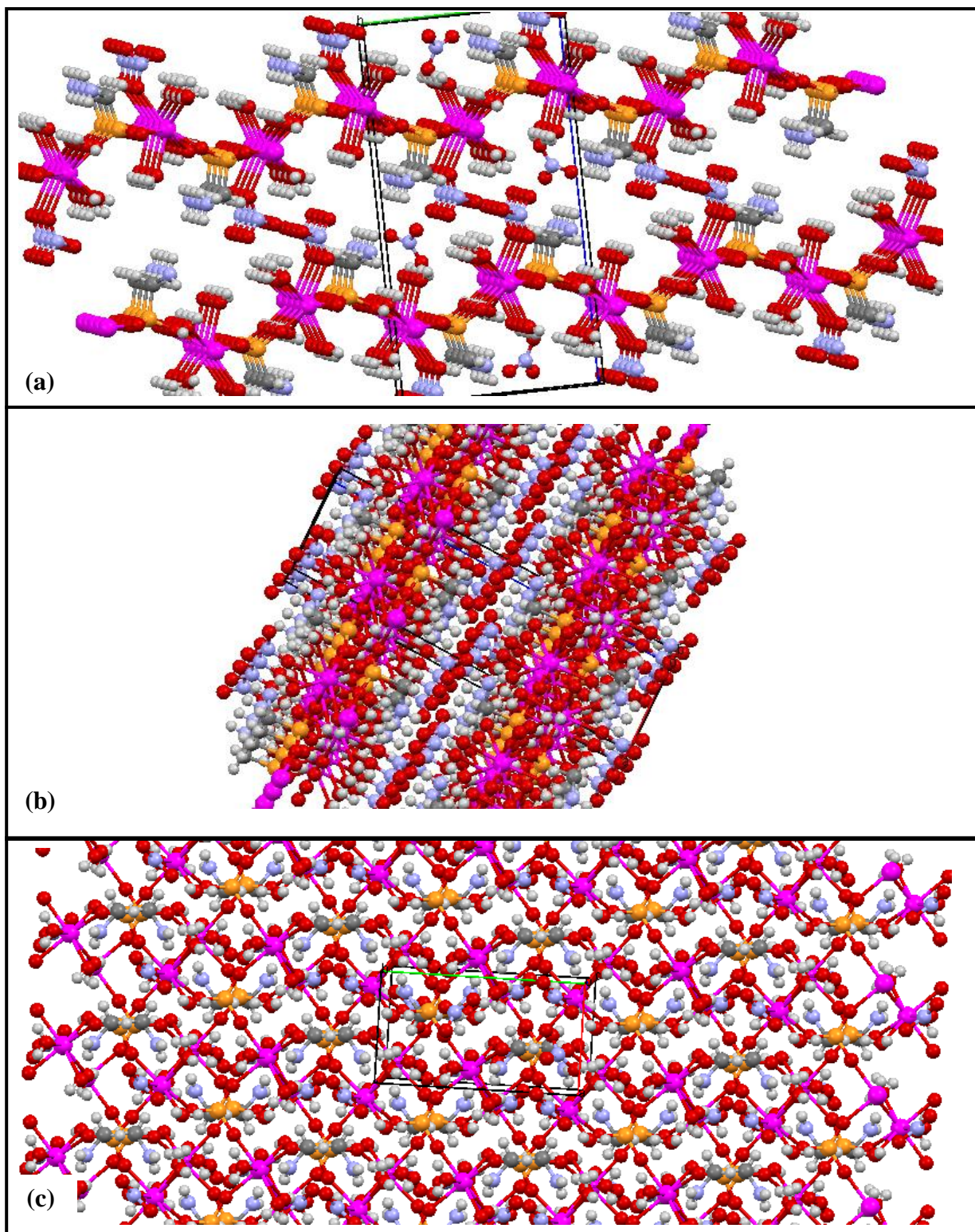
Figure 4.12 Packing diagrams of the expanded network of polymer **19**, [{Gd(NH$_3$CH$_2$PO$_3$)(H$_2$O)$_4$(NO$_3$)}NO$_3$]$_n$. **(a)** Viewed down the *a*-axis **(b)** Viewed down the *b*-axis **(c)** Viewed down the *c*-axis. Unit cell axes: *a* = red, *b* = green, *c* = blue. Atoms: Pink = Gd, orange = P, grey = C, blue = N, red = O, white = H.

4.4 Conclusion

With the aim of investigating the effects of counterion, ligand functionality, and metal choice on the resulting framework motifs, a few conclusions can be drawn. The perchlorate ions present in structures **14** through **17** do not limit the dimensionality of the polymer as did the halide counter ions mentioned in Section 4.3.1, and their presence in the crystal lattice has a significant structural advantage with the increased framework stability due to the hydrogen bonding interactions between the metal-phosphonate layers. The nitrate ions did coordinate to the lanthanide cations, however this did not limit dimensionality due to the large coordination spheres.

The choice of divalent transition metal did not alter the overall framework geometries that were formed, however the three trivalent lanthanide polymers resulted in the formation of polymers that incorporate the -1 form of the ampa ligand, as opposed to the neutral zwitterionic form that is present in the polymers employing the divalent cations. Perhaps further research with trivalent transition metal cations such as cobalt(III) or nickel(III) would result in polymers formed from tridentate ampa ligands. Additional work with the unsuccessful iron(III), possibly with careful monitoring of pH increases, might also produce crystalline material for further study. Altering the pH might increase the likelihood of copper(II)'s coordination to the amino nitrogen, which could increase the dimensionality of the final product if the formation of metal hydroxides could be avoided.

As discussed in Section 4.3.2, the flexibility of the ampa ligand did not produce a significant difference in framework architecture when compared to 2-(pyridylmethyl)phosphonic acid, primarily due to the protonation of the amino group that

prevented the chelation and additional bridging opportunities for the ligand. Given the structural similarity of ampa to the amino acid glycine, this ligand is worth further study into its metal coordination properties and two- and three-dimensional polymeric frameworks. The luminescence supported by the zinc(II) and ytterbium(III) polymers is also significant as research into phosphonate sensors continues.

4.5 Experimental

4.5.1 General Methods

(Aminomethyl)phosphonic acid was prepared as described in Section 4.2. Other materials were purchased from Aldrich and used as received. IR spectra were recorded from KBr pellets on a MIDAC M4000 FT-IR spectrometer. Thermogravimetric analyses (TGA) were carried out on a Seiko 220 instrument at a heating rate of 5 ^{o}C/ min. ^{1}H, ^{31}P{H} NMR spectra were recorded in solution on a Varian Mercury 300 MHz spectrometer. Due to limited solubility in common deuterated solvents no meaningful ^{13}C data could be collected. Fluorescence was recorded using a Shimadzu 5301PC spectrofluorimeter at ambient temperature.

Data collection of the compounds were performed at -60 ^{o}C on a Bruker SMART 1000 diffractometer, using Mo Kα radiation (0.71073Å), equipped with cryostream. Crystals were mounted on glass fibers using paratone oil. SAINT[134] was used for data reduction and cell refinement, and SADABS[134] was run for absorption correction on all data. Crystal structures were solved using direct methods and refined with full-matrix least squares treatment (SHELXL).[134] Crystallographic data is summarized in Table 4.2.

4.5.2 Synthesis of 14, [{Zn(NH₃CH₂PO₃H)₂(H₂O)₂}(ClO₄)₂]ₙ

Ampa (0.05 g, 0.5 mmol) and $Zn(ClO_4)_2 \cdot 6H_2O$ (0.17 g, 0.45 mmol) were combined in a vial containing 3 mL of water. The reaction mixture was stirred at 90 °C for 30 minutes, with the immediate precipitation of a gelatinous white solid. The mixture was filtered. Colorless crystals suitable for X-ray crystallography were obtained by slow evaporation of the clear solution at ambient temperature. Yield = 0.XX g (XX %). Melting point: turned light grey at 176 °C, with a few dark-brown spots; melted at 250 °C with accompanying decomposition. IR (KBr pellet, cm^{-1}) 3503 (br), 3154 (br), 2950 (br), 2357 (w), 1622 (s), 1514 (s), 1429 (w), 1306 (w), 1150 (s), 1083 (s), 940 (m), 808 (m), 729 (s), 627 (s), 538 (w), 467 (m). ^1H NMR (300 MHz, 25 °C, D_2O): δ 2.6 ppm (d, 2H, J = 13.5 Hz). $^{31}P\{H\}$ NMR (121 MHz, 25 °C, D_2O): δ 25 ppm.

4.5.3 Synthesis of 15, [{Co(NH₃CH₂PO₃H)₂(H₂O)₂}(ClO₄)₂]ₙ

Ampa (0.05 g, 0.5 mmol) and $Co(ClO_4)_2 \cdot 6H_2O$ (0.16 g, 0.45 mmol) were combined in a vial containing 3 mL of EtOH/H_2O (50/50). The reaction mixture was stirred at 60 °C for 60 minutes, with no precipitation of any solid. Bright pink crystals suitable for X-ray crystallography were obtained by slow evaporation of the clear solution at ambient temperature. Yield = 0.094 g (81 %). Melting point: 200 °C color changed to lavender; melted at 239 °C and color completely changed to bright dark purple. IR (KBr pellet, cm^{-1}) 3496 (m), 3434 (w), 3401 (w), 3369 (w), 3310 (w), 3120 (w), 3080 (w), 2996 (w), 2944 (w), 2872 (w), 2525 (m), 2350 (w), 2289 (m), 1613 (s), 1489 (s), 1465 (s), 1425 (m), 1301 (m), 1106 (s), 1013 (w), 971 (w), 932 (s), 811 (m), 727 (s), 672 (w), 627 (s), 565 (w), 507 (w), 476 (w).

4.5.4 Synthesis of 16, [{Mn(NH$_3$CH$_2$PO$_3$H)$_2$(H$_2$O)$_2$}(ClO$_4$)$_2$]$_n$

Ampa (0.05 g, 0.5 mmol) and Mn(ClO$_4$)$_2$·H$_2$O (0.11 g, 0.45 mmol) were combined in a vial containing 3 mL of H$_2$O. The reaction mixture was stirred at 90 °C for 60 minutes, with no precipitation of any solid. Colorless crystals suitable for X-ray crystallography were obtained by slow evaporation of the clear solution at ambient temperature. Yield = 0.098 g (85 %). Melting point: a few brown spots appeared at 220 °C, capillary tube fogged up at 334 °C, with apparent decomposition of the crystalline material at 350 °C. IR (KBr pellet, cm^{-1}) 3403 (br), 2349 (w), 1622 (s), 1487 (m), 1430 (w), 1309 (w), 1146 (s), 1111 (s), 1088 (s), 954 (w), 904 (m), 807 (w), 727 (m), 628 (s), 537 (m), 466 (m).

4.5.5 Synthesis of 17, [{Cu(NH$_3$CH$_2$PO$_3$H)$_2$(H$_2$O)}(H$_2$O)$_2$(ClO$_4$)$_2$]$_n$

Ampa (0.05 g, 0.5 mmol), copper(I) iodide (0.086 g, 0.45 mmol), and copper(II) perchlorate hexahydrate (0.167 g, 0.45 mmol) were combined in a vial containing 3 mL of water. The reaction mixture was stirred at 90 °C for 1 hour, with the precipitation of a fine light-blue solid. The mixture was filtered. Crystals suitable for X-ray crystallography were obtained by slow evaporation of the clear solution at ambient temperature. Yield = 0.019 g (16 %). Melting point: >250 °C. IR (KBr pellet, cm^{-1}) 3565 (s), 3510 (s), 3392 (s), 3210 (s), 3150 (s), 3050 (s), 2883 (m), 2654 (w), 2513 (w), 2362 (w), 2343 (w), 1598 (s), 1487 (s), 1462 (s), 1436 (m), 1397 (w), 1309 (w), 1112 (s), 1081 (s), 1040 (s), 1011 (s), 994 (s), 937 (m), 827 (m), 733 (s), 628 (s), 587 (s), 503 (s), 482 (s).

4.5.6 Synthesis of 18, [{Yb$_2$(NH$_3$CH$_2$PO$_3$)$_2$(NO$_3$)$_3$(H$_2$O)$_3$}NO$_3$]$_n$

Ampa (0.07 g, 0.6 mmol) and Yb(NO$_3$)$_3$·5-6H$_2$O (0.28 g, 0.6 mmol) were combined in a vial containing 2 mL of water. The reaction mixture was stirred at 80 °C for 10 minutes, with the

precipitation of a fine white solid within 7 minutes. The mixture was filtered. Colorless crystals suitable for X-ray crystallography were obtained by slow evaporation of the clear solution at ambient temperature. Yield = 0.062 g (32 %). Melting point: >300 °C; loss of water between 186 and 190 °C. IR (KBr pellet, cm^{-1}) 3435 (br), 3402 (br), 2360 (s), 2340 (s), 1632 (s), 1472 (s), 1383 (s), 1354 (s), 1160 (m), 1109 (w), 1015 (m), 813 (m), 743 (m), 669 (m), 654 (w), 591 (w), 537 (w), 454 (w).

4.5.7 Synthesis of 19, [{Gd(NH$_3$CH$_2$PO$_3$)(H$_2$O)$_4$(NO$_3$)}NO$_3$]$_n$

Ampa (0.07 g, 0.6 mmol) and Gd(NO$_3$)$_3$·6H$_2$O (0.28 g, 0.6 mmol) were combined in a vial containing 3 mL of water. The reaction mixture was stirred at 80 °C for 30 minutes, with the appearance of a fine white precipitate within 20 minutes. The solution was filtered. White crystals suitable for X-ray crystallography were obtained by slow evaporation of the solvent at ambient temperature. Yield = 0.038 g (18 %). Melting point: >300 °C; loss of water around 150 °C. IR (KBr pellet, cm^{-1}) 3546 (s), 3490 (s), 3262 (s), 3173 (s), 3018 (m), 2771 (s), 2681 (s), 2554 (s), 2408 (m), 2350 (m), 1994 (w), 1765 (w), 1637 (s), 1590 (m), 1534 (s), 1422 (s), 1381 (s), 1357 (s), 1301 (m), 1150 (s), 1076 (s), 1015 (s), 987 (s), 823 (s), 758 (s), 560 (s), 457 (s).

4.5.8 Synthesis of 20, [{Sm(NH$_3$CH$_2$PO$_3$)(H$_2$O)$_4$(NO$_3$)}NO$_3$]$_n$

Ampa (0.07 g, 0.6 mmol) and Sm(NO$_3$)$_3$·6H$_2$O (0.28 g, 0.6 mmol) were combined in a vial containing 3 mL of water. The reaction mixture was stirred at 80 °C for 45 minutes, with the appearance of a fine white precipitate within 30 minutes. The solution was filtered. Off-white crystals suitable for X-ray crystallography were obtained by slow evaporation of the solvent at ambient temperature. Yield = 0.029 g (14 %). Melting point: >300 °C; loss of water at ~150

°C. IR (KBr pellet, cm^{-1}) 3547 (s), 3489 (s), 3262 (s), 3044 (m), 2771 (s), 2684 (s), 2558 (s), 2412 (m), 2355 (m), 1985 (w), 1764 (w), 1659 (m), 1634 (s), 1590 (m), 1536 (s), 1502 (w), 1462 (w), 1424 (s), 1385 (s), 1303 (m), 1149 (s), 1075 (s), 1017 (s), 988 (s), 823 (s), 755 (s), 556 (s), 457 (s).

Table 4.2: Crystal Data for Compounds 14 - 20

Compound Name	14	15	16	17
Chemical Formula	$C_2H_{16}Cl_2N_2O_{16}P_2Zn$	$C_2H_{16}Cl_2N_2O_{16}P_2Co$	$C_2H_{16}Cl_2N_2O_{16}P_2Mn$	$C_2H_{16}Cl_2N_2O_{16}P_2Cu$
Formula Weight	522.40	515.94	511.95	538.57
Crystal System	Monoclinic	Monoclinic	Monoclinic	Monoclinic
Space Group	P2$_1$/c	P2$_1$/c	P2$_1$/c	C2/C
T(K)	298(2)	298(2)	213(2)	298(2)
a (Å)	9.8950(11)	9.8871(17)	9.844(2)	24.605(2)
b (Å)	8.2412(10)	8.2546(14)	8.2715(17)	7.3173(6)
c (Å)	9.7759(11)	9.7966(17)	9.965(2)	9.8685(8)
α (°)	90	90	90	90
β (°)	97.550(2)	97.618(3)	97.610(3)	103.794(1)
γ (°)	90	90	90	90
V (Å^3)	790.28(16)	792.5(2)	804.2(3)	1725.5(2)
Z	2	2	2	10
Reflections collected	4757	5114	3755	4533
Independent	1793	1798	1449	2070

reflections				
Data/restraints /parameter ratio	1793 / 3 / 139	1798 / 3 / 127	1449 / 2 / 139	2070 / 5 / 153
Unique Data (*R int*)	0.0300	0.0296	0.0258	0.0208
D_{calc} (Mg/m^3)	2.195	2.154	2.114	2.0730
F(000)	528	518	518	1096
R indices (all data)	R1 = 0.0429 wR2 = 0.0803	R1 = 0.0494 wR2 = 0.0955	R1 = 0.0347 wR2 = 0.0726	R1 = 0.0447 wR2 = 0.0845
Final R indices [I > 2σ(I)]	R1 = 0.0312 wR2 = 0.0734	R1 = 0.0362 wR2 = 0.0873	R1 = 0.0280 wR2 = 0.0683	R1 = 0.0309 wR2 = 0.0804
Largest difference in peak and hole (e Å^{-3})	0.449 and -0.377	0.513 and -0.584	0.444 and -0.299	0.55 and -0.39

Compound Name	18	19	20
Chemical Formula	$C_2H_{10}N_6O_{21}P_2Yb_2$	$C_1H_{12}Gd1N_1O_{13}P_1$	$C_1H_{12}N_3O_{13}P_1Sm_1$
Formula Weight	862.18	462.36	455.46
Crystal System	Orthorhombic	Monoclinic	Monoclinic
Space Group	$P2_12_12_1$	$P2_1/c$	$P2_1/c$
T(K)	298(2)	297(2)	223(2)
a (Å)	8.8410(10)	5.7753(13)	5.7776(6)
b (Å)	13.2006(16)	10.523(2)	10.5495(11)
c (Å)	18.135(2)	19.962(5)	19.977(2)
α (°)	90	90	90
β (°)	90	92.772(4)	92.598(2)
γ (°)	90	90	90

V (Å^3)	2116.5(4)	1211.7(5)	1216.3(2)
Z	4	4	4
Reflections collected	18505	11986	7245
Independent reflections	5039	2900	2878
Data/restraints /parameter ratio	5039/6/322	2900 / 8 / 204	2878 / 8 / 204
Unique Data ($R\ int$)	0.0341	0.0435	R(int) = 0.0478
D$_{calc}$ (Mg/m^3)	2.706	2.535	2.487
F(000)	1608	888	880
R indices (all data)	R1 = 0.0215 wR2 = 0.0479	R1 = 0.0348 wR2 = 0.0697	R1 = 0.0654 wR2 = 0.0812
Final R indices [I > 2σ(I)]	R1 = 0.0201 wR2 = 0.0473	R1 = 0.0273, wR2 = 0.0658	R1 = 0.0360 wR2 = 0.0694
Largest difference in peak and hole (e Å^{-3})	0.656 and -1.093	1.172 and -0.798	1.242 and -1.037

Chapter 5

Investigative Studies with 2-(pyridylmethyl)phosphonic Acid and its Isomers

5.1 Introduction

2-(Pyridylmethyl)phosphonic acid ($2pyCH_2PO_3H_2$) was shown in Chapter 3 as a viable resource for the synthesis of multidimensional coordination polymers. The flexible nature of this ligand provides increased opportunities for the self-assembly of robust coordination frameworks. Building on our previous work with this ligand, we were interested in exploring the effects of selected variables on the structural motif of products formed from similar reactions. A series of seven polymers and two dimers have been synthesized by varying the metal-salt precursors and the structural orientation of the ligand. By structural comparisons to previously analyzed polymers, we will discuss similarities and differences, with the aim of evaluating the relationships between metal choice and counter ion on polymer architecture, as well as the effects of geometric constraints of the ligand.

5.2 Results and Discussion

2-(Pyridylmethyl)phosphonic acid was prepared as discussed in Section 3.1.1, with its isomers 3-(pyridylmethyl)phosphonic acid and 4-(pyridylmethyl)phosphonic acid prepared by employing 3- and 4-(bromomethyl)pyridine hydrobromide. For typical transition metal experiments, stoichiometric quantities of metal salt and ligand were dissolved in water/ethanol and stirred with gentle heating for ~3 hours. Crystalline products were obtained after slow evaporation of the solution.

5.2.1 Discussion of Calcium Dimer 21: [Ca(2PyHCH$_2$PO$_3$H)$_2$(H$_2$O)$_5$]Br$_2$ and the 2D Polymer 22: [{Ca(2PyHCH$_2$PO$_3$H)$_2$(H$_2$O)$_2$}(ClO$_4$)$_2$]$_n$.

Bisphosphonates have been well documented for their treatment of osteoporosis,[188] and the presence of a heterocyclic nitrogen atom has proven beneficial to the action of this class of therapeutic agents.[189] The ability of bisphosphonate compounds to bind to the bone mineral hydroxyapatite is due to the affinity of the phosphonate moieties for the divalent calcium ion.[190] Therefore, we were interested in examining the coordinative properties of 2PyCH2PO$_3$H$_2$ with selected calcium precursors with the aim of producing multidimensional polymers. Previous work by our group with 4PyCH$_2$PO$_3$H$_2$ demonstrated that this ligand class was capable of supporting a polymeric architecture with main group element gallium under anaerobic conditions.[191]

The halide salt was selected as the metal precursor, mindful of the possibility for post-synthetic modification. The stoichiometric reaction of calcium bromide and 2-(pyridylmethyl)phosphonic acid in THF under anaerobic conditions led to the isolation of the molecular dimer, **21** (Figure 5.1). Attempts in other solvents led to the formation of calcium hydroxides or Ca(H$_2$O)$_6^{2+}$.
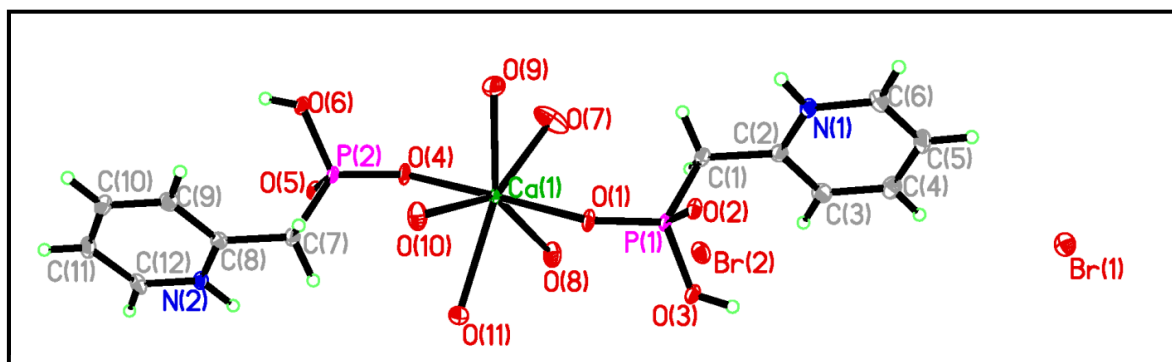
Figure 5.1 Molecular dimer **21**, [Ca(2PyHCH$_2$PO$_3$H)$_2$(H$_2$O)$_5$]Br$_2$. Selected bonds (Å) and angles (°): Ca1-O4 2.290(3), Ca1-O1 2.296(3), Ca1-O9 2.416(3), Ca1-O8 2.472(3), P1-O1 1.482(3), P1-O2 1.519(3), P1-O3 1.580(3), P2-O4 1.483(3), P2-O5 1.520(3), P2-O6 1.582(3), O4-Ca1-O1 177.34(10), O4-Ca1-O9 95.06(11), O1-P1-O3 108.77(16), O4-P2-O6 109.00(17).

The solid-state analysis of **21** showed that the bromide atoms were displaced and located at distances of 5.2 and 11.4 Å from the Ca^{2+} center. The pyridine nitrogen atoms were protonated; thus for charge balance the phosphonic acid is singly deprotonated. This is supported by the sharp band at 3261 cm^{-1}, attributed to POH stretching, as well as the P-O bond lengths: the shortest bond lengths of 1.482(3) Å for P1-O1 and 1.483(3) for P2-O4 are suggestive of P=O bonds, similar to the P=O bond in the neutral phosphine oxide, $[Ph_2P(O)CH_2]C_6H_4Br$, with a bond length of 1.486 Å.[192] O1 and O4 are therefore datively bonded to the calcium atoms. The remaining P-O bonds, such as P1-O2 and P1-O3, have bond lengths of 1.519(3) Å and 1.580(3) Å, respectively, with the latter being the protonated oxygen atom. The seven-coordinate calcium atom has distorted pentagonal bipyramidal geometry, with oxygen atoms occupying all available sites, a common feature in calcium phosphonates.[193] The Ca-O distances vary between 2.290(3) and 2.480(3) Å, with the longer bonds associated with the coordinated water molecules and in the range for similarly reported structures.[194] Hydrogen atoms could be located for these oxygen atoms but would not converge on refinement and consequently were omitted from the final refinements. The protonations of the pyridine nitrogen atom and phosphonate moiety inhibit the growth of the dimensionality of the molecular dimer. Attempts to obtain different structural architectures under basic conditions led to a mixture of amorphous calcium oxide or hydroxides; however, isolation of **21** is not too surprising, given that reacting phenyl phosphonic acid with calcium chloride yields a similar dimeric structure.[195]

The presence of a large number of coordinated water molecules results in lower thermal stability for complex **21**, which melts at 148 – 150 ^{o}C. Infrared spectroscopy shows a strong absorption at 1645 cm^{-1}, characteristic of coordinated H_2O, and the P=O band at 1230 cm^{-1} in

the free ligand shifts to 1219 cm^{-1}, indicating reduction of the double bond P=O character due to metal coordination.[167]

From the isolation of **21**, it was apparent that calcium halides were not going to be suitable precursors for polymeric or cage materials, and the 1:1 reaction of calcium perchlorate with $2PyCH_2PO_3H_2$ was performed in EtOH/ H_2O. After slow evaporation of the solution, colorless crystals of **22** were isolated in high yield. X-ray crystallographic analysis on **22** found it to be a two-dimensional monoclinic coordination polymer, Figure 5.2.
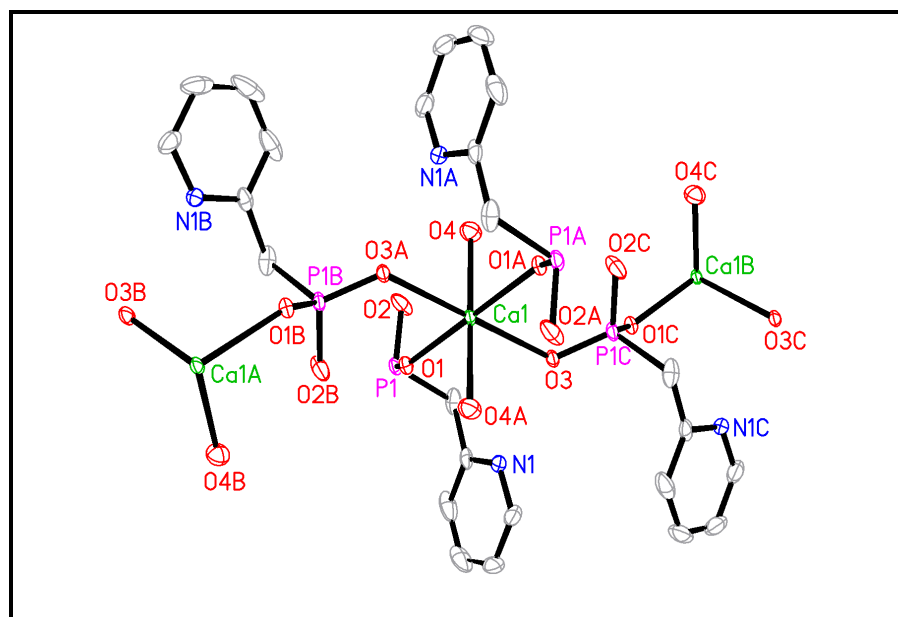
Figure 5.2 2D calcium polymer, **22**, $[\{Ca(2PyHCH_2PO_3H)_2(H_2O)_2\}(ClO_4)_2]_n$, hydrogen atoms omitted for clarity. Thermal ellipsoids at 30% probability. Selected bond lengths (Å) and angles ($^\circ$): Ca1-O1 2.2978(17), Ca1-O3 2.3548(16), Ca1-O4 2.339(2), P1-O1 1.4998(19), P1-O3 1.5029(17), P1-O2 1.568(2), O1-Ca1-O1A 180.00(8), O4-Ca1-O4A 180.0, O3-Ca1-O3A 180.00(5).

In the asymmetric unit of **22** is a calcium ion at half occupancy, one molecule of ligand, a water molecule and a disordered lattice perchlorate ion. The geometry around the calcium atom is almost perfectly octahedral. The coordination sites are occupied by two water molecules, two oxygen atoms from the phosphonate groups, and their symmetry equivalents. The oxygen

atoms coordinated to the calcium center, O1 and O3, have very similar P-O bond lengths of 1.4999(18) Å (P1-O1) and 1.5035(16) Å (P1-O2). The remaining P-O bond is longer, as expected for a protonated phosphonic oxygen atom (P1-O2 1.568(2) Å). The pyridyl nitrogen atom is protonated and provides the charge balance.

The structure of **22** can be compared with $Ca(2\text{-}FC_6H_4CH_2PO_3H)_2\cdot3H_2O$ and $Ca(4\text{-}FC_6H_4CH_2PO_3H)_2\cdot3H_2O$, isolated from the reaction of the corresponding fluorobenzylphosphonic acids with calcium hydroxide.[196] The calcium coordination of both dimers are fairly regular pentagonal bipyramidal, similar to polymer **22**, and the protonation of the ligand is analogous. When examining the packing diagrams of the two crystals, the orientation of the aromatic rings in the 2-isomer of the calcium fluorobenzylphosphonate were similar to that of polymer **22**. While the layers of the 4-isomer are arranged with parallel alignment of adjacent aromatic rings, the layers of the 2-isomer are rotated 180° with respect to each other and are angled in opposite directions. Polymer **22** exhibits a similar rotation of the pyridine rings from adjacent layers as viewed down the *a*-axis (Figure 5.3).
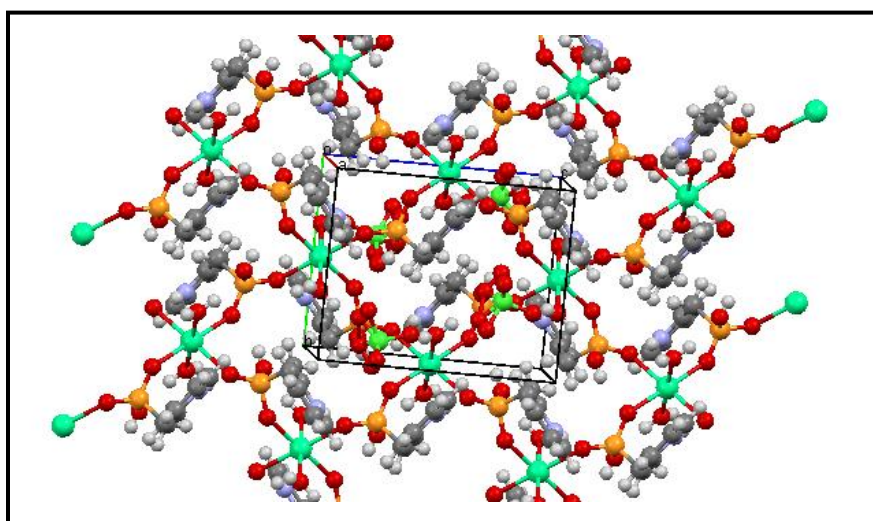
Figure 5.3 Packing diagram of Polymer **22**, $[\{Ca(2PyHCH_2PO_3H)_2(H_2O)_2\}(ClO_4)_2]_n$, viewed down the crystallographic *a*-axis, depicted as the red line of the box. The oppositely-angled phenyl rings can be seen in adjacent layers. Turquoise = Ca, orange = P, red = O, grey = C, blue = N, white = H.

5.2.2 Discussion of 23: [{Co(2PyHCH$_2$PO$_3$H)$_2$(H$_2$O)$_4$}(NO$_3$)$_2$]

In order to investigate the role of the counterion on structural motif, manganese(II) nitrate and cobalt(II) nitrate were reacted with 2PyCH$_2$PO$_3$H$_2$ under the same conditions as used for the synthesis of **6**, **7, 15,** and **16** (see Chapters 3 and 4). From the manganese reaction, unreacted ligand was isolated, indicating no reaction. Various solvents and reaction conditions were attempted but all proved unsuccessful. From the cobalt(II) nitrate reaction, pale pink crystals of the molecular dimer **23**, [{Co(2PyHCH$_2$PO$_3$H)$_2$(H$_2$O)$_4$}(NO$_3$)$_2$], were isolated, Figure 5.4, which crystallized in the triclinic space group P-1.
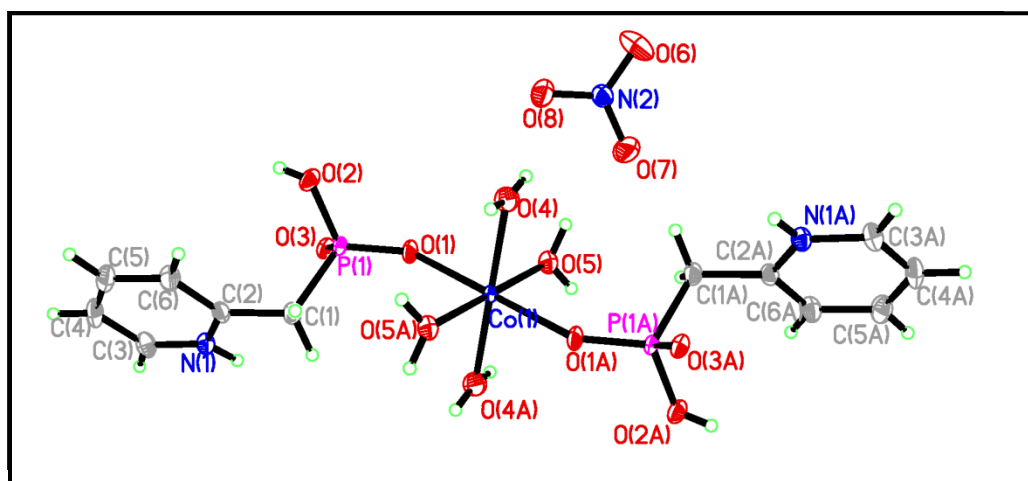
Figure 5.4 Molecular dimer, [{Co(2PyHCH$_2$PO$_3$H)$_2$(H$_2$O)$_4$}(NO$_3$)$_2$], **23**. Selected bond lengths (Å) and angles (°): Co1-O1 2.0926(16), Co1-O4 2.0880(19), Co1-O5 2.0842(18), P1-O1 1.4853(15), P1-O2 1.5762(17), P1-O3 1.5166(16), O5A-Co-O5 180.000(1), O5A-Co1-O4A 89.70(8), O5A-Co1-O4 90.30(8), O1-P1-O3 116.53(10), O1-P1-O2 109.27(10), O3-P1-O2 108.84(9), O1-P1-C1 109.22(10).

Compound **23** is a mononuclear structure consisting of one Co(II), two PyCH$_2$PO$_3$H ligands and four water molecules. The Co atom lies on an inversion center and has close to perfect octahedral geometry, O1-Co-O1A (180°). Only one oxygen atom from the phosphonate group

is coordinated to the cobalt atom, and is part of the shortest P-O bond at 1.4853(15) Å, P1-O1. The P1-O2 is the longest P-O bond, 1.5762(17) Å, and O2 is protonated. The Co-O bond lengths are all similar, within the range 2.0842(18) – 2.0926(16) Å, and comparable to other reported structures.[197] Even though reaction conditions were identical to those used to produce polymers **6** and **7** (Figure 3.3) with 2-(pyridylmethyl)phosphonic acid, the substitution of the nitrate counterion for the perchlorate ion resulted in metal coordination spheres with four aqua groups instead of the two symmetry-related ones in **6** and **7**. This prevented the extension of the M-O-P moiety in the *a*-direction, although an extensive hydrogen bonding network is found among the phosphonate oxygen atoms, protonated nitrogen atom of the pyridyl moiety, water molecules, and the lattice nitrate ion of structure **23**. Further trials with this metal salt and ligand, varying both stoichiometry and solvent, produced amorphous materials.

5.2.3 Discussion of Zinc Phosphonates 24: [Zn(2PyHCH$_2$PO$_3$)Cl]$_n$, 25: [{Zn(2PyHCH$_2$PO$_3$)(2PyHCH$_2$PO$_3$H)}(H$_2$O)(ClO$_4$)]$_n$, and 26: [{Zn$_2$(2PyHCH$_2$PO$_3$H)$_2$(2PyHCH$_2$PO$_3$)$_2$}(H$_2$O)$_2$(NO$_3$)$_2$]$_n$

In the interest of pursuing the effects of the flexible 2pyCH$_2$PO$_3$H$_2$ ligand compared to our first ligand of study, 2PyHPO$_3$H$_2$, as well as investigating the effect of counterion on the resulting structures, 1:1 reactions of 2PyCH$_2$PO$_3$H$_2$ with a series of zinc salts were performed. Polymers isolated from reactions utilizing zinc(II) chloride, **24**, perchlorate, **25**, and nitrate, **26**, were a result of experiments conducted in a similar manner with the goal of examining the effect of the anion on structure architectures. Examination of the crystal structures shows a commonality between **24 – 26**, which is the net-like motif made up of interlinked eight-membered Zn-O-P rings, Figures 5.5, 5.6, and 5.7, as discussed previously in Sections 2.1 and 2.2.1. This structural motif is similar to that found in polymers **1** and **2**, produced from the reaction of 2PyHPO$_3$H with zinc(II) bromide and zinc(II) chloride, respectively.

Crystalline $[Zn(2PyHCH_2PO_3)Cl]_n$, **24** (Figure 5.5), from the zinc(II) chloride reaction, was found to crystallize in the monoclinic space group, $P2_1/c$. Within the asymmetric unit of **24** was found one tetrahedral zinc atom, coordinated to a terminal chloride and three oxygen atoms from separate doubly-deprotonated ligands. The presence of the terminal halide prevents interlinking of the Zn-O-P rings, therefore, the nets are linked through the bridging phosphonates. This same limitation in the growth of the polymer was seen in polymers **1** and **2**, utilizing the halide salts. The 8-membered rings in polymer **24** are smaller than the 12-membered rings of polymers **1** and **2**, and, in fact, resemble the rings found in the dinuclear zinc structure, $[Zn_2(4\text{-}PyHPO_3H)_2Cl_4]$, pictured in Figure 2.5 from Section 2.1.2,[115] which incorporates the more rigid ligand lacking the methylene moiety. In the case of polymer **24**, only one chloride coordinated to the metal center, leaving room for the extension of the framework via another bridging $2\text{-}PyHCH_2PO_3H$ ligand.
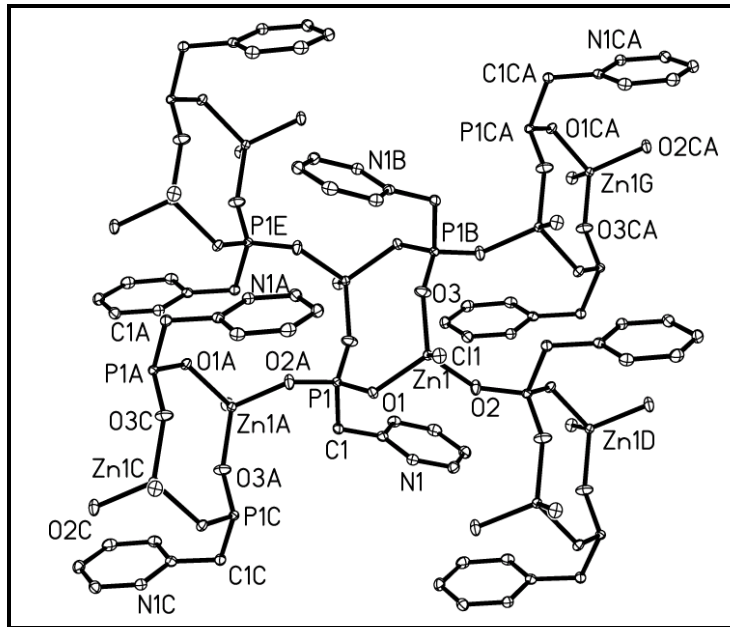
Figure 5.5 Polymeric form of **24**, with thermal ellipsoids drawn at 30% probability level and hydrogen atoms omitted for clarity. Selected bonds (Å) and angles (°): Zn1-O3 1.9181(15), Zn1-O2 1.9494(13), Zn1-O1 1.9705(13), Zn1-Cl1 2.2457(6), P1-O1 1.5382(13), O3-Zn1-O2 112.53(7), O3-Zn1-O1 114.29(6), O2-Zn1-O1 102.13(6), O3-Zn1-Cl1 107.07(5), O2-Zn1-Cl1 112.60(5), O1-Zn1-Cl1 108.25(4).

The two reactions using the labile anions perchlorate and nitrate produced similar structures where the anion remains in the lattice for charge stabilization and hydrogen-bond participation. Polymers **25**, [{Zn(2PyHCH$_2$PO$_3$)(2PyHCH$_2$PO$_3$H)}(H$_2$O)(ClO$_4$)]$_n$, Figure 5.6a, and **26**, [{Zn$_2$ (2PyHCH$_2$PO$_3$H)$_2$(2PyHCH$_2$PO$_3$)$_2$}(H$_2$O)$_2$(NO$_3$)$_2$] $_n$, Figure 5.6b, were both found to crystallize in the triclinic space group P-1.
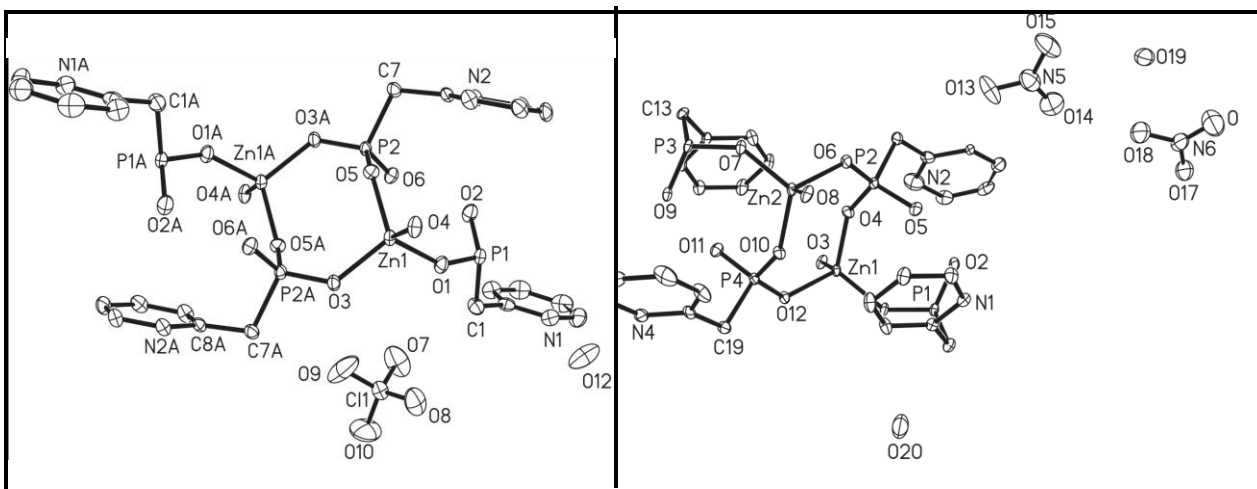
Figure 5.6: Thermal ellipsoids drawn at 30% probability level and hydrogen atoms are omitted for clarity. **(a)** Crystal structure of **25**. Selected bond lengths (Å) and angles (^{o}): Zn1-O1 1.920(3), Zn1-O3 1.935(3), Zn1-O4, 1.946(3), P1-O1 1.495(3), P1-O2 1.555(3), P1-O4A 1.509(3), P2-O5 1.523(3), P2-O6 1.518(3), P2-O3A 1.519(3), O1-Zn1-O3 112.20(14), O4-Zn1-O1 109.35(14), O1-P1-O2 112.83(19). **(b)** Crystal structure of **26**. Selected bond lengths (Å) and angles (^{o}): Zn1-O1 1.915(4), Zn1-O4 1.921(3), Zn1-O3 1.942(3), Zn1-O12 1.953(3), P1-O1 1.518(4), P1-O2 1.526(4), O4-Zn1-O3 104.72(16), O4-Zn1-O12 112.14(15), O1-P1-O2 113.9(2).

The asymmetric unit of **25** contains a lattice perchlorate ion and water molecule, one zinc atom, and two ligands, with each ligand coordinated to the zinc atom through one of its oxygen atoms. In **25** there is a difference between the phosphorus centers in each ligand; the oxygen atom O1, from the P1 phosphonate group, has a short P=O bond of 1.495(3) Å, while the other two P-O bonds are P-O single bonds with O2 protonated. The second phosphonate group, containing P2, has three P-O bonds that are all indicative of single bonds (1.518(3), 1.519(3),

and 1.523(3) Å), and are therefore doubly deprotonated to maintain electroneutrality. The polymeric zinc phosphonate from the zinc nitrate reaction, **26**, has two zinc atoms, four ligands, two lattice nitrate ions and two lattice water molecules in the asymmetric unit. Both polymers exhibit tetrahedral geometry around the zinc(II) centers and the common 8-membered Zn-O-P ring seen in many zinc structures.[115] An examination of the phosphorus-oxygen bond lengths and angles in **26** reveal different phosphonate charges, similar to **25**. P1 and P3 are doubly deprotonated, while P2 and P4 are believed to be singly deprotonated, with oxygen atoms O5 and O11 retaining their protons. Table 5.1 delineates the major structural similarities and differences between the three zinc phosphonate polymers.

Table 5.1: Comparison of Structural Features of **24 - 26**

Complex	Zn—Zn distance	P—P distance	PO$_3$ charge	NH
24: Zn-Cl	4.369	4.816	P1 = -2	yes
25: Zn-ClO$_4$	4.477	4.448	P1 = -1 P2 = -2	yes
26: Zn-NO$_3$	4.516	4.500	P1 = -2 P2 = -1 P3 = -2 P4 = -1	yes

The packing diagrams for structures **24 - 26** reveal similarities in their 3D motifs (Figure 5.7). However, the orientation of the ligand phosphonate moieties create subtle differences in their architectures. Both have interlayer interactions to the lattice counterions and coplanar pyridine rings lining the outside of the M-PO$_3$ core.
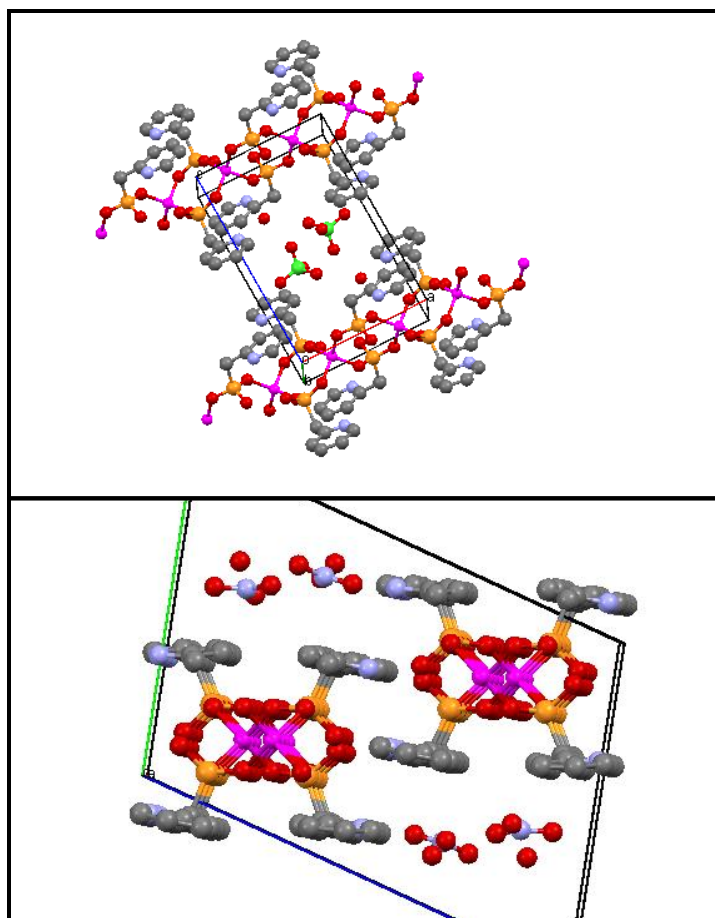
Figure 5.7 (a) Packing diagram of polymer **25**, viewed just off-center of its *b*-axis. **(b)** Packing diagram of polymer **26**, viewed down the *a*-axis. Crystallographic axes box displays geometric centers of molecules in one or more unit cells. Unit cell axes: *a* = red, *b* = green, *c* = blue. Atoms: Pink = Zn, orange = P, red = O, blue = N, grey, = C, green = Cl.

The zinc phosphonates **24 - 26** can be compared with the product from the reaction of hydroxyl(2-pyridyl)methylphosphonic acid with zinc sulfate, which afforded a seven atom zinc cluster[145] (see Figure 3.1, Section 3.1.1). This comparison highlights how metal anion selection and small ligand alterations, such as the addition of a hydroxyl group, can dramatically affect structural dimensionality.

Due to the structural similarity of polymers **24 – 26**, there are many analogous features in their analytical data. All show a single ^{31}P NMR peak at 13 ppm, and show similar IR spectra

with characteristic vibrations observed for the water molecules in **25** and **26**, symmetric and

asymmetric P–OH stretches at ~3200 cm^{-1} (m), and deformation at ~1600 cm^{-1}. PO$_3$ stretching

modes are observed between 1270 and 960 cm^{-1}, and the C–C and C–N stretches associated

with the pyridyl ligand are observed between 1500 and 1410 cm^{-1}.[181] Polymers **25** and **26** are

thermally robust, with no decomposition observed until 200 $^{\circ}$C; polymer **24** is slightly less

robust, melting at 177 – 179 $^{\circ}$C.

5.2.4 Discussion of 27: [{Zn(3PyHCH$_2$PO$_3$H)(3PyHCH$_2$PO$_3$)(H$_2$O)}NO$_3$]$_n$.

For structural comparisons, the reaction of 3PyHCH$_2$PO$_3$H$_2$ with zinc chloride and zinc

nitrate were performed, to investigate how the heterocyclic nitrogen's position might affect

polymer topology.   However, utilizing the same experimental protocol, only crystals from the

zinc nitrate reaction could be isolated, to obtain   polymer **27** (Figure 5.8), crystallizing in

triclinic space group P-1.
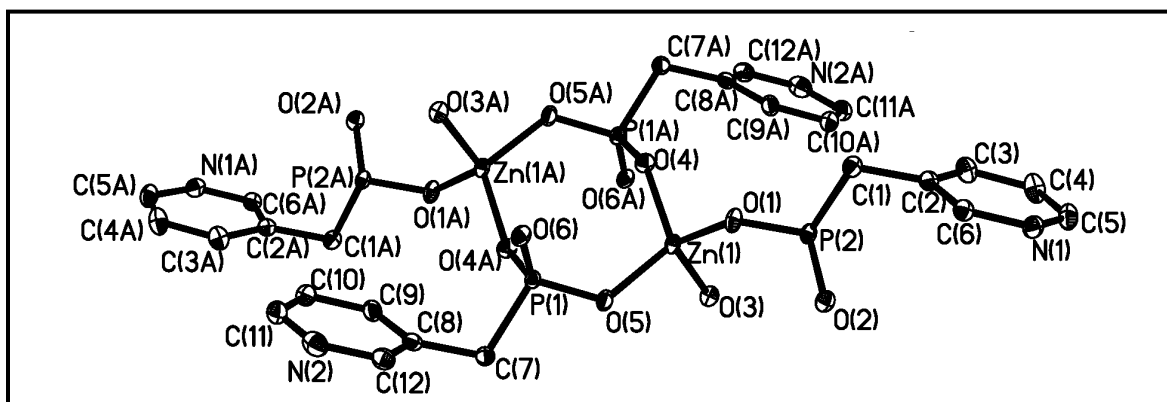
Figure 5.8 Polymeric form of **27**:   [{Zn(3PyHCH$_2$PO$_3$H)(3PyHCH$_2$PO$_3$)(H$_2$O)}NO$_3$]$_n$.
Selected bond lengths (Å) and angles ($^{\circ}$): Zn1-O4 1.910(4), Zn1-O3 1.942(4), Zn1-O5 1.943(4),
Zn1-O1 1.964(4), P1-O4A 1.519(4), P1-O5 1.518(4), P(1)-O(6) 1.535(4), P2-O3A 1.509(4), P2-
O1 1.516(4), P2-O2 1.560(4), O4-Zn1-O3 111.14(17), O3-Zn1-O5 103.86(18), O4-Zn1-O1
104.02(18), O3-Zn1-O1 115.43(17), O5-Zn1-O1 106.37(19), O5-P1-O6 110.1(2).

Within the lattice are one water molecule and a nitrate ion.   The pyridyl nitrogen is

protonated; thus, with two ligands in the asymmetric unit, one of the phosphonic acid molecules

is in the zwitterionic form with one protonated oxygen, while the other phosphonic acid group is doubly deprotonated with the ligand exhibiting a 1- charge. The longer P2-O2 distance of 1.560(4) Å, as seen in previous structures, supports this conclusion. The zinc(II) is in the expected tetrahedral geometry and the 8-membered Zn-O-P ring is analogous to those of polymers **25** and **26**, although the orientation of the pyridyl rings is most similar to the polymer employing the perchlorate salt (**25**), rather than the nitrate (**26**). The zinc(II) structure incorporating the more rigid 3-PyHPO$_3$H, pictured in Figure 2.3 (Section 2.1.2), exhibits a one-dimensional ladder topology with a regular pattern of the organic moiety—one side tilted upward and the other side tilted downward due to the bond angles of the phosphonate group. However, the tetrahedral methylene in between the pyridine and the phosphonate group of 3PyHCH$_2$PO$_3$H$_2$ of structure **27** allows the heterocylic ring to be kept more uniformly close to the plane of the Zn-O-P ring.

5.2.5 Discussion of 28: [Ag$_2$(4PyCH$_2$PO$_3$)]$_n$ and 29: [Ag$_3$(4PyCH$_2$PO$_3$)NO$_3$]$_n$

Given the affinity of silver(I) for nitrogen coordination, we thought that the reactions of silver salts with the 3- and 4-isomers of the PyCH$_2$PO$_3$H$_2$ ligand might provide more suitable coordination geometries, and therefore a better opportunity for chelation of the ligand with the metal center. Given the relative positioning of the phosphonic acid group and of the pyridyl nitrogen (*para* position), it was expected that any steric hindrance, or small bite angle for coordination would be eliminated. Upon reaction of 4-PyCH$_2$PO$_3$H$_2$ with silver(I) triflate and silver(I) nitrate, distinctly different crystalline materials were produced.

Single crystal X-ray analysis reveals that Polymer **28**, [Ag$_2$(4PyCH$_2$PO$_3$)]$_n$ (Figure 5.9a), crystallizes in the monoclinic $P2_1/n$ space group and contains two crystallographically

independent silver centers and no lattice triflate counterion, while polymer **29**, $[Ag_3(4PyCH_2PO_3)NO_3]_n$ (Figure 5.9b), crystallizes in the monoclinic $P2_1/c$ and has three unique silver centers and a lattice nitrate ion.
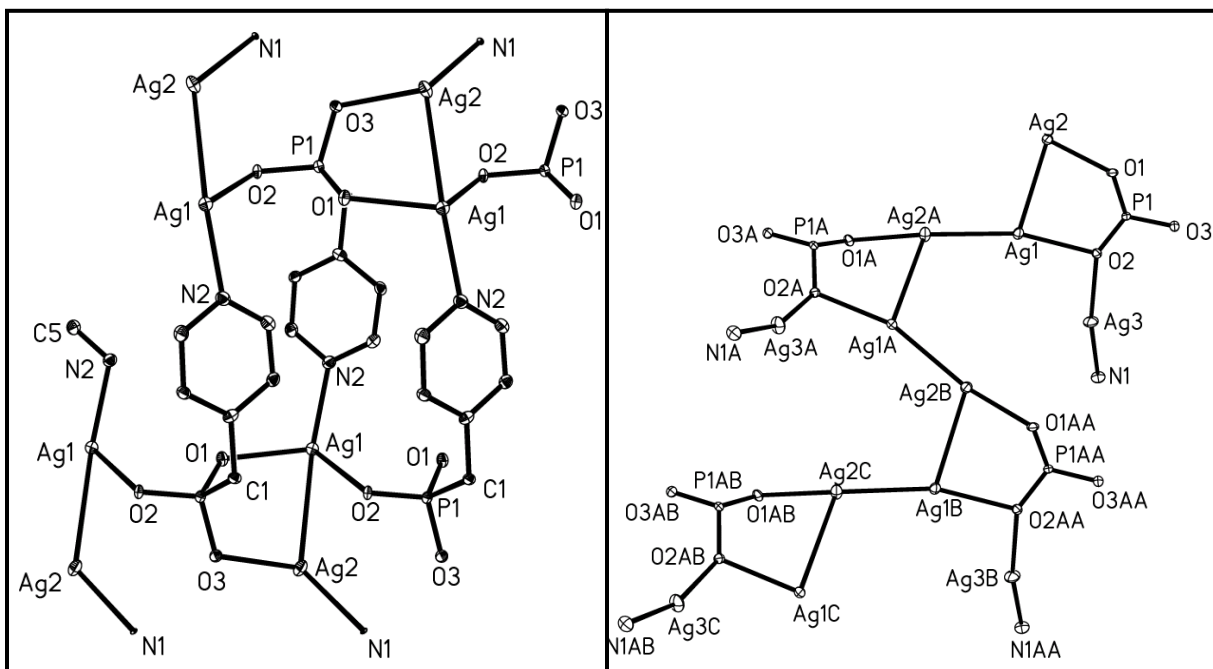
Figure 5.9 (a) Polymer **28**, $[Ag_2(4PyCH_2PO_3)]_n$. Selected bonds (Å) and angles (^{o}): Ag1-N2 2.282(5), Ag1-O2 2.361(4), Ag1-Ag2 3.0849(7), Ag2-N1 2.339(4), P1-O1 1.528(5), P1-O2 1.529(4), P1-O3 1.537(4), N2-Ag1-O2 111.31(17), N2-Ag1-Ag2 168.32(14), O2-Ag1-Ag2 57.68(10). **(b)** Polymer **29**, $[Ag_3(4pyCH_2PO_3)NO_3]_n$. Selected bonds (Å) and angles (^{o}): Ag1-O1 2.2181(3), Ag1-Ag2 3.1857(5), Ag1-Ag2A 3.379(1), P1-O2 1.520(3), P1-O1 1.532(3), P1-O3 1.537(3), O2A-Ag1-O1 168.98(10), O2A-Ag1-O3AA 84.97(9), O1-Ag1-O3AA 105.90(10), O1-Ag1-Ag2A 90.70(7), O3AA-Ag1-Ag2A 162.17(6), O2-P1-O1 114.08(16), O2-P1-O3 110.76(17), O1-P1-O3 111.72(15).

In both **28** and **29** the phosphonate group is doubly deprotonated at both oxygen atoms and links the pair of Ag^+ ions via the formation of $\mu_3\text{-}\eta^3$ phosphonato bridges. These bridges repeat to form an infinite chain. The presence of guest nitrate ions in **29** offset the +1 charge and are located at a distance of 2.169 Å from Ag2.

Crystal packing diagrams for both silver polymers are shown in Figure 5.10, and illustrate the connectivities between the organic and inorganic layers. Polymer **28**, the silver triflate product, has no guest ions present and is a metal organic architecture constructed through Ag-O and Ag-Ag interactions. Each silver atom is at the center of a distorted octahedron. Ag1 coordinates to two symmetry-equivalent Ag2 atoms, a pyridyl nitrogen atom, and three μ_7-η^7 phosphonate ligands, where each oxygen atom bridges two silver centers. This results in a tightly woven network of Ag-O bonds with alternating up-and-down rings, as shown in Figure 5.9a (simple polymeric form) and Figure 5.10a (packing diagram).
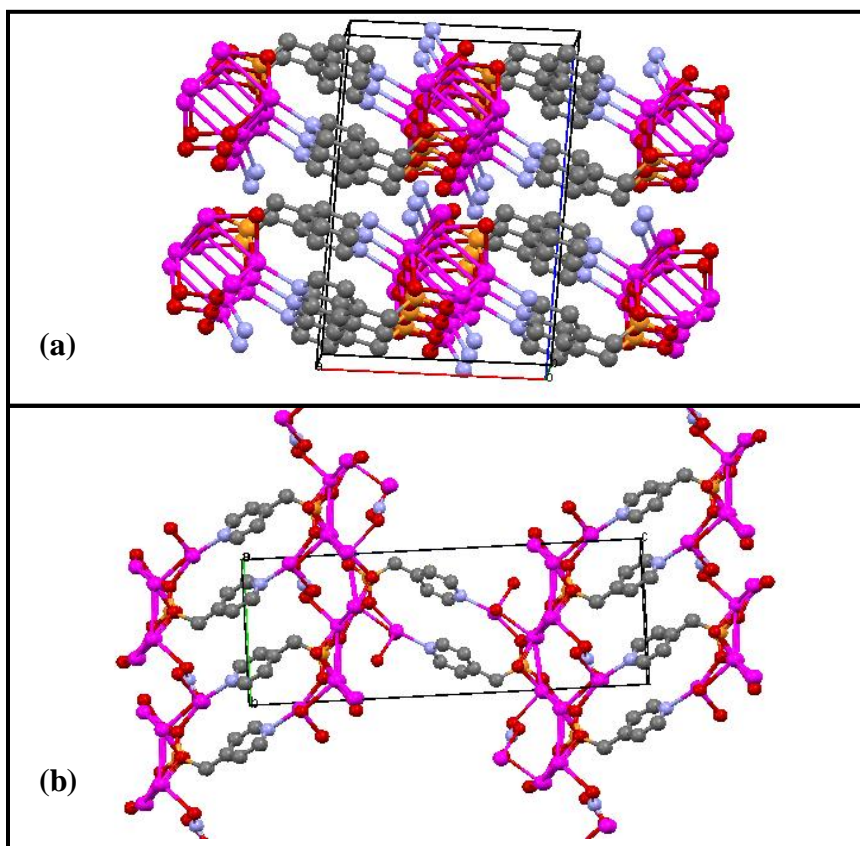
Figure 5.10 **(a)** Packing diagram of polymer **28**, viewed down the *b*-axis. **(b)** Packing diagram of polymer **29**, viewed down the *a*-axis. Crystallographic axes box displays geometric centers of molecules in one or more unit cells. Unit cell axes: *a* = red, *b* = green, *c* = blue. Atoms: Pink = Ag, orange = P, red = O, blue = N, grey, = C.

In **29**, the product formed from the nitrate salt, each silver atom has a different coordination environment, as shown in Figures 5.9b and 5.10b. Ag1 and Ag2 are both six-coordinate, while Ag3 is four-coordinate. Ag1 and Ag2 form an alternating chain of silver(I) centers, with four oxygens occupying the remaining sites on each metal—one oxygen from a nitrate ion and three oxygens from different μ_7-η^7 ligands. Ag3 bridges the two different metal-phosphonate layers, bonding to an oxygen atom from one phosphonate moiety and a pyridyl nitrogen from an adjacent ligand. Ag3 also singly coordinates to two different lattice nitrate ions. The Ag-Ag separation is 3.187 Å between Ag1-Ag2; the van der Waals radii for Ag-Ag is 3.40Å, thus indicating the presence of Ag-Ag interactions. Ag3 has no Ag-Ag interactions.

The similarity of the phosphorus environments in **28** and **29** is evidenced by the similarity in the phosphorus NMR shift at 15 and 16 ppm, respectively. This also indicates that the structural integrity is maintained in solution, as usually where decomposition or breakdown occurs, multiple phosphorus signals are observed.

5.3 Concluding Remarks

It has been well established since the early 1960's that adding a pyridyl moiety as a secondary functional group can increase the stability of metal-organic complexes.[198] In the search for novel supporting scaffolds for various processes (catalysis, sensing, gas storage, etc.) the organic component has an important structure-directing affect on the resulting polymeric architecture. The choice of metal center and counterion combines with the organic ligand to determine the final product's thermal stability, porosity, dimensionality, and functionality. The selection of reaction conditions, including temperature, solvent, and technique, affect the assembly process, and thereby influence the topology of the final product. Utilizing mild

synthetic methods, it has been demonstrated that phosphonic acids containing secondary nitrogen-containing functional groups can support the growth of multidimensional polymers.

More specifically, it has been shown that subtle changes in the position of functional groups can have pronounced effects on the product architecture, through changes in the bridging and chelating modes of the ligand, or simply the bond angles and orientations of the layers within the polymer that can affect pore size and properties. Counterions can participate by coordinating directly to the metal center, as seen with structures **3**, **13** and **18**, or interact within separate layers to add stability to the polymer as demonstrated by most of the polymers that have been discussed. The inherent bias toward obtaining X-ray quality crystals can be a slight disadvantage if the components interfere with desired coordination modes, however, counterions such as nitrates have been shown to increase the connectivity of several of the polymers, including **12** and **29**.

As seen in the previous chapters, metal cation charge and/or ionic radius can affect product geometries, as in the distinctly different Fe(III) and Fe(II) polymers **9** and **10**. The identity of the metal, and its coordination preferences, have been shown to influence the product structure, as with polymers **4** and **5**, as well as have no effect, as in the isotopic lanthanide polymers **19** and **20** and the transition metal polymers **6** and **7**.

The ligand class of phosphonic acids provides a useful platform for the rational design of coordination polymers. The tetrahedral phosphonate group allows for growth in multiple directions, as well as possessing anionic groups whose degree of protonation can be controlled by pH. Increasing the flexibility of the organic group and altering the source of nitrogen donor result in a rich variety of products; however the limitation imposed by a protonated nitrogen is

motivation to discover improved methods to maximize the contributions of the pyridyl and amino groups for metal coordination. Perhaps this might be accomplished by continuing the search for better ways to influence the aqueous equilibria for the nitrogen protonation reaction. Given the ease with which metal hydroxides precipitate, a methodical microscale rise in reaction pH could bear fruit with new structural frameworks that include additional metal-nitrogen binding sites to increase product dimensionality. Additionally, it would be worthwhile to investigate ways to utilize ball-milling as a synthetic method for phosphonic acid polymers, which could eliminate some of the difficulties of aqueous reactions due to functional group pK_a's.

Metal coordination preferences can direct polymer assembly, as demonstrated by the multiple polymer structures attained using a given ligand. Just as the presence of the lead(II) cation encourages the silver(I) to coordinate to the heterocyclic nitrogen in polymer **11**, the presence of a "hard" lanthanide cation coordinating to the phosphonate oxygen atoms could allow another metal to coordinate to the softer pyridine nitrogen atom as seen in the bimetallic polymer in Section 2.1.1. Therefore, future work should be done utilizing the bimetallic route in the pursuit of higher-dimensionality phosphonate polymers. The continued study into the luminescent and magnetic properties of such polymers should provide many opportunities to further our knowledge of the characteristics and functionalities of phosphonic acid polymers. Such studies will also add to the depth and breadth of data pertaining to the factors that affect polymer motifs, as we continue to examine these patterns to reach the goal of intelligent design of polymers with desired structural and functional properties.

5.4 Materials and Methods

All manipulations were performed under aerobic conditions, unless otherwise stated. 2-PyCH$_2$PO$_3$H$_2$, 3-PyCH$_2$PO$_3$H$_2$, and 4-PyCH$_2$PO$_3$H$_2$ were prepared by a modified published method.[137b] All other reagents were purchased from Aldrich and used as received. Crystal data were collected with a Bruker SMART 1000 diffractometer, molybdenum Kα radiation (0.71073Å) at –50, -60 ^{o}C. Crystals were mounted on glass fibers using paratone oil. The data were corrected for absorption. Structures were solved by direct methods[134] and refined[134] via full-matrix least squares. Crystal data for **21-29** can be found in Table 5.2. ^{1}H and ^{31}P{H} NMR spectra were recorded in solution on a Varian Mercury 300 MHz spectrometer. IR analysis was conducted as KBr discs on a MIDAC M4000 FT IR spectrometer. Melting points were determined in capillaries and are uncorrected.

5.5 General Experimental

5.5.1 Synthesis of 21: [Ca(2PyHCH$_2$PO$_3$H)$_2$(H$_2$O)$_5$]Br$_2$

2-(Methyl) pyridine phosphonic acid (0.10 g, 0.58 mmol) and calcium(II) bromide (0.16 g, 0.58 mmol) were mixed together under nitrogen atmosphere in tetrahydrofuran. After 4 hours, the reaction mixture was filtered using anaerobic techniques. However a large amount of precipitate was observed, which was redissolved in water. Slow evaporation of the aqueous solution at room temperature afforded complex **2** in 28 % yield. Melting point: 147-150 ^{o}C. IR (KBr pellet,cm^{-1}) 3261(s), 1645(s), 1536(m), 1466(m), 1416(m), 1390(m), 1314(m), 1253(s), 1219(s), 949(s). ^{1}H NMR (D$_2$O, 300 MHz, 25 ^{o}C): 3.4 (d, 2H, J = 20.4 Hz), 7.8 (m, 2H), 8.4 (t, 1H, J = 8.5Hz), 8.6 (s, 1H, J = 5Hz) ppm. ^{31}P NMR 13 ppm (s).

5.5.2 Synthesis of 22: [{Ca(2PyHCH$_2$PO$_3$H)$_2$(H$_2$O)$_2$}(ClO$_4$)$_2$]$_n$.

2-(Methyl) pyridine phosphonic acid (0.10 g, 0.58 mmol) and calcium perchlorate tetrahydrate (0.18 g, 0.58 mmol) were added to 3 mL of 50/50 EtOH/H$_2$O solution in a scintillation vial and stirred for 3 hours at 60 °C. Crystals suitable for X-ray analysis were formed after slow evaporation of the solvent.

5.5.3 Synthesis of 23: [{Co(2PyHCH$_2$PO$_3$H)$_2$(H$_2$O)$_4$}(NO$_3$)$_2$]

2-(Methyl) pyridine phosphonic acid (0.10 g, 0.58 mmol) and cobalt nitrate hexahydrate (0.17 g, 0.58 mmol) were added to 3 mL of 50/50 EtOH/H$_2$O solution in a scintillation vial and stirred for 3 hours at 60 °C. Crystals suitable for X-ray analysis were formed after slow evaporation of the solvent.

5.5.4 Synthesis of 24 – 26, [Zn(2PyHCH$_2$PO$_3$)Cl]$_n$, [Zn(2PyHCH$_2$PO$_3$)(2PyHCH$_2$PO$_3$H)(ClO$_4$)] $_n$,

[{Zn$_2$(2PyHCH$_2$PO$_3$H)$_2$(2PyHCH$_2$PO$_3$)$_2$}(H$_2$O)$_2$(NO$_3$)$_2$] $_n$

General method: The metal salt and ligand were added to a glass scintillation vial with a stir-bar. A 75/25 mixture of ethanol and water was added and the reaction mixture stirred at ~60 °C for 3 hours. The clear solutions were left to allow evaporation of the solvent. Storage at room temperature for 7 – 10 days afforded colorless crystals that were suitable for X-ray diffraction.

Polymer **24**: ZnCl$_2$, (0.05 g, 0.4 mmol), 2PyCH$_2$PO$_3$H$_2$ (0.06 g, 0.4 mmol). Yield = 0.05 g (50 %). Melting Point: 177 – 179 °C. IR (KBr pellet, cm^{-1}): 3466(s), 1622(s), 1542(w), 1504(w), 1466(w), 1420(w), 1310(w), 1257(w), 1219(m), 1143(s), 1078(s), 1002(w), 940(w), 793(w). ^{1}H NMR (D$_2$O, 300 MHz, 25 °C): 3.3 (d, 2H, J = 20.8 Hz), 7.8 (m, 2H), 8.5 (m, 1H), 8.6 (d, 1H, J = 5.3 Hz) ppm. ^{31}P NMR 13 ppm (s).

Polymer **25**: $Zn(ClO_4)_2$, (0.11 g, 0.29 mmol), $2PyCH_2PO_3H_2$ (0.05 g, 0.3 mmol). Yield = 0.08 g (50 %). Melting Point: 238 – 240 ^{o}C. IR (KBr pellet, cm^{-1}): 3491 (s), 2023 (w), 1628 (s), 1537 (m), 1469 (m), 1419 (w), 1205 (s), 941 (w), 790 (m). ^{1}H NMR (D_2O, 300 MHz, 25 ^{o}C): 3.5 (d, 2H, J = 21.1 Hz), 7.9 (d, J = 8.4 Hz, 1H), 7.8 (tr. of doublets, J = 7.9 Hz, 1H), 8.6 (d, J = 5.8 Hz, 1H) ppm. ^{31}P NMR 13 ppm (s).

Polymer **26**: $Zn(NO_3)_2$, (0.05 g, 0.3 mmol), $2PyCH_2PO_3H_2$ (0.05 g, 0.3 mmol). Yield = 0.11 g (39 %). Melting Point: 98 ℃ "sweat"; expanded in size at 155 ℃ , melting point > 250 ℃, IR (KBr pellet, cm^{-1}): 3450(s), 3277 (w), 2428 (w), 1762 (m), 1643 (s), 1541 (s), 1367 (s). ^{1}H NMR (D_2O, 300 MHz, 25 ^{o}C): 3.4 (d, CH_2, J = 20.9 Hz), 7.8 (overlapping dd, 2H), 8.2 (s, 1H), 8.6 (d, J = 5.2 Hz, 1H) ppm. ^{31}P NMR 13 ppm (s).

5.5.5 Synthesis of 27: [{Zn(3PyHCH₂PO₃H)(3PyHCH₂PO₃)(H₂O)}NO₃]ₙ.

In a scintillation vial, 2-(methyl) pyridine phosphonic acid (0.05 g, 0.29 mmol) and zinc nitrate hexahydrate (0.09 g, 0.29 mmol) were added to 3 mL of 50/50 $EtOH/H_2O$ solution and stirred for 3 hours at 60 ^{o}C. Crystals suitable for X-ray analysis were formed after slow evaporation of the solvent.

5.5.6 Synthesis of 28: [Ag₂(4PyCH₂PO₃)]ₙ

In a scintillation vial, 4-(methyl) pyridine phosphonic acid (0.10 g, 0.58 mmol) and silver triflate (0.15 g, 0.58 mmol) were added to 3 mL of 50/50 $EtOH/H_2O$ solution. The vial was covered with aluminum foil, stirred for 3 hours at 150 ^{o}C, and then filtered. The filtrate was kept in the dark. Slow evaporation of the solution afforded crystals suitable for X-ray analysis. Yield = 0.026 g (11 %). Melting Point: 137 – 139 ^{o}C. IR (KBr pellet, cm^{-1}): 3564(m), 3483(m), 2955(s), 2907(m), 2883(m), 1647(m), 1605(s), 1424(s), 1253(s), 1191(s), 1050(s), 958(m),

864(m), 832(s), 529(s), 411(m). ^{1}H NMR (D$_2$O, 300 MHz, 25 ^{o}C): 3.4 (d, 2H, J = 6.7 Hz), 7.9 (d, 2H, J = 5.3 Hz), 8.6 (d, 2H, J = 21.7 Hz) ppm. ^{31}P NMR 15 ppm (s).

5.5.7 Synthesis of 29: [Ag$_3$(4PyCH$_2$PO$_3$)NO$_3$]$_n$

In a scintillation vial, 4-(methyl) pyridine phosphonic acid (0.10 g, 0.58 mmol) and silver nitrate (0.10 g, 0.58 mmol) were added to 3 mL of 50/50 EtOH/H$_2$O solution. The vial was covered with aluminum foil, stirred for 3 hours at 150 ^{o}C, and then filtered. The filtrate was kept in the dark. Slow evaporation of the solution afforded crystals suitable for X ray analysis. Yield = 0.041 g (13 %). The compound decomposes at 147 ^{o}C. IR (KBr pellet, cm^{-1}): 3398(m), 3145(m), 3072(s), 2960(s), 2851(s), 1635(s), 1384(s), 1248(m), 1088(m), 1034(m), 954(m), 837(s), 695(m), 589(m), 523(m). ^{1}H NMR (D$_2$O, 300 MHz, 25 ^{o}C): 3.4 (d, 2H, J = 21.9 Hz), 7.9 (d, 2H, J = 8.9 Hz), 8.6 (d, 2H, J = 6.7 Hz) ppm. ^{31}P NMR 16 ppm (s).

Table 5.2: Crystal Data for Compounds 21 - 29

Compound Name	21	22	23
Chemical Formula	C$_{12}$H$_{16}$Br$_2$CaN$_2$O$_{11}$P$_2$	C$_{12}$H$_{20}$CaCl$_2$N$_2$O$_{16}$P$_2$	C$_{12}$H$_{24}$CoN$_4$O$_{16}$P$_2$
Formula Weight	626.11	621.22	601.22
Crystal System	Triclinic	Monoclinic	Triclinic
Space Group	P-1	P2$_1$/c	P-1
T(K)	213(2)	173(2)	298(2)
a (Å)	6.0955(6)	13.4951(5)	6.0730(17)
b (Å)	13.7028(13)	8.2626(3)	9.684(3)
c (Å)	14.1738(13)	10.3988(3)	10.143(3)

α (°)	81.314(2)	90	90.725(4)
β (°)	84.839(2)	97.136(3)	97.803(5)
γ (°)	82.761(2)	90	105.582(4)
V (Å^3)	1157.93(19)	1150.53(7)	568.5(3)
Z	2	2	1
Reflections collected	5563	24597	3295
Independent reflections	4051	2909	2514
Data/restraints/ parameter ratio	4051 / 1 / 287	2909 / 4 / 192	2514 / 2 / 179
Unique Data (*R int*)	0.0235	0.0539	0.0154
D_{calc} (Mg/m^3)	1.796	1.793	1.756
F(000)	620	636	309
R indices (all data)	R1 = 0.0574 Wr2 = 0.1388	R1 = 0.0725 wR2 = 0.1048	R1 = 0.0387 wR2 = 0.0996
Final R indices [I > 2σ(I)]	R1 = 0.0459 wR2 = 0.1227	R1 = 0.0439 wR2 = 0.0887	0.0354 wR2 = 0.0965
Largest difference in peak and hole (e Å^{-3})	1.941 and -0.789	0.391 and -0.410	0.639 and -0.569

Compound Name and metal precursor used	**24:** $ZnCl_2$	**25:** $Zn(ClO_4)_2$	**26:** $Zn(NO_3)_2$
Chemical Formula	$C_6H_7Cl_1NO_3PZn$	$C_{12}H_{18}Cl_1N_2O_{11}P_2Zn$	$C_{24}H_{34}N_6O_{20}P_4Zn_2$
Formula Weight	272.92	529.04	981.19
Crystal System	Monoclinic	Triclinic	Triclinic
Space Group	P2$_1$/c	P-1	P-1
T(K)	213(2)	213(2)	213(2)
a (Å)	10.1187(13)	8.7310(9)	8.6038(16)

b (Å)	10.8336(14)	9.3925(9)	12.493(2)
c (Å)	8.2581(10)	13.2576(13)	17.936(3)
α (°)	90	107.947(2)	104.318(4)
β (°)	101.107(2)	90.277(2)	101.588(3)
γ (°)	90	105.855(2)	95.099(3)
V (Å^3)	888.31(19)	990.23(17)	1810.3(6)
Z	4	2	2
Reflections collected	7670	5692	8808
Independent reflections	2103	3528	6373
Data/restraints/ parameter ratio	2103/ 0 /122	3528 / 0 / 270	6373/7/521
Unique Data ($R int$)	0.0226	0.0238	0.0263
D_{calc} (Mg/m^3)	2.041	1.774	1.768
F(000)	544	538	534
R indices (all data)	R1 = 0.0261 wR2 = 0.0550	R1 = 0.0638 wR2 = 0.1255	R1 = 0.0923 wR2 = 0.1503
Final R indices [I > 2σ(I)]	R1 = 0.0206 wR2 = 0.0515	R1 = 0.0454 wR2 = 0.1133	R1 = 0.0507 wR2 = 0.1253
Largest difference in peak and hole (e Å^{-3})	0.459 and – 0.299	1.578 and -0.539 e.Å^{-3}	0.569 and -0.611 e.Å^{-3}

Compound Name	**27**	**28:** Ag triflate	**29:** AgNO$_3$
Chemical Formula	$C_{12}H_{14}N_3O_{10}P_2Zn$	$C_6H_6Ag_2N_2O_3P$	$C_{12}H_{12}Ag_6N_4O_{12}P_2$
Formula Weight	487.57	400.84	1113.42
Crystal System	Triclinic	Monoclinic	Monoclinic
Space Group	P-1	P2$_1$/c	P2$_1$/n
T(K)	213(2)	213(2)	213(2)
a (Å)	8.5058(5)	10.3933(7)	5.5353(5)

b (Å)	9.3779(5)	5.6534(4)	8.4968(8)
c (Å)	12.8237(7)	15.2160(11)	23.319(2)
α (°)	109.2560(10)	90	90
β (°)	106.9970(10)	92.5760(10)	91.206(2)
γ (°)	93.8140(10)	90	90
V (Å^3)	908.33(9)	893.15(11)	1096.51(17)
Z	2	4	2
Reflections collected	9050	4969	10696
Independent reflections	4024	2106	2614
Data/restraints/ parameter ratio	4024 / 3 / 233	2106 / 0 / 127	2614 / 0 / 163
Unique Data (*R int*)	0.0188	0.0377	0.0345
D$_{calc}$ (Mg/m^3)	1.783	2.981	3.372
F(000)	494	756	1040
R indices (all data)	R1 = 0.0776 wR2 = 0.2155	R1 = 0.0579 wR2 = 0.0928	R1 = 0.0402 wR2 = 0.0663
Final R indices [I > 2σ(I)]	R1 = 0.0730 wR2 = 0.2102	R1 = 0.0365 wR2 = 0.0816	R1 = 0.0296 wR2 = 0.0621
Largest difference in peak and hole (e Å^{-3})	3.357 and -1.966	1.266 and -0.786	1.756 and -0.810

Experimental Supporting Information

Electrochemical Studies: 0.3 M [TBA]PF6 and KCl solutions were prepared in DMF and water respectively. 10 mM solutions of **6** and **8** were prepared by dissolving each in DMF, then adding [TBA]PF6 /DMF solution in a 2:1 complex to electrolyte solution ratio. Aqueous samples were prepared similarly using KCl solution. A three-electrode configuration was employed in all experiments with a 0.3 mm Pt wire as the counter electrode, Ag/3 M AgCl as the reference electrode, and a 1 mm diameter glassy carbon electrode. Cyclic voltammograms were recorded using a microautolab type 2/PGSTAT12 potentiostat using NOVA 1.5.

Mn complex
0.1M KCl
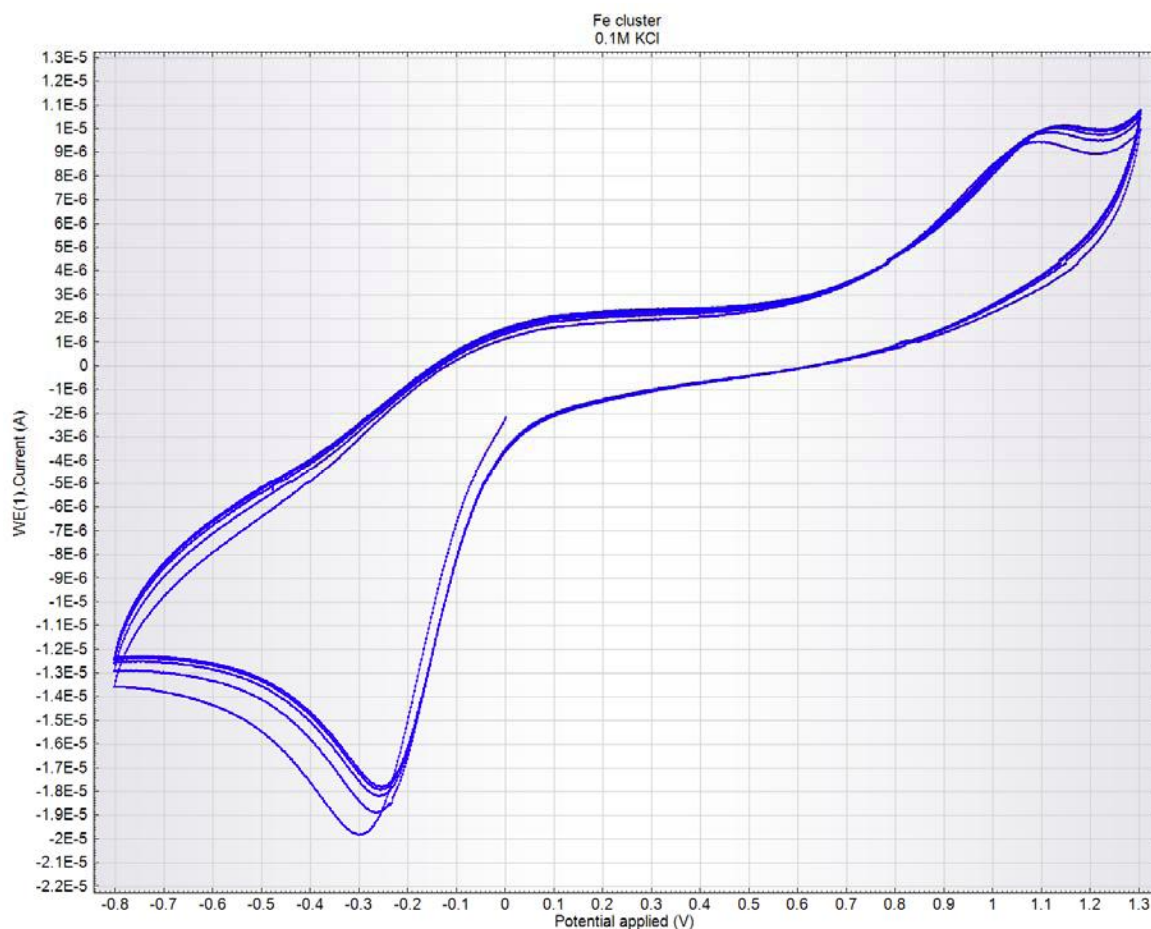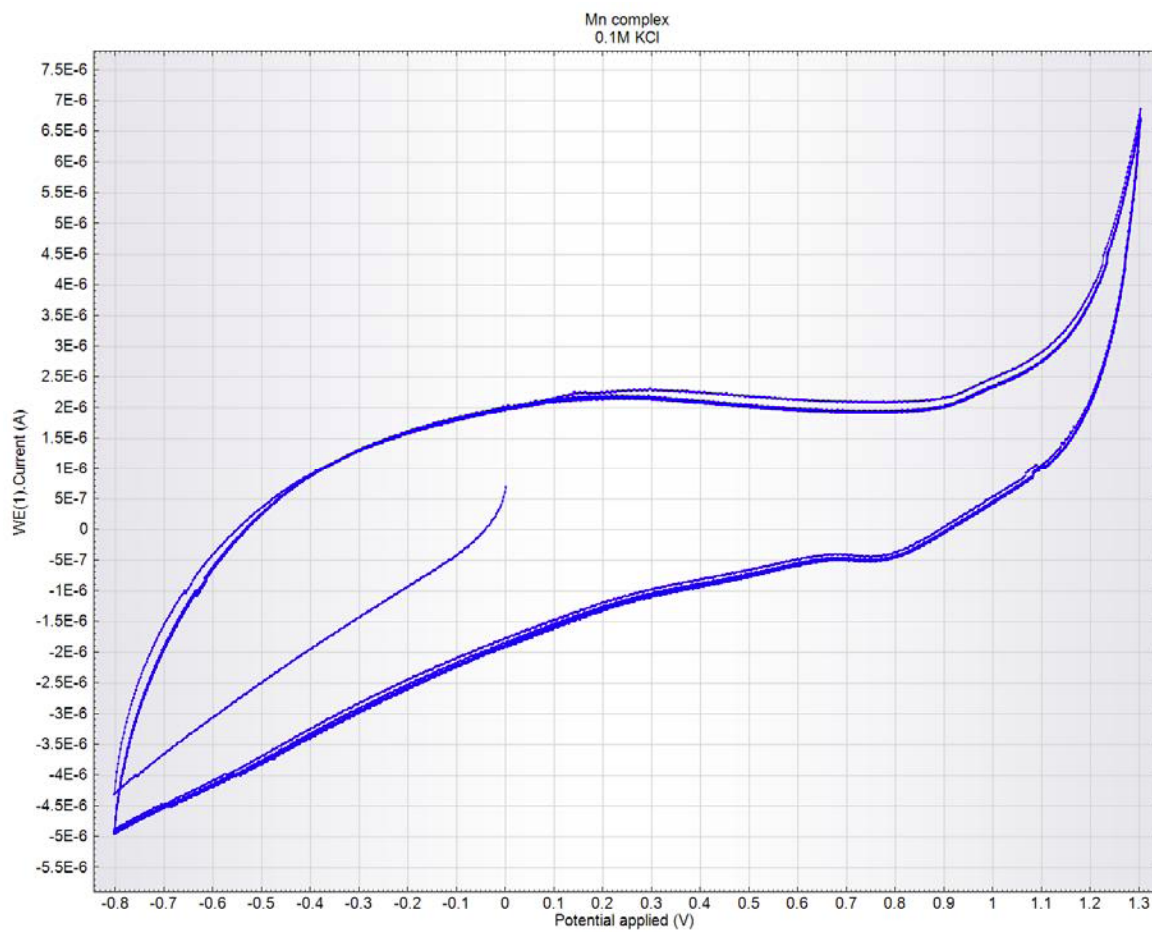
REFERENCES

[1] James, S. L., *Chem. Soc. Rev.,* **2003**, *32*, 276.

[2] Férey, G., *Chem. Soc. Rev.,* **2008**, *37*, 191

[3] Yaghi, O. M., O'Keeffe, M., Ockwig, N. W., Chae, H. K., Eddaoudi, M., Kim, J., *Nature,* **2003** , *423*, 705.

[4] Cheetham, A. K., Rao, C. N., Feller, R. K., *Chem. Commun.*, **2006**, 4780.

[5] Kim, J., Chen, B., Reineke, T. M., Li, H., Eddaoudi, M., Moler, D. B., O'Keeffe, M., Yaghi, O. M., *J. Am. Chem. Soc.,* **2001**, *123,* 8239.

[6] Long, D.-L., Blake, A. J., Champness, N. R., Wilson, C., Schröder, M., *J. Am. Chem. Soc.*, **2001**, *123,* 3401.

[7] Gan, X.-M., Rapko, B. M., Fox, J., Binyamin, I., Pailloux, S., Duesler, E. N., Paine, R. T., *Inorg. Chem.*, **2006**, *45,* 3741.

[8] Shi, X.; Wang, X.; Li, L.; Hou, H.; Fan, Y., *Cryst. Growth Des.,* **2010**, *10*, 2490.

[9] O'Keeffe, M., Stuart, J. A., *Inorg. Chem.*, **1983**, *22*, 177.

[10] Hoskins, B. F. and Robson, R., *J. Am. Chem. Soc.*, **1989**, *111*, 5962.

[11] Chapman, M. E., Ayyappan, P., Foxman, B. M., Yee, G. T., Lin, W. B., *Cryst. Growth Des.*, **2001**, *1*, 159.

[12] a) Moulton, B., Zaworotko, M. J., *Chem. Rev.,* **2001**, *101*, 1629. b) Agou, T., Sébastian, M., Lescop, C., Réau, R., *Inorg. Chem.,* **2011**, *50*, 3183.

[13] Yaghi, O. M., Davis, C. E., Li, G., Li, H., *J. Am. Chem. Soc.*, **1997**, *119*, 2861.

[14] Kitagawa, S., Kitaura, R. and Noro, S., *Angew. Chem., Int. Ed.,* **2004**, *43,* 2334.

[15] Sonnauer, A., Nather, C., Hoeppe, H. A., Senker, J., Stock, N., *Inorg. Chem.*, **2007**, *46*, 9968.

[16] IUPAC Nomenclature for Inorganic compounds. http://old.iupac.org/publications/books/rbook/Red_Book_2005.pdf (accessed July 17, 2011).

[17] Li, H., Eddaoudi, M., Groy, T. L., Yaghi, O. M., *J. Am. Chem. Soc.*, **1998**, *120*, 8571.

[18] Li, H., Eddaoudi, M., O'Keeffe, M., Yaghi, O. M., *Nature*, **1999**, *402*, 276.

[19] (a) Bish, D. L., Ming, D. W., *Natural Zeolites: Occurrence, Properties, and Applications,* Mineralogical Society of America: Washington, D. C., 2001. (b) Zaworotko, M. J., *Nature*, **1999**, *402*, 242.

[20] Côté, A. P., Benin, A. I., Ockwig, N. W., O'Keeffe, M., Matzger, A. J., Yaghi, O. M., *Science*, **2005**, *310*, 1166.

[21] Eddaoudi, M., Kim, J., Rosi, N., Vodak, D., Wachter, J., O'Keeffe, M., Yaghi, O. M., *Science*, **2002**, *295*, 469.

[22] Park, K. S., Ni, Z., Côté, A. P., Choi, J. Y., Huang, R., Uribe-Romo, F. J., Chae, J. K.,O'Keeffe, M., Yaghi, O. M., *Proc. Natl. Acad. Sci. USA,* **2006**, *103*, 10186.

[23] Férey, G., Draznieks, C. M., Serre, C., Millange, F., Dutour, J., Surblé, S., Margiolaki, I., *Science*, **2005**, *309*, 2040.

[24] Chui, S. S.-Y., Lo, S M.-F., Charmant, J. P. H., Orpen, A. G., Williams, I. D., *Science*, **1999**, *283*, 1148.

[25] IUPAC "Project: Coordination polymers and metal organic frameworks: terminology and nomenclature guidelines." http://iupac.org/web/ins/2009-012-2-200 (accessed July 17, 2011).

[26] Janiak, C., *Dalton Trans.*, **2003**, 2781.

[27] Perry IV, J. J., Perman, J. A., Zaworotko, M. J., *Chem. Soc. Rev.,* **2009**, *38*, 1400.

[28] Tranchemontagne, D. J.; Mendoza-Cortés, J. L.; O'Keeffe, M.; Yaghi, O. M., *Chem. Soc. Rev.,* **2009**, *38,* 1257.

[29] Schlapbach, L., Züttel, A., *Nature*, **2001**, *414*, 353.

[30] Biradha, K., Seward, C., Zaworotko, M. J. *Angew. Chem., Int. Ed.* **1999** *38*, 492.

[31] Fujita, M., Kwon, Y. J., Sasaki, O., Yamaguchi, K., Ogura, K. *J. Am. Chem. Soc.,* **1995**, *117*, 7287.

[32] Bauer, S., Marrot, J., Devic, T., Ferey, G., Stock, N., *Inorg. Chem.,* **2007**, *46*, 9998.

[33] Deng, Z.-P., Zhu, Z.-B., Zhang, X.-F., Huo, L.-H., Zhao, H., Gao, S., *CrystEngComm*, **2011**, *13*, 3895.

[34] Kitaura, R., Onoyama, G., Sakamoto, H., Matsuda, R., Noro, S., Kitagawa, S., *Angew. Chem., Int. Ed.,* **2004**, *43*, 2684.

[35] Pearson, R. G., *J. Chem. Educ.*, **1968**, *45*, 581.

[36] Serre, C., Millange, F., Thouvenot, C., Nogues, M., Marsolier, G., Louer, D., Férey, G., *J. Am. Chem. Soc.,* **2002**, *124,* 13519.

[37] Biradha, K., Fujita, M., *Angew. Chem., Int. Ed.*, **2002**, *41*, 3392.

[38] Li, J.-R.; Kuppler, R. J.; Zhou, H.-C., *Chem. Soc. Rev.,* **2009**, *38*, 1477.

[39] Maji, T. K., Mostafa, G., Chang, H. C., Kitagawa, S., *Chem. Commun.,* **2005**, 2436.

[40] IUPAC Manual of Symbols and Terminology Appendix II, Part I, Colloid and Surface Chemistry, p. 585. http://www.iupac.org/publications/pac/pdf/1972/pdf/3104x0577.pdf (accessed July 17, 2011).

[41] Mal, N. K., Fujiwara, M., Tanaka, Y., *Nature*, **2003**, *421*, 350.

[42] Zhang, J. P., Chen, X. M., *J. Am. Chem. Soc.,* **2008**, *130,* 6010.

[43] Chae, H. K., Siberio-Pérez, D. Y., Kim, J., Go, Y. B., Eddaoudi, M., Matzger, A. J., O'Keeffe, M., Yaghi, O. M., *Nature*, **2004**, *427*, 523.

[44] Kaye, S. S., Dailly, A., Yaghi, O. M., Long, J. R., *J. Am. Chem. Soc.*, **2007**, *129*, 14176.

[45] Furukawa, H., Miller, M. A., Yaghi, O. M., *J. Mater. Chem.*, **2007**, *1*7, 3197.

[46] Department of Energy Targets for Onboard Hydrogen Storage Systems for Light-Duty Vehicles http://www1.eere.energy.gov/hydrogenandfuelcells/storage/pdfs/targets_onboard_hydro_storage.pdf. (accessed July 17, 2011).

[47] Czaja, A. U., Trukhan, N., Muller, U., *Chem. Soc. Rev.,* **2009**, *38*, 1284.

[48] Furukawa, H., Ko, N., Go, Y. B., Aratani, N., Choi, S. B., Choi, E., Yazaaydin, A. Ö., *Science,* **2010**, *329*, 424.

[49] Roswell, J. L. C., Millward, A. R., Park, K. S., Yaghi, O. M., *J. Am. Chem. Soc.*, **2004**, *126*, 5666.

[50] Dincă, M., Long, J. R., *J. Am. Chem. Soc.*, **2007**, *129*, 11172.

[51] Dincă, M., Han, W. S., Liu, Y., Dailly, A., Brown, C. M., Long, J. R., *Angew. Chem., Int. Ed.,* **2007**, *45*, 1419.

[52] Suh, M. P., Cheon, Y. E., Lee, E. Y., *Coord. Chem. Rev.*, **2008**, *252*, 1007.

[53] Murray, L. J., Dincă, M., Long, J. R., *Chem. Soc. Rev.,* **2009**, *38*, 1294.

[54] Yang, J., Grzech, A., Mulder, F. M., Dingemans, T. J., *Chem. Commun.,* **2011**, *47*, 5244.

[55] National Research Council, *Catalysis Looks to the Future (Panel on New Directions in Catalytic Science and Technology),* National Academy Press: Washington DC, 1992.

[56]Mueller, T., Ceder, G., *J. Phys. Chem. B,* **2005**, *109*, 17974.

[57] Cho, S.-H., Ma, B., Nguyen, S.-B., T., Hupp, J. T., Albrecht-Schmitt, T. E., *Chem. Commun.*, **2006**, 2563.

[58] Corma, A., Garcia, H., Llabrés i Xamena, F. X., *Chem. Rev.*, **2010**, *110*, 4606.

[59] Fujita, M., Kwon, Y. J., Washizu, S., Ogura, K, *J. Am. Chem. Soc.,* **1994**, *116*, 1151.

[60] Bernin, M. C., Gándara, F., Iglesias, M., Snejko, N., Gutiérrez-Puebla, E., Brusau, E. V., Narda, G. E., Monge, M. Á., *Chem. Eur. J.*, **2009**, 4896.

[61] Sun, Y., Prins, R., *Journal of Catalysis*, **2009**, 193.

[62] Allendorf, M. D., Bauer, C. A., Bhakta, R. K., Houk, R. J. T., *Chem. Soc. Rev.,* **2009**, *38,* 1330.

[63] Chen, Z.-F., Xiong, R.-G., Zhang, J., Chen, X.-T., Xue, Z.-L., You, X.-Z., *Inorg. Chem.*, **2001**, *40*, 4075.

[64] Fun, H.-K., Raj, S. S. S., Xiong, R.-G., Zuo, J.-L., Yu, Z., You, X.-Z., *J. Chem. Soc., Dalton Trans.,* **1999**, 1915.

[65] Bauer, C. A., Timofeeva, T. V., Settersten, T. B., Patterson, B. D., Liu, V. H., Simmons, B. A., Allendorf, M. D., *J. Am. Chem. Soc.,* **2007**, *129*, 7136.

[66] Li, M.-X., Miao, Z.-X., Shao, M., Liang, S.-W., Zhu, S.-R., *Inorg. Chem.*, **2008**, *47*, 4481.

[67] Zhang, S., Wang, Z., Zhang, H. H., Cao, Y. N., Sun, Y. X., Chen., Y. P., Huang, C. C., Yu, X. H., *Inorg. Chim. Acta,* **2007**, *360*, 2704.

[68] Singleton, R., Bye, J., Dyson, J., Baker, G., Ranson, R. M., Hix, G. B., *Dalton Trans.*, **2010**, *39*, 6024.

[69] Huang, Y.-Q., Ding, B., Song, H.-B., Zhao, B., Ren, P., Cheng, P., Wang, H.-G., Liao, D.-Z., Yan, S.-P., *Chem. Commun.,* **2006**, 4906.

[70] Jenkins, A. L., Uy, O. M., Murray, G. M., *Anal. Chem.,* **1999**, *71*, 373.

[71] Yaghi, O. M., Li, H. *J. Am. Chem. Soc.,* **1995**, *117*, 10401.

[72] Forster, P. M., Thomas, P. M., Cheetham, A. K., *Chem. Mater.,* **2002**, *14*, 17.

[73] Klinowski, J., Almeida P., Filipe A., Silva, P., Rocha, J., *Dalton Trans.,* **2011**, *40*, 321.

[74] Garay, A. L., Pichon, A., James, S. L., *Chem. Soc. Rev.,* **2007**, *36*, 846.

[75] Bowmaker, G. A., Chaichit, N., Pakawatchai, C., Skelton, B. W., White, A. H., *Dalton Trans.*, **2008**, 2926.

[76] Sheldon, R. A., *Green Chem.,* **2005**, 267.

[77] Orita, A., Jiang, L., Nakano, T., Ma, N., Otera, J., *Chem. Commun.,* **2002**, 1362.

[78] Fujita, M., Yazaki, J., Ogura, K., *J. Am. Chem. Soc.*, **1990**, *112*, 5645.

[79] Braga, D., Cojazzi, G., Maini, L., Polito, M., Grepioni, F., *Chem. Commun.*, **1999**, 1949.

[80] Mellot-Draznieks, C., Dutour, J., Ferey, G., *Angew. Chem., Int. Ed.*, **2004**, *43*, 6291.

[81] Devic, T., Horcajada, P., Serre, C., Salles, F., Maurin, G., Moulin, B., Heurtaux, D., Clet, G., Vimont, A., Grenèche, J.-M., Le Ouay, B., Moreau, F., Magnier,E., Filinchuk, Y., Marrot, J., Lavalley, J. C., Daturi, M., Férey, G., *J. Am. Chem. Soc.,* **2010**, *132*, 1127.

[82] Jessop, P. G., *Green Chem.*, **2011**, *13*, 1391.

[83] Sharma, M. K., Bharadwaj, P. K., *Inorg. Chem.,* **2011**, *50*, 1889.

[84] Singh, M., Kumar, D., Thomas, J., Ramanan, A., *J. Chem. Sci.*, **2010**, *122*, 757.

[85] Hoskins, B. F., Robson, R., *J. Am. Chem. Soc.,* **1990**, *112*, 1546.

[86] Ramanan, A., Whittingham, M. S., *Cryst. Growth Des.*, **2006**, *6*, 2419.

[87] Shoaee, M., Anderson, M. W., Attfield, M. P., *Angew. Chem., Int. Ed.*, **2008**, *47*, 8525.

[88] Morris, R. E., *ChemPhysChem*, **2009**, *10*, 327.

[89] Aakeröy, C. B., Desper, J., Levin, B., Valdés-Martínez, J., *Inorg. Chim. Acta*, **2006**, 1255.

[90] Kitazawa, T., Kikuyama, T., Takeda, M., Iwamoto, T., *Dalton Trans.*, **1995**, *22*, 3715.

[91] Lee, E. Y., Jang, S. Y., Suh, M. P., *J. Am. Chem. Soc.*, **2005**, *127*, 6374.

[92] Suh, M. P., Cheon, Y. E., Lee, E. Y., *Chem.—Eur. J.*, **2007**, *13*, 4208.

[93] Stock, N., Bein, T., *J. Mater. Chem.*, **2005**, *15*, 1384.

[94] Withersby, M. A., Blake, A. J., Champness, N. R., Hubberstey, P., Li, W. S., Schroder, M., *Angew. Chem., Int. Ed.*, **1997**, *36*, 2327.

[95] Bauer, S., Bein, T., Stock, N., *Inorg. Chem.*, **2005**, *44*, 5882.

[96] Mondal, R., Basu, T., Sadhukhan, D., Chattopadhyay, T., Bhunia, M. K., *Cryst. Growth Des.*, **2009**, *9*, 1095.

[97] Du, Z.-Y., Xu, H.-B., Mao, J.-G., *Inorg. Chem.*, **2006**, *45*, 9780.

[98] Yang, T.-H., Cao, D.-K., Li, Y.-Z., Zheng, L.-M., *J. Solid State Chem.,* **2010**, *183*, 1159.

[99] Shimizu, G. K. H., Vaidhyanathan, R., Taylor, J. M., *Chem. Soc. Rev.*, **2009**, *38*, 1430.

[100] Lamshöft, M., Storp, J., Ivanova, B., Spiteller, M., *Polyhedron*, **2011**, *30*, 2564.

[101] Nishiyabu, R., Kubo, Y., James, T., Fossey, J. S., *Chem. Commun.,* **2011**, *47*, 1124.

[102] (a) Hall, D., *Boronic Acids*, Wiley: Weinheim, 2005, (b) Christinat, N., Scopelliti, R., Severin, K., *Angew. Chem., Int. Ed.,* **2008**, *47*, 1848.

[103] Alberti, G., Costantino, U., in *Comprehensive Supramolecular Chemistry vol. 7*, ed. J. L. Atwood, J. E. D. Davies, D. D. MacNicol, and F. Vogtle, Elsevier Science: New York, 1996.

[104] Alberti, G.; Constantino, U.; Allulli, S.; Tomassini, N. *Inorg. Nucl. Chem.,* **1978**, *40*, 1113.

[105] Samanamu, C. R., Olmstead, M. M., Montchamp, J.-L., Richards, A. F., *Inorg. Chem.*, **2008**, *47*, 3879.

[106] Bulot, J. J., Aboujaoude, E., Collignon, N., Savignac, P., *Phosphorus Sulfur Relat. Elem.*, **1984**, *21*, 197.

[107] (a) Wan, B.-Z., Anthony, R. G., Peng, G.-Z., Clearfield, A. *J. Catal.* **1994**, *101*, 19. (b) Colon, J. L., Thakur, D. S., Yang, C.-Y., Clearfield, A., *J. Catal.* **1990**, *124*, 148. (c) Deniaud, D., Schollorn, B., Mansuy, D., Rouxel, J, Battioni, P., Bujoli, B., *Chem. Mater.* **1995**, *7*, 995.

[108] (a) Cao, G., Hong, H., Mallouk, T. E., *Acc. Chem. Res.* **1992**, *25*, 420. (b) Alberti, G., Polombari, R., *Solid State Ionics* **1989**, *35*, 153. (c) Alberti, G., Casciola, M., Palombari, R., *Solid State Ionics* **1992**, *52*, 291. (d) Thompson, M. E., *Chem. Mater.* **1994**, *6*, 1168.

[109] Evans, O. R., Ngo, H. L., Lin, W., *J. Am. Chem. Soc.*, **2001**, *123*, 10395.

[110] Byrd, H., Clearfield, A., Poojary, D., Reis, K. P., Thompson, M. E., *Chem. Mater.*, **1996**, *8*, 2239.

[111] (a) Xu, Z., Thompson, L. K., Black, D. A., Ralph, C., Miller, D. O., Leech, M. A., Howard, J. A. K., *Dalton Trans.*, **2001**, 2042. (b) Luo, J., Jiang, F., Wang, R., Han, L., Lin, Z., Cao, R., Hong, M. *J. Mol. Struct.*, **2004**, *707*, 211. (c) Hu, C., Kalf, I., Unglert, U., *CrystEngComm*, **2007**, *9*, 603.

[112] Belabassi, Y., Alzghari, S., Montchamp, J.-L., *J. Organomet. Chem.,* **2008**, *693*, 3171.

[113] McKenna, C. E., Schmidhuser, J., *J. Chem. Soc. Chem. Commun.*, **1979**, 739.

[114] Ayyappan, P., Evans, O. R., Foxman, B. M., Wheeler, K. A., Warren, T. H., Lin, W., *Inorg. Chem.* **2001**, *40*, 5954.

[115] Konar, S., Zoń, J., Prosvirin, A. V., Dunbar, K. R., Clearfield, A., *Inorg. Chem.* **2007**, *46*, 5229.

[116] Perry, H., Zoń, J., Law, J., Clearfield, A., *J. Sol. State Chem.*, **2010**, *183*, 1165.

[117] (a) Ma, Y.-S., Song, Y., Du, W.-X., Li, Y.-Z., Zheng, L.-M., *Dalton Trans.* **2006**, 3228. (b) Ma, Y.-S., Li, H., Wang, J.-J., Bao, S.-S., Cao, R., Li, Y.-Z., Ma, J., Zheng, L.-M., *Chem. Eur. J.* **2007**, 13, 4759. (c) Ma, Y.-S., Song, Y., Zheng, L.-M., *Inorg. Chim. Acta,* **2008**, *361* 1363.

[118] (a) Yu, J., Wang, Y., Shi, Z., Xu, R., *Chem. Mater.* **2001**, *13*, 2972. (b) Alexios, M., Dendrinou-Samara, C., Raptopoulou, C. P., Terzis, A., *Inorg. Chem.* **2002**, *41*, 4732. (c) Kubieck, V., Vojtisek, P., Rudovsky, J., Hermann, P., Lukes, I., *Dalton Trans.* **2003**, 3927. (d) Videra, V., Chauvin, A. S., Varbanov, S., Baux, C., Scopelith, R., *Eur. J. Inorg. Chem.* **2004**, 2173. (e) Looney, A., Lornebise, M., Miller, D., Parkin, G., *Inorg. Chem.* **1992**, *31*, 989. (f) Poat, J. C., Slawin, A. M. Z., Williams, D. J., Woollins, J. D., *Polyhedron* **1992**, *11*, 2125. (g) Clearfield, A., Sharma, C. V. K., Zhang, B., *Chem. Mater.* **2001**, *13*, 3099. (h) Drumel, S., Janvier, P., Deniaud, D., Bujoli, B., *Chem. Commun.* **1995**, 1051. (i) Drumel, S., Janvier, P., Barboux, M., Bujoli-Doueff, M., Bujoli, B., *Inorg. Chem.* **1995**, *34*, 148. (j) Harrison, W. T. A., Martin, T. E., Gier, T. E., Stucky, G. D., *J. Mater. Chem.* **1992**, *2*, 175.

[119] (a) Nakamoto, K., *Infrared spectra of inorganic and coordination compounds,* Wiley: New York, 1963. (b) Corbridge, D. E. C., *P an outline of its biochemistry and technology, 4th edition.* Elsevier: Amsterdam, 1990.

[120] Redmore, D., *J. Org. Chem.*, **1970**, *35*, 4114.

[121] (a) Teixidor, F., Escriche, L., Rodriguez, I., Casabo, J., Rius, J., Molins, E., Martinez, B., Miravitlles, C., *J. Chem. Soc., Dalton Trans.* **1989**, 1381. (b) Loi, M., Graf, E., Hosseini, M. W., De Cian, A., Fischer, J., *Chem. Commun.* **1999**, 603. (c) Matthews, C. J., Clegg, W., Heath, S. L., Martin, N. C., Hill, M. N. S., Lockhart, J. C., *Inorg. Chem.* **1998**, *37*, 199. (d) Cannas, M., Marongiu, G., Saba, G., *J. Chem. Soc., Dalton Trans.* **1980**, 2090.

[122] Bondi, A., *J. Phys. Chem.* **1964**, *68*, 441.

[123] Desiraju, G. R. *Crystal engineering: The design of organic solids,* Elsevier: New York, 1989.

[124] Meyer, G., Nockemann, P., *Z. Anorg. Allg. Chem.* **2003**, *629*, 1294.

[125] (a) Bebout, D. C., DeLanoy, A. E., Ehmann, D. E., Kastner, M. E., Parrish, D. A., Butcher, R. J., *Inorg. Chem.* **1998**, *37*, 2952. (b) Batten, S. R., Hoskins, B. F., Robson, R., *Angew. Chem., Int. Ed. Engl.* **1995**, *34*, 820. (c) Deacon, G. B., Raston, C. L., Tunaley, D., White, A. H., *Aust. J. Chem.* **1979**, *32*, 2195. (d) Aakesson, R., Sandstroem, M., Staalhandske, C., Persson, I., *Acta Chem. Scand.* **1991**, *45*, 165. (e) Short Hg-N bond length, 2.229 Ǻ: Grdenic, D., Kamenar, B., Hergold-Brundic, A., *Croat. Chem. Acta* **1979**, *52*, 339.

[126] Canty, A. J., Deacon, G. B., *Inorg. Chim. Acta.* **1980**, *45*, L225.

[127] (a) Hoskins, B.F., Rohron, R. J., *J. Am. Chem. Soc.* **1990**, *112*, 1546. (b) Carlucci, L., Ciani, G., Proserpio, D., Sironic, A., *J. Chem. Soc., Chem. Commun.* **1994**, 2755. (c) Carlucci, L., Ciani, G., Proserpio, D., Sironic, A., *J. Am. Chem. Soc.* **1995**, *117*, 4562. (d) Carlucci, L., Ciani, G., Proserpio, D., Sironic, A., *Inorg. Chem.* **1995**, *34*, 5698.

[128] (a) Makinen, S. K., Melcer, N. J., Parvez, M., Shimizu, G. K. H., *Chem. Eur. J.* **2001**, *7*, 5176. (b) Smith, G., Cloutt, B. A., Lynch, D. E., Byriel, K. A., Kennard, C. H. L., *Inorg. Chem.* **1998**, *37*, 3236. (c) Kulynych, A. D., Shimizu, G. K. H., *CrystEngComm* **2002**, *4*, 102. (d) Yu, J. O., Cote, A. P., Enright, G. D., Shimizu, G. K. H*., Inorg. Chem.* **2001**, *40*, 582.

[129] (a) Lawrance, G. A., *Chem. Rev.* **1986**, *86*, 17. (b) Ning, G. L., Munakata, M., Wu, L. P., Maekawa, M., Suenaga, Y., Kuroda-Sowa, T., Sugimoto, K., *Inorg. Chem.* **1999**, *38*, 5668. (c) Munakata, M., Wu, L. P., Kuroda-Sowa, T., Maekawa, M., Suenaga, Y., Sugimoto, K., Ino, I*., Dalton Trans.* **1999**, 373. (d) Timmermans, P. J., Mackor, A., *J. Organomet. Chem.* **1984**, *276*, 287. (e) Ning, G. L., Wu, L. P., Sugimoto, K., Munakata, M., Kuroda-Sowa, T., Maekawa, M., *Dalton Trans.* **1999**, 2529.

[130] Khlobystar, A. N., Blake, A. J., Champness, N. R., Lemonovskii, D. A., Majouga, A. G., Zyk, N. V., Schröder, M., *Coord. Chem. Rev.* **2001**, 155.

[131] (a) Jansen, M., *Angew. Chem., Int. Ed. Engl.* **1987**, *26*, 1098. (b) Su, W. P., Cao, R., Hong, M. C., Wong, W. T., Lu, J. X., *Inorg. Chem. Commun.* **1999**, *2*, 241. (c) Ahmed, L. S., Dilworth, J. R., Miller, J. R., Wheatley, N., *Inorg. Chim. Acta* **1998**, *278*, 229. (d) Hartshorn, C. M., Steel, P. J., *Inorg. Chem. Commun.* **2000**, *3*, 476. (e) Yang, S. P., Zhu, H. L., Yin, X. H., Chen, X. M., Ji, L. N., *Polyhedron* **2000**, *19*, 2237. (f) Yoon, I., Lee, Y. H., Jung, J. H., Park, K. M., Kim, J., Lee, S. S., *Inorg. Chem. Commun.* **2002**, *5*, 820. (g) Yam, V. W. W., Yeung, P. K. Y., Cheung, K. K., *Angew. Chem., Int. Ed. Engl.* **1996**, *35*, 739. (h) Tong, M. L., Chen, X. M., Ye, B. H., Ji, L. N., *Angew. Chem., Int. Ed.* **1999**, *38*, 2237. (i) Tong, M. L., Chen, X. M., Ye, B. H., *Inorg. Chem.* **1998**, *37*, 5278. (j) Tong, M. L., Zheng, S. L., Chen, X. M*., Chem. Commun.* **1999**, 561. (k) Zheng, S. L., Zhang, J. P., Wong, W. T., Chen, X. M., *J. Am. Chem. Soc.* **2003**, *125*, 6882. (l) Che, C. M., Yip, H. K., Li, D., Peng, S. M., Lee, G. H., Wang, Y. M., Liu, S. L., *J. Chem. Soc., Chem. Commun.* **1991**, 1615. (m) Pyykkö, P., Zhao, Y., *Angew. Chem., Int. Ed.* **1991**, *30*, 604. (n) Li, J., Pyykkö, P., *Chem. Phys. Lett.* **1992**, *197*, 586.

[132] Carlucci, L., Ciani, G., Gudenberg, D. W. V., Proserpio, D., *Inorg. Chem.* **1997**, *36*, 3812.

[133] (a) Zheng, S.-L., Yang, J.-H., Yu, X.-L., Chen, X.-M., Wong, W.-T., *Inorg. Chem.* **2004**, *43*, 830. (b) Wang, R.-H., Han, L., Jiang, F.-L., Zhou, Y.-F., Yuan, D.-Q., Hong, M.-C., *Cryst. Growth Des.* **2005**, *5*, 129.

[134] (a) Sheldrick, G. M., SHELXS-97, Program for the solution of crystal structures, University of Göttingen, Germany, 1997. (b)Sheldrick, G. M., SHELXL-97, Program for the refinement of crystal structures, University of Göttingen, Germany, 1997.

135 (a) Fry, J. A. , Samanamu, C. R., Montchamp, J.-L., Richards, A. F., *Eur. J. Inorg. Chem.* **2008**, *3*, 463. (b) Samanamu, C. R., Montchamp, J.-L., Richards, A. F., *J. Solid State Chem.* **2008**, *181*, 1462. (c) Samanamu, C. R., Olmstead, M. M., Montchamp, J.-L., Richards, A. F., *Inorg. Chem.* **2008**, *47*, 3879. (d) Pailloux, S., Shirima, C. E., Smith, K. A., Duesler, E. N., Paine, R. T., Williams, N. J., Hancock, R. D., *Inorg. Chem.* **2010**, *49*, 9369.

136 Ohba, M., Tamaki, H., Matsumoto, N., Okawa, H., *Inorg. Chem.,* **1993**, *32*, 5385.

137 Sessoli, R., Tsai, H.-L., Schake, A. R., Wang, S., Vincent, J. B., Folting, K., Gatteschi, D., Christou, G., Hendrickson, D. N., *J. Am. Chem. Soc.*, **1993**, *115*, 1804.

138 (a) Konar, S., Bhuvanesh, N., Clearfield, A. *J. Am. Chem. Soc.*, **2006**, *128*, 9604. (b) Langley, S., Helliwell, M., Sessoli, R., Teat, S. J., Winpenny, R. E. P. *Inorg. Chem.*, **2008**, *47*, 497. (c) Langley, S., Helliwell, M., Sessoli, R., Teat, S. J., Winpenny, R. E. P., *Dalton Trans.*, **2009**, 3102. (d) Zheng, Y.-Z., Breeze, B. A., Timco, G. A., Tuna, F., Winpenny, R. E. P., *Dalton Trans.*, **2010**, *39*, 6175. (e) Du, Z.-Y., Sun, Y.-H., Liu, Q.-Y., Xie, Y.-R., Wen, H.-R., *Inorg. Chem.*, **2009**, *48*, 7015.

139 Helliwell, M., Langley, S., Raftery, J., Tolis, E. I., Winpenny, R. E. P. *Angew. Chem., Int. Ed.,* **2003**, *42,* 3804.

140 Chandrasekhar, V., Kingsley, S. *Angew. Chem., Int. Ed.*, **2000**, *39*, 2320.

141 Khan, M. I., Zubieta, J., *Prog. Inorg. Chem.*, **1995**, *43*, 1.

142 Wasson, A. E., LaDuca, R. L., *Acta Crystallogr. Sect.E: Struct. Rep. Online,* **2007**, *63*, m462.

143 (a) Gan, X.-M., Rapko, B. M., Fox, J., Binyamin, I., Pailloux, S., Duesler, E. N., Paine, R. T., *Inorg. Chem.*, **2006**, *45*, 3741. b) Gan, X. M., Binyamin, I., Rapko, B. M., Fox, J., Duesler, E. N., Paine, R. T., *Inorg. Chem.*, **2004**, *43*, 2443. (c) Gan, X., Binyamin, I., Rapko, B. M., Fox, J., Duesler, E. N., Paine, R. T., *Polyhedron,* **2006**, *25*, 3387.

144 (a) Du, M., Bu, X.-H., Shionoya, M., Shiro, M., *J. Mol. Struct.*, **2002**, *607*, 155. (b) Mamula, O., Lama, M., Stoeckli-Evans, H., Shova, S., *Angew. Chem., Int. Ed.*, **2006**, *45*, 4940. (c) Thuery, P., *Acta Crystallogr. Sect. C: Cryst. Struct Commun.*, **2008**, *64*, m50.

145 Cao, D.-K., Li, Y.-Z., Zheng, L.-M., *Inorg. Chem.*, **2005**, *44*, 2984.

146 Ochocki, J., Graczyk, J., Reedijk, J., *J. Inorg. Biochem.,* **1995**, *59*, 240.

147 Caution: Metal perchlorate salts can be explosive.

148 (a) Meng, L., Li, J., Sun, Z.-G., Zheng, X., Dong, D.-P., Yan, Z., Chen, H., Zhu, Y. Y., Zhao, Y., Zhang, J., *Z. Anorg. Allg. Chem.,* **2008**, *634*, 571. (b) Fanucci, G. E., Krzystek, J., Meisel, M. W., Brunel, L.-C., Talham, D. R., *J. Am. Chem. Soc.*, **1998**, *120*, 5469. (c) Bakhmutova, E. V., Ouyang, X., Medvedev, D. G., Clearfield, A., *Inorg. Chem.*, **2003**, *42*,

7046. (d) Turner, A., Jaffres, P.-A., MacLean, E. J., Villemin, D., McKee, V., Hix, G. B., *Dalton Trans*., **2003**, *7*, 1314.

[149] (a) Reedijk, J., Driessen, W. L., Groeneveld, W. L., *Recl. Trav. Chim. Pays-Bas.,* **1969***, 88*, 1095. (b) Lever, A. B. P., *Inorganic Electronic Spectroscopy*, Elsevier: Amsterdam, 1986.

[150] (a) Hathaway, B. J., Underhill, A. E., *J. Chem. Soc*., **1961**, 3091. (b) Dickson, I. E., Robson, R., *Inorg. Chem*., **1974**, *13*, 1301. (c) Grzybowski, J. J., Merrel, P. M., Urbach, F. L., *Inorg. Chem*., **1978**, *17*, 3078.

[151] Tolis, E. I., Helliwell, M., Langley, S., Raftery, J., Winpenny, R. E. P, *Angew Chem., Int. Ed*., **2003**, *42*, 3804.

[152] Roesky, H. W., Murugavel, R., *Acc. Chem. Res*., **1999**, *32*, 117.

[153] Ye, B.-H., Li, X.-Y., Mak, T. C. W., *Chem. Comm*., **1997**, 2407.

[154] (a) Lippard, S. J., *Angew. Chem., Int. Ed.,* **1988**, *27*, 344. (b) Vincent, J. B., Olivier-Lilley, G. L., Averill, B. A., *Chem. Rev*., **1990**, *90*, 1447. (c) Susse, P., *Z. Kristallogr*., **1968**, *127*, 261. (d) Moore, P. B., *Am. Mineral*., **1972**, *57*, 397.

[155] Drüeke, S., Wieghardt, K., Nuber, B., Weiss, J., Fleischhauer, H.-P., Gehring, S., Haase, W., *J. Am. Chem. Soc*., **1989**, *111*, 8622.

[156] (a) Armstrong, W. H., Roth, M. E., Lippard, S. J., *J. Am. Chem. Soc*., **1987**, *109*, 6318. (b) Toftlund, H., Murray, K. S., Zwack, P. R., Taylor, L. F., Anderson, O. P., *J. Chem. Commun*., **1986**, 191.

[157] NIST X-ray Photoelectron Spectroscopy Database, NIST Standard Reference Database 20, V.3.5.

[158] (a) Kang, S. A., Hoke, K. R., Crane, B. R., *J. Am. Chem. Soc.,* **2006**, *128*, 2346. (b) Glowiak, T., Huskowska, E., Legendziewiz *J., Polyhedron*, **1991**, *10*, 175.

[159] Pauling, L., *The Nature of the Chemical Bond* (3rd Ed.), Cornell University Press: 1960.

[160] (a) Cavellec, M. R., Grenèche, J.-M., Riou, D., Férey, G., *Chem. Mater*., **1998**, *10*, 2434. (b) Lethbridge, Z. A. D., Lightfoot, P., *J. Solid State Chem*., **1999**, *143*, 58. (c) Du, Z.-Y., Wen, H.-R., Liu, C.-M., Sun, Y.-H., Lu, Y.-B., Xie, Y.-R., *Cryst. Growth Des.,* **2010**, *10*, 3721.

[161] (a) Noro, S., Miyasaka, H., Kitagawa, S., Wada, T., Okuba, T., Yamashita, M., Mitani, T., *Inorg. Chem*., **2005**, *44*, 133. (b) Yan, B., Capracotta, M. D., Maggard, P. A., *Inorg. Chem*., **2005**, *44*, 6509. (c) Schultheiss, N., Barnes, C. L., Bosch, E., *Cryst. Growth Des*. **2003**, *3*, 573.

[162] (a) Zhao, L., Mak, T. C. W., *Inorg. Chem.*, **2009**, *48*, 6480. (b) Fenton, H., Tidmarsh, I. S., Ward, M. D., *Dalton Trans.*, **2009**, *21*, 4199. (c) Du, M., Li, C. P., Zhao, X.-J., *Cryst. Growth Des.*, **2006**, *6*, 335.

[163] (a) Yang, B. P., Mao, J. G., Sun, Y. Q., Zhao, H. G., Clearfield, A., *Eur. J. Inorg. Chem.,* **2003**, 4211. (b) Song, J. L., Lei, C., Sun, Y. Q., Mao, J. G., *J. Solid State Chem.*, **2004**, *177*, 2557.

[164] (a) Bowen, S. M., Deusler, E. N., Paine, R. T., Campana, C. F., *Inorg. Chim. Acta,* **1982***, 59*, 53. (b) Tikhonova, I. A., Dolgushin, F. M., Tugashov, K. J., Petrovskii, P. V., Purin, G. G., Shur, V. B., *J. Organomet. Chem.*, **2002**, *654*, 123. (c) Cabeza, A., Aranda, M. A. G., Martinez-Lara, M., Bruque, S., Sanz, J., *Acta. Crystallogr. B.*, **1996**, *52*, 982.

[165] (a) Gomez-Alcantara, M. M., Cabeza, A., Aranda, M. A. G., Guagliardi, A., Mao, J. G., Clearfield, A., *Solid State Sciences*, **2004**, *6*, 479. (b) Tran, D. T., Kam, Y. S., Zavaliji, P. Y., Oliver, S. R., *Inorg. Chem.*, **2003**, *42*, 2165.

[166] Dong, Y. B., Wang, H.-Y., Ma, J.-P., Shen, D.-Z., Huang, R.-Q., *Inorg. Chem.*, **2005**, *44*, 4679.

[167] Ochocki, J., Kostka, K., Zurowska, B., Mrozinski, J., Galdecka, E., Galdecki, Z., Reedijk, J., *Dalton Trans.,* **1992**, 2955.

[168] Glowiak, T., Sawka-Dobrowolska, W., Jezowska-Trzebiatowska, B., Antonow, A., *J. Mol. Struct.*, **1980**, *10*, 1.

[169] Komossa, D., Gennity, I., Sandermann, H., Jr., *Pestic. Biochem. Physiol,* **1992**, *43*, 85.

[170] Giannousis, P. G., Bartlett, P. A., *J. Med. Chem.*, **1987**, *30*, 1603.

[171] (a) Fe(III): Barja, B. C., Herszage, J., dos Santos Afonso, M., *Polyhedron*, **2001**, *20*, 1821. (b) Mg(II): Lutz, M., Muller, G. *Inorg. Chim. Acta*, **1995**, *232*, 189.

[172] Samanamu, C. R., Zamora, E. N., Montchamp, J.-L., Richards, A. F., *J. Solid State Chem.*, **2008**, *181*, 1462.

[173] Song, B., Chen, D., Bastian, M., Martin, R. B., Sigel, H., *Helv. Chim. Acta*, **1994**, *77*, 1738.

[174] Hirschmann, R., Yager, K. M., Taylor, C. M., Witherington, J., Sprengeler, P. A., Phillips, B. W., Moore, W., and Smith, III, A. B., *J. Am. Chem. Soc.*, **1997**, *119*, 8177.

[175] Soroka, M., Zygmunt, J., *Synthesis*, **1988**, 370.

[176] (a) Sergienko, V. S., Afonin, E. G., Aleksandrov, G. G., *Russ. J. Inorg. Chem.*, **1998**, *43*, 1002. (b) Lei, C., Mao, J.-G., Sun, Y.-Q., Zeng, H.-Y., Clearfield, A., *Inorg. Chem.*, **2003**, *42*, 6157. (c) Ayi, A. A., Choudhury, A., Natarajan, S., Neeraj, S., Rao, C. N. R., *J. Mater. Chem.*, **2001**, *11*, 1181.

[177] Bakhmutova, E. V., Ouyang, X., Medvedev, D. G., Clearfield, A. *Inorg. Chem.*, **2003**, *42*, 7046.

[178] Bellamy, L. J., *The Infrared Spectra of Complex Molecules*, Wiley: New York, 1958**.**

[179] Nakamoto, K., *Infrared spectra of inorganic and coordination compounds Part A: Theory and Applications in Inorganic Chemistry*, 5th edition, Wiley: New York, 1997.

[180] Nakamoto, K, *Infrared spectra of inorganic and coordination compounds Part B: applications in coordination, organometallic, and bioinorganic Chemistry*, 5th edition, Wiley: New York, 1997.

[181] Silverstein, R. M., Bassler, G. C., Morrill, T. C., *Spectrometric identification of organic compounds*, Wiley: New York, 1981.

[182] (a) Chen, Z.-F., Xiong, R.-G., Zhang, J., Chen, X.-T., Xue, Z.-L., and You, X.-Z., *Inorg. Chem.*, **2001**, *40*, 4075. (b) Zhong, R.-Q., Zou, R.-Q., Du, M., Jiang, L., Yamada, T., Maruta, G., Takeda, S., and Xu, Q., *CrystEngComm*, **2008**, *10*, 605.

[183] (a) Cao, D.-K., Xie, X.-J., Li, Y.-Z., Zheng, L.-M., *Dalton Trans.*, **2008**, 5008. (b) Aleksandrov, G. G., Sergienko, V. S., *Kristallografiya*, **1999**, *44*, 1061.

[184] Massa, W., *Crystal Structure Determination*, Springer-Verlag: Berlin-Heidelberg, 2004.

[185] Nash, K. L., Rogers, R. D., Ferraro, J., Zhang, J., *Inorg. Chim. Acta*, **1998**, *269*, 211.

[186] (a) Cotton, A., Franckevicius, V., Mahon, M. F., Ooi, L. L., Raithby, P. R., Teat, S. J., *Polyhedron***, 2006**, *25*, 1057. (b) Drew, M. G. B., Hudson, M. J., Iveson, P. B., Madic, C., Russell, M. L., *Dalton Trans*., **2000**, 2711. (c) Al-Rasoul, K., Weakley, T. J. R., *Inorg. Chim. Acta*, **1982**, *60*, 191.

[187] Curtis, N. F., Curtis, Y. M., *Inorg. Chem.*, **1964**, *4*, 804.

[188] Benford, H. L., Frith, J. C., Auriola, S., Monkkonen, J., Rogers, M. J., *Mol. Pharmacol.*, **1999**, *56*, 131.

[189] Major, P., *Oncologist*, **2002**, *7*, 481.

[190] Lawson, M. A., Xia, Z., Barnett, B. L., Triffitt, J. T., Phipps, R. J., Dunford, J. E., Locklin, R. M., Ebetino, F. H., Russell, R. G. G., *J. Biomed. Mat. Res. Part B: App. Biomat.*, **2009**, *92B*, 149.

[191] Samanamu, C., PhD. Dissertation, Texas Christian University, **2009**.

[192] Bew, S. P., Brimage, R. A., Hughes, D. L., Legentil, L., Sharma, S. V., Wilson, M. A., *J. Org. Chem.*, **2007**, *72*, 2655.

[193] Kontturi, M., Peraniemi, S., Vepsalainen, J. J., Ahlgren, M., *Eur. J. Inorg. Chem.*, **2004**, 2627.

[194] K. J. Langley, P. J. Squattrito, F. Adani, E. Montoneri, *Inorg. Chim. Acta*. **1996**, *253*, 77.

[195] Cao, G., Lee, H., Lynch, V. M., Mallouk, T. E., *Inorg. Chem.,* **1988***, 27*, 2781.

[196] Langley, K. J., Squattrito, P. J., Adani, F., Montoneri, E., *Inorg. Chim. Acta*, **1996**, *253*, 77.

[197] Cao, D.-K., Li, Y.-Z., Zheng, L.-M., *Inorg. Chem.*, **2007**, *46*, 7571.

[198] Uhlig, E., Keil, D., *Zeitschrift fur anorganische und allgemeine Chemie*, **1964**, *332,* 69.

VITA

Julie Ann Fry was born April 15, 1967, at Mather Air Force Base, Sacramento, California. She is the daughter of Colonel Johnnie and Mrs. Janice Vaught. A 1985 graduate of Rogers High School, Newport, Rhode Island, she went on to Abilene Christian University in Abilene, Texas to begin her undergraduate degree. In June, 1987, she was married to Dean M. Fry, D.D.S. and received her Bachelor of Arts degree with a major in Biology from Rice University, Houston, in 1989. She was awarded the Donald I. Woods Award for Teaching Excellence from the Education Department of Rice University, and earned her Texas State Teaching Certifications in Biology and Chemistry.

She then began a twenty-one-year teaching career. Teaching at Episcopal High School in Houston, Texas and Southwest Christian School (SCS) in Fort Worth, Texas, she has taught sixteen years of AP Biology and AP Chemistry, as well as first-year courses in both subjects. She has served as Science Department Chair at SCS since 1998 and has mentored many fine teachers over the years.

She is the mother of five wonderful children: Jenna, Erin, Hayley, Dallas, and Anna, ranging in age from 21 to 11.

In August, 2006, she enrolled in graduate study at Texas Christian University, where she received her Doctor of Philosophy degree in December of 2011. In August, 2009, she became a lecturer of General Chemistry for Texas Christian University, and has taught General Chemistry and Quantitative Analysis for the past three years. She is a member of the American Chemical Society, the National Science Teachers Association, and the Association of Chemistry Teachers of Texas.

ABSTRACT

CRYSTALLOGRAPHIC STUDIES FOR THE RATIONAL DESIGN OF
N-FUNCTIONALIZED PHOSPHONIC ACID COORDINATION POLYMERS

By Julie Ann Fry, Ph.D., 2011
Department of Chemistry
Texas Christian University
Dissertation Advisors: Anne F. Richards, Assistant Professor
Robert H. Neilson, Professor

Metal-organic frameworks (MOFs)[1] are dynamic one-, two-, and three-dimensional networks that reveal unprecedented gas adsorption and storage capabilities, catalytic function, and other useful properties such as luminescence and magnetism.[2] While we begin to see many possibilities for applications of these polymers,[3] the goal of true rational design will only be achieved on the basis of intensive systematic investigations.[4]

The following five chapters will detail our efforts to advance the research goal of utilizing mild synthetic methods to investigate factors controlling the structure of crystalline, thermally stable coordination polymers utilizing *N*-functionalized phosphonic acids. Studies into preferred metal geometry and coordination modes, ligand flexibility, counterion, solvent, and pH will be addressed to discern useful patterns for future synthetic endeavors.

Chapter 1 presents an introduction to the terminology, structural diversity, and chemical applications of this emerging field. Chapter 2 describes the synthesis and crystallographic analysis of five polymers employing a bifunctional, zwitterionic 2-(pyridyl)phosphonic acid ligand, $2PyHPO_3H$, and salts of Zn(II), Cd(II), Hg(II), and Ag(I). Chapter 3 reports the influence that cation choice and ligand flexibility have on the dimensionality and structure of eight products containing Mn(II), Co(II), Fe(II), Fe(III), Ag(I), and Pb(II) cations and 2-(pyridylmethyl)phosphonic acid, $2PyCH_2PO_3H_2$. Chapter 4

explores the use of (aminomethyl)phosphonic acid ($NH_3CH_2PO_3H$) as a bifunctional organic linker for the production of coordination polymers. The substitution of the amino group for the rigid heterocyclic ring of 2-(pyridylmethyl)phosphonic acid results in two-dimensional organophosphonate frameworks with Zn(II), Mn(II), Co(II), Cu(II), Gd(III), Sm(III), and Yb(III) cations. Chapter 5 relates our efforts to evaluate the relationships between metal choice, counterion, and ligand geometric constraints on polymer architectures. Ca(II), Co(II) and Zn(II) salts produce both dimers and polymers with 2-(pyridylmethyl)phosphonic acid, and Ag(I) and Zn(II) salts form unique polymers with 3- and 4-(pyridylmethyl)phosphonic acid. Crystal structures of the compounds allow us to compare and contrast the final products of the self-assembly process. Other analytical techniques, such as IR, NMR, TGA, and mass spectroscopy, are used to support and interpret the crystallographic results.

[1] James, S. L., *Chem. Soc. Rev.,* **2003**, *32*, 276.

[2] Férey, G., *Chem. Soc. Rev.,* **2008**, *37*, 191

[3] Kitagawa, S., Kitaura, R. and Noro, S., *Angew. Chem., Int. Ed.,* **2004**, *43,* 2334.

[4] Sonnauer, A., Nather, C., Hoeppe, H. A., Senker, J., Stock, N., *Inorg. Chem.*, **2007**, *46*, 9968.